DOCTOR OF PHILOSOPHY

Tat signal peptide recognition during protein maturation and export

Grahl, Sabine

Award date:
2011

Awarding institution:
University of Dundee

Link to publication

Tat signal peptide recognition during protein maturation and export

Sabine Grahl

2011

University of Dundee

Tat signal peptide recognition during protein maturation and export

by

Sabine Grahl

College of Life Sciences

November 2011

Thesis submitted to the University of Dundee in partial fulfilment of the requirements for the degree of Doctor of Philosophy

Abstract

Nitrogen is one of the most abundant elements on Earth and mostly found in the atmosphere as the inert gas N_2. Therefore the nitrogen cycle is important for maintaining the bioavailabilty of nitrogen for organisms. Denitrification is a process that closes the nitrogen cycle by subsequent conversion of nitrate to dinitrogen with reduction of nitrate to nitrite being the very first necessary step. The bacterial periplasmic nitrate reductase NapA is one of those nitrate reducing enzymes and contains a molybdenum cofactor and a [4Fe-4S] cluster as cofactors. As a periplasmic terminal reductase NapA has an N-terminal signal peptide harbouring a Tat (twin-arginine translocation) motif, which follows closely the consensus S/T-R-R-x-F-L-K. As with other proteins transported *via* the Tat pathway, NapA needs to be fully folded, and cofactor insertion needs to be completed, prior to export. This is assured by an individual chaperone in a process called 'Tat-proofreading'. The proofreading chaperone for NapA is NapD, which had been previously shown to interact tightly with the signal peptide of NapA.

In this work the binding epitope on the *Escherichia coli* NapA signal peptide recognised by NapD was mapped for the first time. The key amino acid residues (NapA R6, K10, A17) overlapped with the Tat targeting motif and were further characterized *in vitro* and *in vivo* for their importance in NapD binding, Tat transport and NapA biosynthesis. In addition, *napD* suppressor mutants able to re-bind the NapA A17Q variant were isolated.

NMR spectroscopy revealed the 3D solution structure of NapD in complex with the NapA signal peptide. Interestingly, the signal peptide of NapA is α-helical when bound to NapD. Overall, the structure supports strongly that NapA residues R6, K10 and A17 interact with NapD. Pulsed EPR spectroscopy on the isolated signal peptide indicated structural changes of the NapA signal peptide between NapD bound and unbound states, though it was believed that an overall α-helical structure was maintained.

Co-purification studies of the complete NapDA complex for crystallisation trials resulted in increased information on the behaviour of the complex and the order of cofactor insertion into NapA.

Finally, an *in vitro* translation and cross-linking approach was attempted with the aim of addressing whether direct contact was made between NapD and the Tat translocase. In addition, functional chromosomal fusions of either NapD or NapA with fluorescent proteins were generated to form a basis for a future project based on fluorescence correlation spectroscopy in living cells.

This project has therefore provided fresh insight into the NapA-NapD interaction at the molecular level and laid the foundations for future research in this area.

Table of contents

Table of figures

Table of tables

List of abbreviations

acetyl-CoA	acetyl coenzyme A
ATP	adenosine triphosphate
BiFC	bimolecular fluorescence complementation
BN-PAGE	blue native polyacrylamide gel electrophoresis
BTH	bacterial two-hybrid
cAMP	cyclic adenosine monophosphate
CD	circular dichroism
Cml	chloramphenicol
CRP	cAMP receptor protein
CAT	chloramphenicol acetyl transferase
Cml	chloramphenicol
Da	Dalton
DMF	dimethylformamide
DMSO	diemthylsulfoxide
EPR	electron paramagentic resonance
FCS	fluorescence correlation spectroscopy
GFOR	glucose-fructose oxidoreductase
HiPIP	high potential iron-sulphur protein
HSQC	heteronuclear single quantum correlation
ICP-MS	inductively coupled plasma mass spectrometry
IMAC	immobilised metal affinity chromatography
INV	inside-out inner membrane vesicle
ITC	isothermal titration calorimetry
FNR	fumarate and nitrate regulatory protein
K_D	binding (dissociation) constant
LB	Luria-Bertani
LPS	lipopolysaccharide
MALDI-TOF	matrix assisted laser desorption ionisation – time of flight
MalE	maltose binding protein
mCer	mCerulean
MTSL	S-(2,2,5,5-tetramethyl-2,5-dihydro-1H-pyrrol-3-yl)methyl methanesulfonothioate
N	binding stoichiometry
NapA$_{SP}$	NapA signal peptide
NED	N-(1-naphthyl)ethylenediamine
NMR	nuclear magnetic resonance
NTP	nucleotide triphosphate
OCD	oriented CD
OM	outer membrane
pBpa	p-benzoyl-L-phenylalanine
PCR	polymerase chain reaction
PELDOR	pulsed electron-electron double resonance
PDB	protein data bank
PK	Proteinase K
pmf	proton motif force
PURE	protein synthesis using recombinant elements
SDS-PAGE	sodium dodecyl sulfate polyacrylamide gel electrophoresis
Sec	secretory
SDSL	site-directed spin labelling
SRP	signal recognition particle
Tat	twin-argine translocation
TF	trigger factor
TMAO	trimethylamine N-oxide
UV	ultra violet

Acknowledgements

Declaration

I declare that I am the author of this thesis and that, unless otherwise stated, all references cited have been consulted; that the work of which this thesis is record of has been performed by me, and that it has not been previously accepted for a higher degree: where the thesis is based upon joint research, the nature and extent of my individual contribution is defined.

Sabine Grahl

1 Introduction

1.1 THE NITROGEN CYCLE

Nitrogen is the fourth most abundant element in biomass and as a key constituent of nucleic acids and proteins it is essential to life on Earth. Nitrogen makes up to 80% of the atmosphere of the Earth, but its bioavailability is limited since the atmospheric form is almost completely in the largely inert dinitrogen gas (N_2) form. Paradoxically, however, this places atmospheric N_2 as the biggest nitrogen source on the planet and as such is of great ecological importance (Dance, 2007). The triple bond between the N atoms in dinitrogen makes this compound thermodynamically and kinetically very stable, and thus inaccessible to most organisms (Moir, 2011). Nature has found a way of both capturing and replenishing atmospheric N_2 for living things. In the biogeochemical nitrogen cycle the nitrogen molecule is converted through a number of redox reactions by various microorganisms (Martínez-Espinosa et al, 2011). The N_2 is transformed through a number of enzymatic reactions to generate different intermediates and compounds with a wide range of redox states ranging from +V to −III (Figure 1.1).
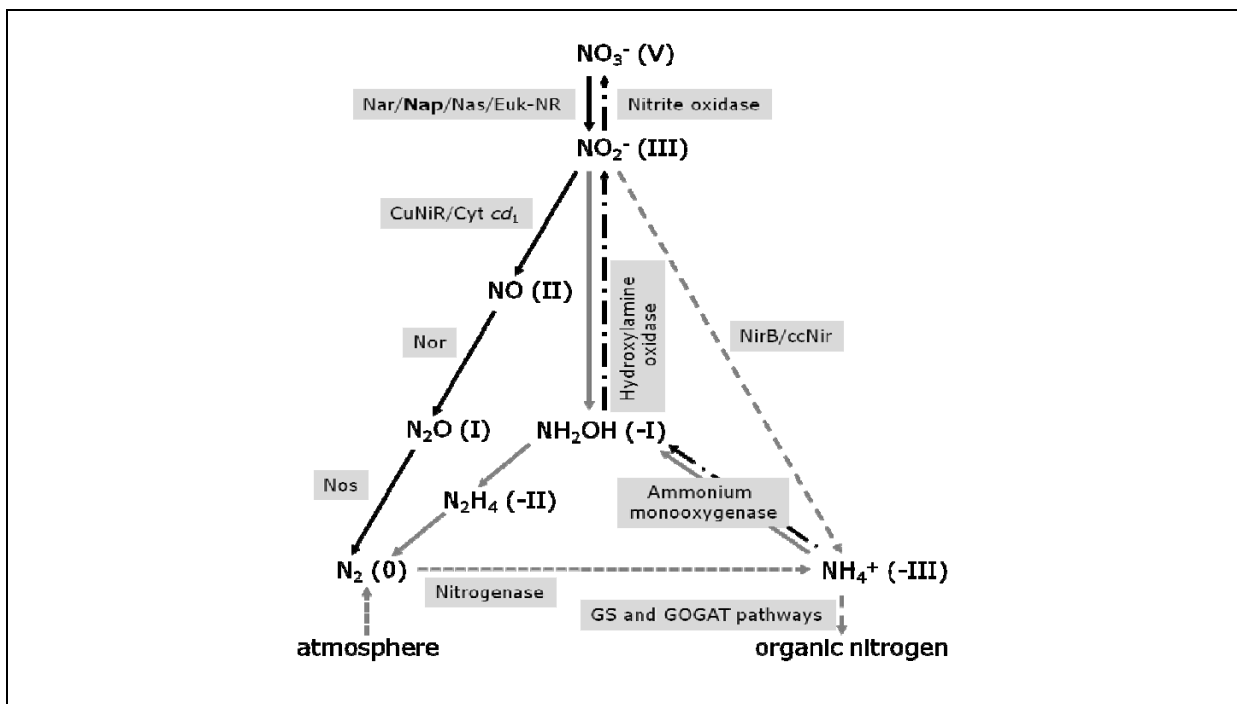
Figure 1.1 The inorganic nitrogen cycle (including the enzymes responsible for each step). The oxidation state of each compound is indicated between parentheses. The pathways are identified as follow: black solid line, respiratory pathway (denitrification); dashed line, dissimilatory and assimilatory ammonification (note that nitrate reduction is indicated only as solid arrow); dotted line, nitrogen fixation; dash-dot line, nitrification; grey solid line, anaerobic ammonium oxidation (ANAMMOX). GS – glutamine synthetase, GOGAT – glutamine synthetase-glutamate synthetase (González et al, 2006).

1.1.1 Nitrogen fixation

The fixation of nitrogen is probably best understood in legume symbionts such as *Rhizobium or Bradyrhizobium* species, which grow in the nodules of leguminous plants. However, nitrogen fixers are wide spread in the prokaryotic world with free-living *Azotobacter vinelandii* and *Klebsiella pneumonia* as some of the best studied examples. Also some cyanobacteria and methanogenic archea are able to produce ammonium from nitrogen (Peters et al, 2011).

The enzyme that performs this energy-consuming reaction is the nitrogenase. The majority of nitrogenases contain molybdenum and iron in their active centre (*nif*), however, vanadium and iron (*vnf*), and iron only (*anf*), nitrogenases have also been identified (Walmsley et al, 1994).
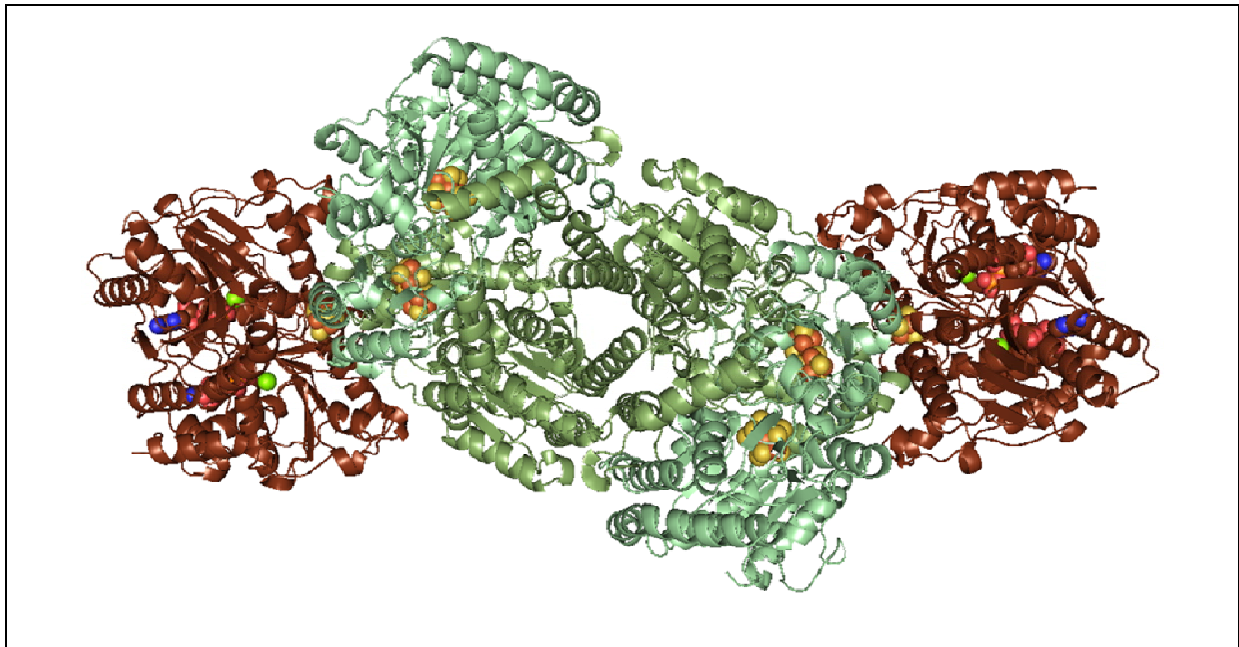
Figure 1.2 Overall structure of the nitrogenase complex of *Azotobacter vinelandii*. The MoFe α-subunit (light green), the β-subunit (green) and the dimeric Fe-protein (brown) are shown. The cofactors and bound nucleotides MgADP are shown as spheres. Atoms are colour coded with Mg in grass green and Mo in cyan, Fe in light brown, S in yellow, O in red and N in blue. (Taken from Schindelin et al, 1997; PDB ID code 1n2c)

Nitrogenases consist of two proteins – a Fe protein (NifH) and a MoFe protein (NifD and NifK assembling as α- and β-subunit, respectively) (Hu et al, 2008; Figure 1.2.). Dinitrogen is reduced in a cycle of eight steps each needing a single electron. This is achieved by constant association and dissociation of the Fe protein with the MoFe protein coupled with electron transfer from ATP hydrolysis by the Fe protein (Equation 1.1). Thus ATP is bound and hydrolyzed after complex formation between the two proteins. Electrons are then transferred from the Fe protein's [4Fe-4S] cluster to an iron containing P-cluster in the α-subunit to the final active MoFe site (Seefeldt et al, 2009).

$$N_2 + 16MgATP + 8e^- + 8H^+ \quad \rightarrow \quad 2NH_3 + H_2 + 16MgADP + 16P_i \qquad \text{Equation 1.1}$$
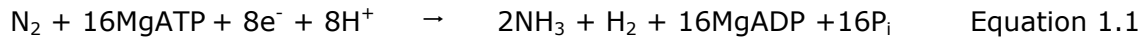
1.1.2 Ammonification

The respiratory reduction of nitrite to produce ammonium only occurs in γ-, δ- or ε-proteobacteria under anaerobic conditions and allows the generation of an electrochemical proton gradient (Δp) across the inner membrane for ATP synthesis. Normally a formate dehydrogenase or a hydrogenase provide electrons by oxidation of formate or hydrogen (Equation 1.2 and 1.3), respectively, which are transferred *via* the quinone pool to a cytochrome *c* nitrite reductase, NrfA. In addition, sulphide was also shown to be used as electron donor (Simon, 2002).

$$3HCO_2^- + NO_2^- + 5H^+ \quad \rightarrow \quad 3CO_2 + NH_4^+ + 2H_2O \qquad \text{Equation 1.2}$$

$$3H_2 + NO_2^- + 2H^+ \quad \rightarrow \quad NH_4^+ + 2H_2O \qquad \text{Equation 1.3}$$
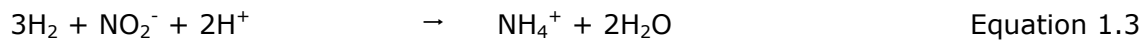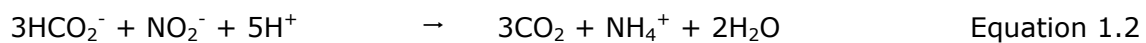
NrfA contains five haem *c* groups and is anchored to the membrane by a tetrahaem cytochrome *c* (NrfH in *Wolinella succinogenes*), which oxides menaquinol (Figure 1.3; Einsle, 2011). However, according to phylogenetic analysis, it seems that pathways for electron transfer to nitrite reductase are different for each bacterial group (Simon, 2002).
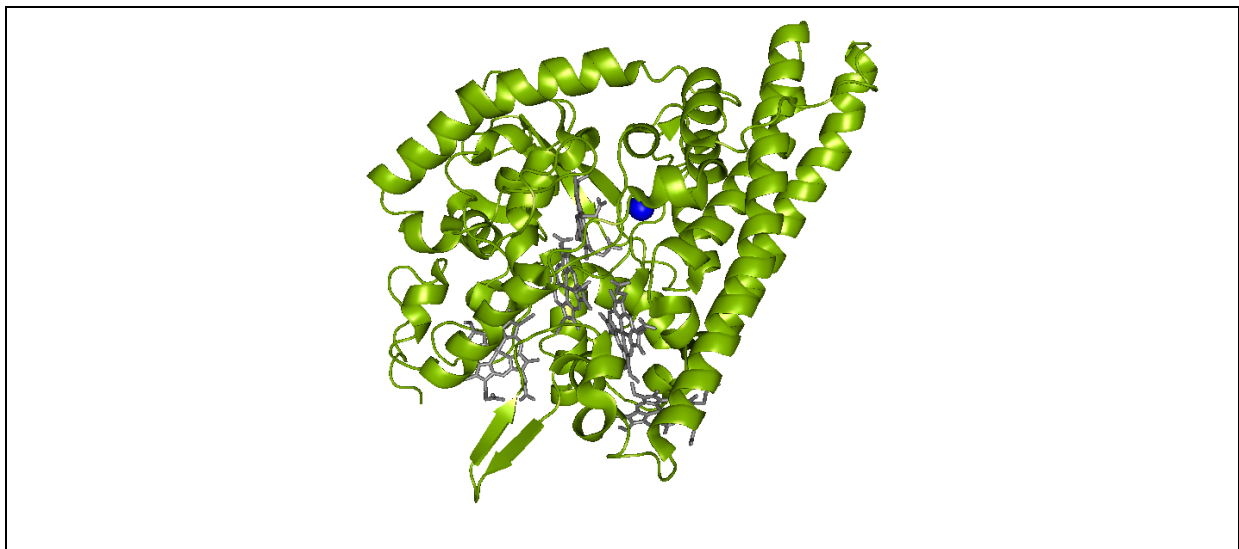
Figure 1.3 Crystal structure of NrfA from *W. succinogenes*. NrfA exists as a dimer, however here only the monomeric form is shown. The five haem groups are depicted in stick formate. The Ca^{2+} ion (blue) was shown to be important for activity and might influence the stability of the protein (Einsle et al, 2002; Cunha et al, 2003). (PDB ID code 1fs7)

1.1.3 Nitrification

In contrast to ammonification, nitrification is the oxidation of ammonium to nitrate *via* nitrite. The nitrification process is found in soil and water, but has also a major role in waste water treatment in combination with denitrification. The conversion of

ammonium/ammonia is performed by bacteria belonging to the genera *Nitrosomonas, Nitrosococcus and Nitrosospira*. The so far best described organism is *Nitrosomonas europaea*. This bacterium contains a membrane-bound ammonia monoxygenase enzyme (Amo), which performs the first reaction described in Equation 1.4, where ammonium in the presence of oxygen is transformed into hydroxylamine. Amo is a copper enzyme possibly consisting of a heterotrimeric complex with AmoABC subunits (Arp et al, 2002).

$$NH_3 + O_2 + 2H+ + 2e^- \rightarrow NH_2OH + H_2O \quad\quad\quad \text{Equation 1.4}$$
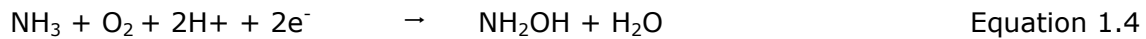
Next, a hydroxylamine oxidoreductase (Hao) oxidizes NH_2OH to NO_2^- (Equation 1.5). Hao is located in the periplasm and forms a homotrimeric octahaem cytochrome *c* complex (Figure 1.4; Klotz et al, 2008).

$$NH_2OH + H_2O \rightarrow NO_2^- + 5H^+ + 4e- \quad\quad\quad \text{Equation 1.5}$$
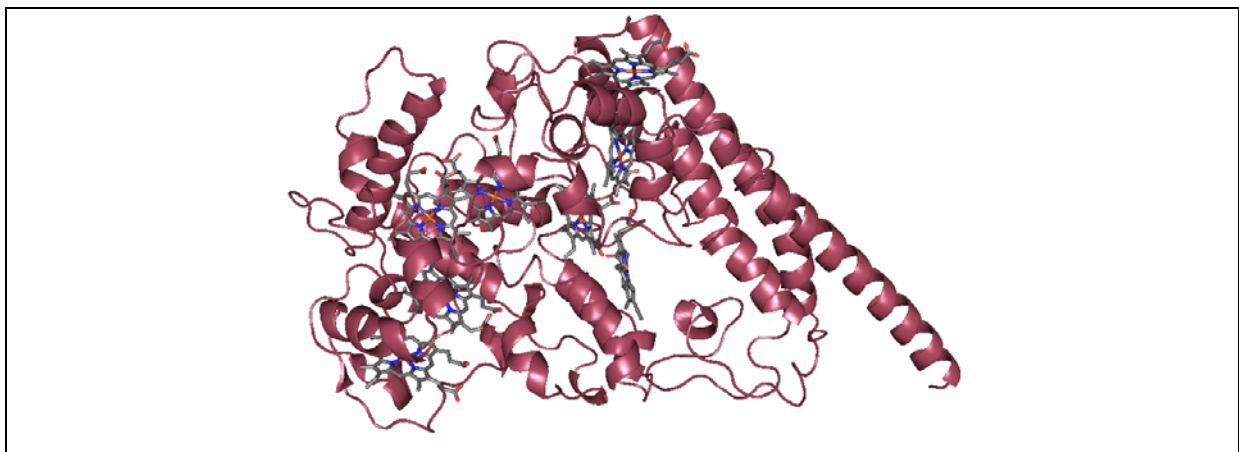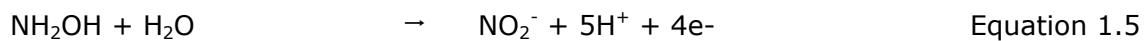
Figure 1.4 Crystal structure of the hydroxylamine oxidoreductase from *N. europaea*. The protein is shown in its monomeric form. The eight haems are highlighted as sticks. (PDB ID code 1fgj)

Recently, archea of the new phylum *Thaumarcheota* have been described, which encode homologues genes to *amo* and were able to oxidise ammonium (Martens-Habbena & Stahl, 2011).

The last step in the nitrification process, the oxidation of nitrite to nitrate is performed by bacteria of the genera *Nitrobacter*, *Nitrococcus* and *Nitrospira* (Equation 1.6). The reaction is carried out by a nitrite oxidoreductase (Nxr), a membrane-associated complex comprising a molybdenum-containing α-subunit and a [Fe-S]-containing β-subunit. So far not much is known about localisation, structure or molecular mechanism of Nxr. However, sequences analysis in *Nitrobacter hamburgensis* shows remarkable similarities to the membrane-bound nitrate reductase (Nar), thus it is assumed that Nxr

is facing the cytoplasmic site of the membrane and has similar mechanisms for quinol reduction and electron transfer (Poly et al, 2008; Starkenburg et al, 2008).

$$NO_2^- + H_2O \quad \rightarrow \quad NO_3^- + 2H^+ + 2e^- \qquad \text{Equation 1.6}$$
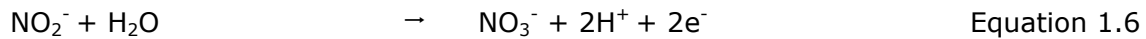
1.1.4 ANAMMOX

The relatively recent discovery of anaerobic ammonium oxidation (ANAMMOX) is a process that removes ammonium from the system through reduction of nitrite and can be described with the following overall reaction:

$$NH_4^+ + NO_2^- \quad \rightarrow \quad N_2 + 2H_2O \qquad \text{Equation 1.7}$$
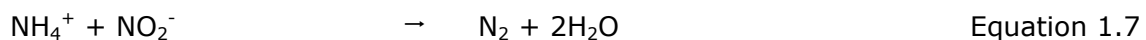
The ANAMMOX process was first discovered in a waste water plant and in general is important for the global marine nitrogen cycle. There it is a sink for fixed dinitrogen contributing up to 50% to the overall amount of N_2 (Penton et al, 2006). ANAMMOX is carried out by both bacteria and archaea and those microorganisms contain a membrane-bound intracellular organelle, the anammoxosome, which consists of highly impermeable ladderane lipids (van Niftrik et al, 2008). For bacteria, *Candidatus* 'Kuenenia stuttgartiensis' from the order *Brocadiales*, phylum *Planctomycetes* is one of the best described based on *in silico* and *in vitro* studies (Strous et al, 2006).

Oxidation of ammonium occurs in three steps and for each step the corresponding enzyme has been isolated and characterized from *Ca.* 'Kuenenia stuttgartiensis' (Kartal et al, 2011). In the first reaction nitrite is reduced to nitric oxide by a cd_1 nitrite:nitric oxide oxidoreductase (NirS, Equation 1.8).

$$NO_2^- + 2H^+ + e^- \quad \rightarrow \quad NO + H_2O \qquad \text{Equation 1.8}$$
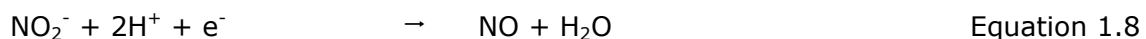
This is followed by condensation of NO with ammonium to produce hydrazine (Equation 1.9), which is carried out by a hydrazine synthetase (HZS).

$$NO + NH_4^+ + 2H^+ + 3e^- \quad \rightarrow \quad N_2H_4 + H_2O \qquad \text{Equation 1.9}$$
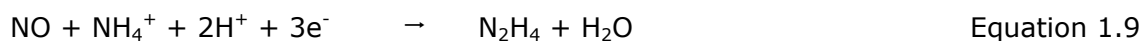
In the final reaction a hydrazine dehydrogenase (HDH) oxidizes quickly N_2H_4 to N_2 (Equation 1.10).

$$N_2H_4 \quad \rightarrow \quad N_2 + 4H^+ + 4e^- \qquad \text{Equation 1.10}$$
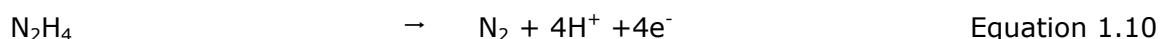
1.1.5 Denitrification

Another key process in the N-cycle is denitrification, which involves the reduction of nitrate to dinitrogen and its subsequent release back into the atmosphere. It is carried

out by many bacteria and some fungi. Denitrification proceeds in a step-wise manner, from $NO_3^- \rightarrow NO_2^- \rightarrow NO \rightarrow N_2O \rightarrow N_2$. The first key step in this reaction scheme is performed by nitrate reductases (Equation 1.11).

$$NO_3^- + 2e^- + 2H^+ \qquad \rightarrow \qquad NO_2^- + H_2O \qquad \qquad \text{Equation 1.11}$$
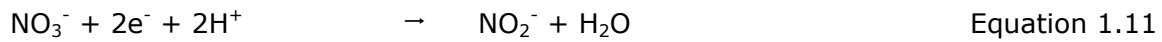
During anaerobic growth many bacteria use especially nitrate as preferred electron acceptor. Almost all nitrate reductases are mononuclear molybdenum-containing enzymes with additional prosthetic groups such as iron-sulphur or haem cofactors. These are further described in Section 1.3 using the example of *Escherichia coli*.

1.1.5.1 Nitrite reductase

Nitric oxide (NO), the product of nitrite reduction in the denitrification process (Equation 1.12) is formed either by a copper containing nitrate reductase (NirK) or a cytochrome cd_1-type nitrite reductase (NirS). NirK forms a homotrimer with copper ions participating in electron transfer and catalytic NO reduction. The *nirK* gene is found together with *nirV*, a desulfarase homologue possibly involved in copper insertion. In contrast, NirS is homodimeric. Each subunit has an N-terminal α-helical domain harbouring the *c*-type haem for electron uptake and an eight-bladed β-propeller domain, where the d_1 haem forms the catalytic site. The general operon *nirSECFDLGHJN* encodes beside the catalytic protein a number of transcriptional regulators and proteins involved in synthesis and assembly of haem d_1 (van Spanning, 2011).

$$NO_2^- + e^- + 2H^+ \qquad \rightarrow \qquad NO + H_2O \qquad \qquad \text{Equation 1.12}$$
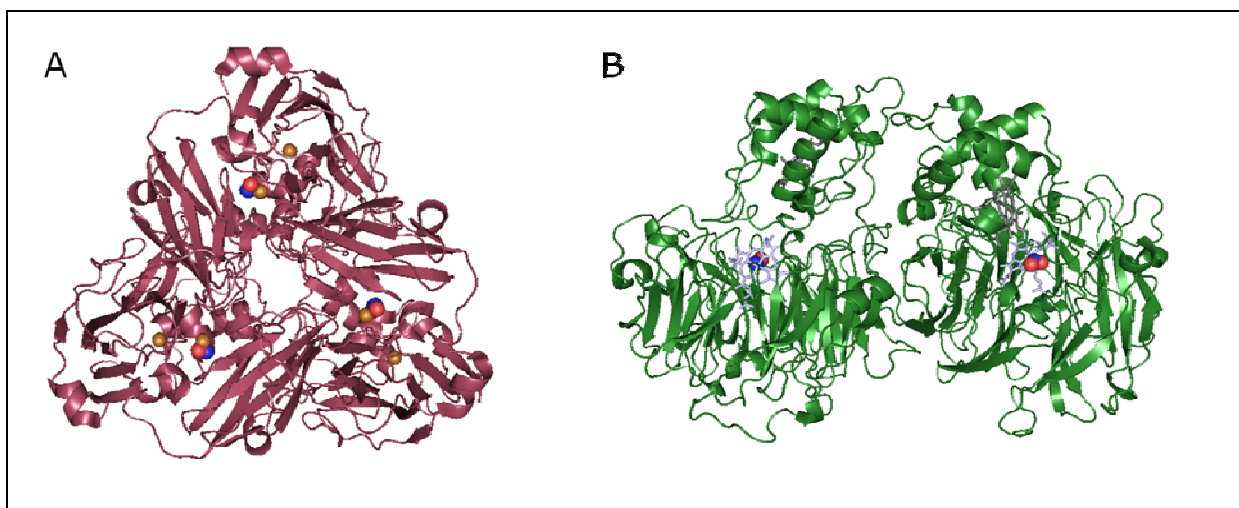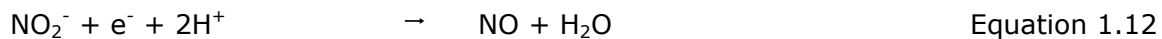
Figure 1.5 Crystal structures of the different nitrite reductases in the denitrification process. (A) The trimeric Cu nitrate reductase NirK from *Alcaligenes faecalis*. Each subunit contains two copper ions (brown) and is shown here with bound nitrite (O in red, N in blue). (PDB ID code 1j9q) (B) The cd_1 nitrite reductase NirS from *Paracoccus pantotrophus*. The *c* and d_1 haem are shown in stick format in grey and light blue, respectively. Bound nitrite is shown as spheres. (PDB ID code 1aoq).

NirK was identified in archaea, bacteria of the genus Actinobacteria, Firmigutes, as well as α-, β- and γ-proteobacteria. NirS is encoded in β-, γ-, ε-proteobacteria, Aquifacea and there are also homologues in archaea. Interestingly, NirK is not found in ε-proteobacteria and Aquifacea. So far no organism has been discovered that encodes both nitrite reductases within its genome (Jones et al, 2008).

1.1.5.2 Nitric oxide reductase

Nitric oxide reductase (NOR) performs the difficult task of bonding N-N by reduction of two molecules nitric oxide to nitrous oxide (Equation 1.13).

$$2NO + 2e^- + 2H^+ \quad \rightarrow \quad N_2O + H_2O \qquad \text{Equation 1.13}$$
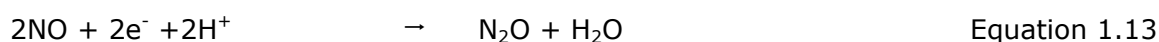
Usually NOR is isolated as a heterodimeric complex, NorBC. NorC has an N-terminal transmembrane helix anchoring its haem c-type cytochrome to the periplasmic site of the membrane. This protein obtains electrons from pseudoazurin or cytochrome c_{550} to NorB. Then, NorB shuttles the electron through two haem b to the haem b::Fe_B dinuclear centre, where the catalytic reaction is performed. This subunit contains 12 transmembrane domains burying its active centre in the membrane (Figure 1.6; Zumft, 2005). Sequence analysis revealed five highly conserved glutamine residues, where Glu211 and Glu280 (positioning based on *Pseudomonas aeriginosa* NorB) are possibly proton donors for the NO reduction, Glu215 contributes to an electro-negative environment at the catalytic centre and Glu135 and Glu138 participate in stabilizing the structure of NorB (Hino et al, 2011).
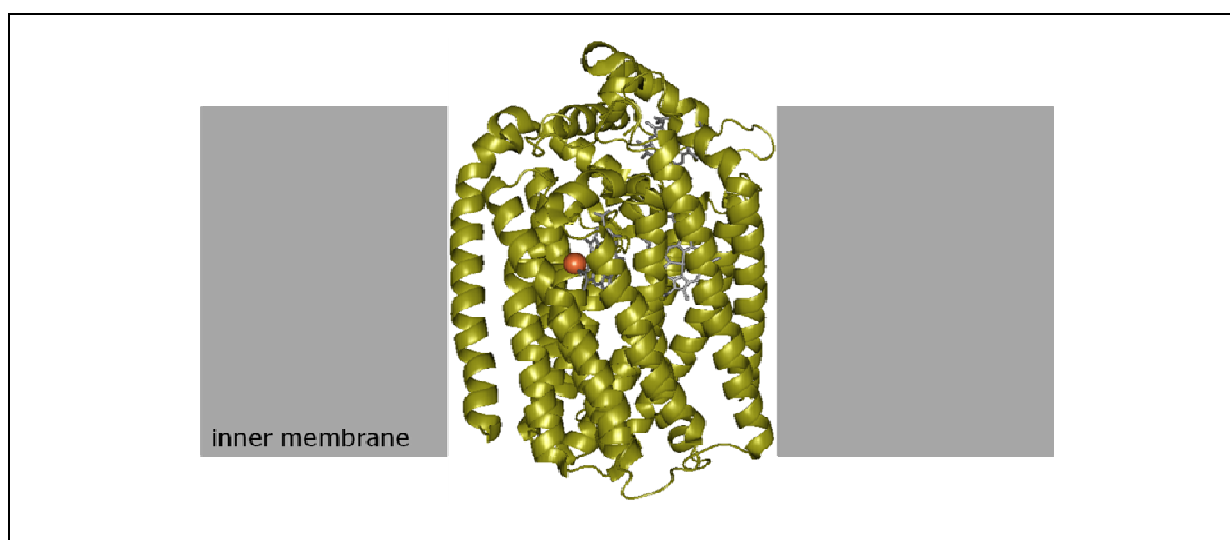
Figure 1.6 Crystal structure of nitric oxide reductase subunit NorB from *P. aeriginosa*. NorB is a transmembrane protein, which contains an iron (brown sphere) in its active centre. The haem groups are depicted as sticks. (PDB ID code 3o0r)

1.1.5.3 Nitrous oxide reductase

The last step in the denitrification process, reduction of N_2O to N_2, is performed by a nitrous oxide reductase (N_2OR), which is encoded by the *nosZ* gene (Equation 1.14).

$$N_2O + 2e^- + 2H^+ \quad \rightarrow \quad N_2 + H_2O \qquad \text{Equation 1.14}$$
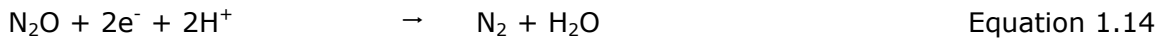
N_2OR is a dimeric periplasmic protein with each subunit containing two copper centres (Figure 1.4). The di-copper Cu_A is the entrance site for electrons, whereas Cu_Z is the reactive centre. In some species N_2OR has been found to contain a Tat (twin-arginine translocation) signal peptide, suggesting protein folding occurs in the cytoplasm prior to export (Hoeren et al, 1993). Indeed, a mutation of the first arginine in the Tat motif of *P. stutzeri* N_2OR to aspartate prevented translocation of the reductase to the periplasm (Dreusch et al, 1997). Nevertheless, copper insertion and full assembly need to be carried out in the periplasm. The *nosZ* gene is found in an operon together with *nosDFY*, the resulting proteins participate in sulphur transport (NosFY) for copper-sulphide-bridging and provide an assembly platform (NosD) for copper insertion and final folding of NosZ. It is proposed that electrons are provided from the quinol pool *via* two flavoproteins, NosR and NosX to drive N_2O reduction (van Spanning, 2011).
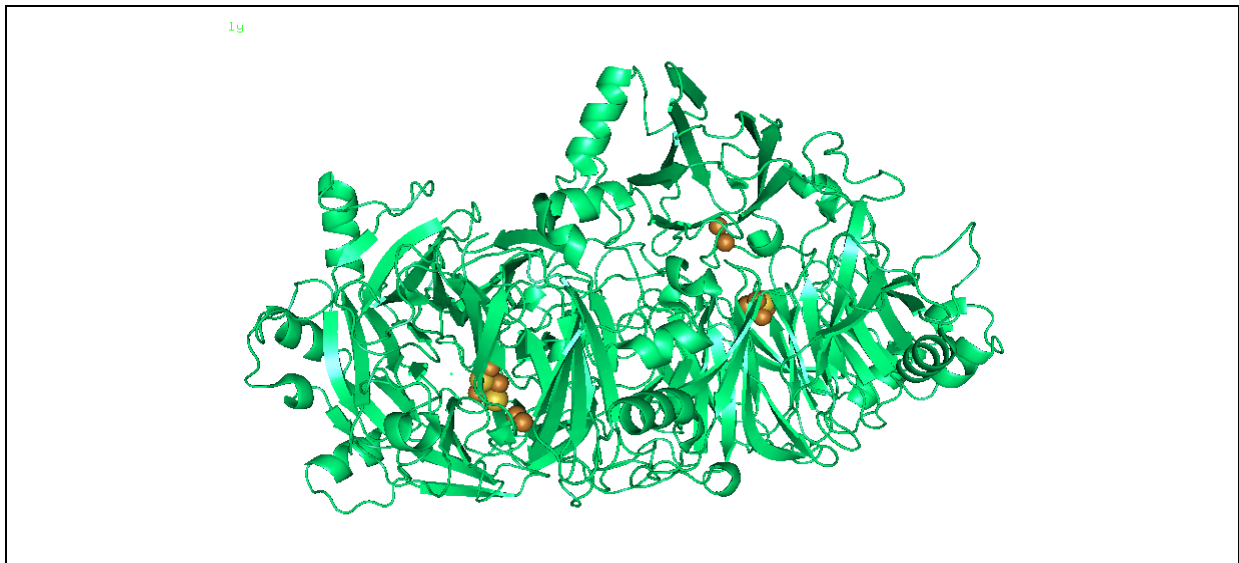
Figure 1.7 Nitrous oxide reductase (N_2OR) from *P. stutzeri*. Shown is the homodimer in a head-to-tail orientation. For each subunit the tetranuclear Cu_Z active site is located in the N-terminus, a seven-bladed β-propeller domain. The binuclear Cu_A site is in the C-terminal cupredoxin domain. (Taken from Pomowski et al, 2011; PDB ID code 3sbq)

1.2 ESCHERICHIA COLI

E. coli was first described in 1885 by Theodor Escherich, a bacteriologist and paediatrician, who isolated the bacterium from infant stool samples. Escherich named the bacterium initially *Bacterium coli* due to its presence in the small intestines and the colon. Later on, in honour of its discoverer, it was renamed '*Escherichia coli*', which has been commonly accepted since 1958 (Shulman et al, 2007).

E. coli belongs to the family of *Enterobacteriaceae* in the phylum of γ-*proteobacteria*. Cells of *E. coli* are Gram-negative, rod-shaped with a length of 2 µm and a diameter of 0.5 µm. It is motile through peritrichous flagella and is able to attach to surfaces by fimbriae formation.

E. coli is a facultative-anaerobe able to use aerobic and anaerobic pathways for energy production, where different electron acceptors can be adopted to suit the individual growth conditions (Sargent, 2007a). Through the respiratory chain a substrate-specific dehydrogenase oxidises its substrate and transfers electrons to the quinone pool in the membrane. In *E. coli* three different types of quinone are available: ubiquinone, menaquinone and demethylmenaquinone, which are produced under the different growth conditions. Those quinones in their reduced form (quinols) further transfer electrons *via* another oxidoreductase to a terminal electron acceptor.

During aerobic growth *E. coli* uses oxygen as terminal electron acceptor. However, under anaerobiosis nitrate, nitrite, TMAO (trimethylamine *N*-oxide), DMSO (dimethyl sulfoxide) or fumarate can be used.

Under anaerobic conditions, and if no terminal electron acceptor is available, *E. coli* performs mixed acid fermentation producing ethanol, lactate, succinate, acetate and formate (which can be further converted to hydrogen gas and carbon dioxide).

As one of the first, complete genomes to be assembled, the sequence of the single *E. coli* chromosome was published in 1997 (Blattner et al, 1997). In addition, *E. coli* is relatively easy to manipulate genetically, straight forward to culture, and has a relatively short doubling time (under ideal growth conditions this can be less than 20 minutes). *E. coli* is also closely related to pathogenic bacteria such as *Salmonella*, *Shigella*, *Yersinia*, and *E. coli* strains exist, of course, which cause different infections in humans including urinary tract infections, neonatal meningitis and intestinal diseases (gastroenteritis).

Therefore *E. coli* is an ideal model organism in the field of molecular biology, biochemistry, medicine and biotechnology.

1.3 NITRATE REDUCTASES OF E. COLI

There are three distinct isoenzymes responsible for nitrate reduction in *E. coli*: nitrate reductase-A; nitrate reductase-Z; and the periplasmic nitrate reductase, Nap. Each are genetically distinct, differentially expressed, and have subtly different roles in nitrate respiration.

1.3.1 The nitrate reductase-A, NarGHI

The *narGHJI* operon in *E. coli* encodes for a membrane-bound nitrate reductase (Sodergren & DeMoss, 1988). Crystal structures of the reductase have been solved and show a heterohexameric complex with $[NarG]_2[NarH]_2[NarI]_2$ (Bertero et al, 2003; Jormakka et al, 2004). NarGH is active in the cytoplasm and attached to the membrane *via* NarI, a five transmembrane spanning protein (Figure 1.8).
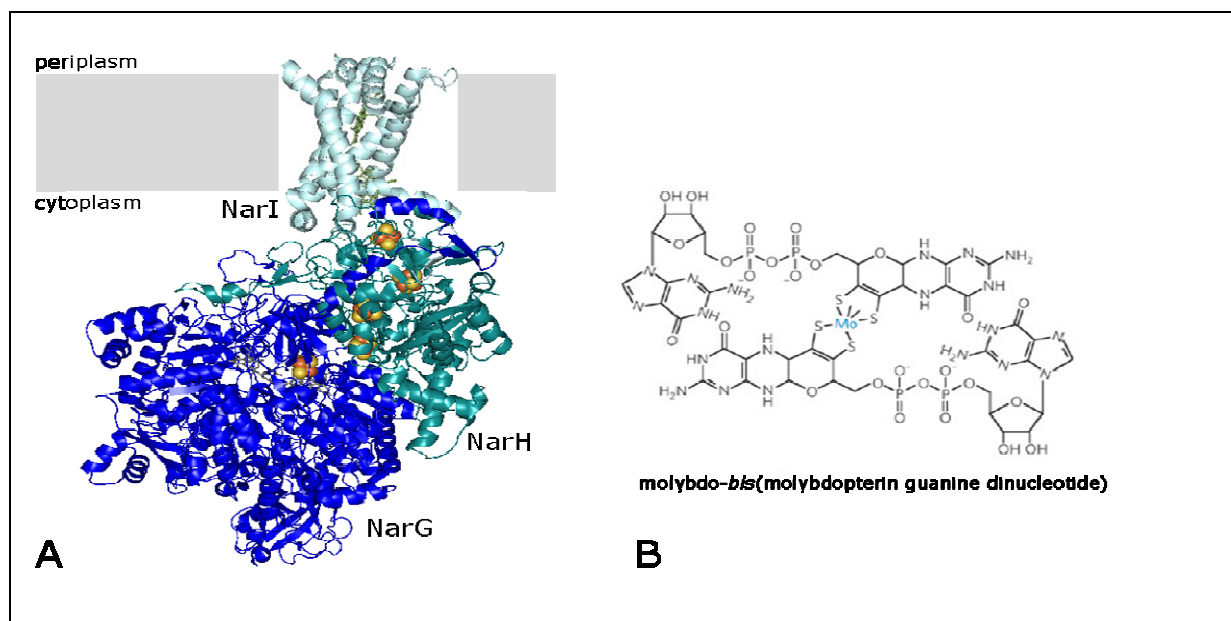
Figure 1.8 Crystal structure of the nitrate reductase-A from *E. coli*. (A) NarGHI is viewed parallel to the membrane. NarG is shown in blue, NarH in cyan and NarI in light blue. Mo-*bis*-MGD and the two haems are depicted in stick rendering in grey and green, respectively. Molybdenum (light green) and [Fe-S] cluster (brown-yellow) are shown as sphares. (PDB ID code 1q16). (B) Chemical structure of Mo-*bis*-MGD [molybdo-*bis*(molybdopterin guanne dinucleotide)] (Schwarz et al, 2009).

NarI is a *b*-type cytochrome binding two haems, which provides electrons from the oxidation of quinol to the iron-sulphur containing subunit NarH and further to the catalytic active site of NarG (Figure 1.9) (Bertero et al, 2005; Rothery et al, 2001). In addition to a [4Fe-4S] cluster NarG contains a molybdenum-*bis*-molybdopterin guanine dinucleotide (Mo-*bis*-MGD) (Magalon et al, 1998; Rothery et al, 2004). The NarJ protein has a chaperone-like function mediating NarGH assembly and attachment to NarI (Lanciano et al, 2007). In *E. coli* the *narGHJI* operon is expressed under high nitrate concentrations and is part of an energy conserving process in the cell (Richardson et al, 2001).
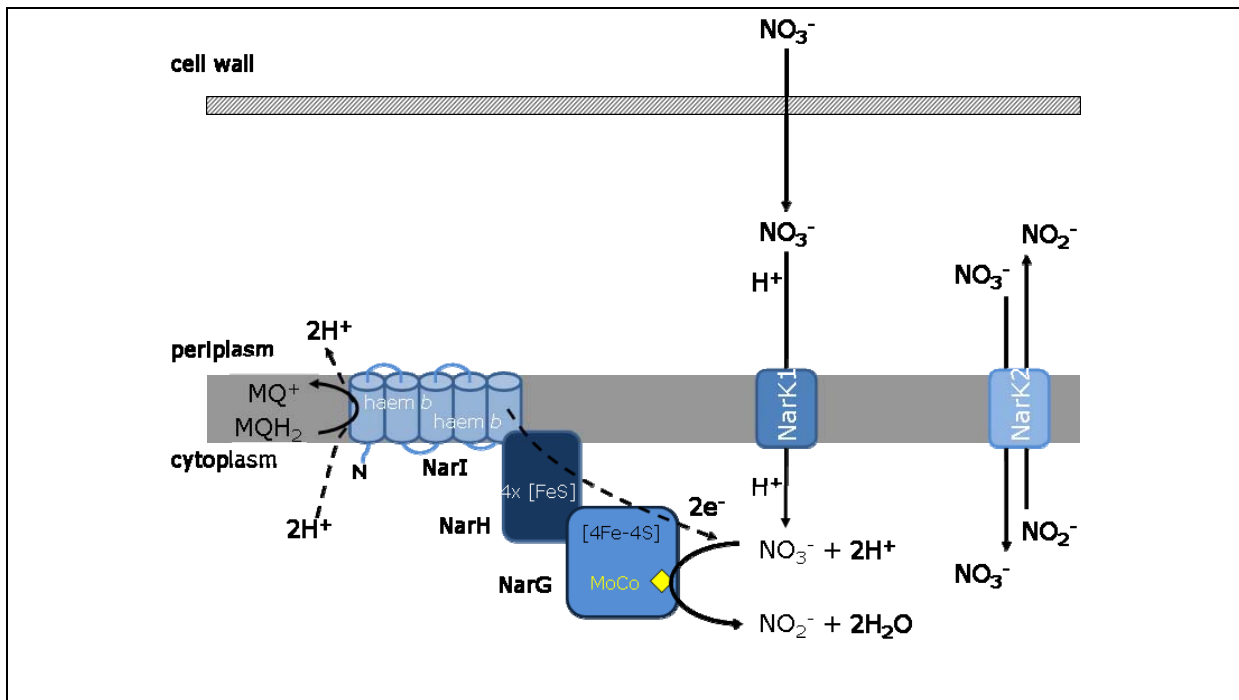
Figure 1.9 Respiratory nitrate reduction by the nitrate reductase-A. NarI oxidises quinol from the membrane pool close to the periplasmic side of the membrane, which in turn releases two protons into the periplasm. The electrons are then transferred *via* NarH to the catalytic site of NarG (molybdenum cofactor - MoCo), where nitrate is reduced to nitrite. The Nar complex exists actually as a dimer of heterotrimers, but for clarity only one heterotrimer is shown. Because NarGHI is located on the cytoplasmic site of the membrane nitrate needs be imported into the cytoplasm in order to be reduced. The proton:nitrate symporter NarK1 is active in the beginning of nitrate reduction. Later, when nitrite accumulates NarK2 is activated, a nitrate:nitrite antiporter, which maintains the steady state. The cytoplasmically located NarJ chaperone is not shown. Modified from Gonzalez et al, 2006.

1.3.2 The nitrate reductase-Z, NarZYV

Another membrane-bound nitrate reductase in *E. coli* is encoded by the *narZYWV* operon, where the NarZYV complex is homologous to NarGHI and NarW is homologous to NarJ, and so possibly also a private chaperone for the assembly of the reductase (Blasco et al, 1990; Blasco et al, 1992). It was originally hypothesised that *narZYWV* is a gene duplication of *narGHJI*, which is constitutively expressed at very low levels regardless of growth conditions. It has been suggested that NarZYV is used by the cell during the initial stages of the switch between aerobic to anaerobic growth in the presence of nitrate (Iobbi-Nivol et al, 1990).

1.3.3 The periplasmic nitrate reductase, Nap

The *E. coli nap* operon is expressed during anaerobiosis under nitrate limiting conditions (Figure 1.11A). The *napA* gene encodes the 93 kDa large catalytic subunit of the periplasmic nitrate reductase, which contains a [4Fe-4S] cluster and a Mo-*bis*-MGD cofactor (Figure 1.10; Jepson et al, 2007). NapA is located in the periplasm and forms a loose complex with the 16 kDa di-haem cytochrome *c* NapB (Figure 1.11B; Jepson et al, 2007). The NapA precursor contains an N-terminal twin-arginine signal peptide, and is thus exported to the periplasm *via* the Tat pathway (Thomas et al, 1999). There, NapA

11

interacts with NapB, which itself is transported *via* the Sec pathway (González et al, 2007).
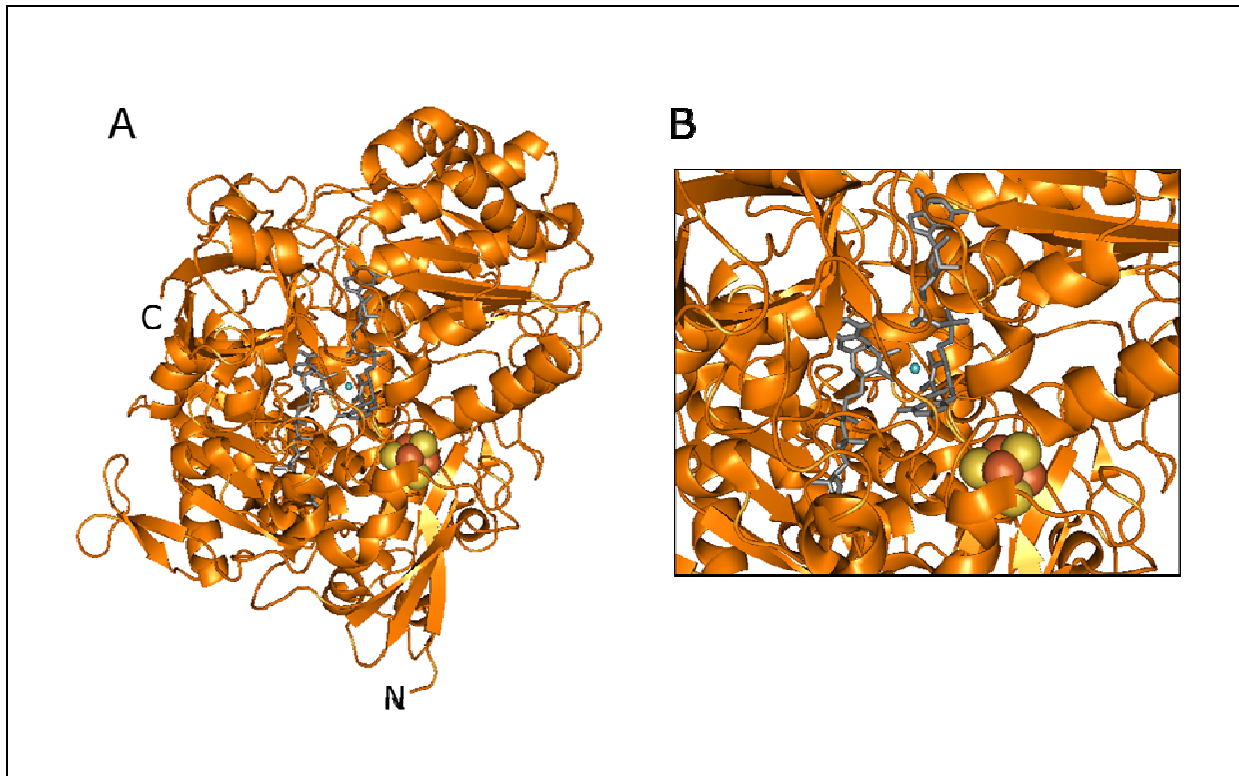
Figure 1.10 NapA, the catalytic subunit of the periplasmic nitrate reductase. (A) Crystal structure of NapA. Mo-*bis*-MGD is depicted with grey sticks, molybdenum (light green) and the [4Fe-4S] (brown-yellow) are shown as spheres. (B) Enlargement of the catalytic site of NapA. (PDB ID code 2nya)

In order to reduce nitrate electrons need to be transferred from the quinol pool in the membrane to NapB and further to NapA. Therefore, the complete Nap complex comprises three proteins bound to or associated with the membrane: NapC, NapG and NapH, which are involved in two different electron transport chains (Figure 1.11B). NapC is a *c*-type cytochrome anchored to the inner membrane by a single N-terminal transmembrane domain. This protein is able to reduce menaquinol, which provides electrons directly to NapB and NapA.

Interestingly, the *E. coli* Nap system includes an alternative route for electron transfer to NapA that includes NapG and NapH. *In silico* analysis predicts NapH to be a four transmembrane protein with N- and C-terminus located in the cytoplasm with a soluble cytoplasmic domain containing two [4Fe-4S] clusters (Brondijk et al, 2004). NapG is predicted to bind four [4Fe-4S] clusters and possesses an N-terminal Tat signal peptide, which targets NapG into the periplasm. The periplasmic localisation of NapG, and its subsequent binding to NapH, was supported by bacterial two-hybrid assays (Brondijk et al, 2004). The same study showed also strong interactions between NapC and NapH. From this work the authors concluded that NapGH is a quinol dehydrogenase and

electrons are directed to NapC, NapB and finally to NapA (Brondijk et al, 2004). Thus the *E. coli* Nap system is able to use both ubiquinol and menaquinol as electron donors.
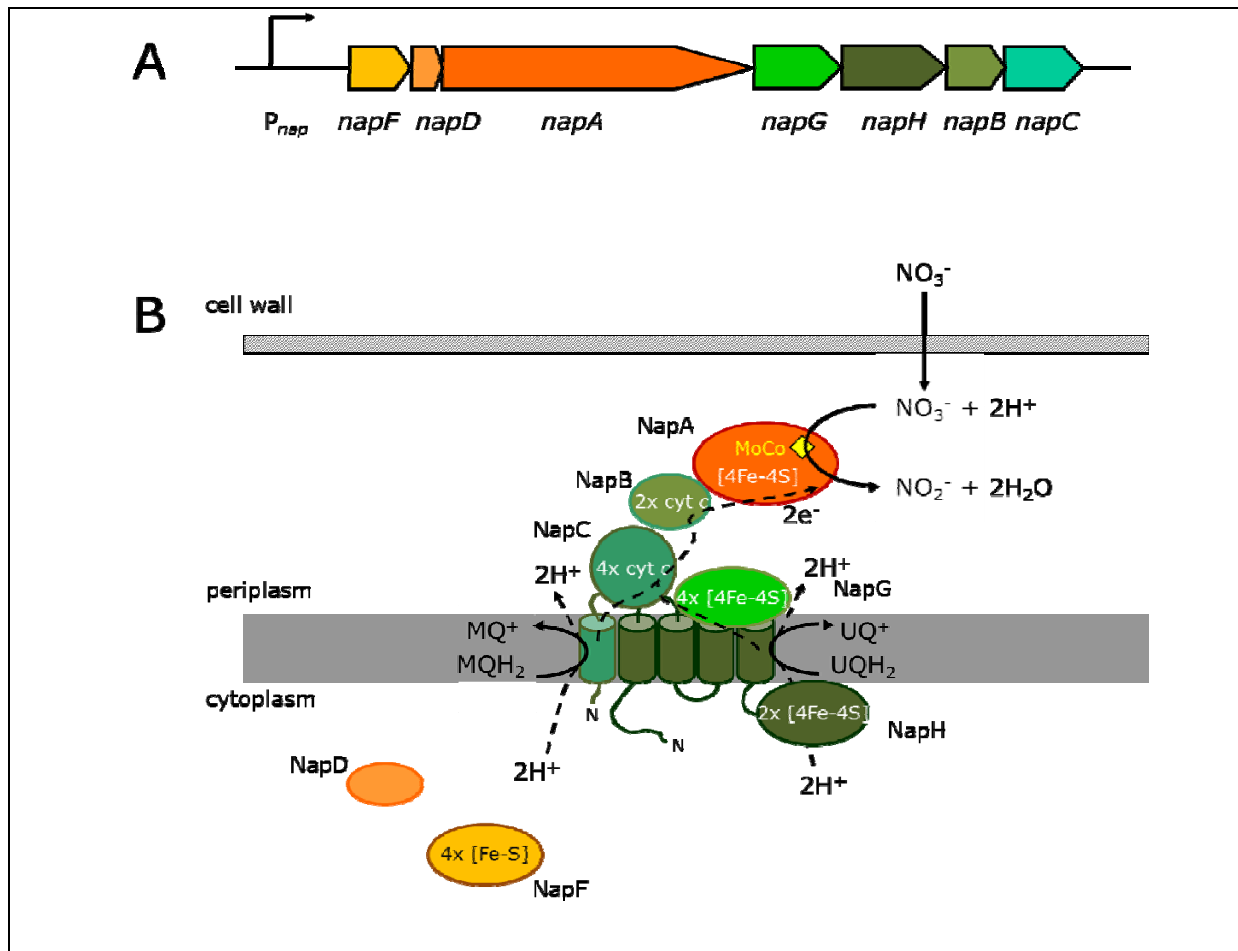
Figure 1.11 The *nap* operon and cellulare localisation of its gene products. (A) The *napFDAGHBC* operon is located at min 46.5 on the *E.coli* chromosome. (B) Cellular localisation of Nap components and possible electron transfer routes. NapD and NapF are cytoplasmically located and take part in NapA maturation.

1.3.3.1 NapD

NapD is a small 9.3 kDa cytoplasmic protein that was originally suggested to have a role in NapA maturation (Figure 1.11; Berks et al, 1995). A knock-out of *napD* on the chromosome of *E. coli* resulted in a complete loss of periplasmic nitrate reductase activity and subsequent degradation of the now unstable NapA polypeptide (Maillard et al, 2007; Potter & Cole, 1999). Protein-protein interaction studies using a bacterial two-hybrid system and *in vitro* analysis by isothermal titration calorimetry showed a very specific and tight binding of NapD to both full-length NapA (Nilavongse et al, 2006) and the Tat signal peptide of NapA (Maillard et al, 2007). NMR analysis of purified NapD revealed a β-α-β-β-α-β 'ferredoxin-like' structure (Figure 1.12; Maillard et al., 2007).
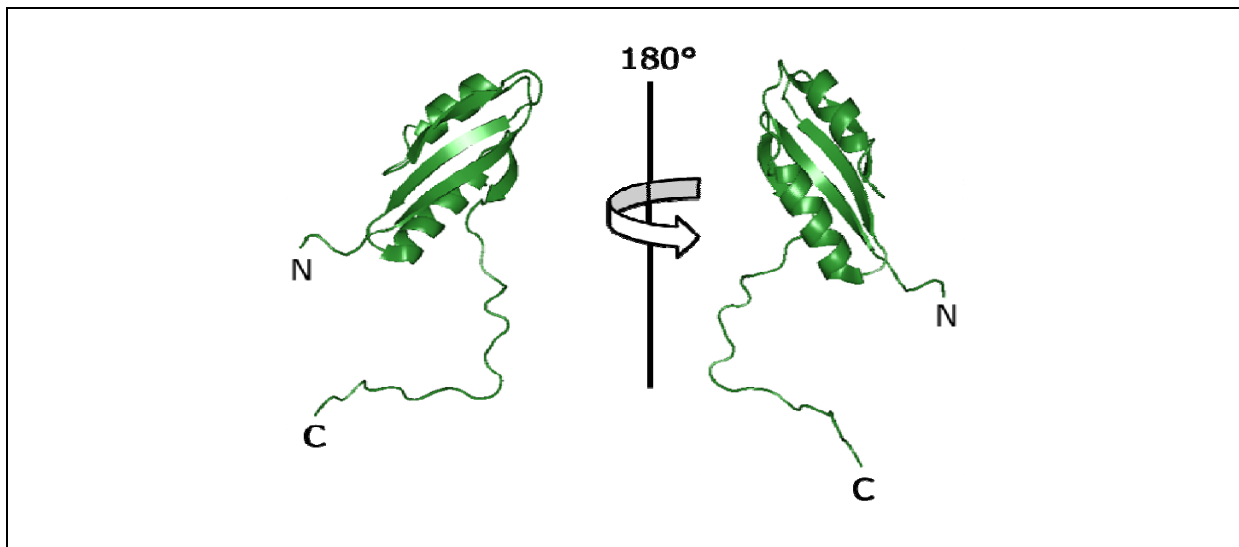
Figure 1.12 NMR structure of the proofreading chaperone NapD. NapD is a cytoplasmic protein involved in maturation of the periplasmic nitrate reductase NapA. NMR analysis revealed a ferredoxin-like fold comprising a β-α-β-β-α-β order. In addition, NapD contains a long flexible C-terminus. (PDB ID code 2jsx)

1.3.3.2 NapF

In *E. coli*, NapF is an 18 kDa iron-sulphur protein predicted to be located in the cytoplasm (Figure 1.11) (Nilavongse et al, 2006). Sequence analysis of NapF proteins shows four potential iron-sulphur cluster binding motifs. Furthermore, purified NapF from *Rhodobacter sphaeroides* displayed a characteristic absorption spectrum indicative for [Fe-S] cluster (Olmo-Mira et al, 2004). Mutation studies on *W. succinogenes* NapF carried out by Kern and Simon (2009) highlighted that only the third poly-cysteine motif is important for the activity of the periplasmic nitrate reductase.

Protein-protein interaction studies showed that NapA probably interacts with NapF in the cytoplasm before its export to the periplasm (Nilavongse et al, 2006). However, NapF is not essential for NapA activity (Brondijk et al, 2002; Potter & Cole, 1999). For the photosynthetic α-proteobacterium *R. sphaeroides*, NapF was able to catalyse insertion of the iron-sulphur cluster *in vitro* into a version of NapA that had been chemically treated to first destroy the cluster (Olmo-Mira et al, 2004). Furthermore, a deletion of *napF* in the ε-proteobacterium *W. succinogenes* resulted in the cytoplasmic accumulation of inactive NapA (Kern & Simon, 2009). Taken together, this would suggest a role for NapF as an accessory protein involved in the assembly of NapA.

1.3.3.3 The nap *operon and its regulation*

The *napFDAGHBC* operon of *E. coli* is encoded at minute 46.5 on the chromosome (Figure 1.11A) (Choe & Reznikoff, 1993; Grove et al, 1996). Gene products of *napABCD* have been shown to be essential for nitrate reduction (Potter & Cole, 1999). Activation of transcription of the *nap* operon is a complex process regulated by several factors. During anaerobic growth the FNR (fumarate and nitrate regulatory) protein utilises its oxygen-

sensitive iron-sulphur cluster as a sensor to then allow binding of the protein to a specific DNA sequence upstream of *napF* (Figure 1.13; Kiley & Beinert, 1998). Furthermore, the NarQ-NarP and NarX-NarL two component regulatory systems are recruited in response to nitrate and nitrite availability (Figure 1.13; Stewart & Rabin, 1995). NarP~P and NarL~P bind downstream of FNR upon phosphorylation by the NarQ and NarX sensor kinases, respectively, whereas NarP~P activates *nap* transcription and NarL~P represses transcription (Choe & Reznikoff, 1993; Darwin & Stewart, 1995; Rabin & Stewart, 1993). Overall, maximal *nap* expression occurs in a nitrate-limiting environment to scavenge low levels of available nitrate and to maintain the redox balancing during anaerobic growth (Richardson et al, 2001).

Three *nap* promoter regions have been identified. Promoter P1 is synergistically activated by FNR and NarP~P during anaerobic growth in the presence of low levels of nitrate (Figure 1.13; Darwin et al, 1998). In contrast, transcription from the overlapping promoter P2 occurs in the absence of nitrate under aerobic or anaerobic conditions (Figure 1.13; Stewart et al, 2003). The [Fe-S] cluster-containing transcriptional repressor IscR binds to promoter region P3 and inhibits transcription during aerobic growth, and is released from the DNA under anaerobic or iron-sulphur stress, conditions (Figure 1.13; Giel et al, 2003).

In addition, it has been shown that *nap* expression depends on the availability of environmental molybdenum controlled by the molybdate-responsive regulator ModE (Figure 1.13; McNicholas & Gunsalus, 2002). Recently, another transcription factor has been discovered, NsrR, which senses nitric oxide and also represses the *nap* operon (Figure 1.13; Filenko et al, 2007), thus reinforcing the intimate link between the nitrate reduction and other reactions of the N-cycle.

Finally, a role for CRP (cAMP receptor protein) was predicted (Brown & Callan Jr, 2004) and later shown to activate *nap* transcription in conjunction with FNR when nitrate is absent and less favourable carbon sources are dominant (Figure 1.13; Stewart et al, 2009).

IscR Footprint

```
                    -134.5              T3 >            -105.5
                      |                  |                 |
CTCTGGTGAATCAATCGCTATATAAATATATTTATAACCATTTGAAATGTGAGCAAAAGCCCGTTTTTGCCACGCTTCCCGCC
            CGTTATATA■■■■TATATAACG            AAATGTGATCTAGATCACATTT
                ModE                             Crp


          -64.5              -44.5               -29                        T1 >
            |                  |                  |                           |
ACTCTTTTGATCCTGCTACAGGTTTTACCCCGATCGGGGTATGCATCTTTGACACATCCTTTAATATCTTAGCGGCTATA■■■
    TTGAT■■■■■ATCAA        TACYYMTWWAKGGGTA                       TATAAT
        FNR                   NarP       AAGATGYATTT■AAATRCATCTT      -10 (P1)
                                            NsrR


                                          -29                        T2 >
                                            |                           |
                  ■■■GGGGTATGCATCTTTGACACATCCTTTAATATCTTAGCGGCTATA■■■
                        TTGACA            TATAAT
                        -35 (P2)          -10 (P2)
```

Figure 1.13 Transcriptional control region of the *E. coli nap* operon. A part of the sequence is duplicated to show overlaying P2 promoter region separately. T1, T2 and T3 indicate the transcription initiation sites. Binding sites are shaded grey or are underlined (NsrR) with the consensus sequence underneath. Letter code as Y: C or T; M: A or C; K: G or T and W: A or T. The diagram and labelling was adopted from Stewart et al, 2009.

1.4 THE TAT TRANSLOCATION PATHWAY

Protein transport to and across membranes is essential for cellular life. In bacteria, two distinct general protein transport pathways operate in parallel. The general Sec (secretory) pathway exports linear polypeptides through the SecYEG 'tunnel' by essentially a threading mechanism. This process can be co-translational or post-translational where transport is driven by ATP hydrolysis (Du Plessis et al, 2011). In contrast, the Tat pathway transports folded proteins and translocation is solely dependent on the proton motif force (pmf) (Berks et al, 2003; Robinson, 2011)

1.4.1 Tat signal peptide

Targeting of proteins to the Tat export pathway requires a specific targeting signal – the twin-arginine signal peptide. These signal peptides consist of a polar N-terminal 'n-region' of variable length, followed by a moderately hydrophobic (often glycine-rich) 'h-region', and at the C-terminus of the peptide a 'c-region' is usually present that contains the sequence Ala-x-Ala, which is a cleavage recognition site for leader peptidase I (LepB) (Lüke et al, 2009; Palmer et al, 2005). In contrast to Sec signal peptides, which follow very closely the same structural arrangement (Figure 1.14), the Tat signal peptide is longer, more hydrophilic in the h-region, and carries a conserved amino acid motif at the boundary between the n- and h-regions (Cristóbal et al, 1999). The conserved motif is

the most prominent feature of the Tat signal peptide and is known as the 'twin-arginine' motif, which is eponymous for the Tat (twin-arginine translocation) pathway. The Tat motif contains the consensus sequence of S/T-R-R-x-F-L-K (Berks, 1996). The two arginine residues are almost invariant and are critically important for transport. Even a conservative substitution of arginine to lysine has the potential to block protein export *via* the Tat pathway. Early studies of Tat signal peptide activity determined that mutations affecting the second arginine within the motif have bigger negative effects on translocation (Buchanan et al, 2002; Stanley et al, 2000). In addition, the conservation of the phenylalanine residue of the consensus motif seems very important for correct operation of the export pathway (Stanley et al, 2000).

As well as the twin-arginine motif there are other structural aspects of Tat signal peptides that are important for function. It seems that a subtle level of hydrophobicity within the h-region is important for correct substrate targeting pathway (Cristóbal et al, 1999; Stanley et al, 2000). For example, increasing the overall hydrophobicity of a Tat signal peptide closer to that of a Sec signal peptide diverted a reporter protein between the two pathways (Cristóbal et al, 1999). Furthermore, the existence of a 'Sec avoidance' motif with the c-region of Tat signal peptides has been characterised, which comprises basic residues (Blaudeck et al, 2003; Bogsch et al, 1997). However, the existence of such a 'Sec-avoidance' motif is not universally accepted (Tullman-Ercek et al, 2007).
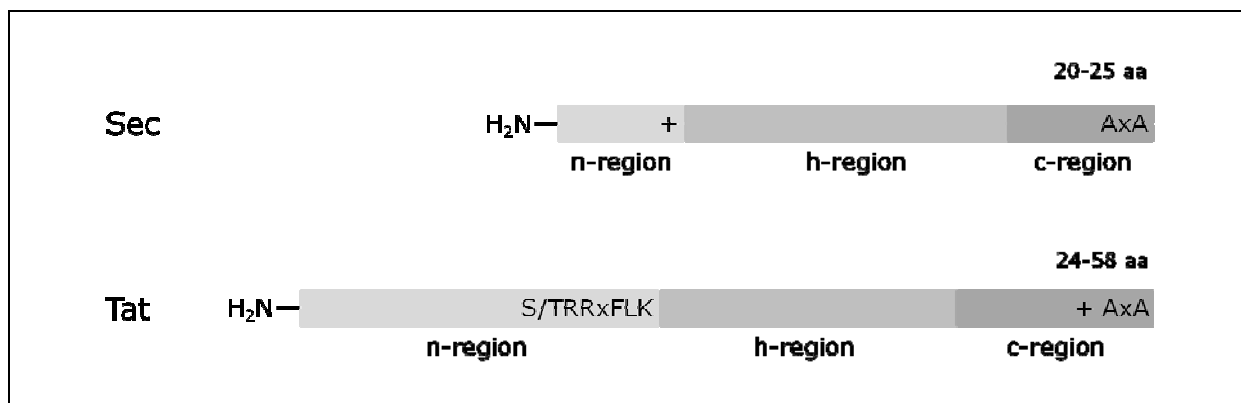
Figure 1.14 Signal peptides of the Sec and Tat pathway. The Sec and Tat systems have similar signal peptides that comprise the n-terminal region, the hydrophobic h-region and the c-terminal region, which contains an A-x-A cleavage site for the leader peptidase I, LepB. The Sec signal peptides have a positively charged n-region (indicated with a black cross). The Tat signal peptides contain the twin-arginine motif S/TRRxFLK between the n- and h-region. The c-region of Tat signal peptides generally also has a positive charge.

It should also be noted that naturally-occurring Tat substrates have been reported that show relaxed amino acid specificity within the twin-arginine motif, but are still transported *via* the Tat pathway. TtrB (a subunit of the tetrathionate reductase from *Salmonella enterica*), for example, has a lysine substitution for the first arginine residue (Hinsley et al, 2001). Moreover, the two arginine residues in pre-pro-penicillin amidase

(ppPA), a plasmid-encoded protein in some clinical strains of *E. coli*, are separated by an asparagine yet it remains Tat-dependent for export (Ignatova et al, 2002).

The number of Tat substrates in a given organism varies considerably but if a genome sequence is available this can be predicted *in silico* – programs called TatFIND and TatP are available (Bendtsen et al, 2005; Rose et al, 2002). Usually such predictions must be verified experimentally. In *Streptomyces ceolicolor*, for example, around 150 proteins were predicted to be exported by the Tat pathway, of which only 25 were later positively confirmed by laboratory-based transport experiments (Bendtsen et al, 2005; Widdick et al, 2006). For comparison, the genome of *E. coli* encodes 27 true Tat substrates (Tullman-Ercek et al, 2007), whereas *Helicobacter pylori* is predicted to have one Tat-dependent protein, the [NiFe] hydrogenase (Wu et al, 2000).

Most bacterial Tat substrates are proteins that contain complex cofactors that must be inserted prior to export. The main examples of such cofactors are molybdopterins, iron-sulphur clusters, Ni-Fe clusters, some non-covalently-bound flavin, some non-covalently-bound haem, some types of copper cofactors, or cobalamin. However, there are also a certain number of proteins that do not contain any known cofactors, or are able to bind metal ions after transport. It was proposed that these proteins folded 'too rapidly' in the cytoplasm, which precludes them from Sec transport (Berks et al, 2003; Sturm et al, 2006). In addition, it was shown that a few proteins with C-terminal transmembrane domains are Tat dependent. However, the mechanism of assembly of such proteins into the cytoplasmic membrane remains unknown (Hatzixanthis et al, 2003).

The Tat system is important for many fundamental bacterial processes, such as respiration (Sargent, 2007a), cell wall biosynthesis and cell division (Ize et al, 2003), production of secondary metabolites (Widdick et al, 2006), degradation of biomolecules (Widdick et al, 2008) and pathogenicity (De Buck et al, 2008). Indeed, the Tat pathway is not only found in bacteria and archaea, but also in the chloroplasts of higher plants, where it was first discovered and initially named the 'Delta pH-dependent pathway' (Mori & Cline, 2001). In chloroplasts the Tat system targets proteins from the stroma across the thylakoid membrane into the lumen. The few proteins transported in this way play critical roles in either the oxygen-evolving complex of Photosystem II or the cytochrome b_6f complex. Sequence analysis of mitochondrial DNA has also revealed the existence putative *tat* genes in these organelles, however their role in protein export in the sea sponge has so far not been investigated (Bogsch et al, 1998; Wang & Lavrov, 2007).

1.4.2 Components of the Tat translocase

1.4.2.1 The homologous proteins TatA, TatB and TatE

The *E. coli* TatA and TatB proteins, with molecular weights of 10 kDa and 18 kDa, respectively, share overall sequence identity of 25%. Both proteins consist of an N-terminal transmembrane domain, followed by an amphipathic helix and an unstructured C-terminus (Figure 1.16A; Chan et al, 2011; Porcelli et al, 2002). Some researchers predict the amphipathic helix lies along the membrane (Gouffi et al, 2004). Recent NMR studies on a *Bacillus subtilis* TatA revealed an L-shaped structure that mirrored precisely these cartoon models (Figure 1.15; Hu et al, 2010; Walter et al, 2010). Truncation studies have shown that the C-termini of TatA and TatB are not important for their function (Lee et al, 2002), however even though the predicted structures and sequences of TatA and TatB share similarities, the proteins are not interchangeable in function (Sargent et al, 1999).
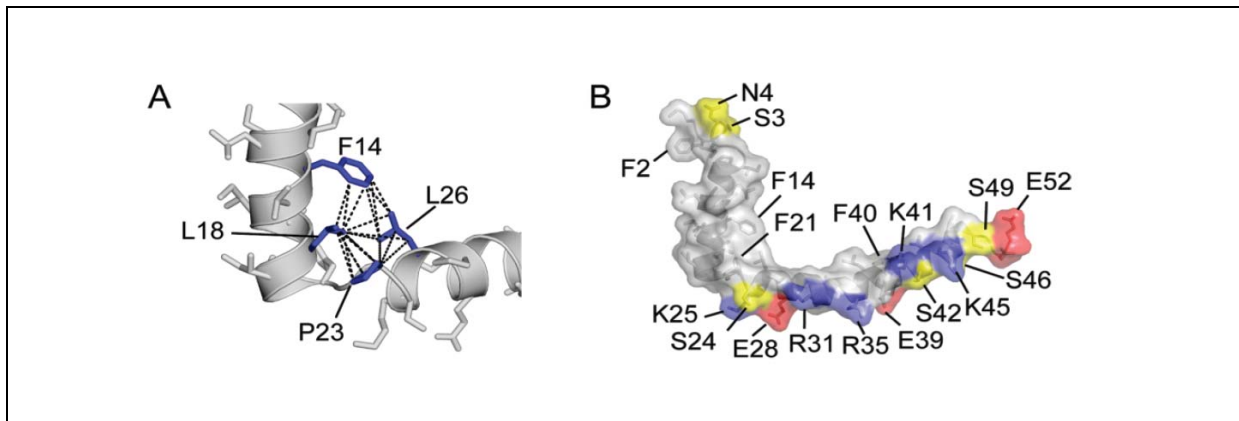
Figure 1.15 NMR analysis of *B. subtilis* TatA$_d$. (A) Local conformation of the hinge region. Close interactions are shown as dashed lines. (B) Surface representation of *Bs*TatA$_d$. The positively charged, negatively charged, and polar residues are coloured in blue, red, and yellow, respectively. Taken from Hu et al., 2010.

Another *E. coli* protein, TatE, is a very close homologue of TatA and can complement a Δ*tatA* strain (Sargent et al, 1998). However, the native expression level of *tatE* is much lower compared to *tatA*, which has given rise to the hypothesis that *tatE* is a cryptic gene duplication of *tatA* (Jack et al, 2001).

1.4.2.2 The polytopic TatC protein

The highly conserved 29 kDa TatC protein is the largest and most hydrophobic of all known Tat components (Bogsch et al, 1998). *In silico* analysis and fusions to reporter proteins suggest TatC consists of six transmembrane domains with N- and C-termini located in the cytoplasm (Figure 1.16A; Behrendt et al, 2004; Drew et al, 2002). Circular dichroism (CD) spectroscopy and oriented CD (OCD) spectroscopy carried out on TatC from *B. subtilis* showed the protein contained ~50% α-helix with the transmembrane helices slightly tilted in the lipid bilayer (Nolandt et al, 2009). Such helix tilting is

supported by cysteine-crosslinking studies on the *E. coli* TatC protein (Punginelli et al, 2007). TatC is believed to form stable, active dimers, where only one TatC protomer is active at any time (Maldonado et al, 2011a).
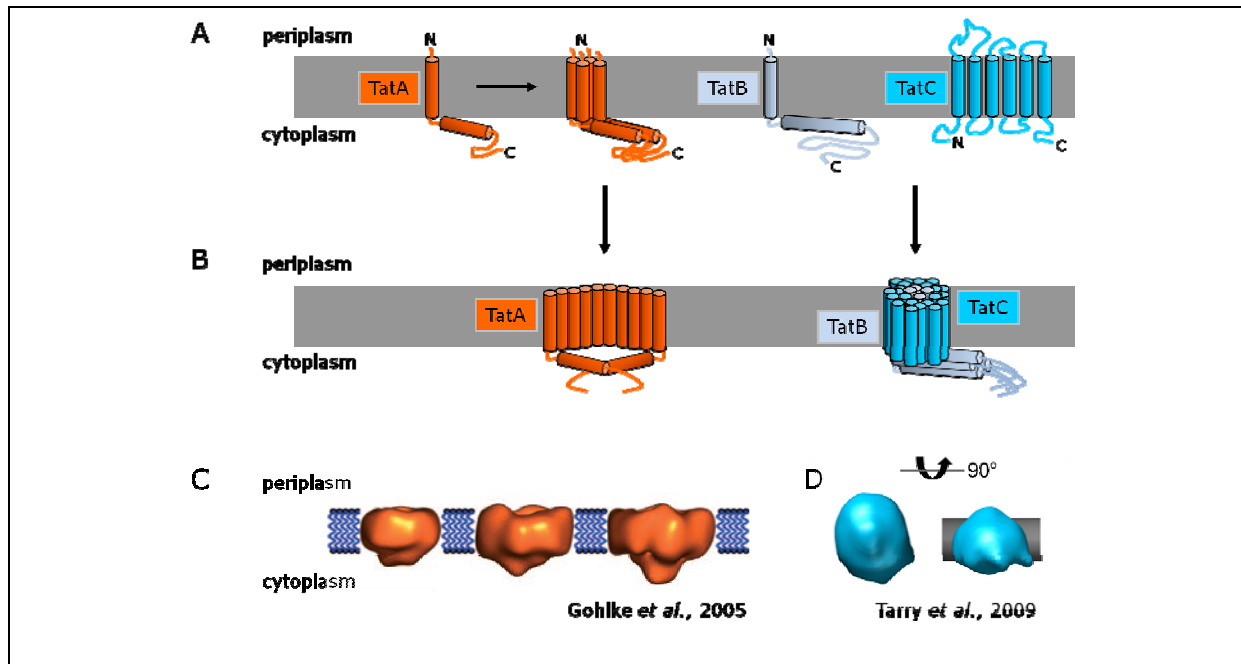
Figure 1.16 Topology of the Tat components and their complexes. (A) Predicted secondary structure of the integral proteins TatA, TatB and TatC. TatA exists as tetramer in the membrane. (B) The TatA complex is variable in size and most likely forms the protein conducting channel. TatB and TatC form a complex in equimolar ratio and functions as a substrate recognition unit. (C) Single-particle electron microscopy of the TatA and (D) TatBC complexes (Gohlke et al, 2005; Tarry et al, 2009).

1.4.2.3 The TatBC complex

TatB and TatC interact in a 1:1 ratio with each subunit present in multiple copies in the final complex (Bolhuis et al, 2001). Crosslinking experiments and protein-protein interaction studies suggest that TatC is organized around TatB (Figure 1.16B; Lee et al, 2006; Maldonado et al, 2011b; Punginelli et al, 2007), with the whole complex possibly adopting a hexameric or heptameric architecture (Oates et al, 2005; Tarry et al, 2009b). Truncation analysis of TatB has established that the transmembrane and/or amphipathic helix are important for the TatC interaction (Maldonado et al, 2011b).

The TatBC complex is the initial recognition complex for Tat signal peptides. TatC is understood to recognise primarily the twin-arginine motif, while TatB interacts with the hydrophobic h-region, of Tat signal peptides (Alami et al, 2003; Gérard & Cline, 2006). Recent *in vitro* transport experiments even show interactions between the mature part of a Tat substrate and TatB (Maurer et al, 2010). Suppressor mutants of *tatC* suggest the first half of the protein, especially the first cytoplasmic and second periplasmic loop, is somehow involved in signal peptide binding (Holzapfel et al, 2007; Kreutzenbeck et al, 2007; Strauch & Georgiou, 2007). Single-particle electron microscopy revealed that one

or two Tat substrates bind to the periphery of the TatBC complex and, in case of two substrates, binding sites are adjacent (Tarry et al, 2009b). For the TatBC homologue Hcf106:cpTatC from chloroplasts even up to four substrates were found to bind, which were subsequently all transported together (Ma & Cline, 2010).

1.4.2.4 The TatA complex

Purification of overproduced and detergent solubilized TatA from *E. coli*, followed by analysis by blue native (BN)-PAGE, resulted in the identification of large homo-oligomeric complexes with variable sizes from 50-500 kDa (Oates et al, 2005; Porcelli et al, 2002). Single-particle electron microscopy of these TatA complexes showed ring-like structures of different sizes and computer-aided 3-D reconstructions suggested each ring contained a 'lid' at one side with an internal channel big enough to accommodate some known Tat substrates (Figure 1.16C; Gohlke et al, 2005). Also fluorescence microscopy in live cells with TatA tagged to YFP pointed to ring formation with 4 to 100 TatA protomers within each complex (Figure 1.16B; Leake et al, 2008). From this it was suggested that a pool of TatA tetramers exist in the membrane (Figure 1.16A; Leake et al, 2008), which are recruited to form an active complex upon TatBC-substrate interaction. This is known as the 'polymerisation model' (Cline & McCaffery, 2007). Pulsed EPR (electron paramagnetic resonance) analysis confirmed a high exchange rate of TatA subunits between the TatA complexes (White et al, 2010).

The Tat transport field is not without controversy, nor is it focussed entirely on the *E. coli* Tat system. Some studies of the *E. coli* TatA protein have suggested that the C-terminus is accessible to proteases and chemical compounds on both sides of the membrane, which suggested a dual topology for TatA C-terminus during channel formation (Chan et al, 2007; Gouffi et al, 2004). In this model the amphipathic helix would intermittently act as a second transmembrane domain, thus forming a helical hairpin in the inner membrane. The widely-accepted topology of TatA (and TatB) is that the N-terminus of the transmembrane helix is located at the periplasmic side, whereas the C-terminus is inside the cytoplasm (Gouffi et al, 2004; Porcelli et al, 2002). This is supported by the 'positive inside' rule and also many transmembrane prediction programmes (Hofmann & Stoffel, 1993; Von Heijne, 1992). However, a further alternative hypothesis suggests the N-terminus of TatA in the cytoplasm (Chan et al, 2011; Chan et al, 2007), which would generate a radical new model for the TatA structure, but which would be difficult to attach to existing biochemical studies on the structure and function of TatA. Another extraordinary observation was the TatC-dependent tube formation of overproduced TatA in the cytoplasm of *E. coli* cells. From this, it was suggested that TatA could act as a targeting factor for substrates on order to initiate TatC binding in the membrane (Berthelmann et al, 2008).

Overall, the TatA complex remains the most likely protein-conducting channel for the Tat system and therefore has the difficult task of allowing transport of large globular proteins while maintaining cell integrity.

1.4.3 The Tat translocation process

A number of different *in vitro* and *in vivo* studies have given insight into the translocation process of proteins by the Tat pathway, and the following model is currently widely accepted. In an initial energy-independent step the Tat substrate binds *via* its signal peptide to the TatBC complex (Figure 1.17B; Cline & Mori, 2001; De Leeuw et al, 2001). Thereby TatC is the primary recognition site of the twin-arginine motif and TatB interacts with the hydrophobic h-region of the signal peptide and the mature part of the protein (Alami et al., 2003; Gérard & Cline, 2006; Maurer et al., 2010). The following process was shown to be ATP-independent (Yahr & Wickner, 2001), however instead uses the proton motive force across the cytoplasmic membrane, which comprises a pH gradient (ΔpH) and an electrical field gradient (ΔΨ) (Bageshwar & Musser, 2007; Braun et al, 2007; Theg et al, 2005): tetramers of TatA recognize the substrate bound TatBC complex and bind to it before assembling themselves as a pore in the vicinity of, or possibly completely surrounding, the Tat substrate (Figure 1.17C) (Cline and Mori, 2001; Gohlke et al., 2005; Leake et al., 2008). At this point the fully assembled Tat translocase is formed, energy is again transduced from the proton motif force, and the Tat substrate is translocated to the periplasmic side of the membrane (Figure 1.17D). It is thought that the unprocessed signal peptide is then released laterally into the lipid phase, where it is then processed by LepB (Sargent et al, 2006). The translocase dissociates back to the TatA subunits and the TatBC complex (Figure 1.17A).

It is worth noting here that a few Tat-targeted enzymes exist that are exported as heterodimers, where only one partner protein contains a Tat signal peptide. In *E. coli* examples are HybO/HybC ([NiFe] hydrogenase-2) and DmsA/DmsB (DMSO reductase). This special mechanism of transporting oligomers *via* the Tat pathway is called 'hitchhiking' (Rodrigue et al, 1999; Stanley et al, 2002).
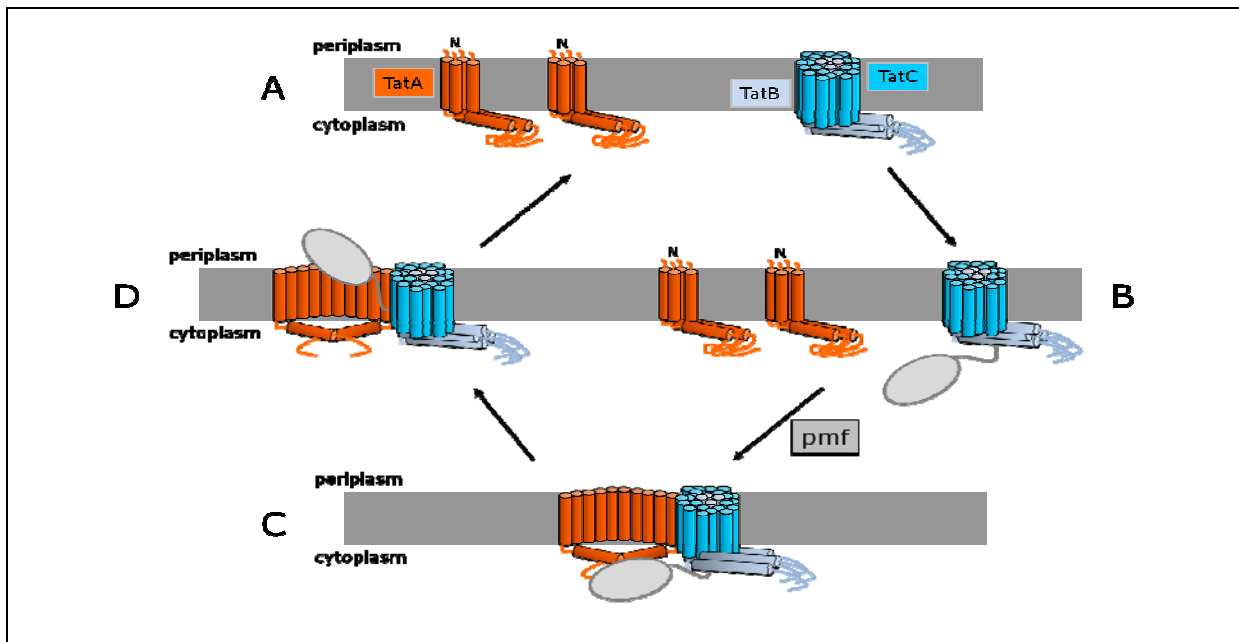
Figure 1.17 The Tat translocation process. (A) Tetrameric TatA and the TatBC complex are separate units in the cytoplasmic membrane. (B) In the first step the substrate binds *via* its Tat signal peptide to the TatBC complex. (C) Using a proton motif force (pmf) TatA associates with the substrate-bound TatBC complex. (D) The Tat substrate is exported through the TatA channel. The peptidase LepB cleaves off the Tat signal peptide and the substrate is released into the periplasm (not shown). This is followed by the dissociation of the TatA and TatBC complexes.

1.4.4 Tat quality control

While it is well established that the Tat pathway is dedicated to the transmembrane translocation of folded proteins, it is often overlooked that initial studies of this system realised that non-transport of unfolded proteins was a key feature of this system (Santini et al, 1998). This led to further studies and the establishment of the hypothesis that the Tat translocase could possess an intrinsic "quality control mechanism" allowing it to recognize unfolded Tat substrates and reject them before transport was attempted. To address this hypothesis DeLisa and co-workers (2003) used the normally Sec-dependent alkaline phosphatase (PhoA) protein as reporter. PhoA requires the oxidizing environment of the periplasm in order to form two disulphide bridges, which are essential for proper protein folding and enzymatic activity. Switching the PhoA Sec signal sequence for a Tat signal peptide initially did not result in periplasmic targeting of the enzyme, possibly due to its unfolded state under the reducing environment of the cytoplasm. However, when expressed in an *E. coli* mutant engineered to have an oxidizing cytoplasm PhoA readily formed disulphide bonds, folded, and was thus transported by the Tat translocase into the periplasm (DeLisa et al, 2003). The overwhelming need for folding for PhoA in order to be transported by the Tat pathway was later confirmed by *in vitro* translation and transport assays (Panahandeh et al, 2008).

Furthermore, it was shown that accumulated mis-targeted or malfolded Tat substrates are degraded in the cytoplasm. This proteolysis is another controversial area but seems to be Tat-independent, and in some cases might occur prior to Tat-specific interactions (Brüser & Sanders, 2003; Lindenstrauß et al, 2010). The pathways for proteolysis of non-exported proteins is so far unknown, but might include FtsH or the Clp machinery (Fisher & Delisa, 2004).

It needs to be noted that the folding status of a protein is not always a prerequisite for export, and that the Tat translocase can show relaxed substrate specificity under some circumstances. For example, it was shown that small hydrophilic unfolded polypeptides fused to long unstructured linkers are still transported, if their length does not exceed 100-150 amino acids (Lindenstrauß & Brüser, 2009; Richter et al, 2007). In addition, unfolded PhoA is targeted to the Tat translocon, where it makes contact with the TatBC complex *via* its Tat signal peptide, however, it is not exported (Panahandeh et al, 2008; Richter & Brüser, 2005). However, all of these studies involve artificial Tat substrates and as such their physiological relevance can be questioned.

1.4.5 The Tat 'proofreading' process

Alongside the "Tat quality control" system a second tier of quality control exists for some proteins. Termed "Tat proofreading" this involves water-soluble chaperones that are usually encoded in operons together with their specific Tat substrate partners (Turner et al, 2004). The structure and function of Tat proofreading chaperones is discussed extensively throughout this thesis. In general, Tat proofreading chaperones bind to the nascent chain of the Tat substrate, most usually directly to the N-terminal twin-arginine signal peptide itself (Figure 1.18, step 1; Jack et al, 2004; Maillard et al, 2007). The physiological roles of Tat proofreading chaperones are not completely clear, but one hypothesis is that binding prevents the signal peptide from indulging in pre-mature interactions with the Tat complex. In some cases binding of the chaperone can prevent the signal peptide from degradation by some proteases, including OmpT (Figure 1.18, step 1; Genest et al, 2006a; Geneste et al. 2006b). For some chaperones a second binding site beside the Tat signal peptide has been implied, but never positively identified, which lies somewhere else on the mature part of the protein (Figure 1.18, step 1; Genest et al, 2008). It is generally agreed that such chaperones keep their substrates in a cofactor-competent state until cofactor insertion and protein folding has occurred (Figure 1.18, step 2; Pommier et al, 2008). Indeed, there is some evidence that some Tat proofreading chaperones interact with proteins of the cofactor insertion machinery as well (Genest et al, 2008; Li et al, 2010). Eventually, the chaperone is released, by a yet unknown mechanism, leaving the Tat substrate to interact with the Tat translocase (Figure 1.18, step 3).

Previously, it has been suggested that perhaps all *E. coli* Tat substrates use specific proofreading chaperones during their maturation (Palmer et al, 2005). However, *in vitro* studies proved that at least non-cofactor containing Tat substrates do not interact with specific proofreading chaperones (Holzapfel et al, 2009).
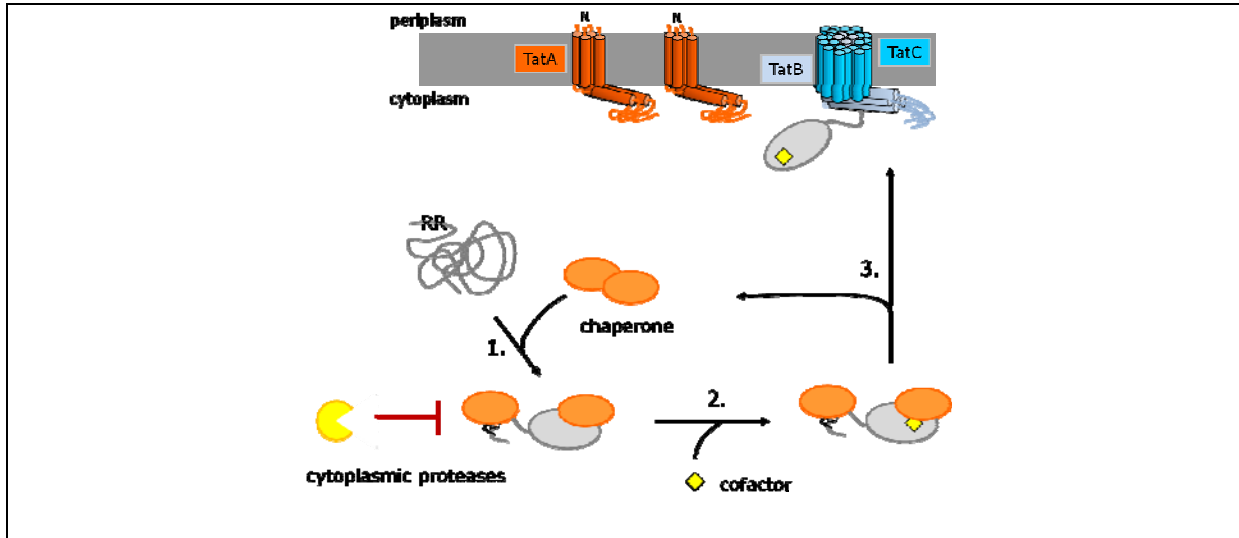
Figure 1.18 The 'proofreading' process. Substrate specific chaperones bind to the polypeptide nascent chain and participate in protein folding. Binding sites are the Tat signal peptide ('RR') and in some cases somewhere on the mature part of the protein. This prevents degradation by cytoplasmic proteases and from pre-mature interaction of the Tat substrate with the translocase (step 1). Proofreading chaperones can also assist in cofactor insertion (step 2). After the substrate is fully assembled and active the chaperones are released through an unknown mechanism and the substrate is able to bind to the TatBC complex *via* its signal peptide (step 3).

1.4.5.1 The TorD/DmsD family

The most heavily studied Tat proofreading chaperones belong to the TorD/DmsD family. Those chaperones like NapD are involved in maturation of TMAO and DMSO reductases, which contain Mo-*bis*-MGD as cofactor (Richardson, 2000). Sequence alignments and phylogenetic tree construction revealed that members of the TorD/DmsD family can be divided into three clades: TorD, DmsD and NarJ (Turner et al, 2004).

TorD and DmsD have been studied as the paradigm Tat proofreading chaperones and several structures of those two proteins from different bacteria have been solved. The overall structure of this family is an all α-helical fold, and they can exist in monomeric and dimeric forms (Figure 1.19; Sarfo et al, 2004; Trainer et al, 2003). Interestingly, TorD from *Shewanella massilia* shows extreme domain-swapping (Figure 1.19; Trainer et al, 2003).

Chaperone activity for TorD was suggested after it was found to stabilize TorA (TMAO reductase) at elevated temperatures (Genest et al, 2005). It was also shown that TorD could prevent degradation of full-length TorA by cytoplasmic proteases (Genest et al, 2006a; Genets et al, 2006b). However, a *torD* mutant still retains TorA activity suggesting its activity is not essential (Pommier et al, 1998). In contrast, DmsA (DMSO

reductase), the specific Tat substrate for the TorD homologue DmsD, shows no activity when *dmsD* is deleted (Ray et al, 2003).
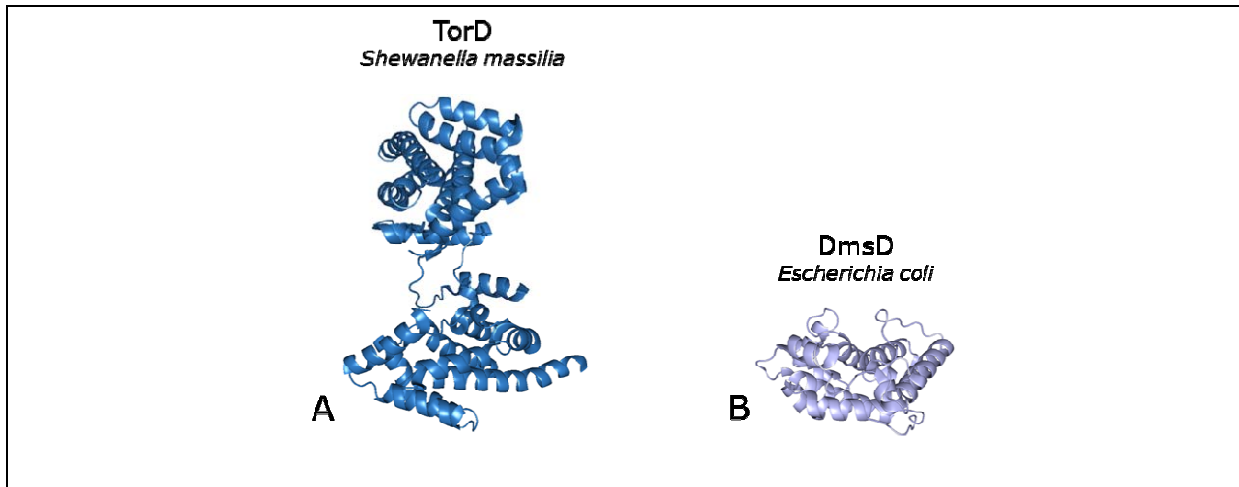
Figure 1.19 Crystal structures of members of the TorD/DmsD family of proofreading chaperones. (A) Dimer of *S. massilia* TorD shows domain swapping between the subunits. (PDB ID code 1n1c) (B) DmsD, here from *E. coli* exists in monomeric form. (PDB ID code 3efp)

It was shown *in vitro* that TorD and DmsD have high affinities for the individual Tat signal peptides of TorA and DmsA, respectively (Oresnik et al, 2001; Hatzixanthis et al, 2005). Also, it was shown that TorD can hydrolyse GTP, an activity that is induced by domain-swapping (Guymer et al, 2010). GTP binding enhances the affinity of TorD for the TorA signal peptide (Hatzixanthis et al, 2005), therefore it is possible that such nucleotide binding regulated TorD-signal peptide interaction and release cycles. In addition, TorD is able to bind somewhere else on the mature part of TorA, where it seems that binding is dependent on its switch between monomeric and dimeric forms (Jack et al, 2004; Tranier et al, 2002).

TorD and DmsD were shown to interact with components of the molybdenum cofactor biosynthesis pathway, and TorD was able to bind the precursor and mature form of Mo-*bis*-MGD *in vitro* (Genest et al, 2008; Li et al, 2010). Also, *in vitro* reconstitution experiments revealed that TorD is able to bind TorA before cofactor insertion, however, that binding affinity is enhanced when Mo-*bis*-MGD was added (Ilbert et al, 2003). Therefore it was proposed that those proofreading chaperones participate in cofactor insertion and so set the Tat substrates in a 'cofactor insertion competent state'.

Another role for TorD and DmsD could be in targeting their respective Tat substrates to the Tat translocase for export. Cell fractionation showed that overproduced DmsD is membrane associated and that this is dependent on the presence of TatB or TatC (Papish et al, 2003). Recently, the interaction of DmsD with the TatBC complex was confirmed by bimolecular fluorescence complementation experiments (BiFC; Kostecki et al, 2010).

1.4.5.2 The NapD family

The NapD family comprises ~100 members (Maillard et al, 2007). The proteins of this family are rather small with sequences of around 100 amino acids. Some sequence motifs were identified, however no clear signature motif could be attributed (Turner et al, 2004). Interestingly, a few NapD proteins show an N-terminal extension containing a putative Tat-like amino acid motif (Maillard et al, 2007). Using *napD* mutants it was shown that NapD is essential for maturation of the periplasmic nitrate reductase NapA (Maillard et al, 2007; Potter & Cole, 1999), while Maillard and co-workers (2007) established binding of NapD to the Tat signal peptide of NapA using a wide variety of *in vivo* and *in vitro* methods.

1.4.6 The role of general chaperones during Tat substrate folding

Crosslinking studies have shown that trigger factor (TF) binds to the nascent chain of different Tat signal peptides immediately at the ribosomal exit tunnel, but that this interaction is apparently not important for overall protein transport (Jong et al, 2004). Furthermore, different protein-protein interaction techniques showed that the DmsD Tat proofreading chaperone from *E. coli* interacts with a surprisingly wide variety of general chaperones like TF, DnaK, DnaJ, GrpE, GroEL and Ef-Tu (translation elongation factor) (Li et al, 2010). Given that there is an existing chaperone cascade of DnaK-DnaJ-GrpE-GroEL (Mayhew & Hartl, 1996), one hypothesis is that DmsD could shuttle its substrate through this cascade of protein folding and maturation steps before reaching the Tat translocase (Li et al, 2010). Indeed, it has been proposed that GroEL could be involved in general maturation of metallo-enzymes (Ribbe & Burgess, 2001), although how the cofactors and their binding-proteins are internalised into the GroEL chamber remains unclear. In addition, DnaK, but also SlyD, were found to interact and stabilize Tat substrates (Graubner et al, 2007; Pérez-Rodríguez et al, 2007; Zhang et al, 2005).

1.4.7 Medical and biotechnological implications of the Tat pathway

The Tat system is present in many bacterial plant and animal pathogens and it has been shown that it strongly contributes in the secretion of virulence factors (De Buck et al, 2008). With the increasing drug-resistance of many pathogens the development of novel drugs has high priority, at least in the academic arena. Because the Tat pathway is absent in mammalian cells, and very well conserved in bacteria, the Tat translocase could be an ideal target for novel antimicrobials.

The Tat system is not essential in all bacteria. However, inactivation of the Tat translocase causes pleiotropic effects in cell division and membrane integrity. Hence, a drug effecting the translocase would perhaps not kill the bacterium (unless the channel was jammed open) but could reduce virulence, so bacterial cells would be more

susceptible to host defence or to secondary drug target effects (Sargent, 2007b). For example, β-lactamases in *Mycobacterium* are Tat substrates, and *tat* mutants therefore become more sensitive to β-lactam antibiotics (Feltcher et al, 2010).

Another application for Tat is in the biotechnology field. The ability of the translocase to export folded, often oligomeric, enzymatically-active proteins provides a great selection mechanism for protein production. The requirements for a heterologous expressed protein to be transported *via* the Tat pathway had been reviewed (Brüser, 2007). The group of DeLisa developed fusions containing the protein of interest with N-terminal Tat signal peptide and C-terminal β-lactamase coupling antibiotic resistance with Tat transport thus monitoring protein folding (Fisher et al, 2006). This method has been already successfully used for antibody production and protein-protein interaction studies (Fisher & DeLisa, 2009; Waraho & DeLisa, 2009). In addition, phage display in combination with the Tat pathway had been successfully used to produce active proteins (Speck et al, 2011; Thammawong et al, 2006).

1.5 AIMS

The work of Maillard et al (2007) identified NapD as the specific proofreading chaperone for the periplasmic nitrate reductase NapA. Furthermore, protein-protein interaction studies showed that NapD interacts specifically with the Tat signal peptide of NapA (Maillard et al, 2007). This previous work guided the direction of my PhD project, analyzing, at the molecular level, interactions between NapD and NapA . The following aims were set:

1. Mapping the binding site for NapD on the Tat signal peptide of NapA by glutamine scanning mutagenesis.

2. Determining the role of specific residues within the Tat motif and hydrophobic region of the NapA signal peptide in biosynthesis and transport of the enzyme *in vivo*.

3. Structural analysis of NapD in complex with NapA and its signal peptide.

4. Setting a foundation for future experiments on targeted NapA transport *via* NapD to the Tat translocase.

2 The role of the twin-arginine signal peptide in NapA maturation, export and biosynthesis

2.1 INTRODUCTION

Periplasmic, molybdenum-dependent, nitrate reductases are widespread in Gram-negative bacteria and can be identified in both pathogens (Stewart & Bledsoe, 2005) and environmentally-important bacteria (Berks et al, 1995). Assembly of a fully functional nitrate reduction system in the periplasm is not trivial and requires co-ordination of gene regulation, protein synthesis, cofactor synthesis, cofactor loading, and protein targeting pathways. To this end the *E. coli nap* operon encodes accessory proteins dedicated to the assembly of the periplasmic nitrate reductase. The work of Maillard et al (2007) established that the NapD protein acts as a Tat proofreading chaperone for the periplasmic nitrate reductase enzyme itself, NapA. As such NapD was shown to bind directly and specifically to the NapA twin-arginine signal peptide (NapA$_{SP}$). One hypothesis put forward was that this interaction shielded the signal peptide from premature interactions with the Tat translocase until folding, cofactor loading and assembly of the enzyme was completed (Sargent, 2007b).

In this Chapter structural features of the NapA signal peptide required for NapD binding were investigated. Following-on from the initial study of Maillard et al (2007), genetic and biochemical approaches were taken in order to map the precise NapD binding epitope on NapA$_{SP}$. In addition, the roles of these key NapA$_{SP}$ residues in Tat transport and enzymatic activity of NapA were investigated.

2.2 RESULTS

2.2.1 Mapping the NapD binding site on the NapA signal peptide *in vivo*

To identify NapA$_{SP}$ residues important for NapD binding a genetic approach was initially chosen that involved a bacterial 'two-hybrid' assay (BTH). The BTH system used here is based on the reconstitution of adenylate cyclase activity in an *E. coli cya* mutant (Karimova et al, 1998). In *E. coli* the *cya* gene encodes a membrane-bound adenylate cyclase that is activated in response to glucose abundance in the cell. Normally, in the absence of glucose the adenylate cyclase is activated and this causes an increase in cAMP (cyclic adenosine monophosphate) levels, which in turn activates transcription of genes for utilisation of alternative carbon sources, e.g. maltose and lactose (Figure 2.1A). The BTH system developed by Karimova et al. (1998) uses cAMP concentration as a readout for protein interactions. *Bordetella pertussis* secretes a large protein toxin called CyaA. This toxin carries, towards its N-terminus, a water-soluble adenylate cylcase domain that can itself be separated into two sub-domains termed T25 and T18

(Karimova et al, 1998). Disconnection of the two adenylate cyclase complementary fragments (T25 and T18) leads to a complete loss of enzymatic activity, however if the sub-domains are covalently fused to two proteins that can physically interact then the adenylate cyclase activity can be restored (Figure 2.1B) (Karimova et al, 1998). Thus when co-expressed in a *cya* deficient *E. coli* strain (BTH101) protein-protein interactions will induce cAMP synthesis and subsequently trigger transcription of the *mal* and *lac* operons (Figure 2.1D). Positive interacting partners can therefore be readily visualized as red colonies on MacConkey indicator plates supplemented with maltose, and semi-quantification of the binding events can be achieved by measuring the β-galactosidase activity. Several studies in the past showed the usefulness of this BTH system in determining signal peptide/chaperone interactions (Buchanan et al, 2008; Maillard et al, 2007).
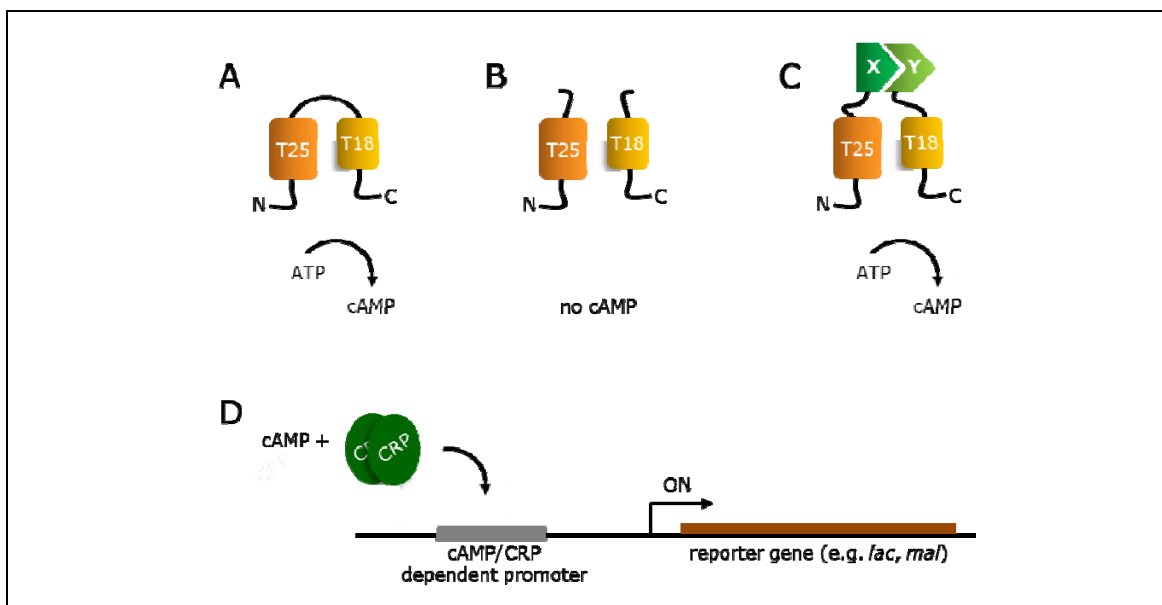
Figure 2.1 The bacterial two-hybrid system. (A) The adenylate cyclase domain of *B. pertussis*' CyaA toxin converts ATP to cAMP. (B) The two sub-domains T25 and T18 form the catalytic subunit of the adenylate cyclase and are not functional unless they are in close proximity of each other. (C) Fusing fragments T25 and T18 to putative interacting proteins (X and Y) can restore adenylate cyclase activity. (D) Cyclic AMP binds to a CRP dimer, which activates different catabolic operons like *lac* or *mal* used for quantifying protein interactions in the bacterial two-hybrid system.

Previously, Maillard et al. (2007) had designed a plasmid encoding a NapA$_{SP}$-T18 fusion protein where the NapA twin-arginine signal peptide was fused to the N-terminus of the T18 fragment. In addition a compatible vector encoding a T25-NapD fusion protein, where NapD was fused to the C-terminus of T25, was also previously constructed. This plasmid pair allowed the clear detection and quantification of the NapD-NapA$_{SP}$ interaction (Maillard et al, 2007).

In this work, the plasmid encoding the NapA$_{SP}$-T18 fusion was subjected to glutamine-scanning mutagenesis such that every NapA$_{SP}$ residue from K2 through to G34 was substituted individually by glutamine (Figure 2.2). The polar amino acid glutamine was chosen because of its very rare natural occurrence in Tat signal peptides (Cristóbal et al, 1999), thus it may be a good candidate to disrupt signal peptide function, and also because its polar nature would interrupt the hydrophobic properties of the signal peptide.
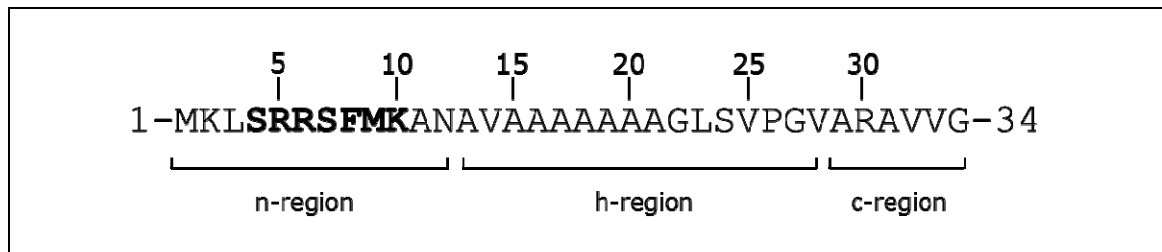
Figure 2.2 Signal sequence of NapA. The Tat motif is in bold and the N-terminal n-, hydrophobic h- and C-terminal c-region are outlined. Individual glutamine substitutions were introduced to residues 2 to 34.

The resultant bank of 33 NapA$_{SP}$ variants was then tested for the ability to interact with T25-NapD *in vivo* (Figure 2.3). Residues covering a broad scope of the signal peptide were identified as being important for NapD binding using this systematic scanning approach. Substitutions of R6, M9, K10, A13, A17 and A21 with glutamine all showed decreased β-galactosidase activity indicating impaired recognition by NapD *in vivo* (Figure 2.3). Further, substitution of residue A17 by the hydrophobic amino acid leucine also showed reduced NapD binding *in vivo* (Figure 2.3), thus reinforcing the important role of A17, which lies in the centre of the predicted h-region (Figure 2.2), in peptide-chaperone recognition.

As well as the h-region (Figure 2.2), the BTH assay data suggest that residues of the Tat motif itself are important for chaperone binding (Figure 2.3). NapA residue R6 is part of the Tat motif and thus predicted to be of critical importance for protein transport (Buchanan et al, 2002; Stanley et al, 2000). Indeed, a double R5Q-R6Q variant signal peptide also showed impaired binding to NapD in this bacterial two-hybrid assay (Figure 2.3).
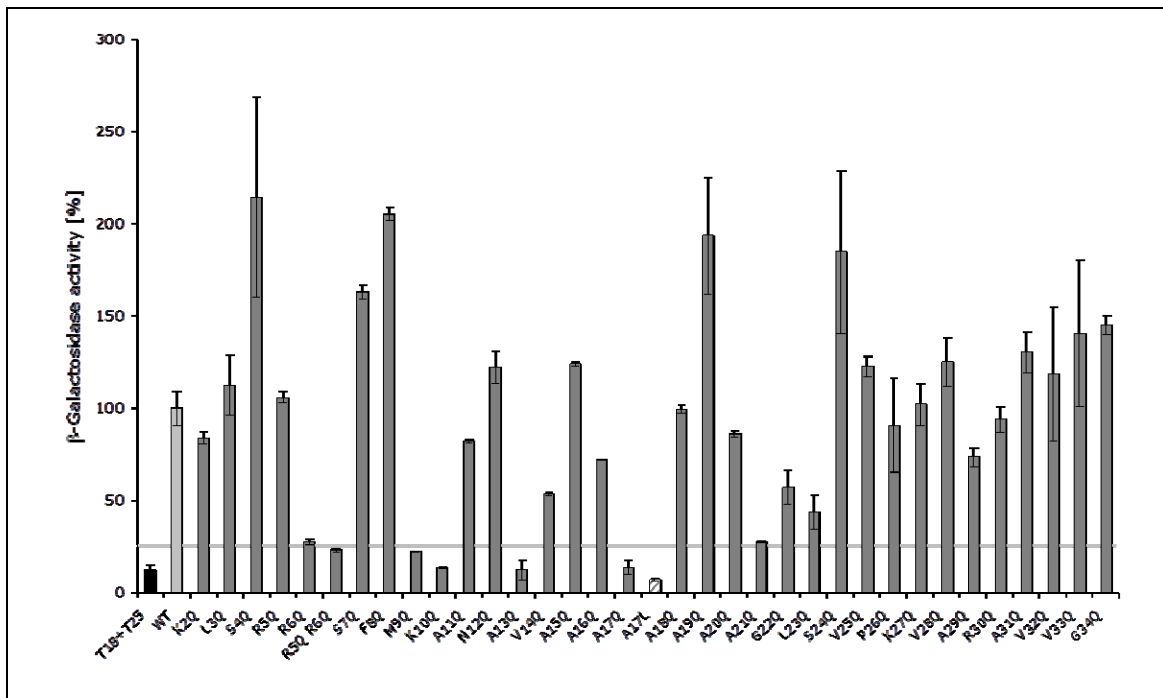
Figure 2.3 Interaction study between the Tat signal peptide of the periplasmic nitrate reductase NapA and its chaperone NapD. Interactions of NapD with the amino acid substituted NapA signal peptide using the bacterial two-hybrid system. β-Galactosidase activity is shown relatively to the native NapA signal peptide (WT). Column marked 'T18+T25' is the negative control. Error bars represent standard deviation of the mean, n = 3-9. The threshold for non-interacting NapA$_{SP}$ glutamine variants was set to ~30% compared to native NapA$_{SP}$ (grey line).
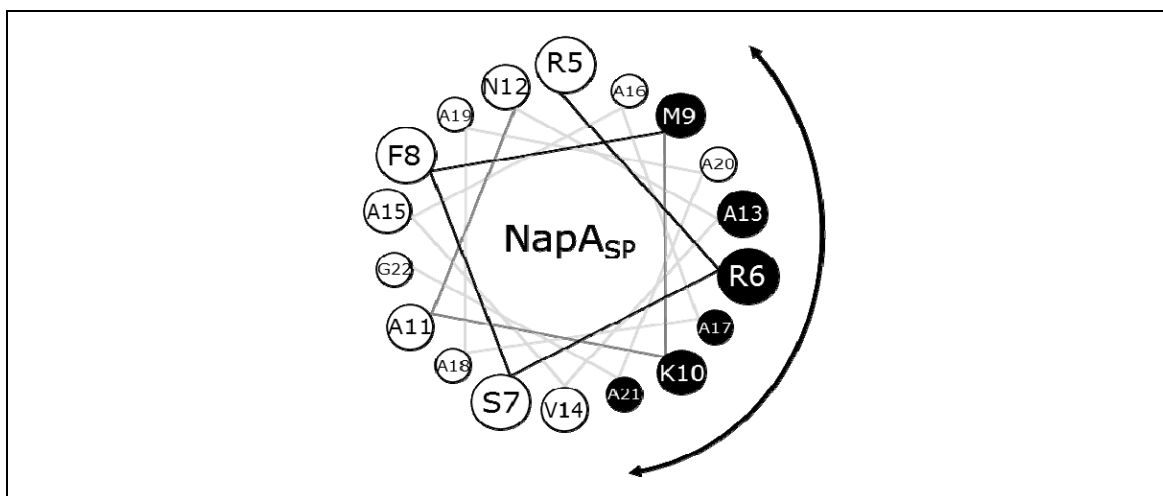
Figure 2.4 Prediction of NapA signal peptide residues required for NapD binding using a genetic approach. An α-helical wheel projection of NapA signal peptide (NapA$_{SP}$) shows residues R5 to G22. Side chains implicated in NapD binding as predicted by BTH and glutamine-scanning mutagenesis are shown in black and highlighted by the double arrow. The online applet at http://cti.itc.virginia.edu/~cmg/Demo/wheel/wheelApp.html was used to generate the helical wheel.

Strikingly, there appears to be an obvious periodicity in the pattern of NapA$_{SP}$ residues implicated in NapD binding (Figure 2.3). Plotting the NapA$_{SP}$ primary sequence as a canonical α-helix (3.6 residues per turn) shows that the residues implicated in NapD binding (R6, M9, K10, A13, A17 and A21) cluster together on one 'face' of the α-helix,

suggesting strongly that the signal peptide adopts a helical structure when bound by NapD (Figure 2.4).

2.2.2 Verification of the NapD binding epitope on NapA$_{SP}$ *in vitro*.

Although the *in vivo* BTH system is very useful for rapid scanning of binding interfaces between proteins, because of the common occurrence of both false-positives and – negatives when taking this approach it is always advisable to verify any interaction data using a second technique. In this case isothermal titration calorimetry (ITC) was selected as a sensitive *in vitro* method to validate the interaction between the twin-arginine signal peptide of NapA and NapD from the bacterial two-hybrid assay. ITC is a thermodynamic technique, which measures the generated or absorbed heat during interaction of two biomolecules. A single experiment can give full information about binding constants (K$_D$), reaction stoichiometry (*N*), enthalpy (ΔH) and entropy (ΔS) providing a detailed thermodynamic profile of the binding event.

Previously, a fusion of the NapA signal peptide to the C-terminus of the *E. coli* maltose binding protein MalE (MalE-NapA$_{SP}$) has been used to study NapD binding by ITC (Maillard et al. 2007). In this initial study the proteins were prepared under native conditions and the ITC experiments involved titration of 50 µM NapD into 5 µM MalE-NapA$_{SP}$. These experiments resulted in a single apparent dissociation constant (K$_D$) of 7 nM, and an *N* value (binding stoichiometry) of 0.59 (Maillard et al, 2007).

However, in this Chapter slight changes regarding protein purification protocols and ITC assay conditions were implemented. Here, the native MalE-NapA$_{SP}$ fusion, its glutamine-substituted variants, as well as the NapD chaperone were purified under denaturing conditions in the presence of high concentrations of urea, followed by in-column re-naturation, before subsequent purification. The denaturation step was needed due to the very high level of proteolytic degradation observed for the glutamine-substituted MalE-NapA$_{SP}$ variants under native conditions (data not shown). It was decided, therefore, to subject all proteins to identical treatment in this section.

Representative purification experiments are shown in Figure 2.5. Briefly, the MalE-NapA$_{SP}$ fusion protein (which also carries a hexa-Histidine affinity tag at its extreme C-terminus) was overproduced as described in Materials & Methods (Section 7.4.3). The cells were lysed in the presence of 5 M urea and loaded on to an immobilised metal affinity chromatography (IMAC) column. The protein was then refolded whilst still bound to the IMAC column by applying a linear gradient of 5-0 M urea, and finally eluted from the column by application of an imidazole gradient (Figure 2.5). This protocol resulted in high yields and purities for both MalE-NapA$_{SP}$ and NapD (Figure 2.5A and 2.5B). Data for the purification of the MalE-NapA$_{SP}$ variants is not shown.
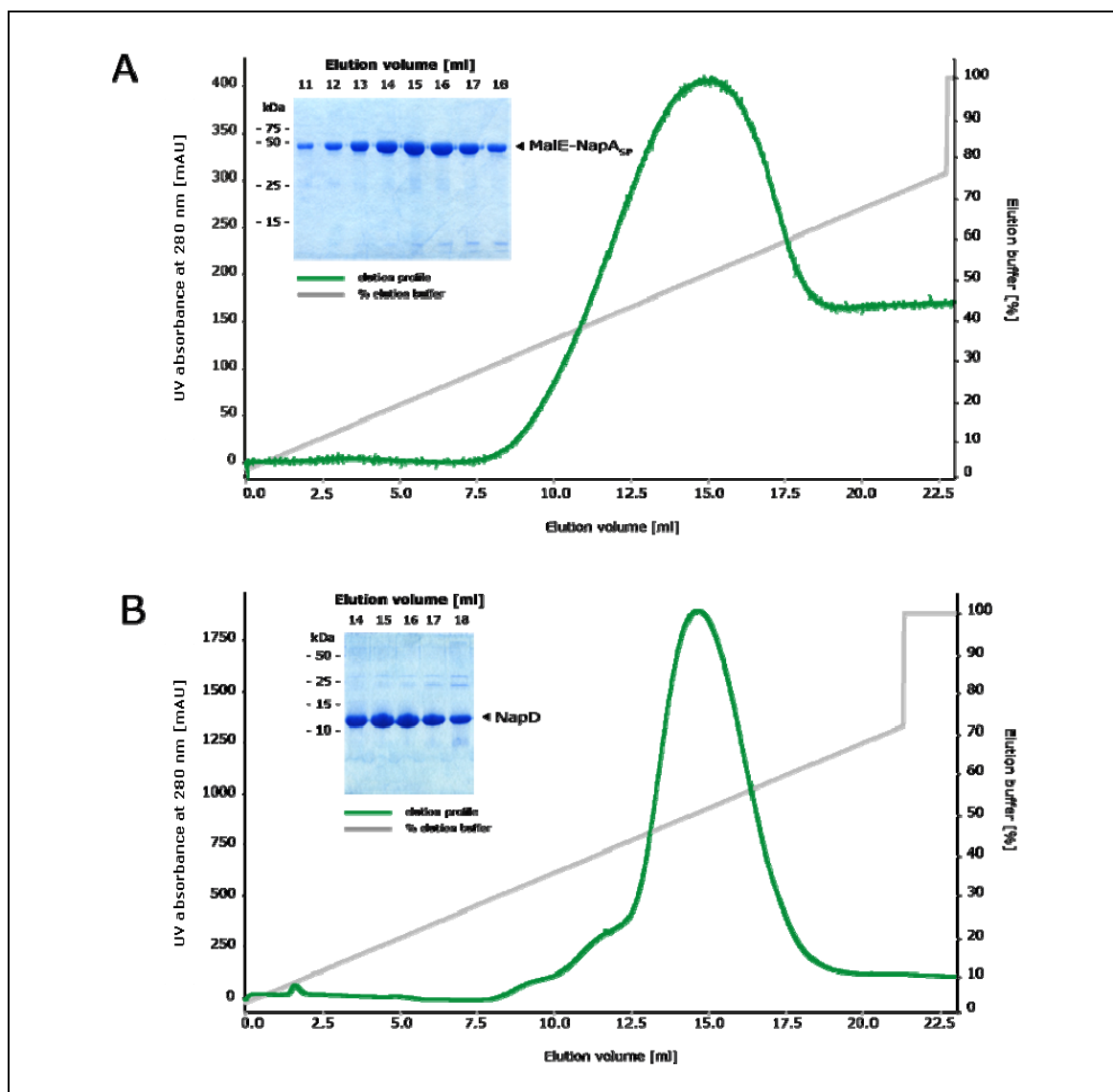
Figure 2.5 Purification of His-tagged MalE-NapA$_{SP}$ and NapD using IMAC. Cells were lysed in the presence of 5 M urea and crude extract loaded on a HisTrap^{TM} HP column. Bound denatured proteins were subsequently refolded on the column and eluted using a linear gradient of imidazole (0-500 mM). Shown are elution profiles of (A) MalE-NapA$_{SP}$ and (B) NapD. Fractions were collected and 1 µl of each 1:1 diluted in Lämmli sample buffer (Bio-Rad). Separation was achieved on a 12% or 15% SDS-PAGE for MalE-NapA$_{SP}$ or NapD, respectively. MalE-NapA$_{SP}$ variants show a very similar purification profile to Figure 4A.

The isolated MalE-NapA$_{SP}$ and NapD were then subjected to an ITC experiment to assess the degree of interaction between the two. In this case a stock of 100 µM NapD was titrated against 10 µM MalE-NapA$_{SP}$ in the sample cell. Under these conditions a bi-phasic binding curve was obtained, clearly indicative of two distinct binding events (Figure 2.6A). Optimal curve fitting suggested the involvement of two separate protein populations: one where 35% of the proteins interacted with an apparent K$_D$ of 3 nM, and a second where the remainder of the proteins (64%) showed an apparent dissociation constant of 143 nM (Table 2.1). Note that ITC experiments using identical concentrations of NapD and MalE-NapA$_{SP}$ but purified under native conditions showed similar binding characteristics (data not shown).
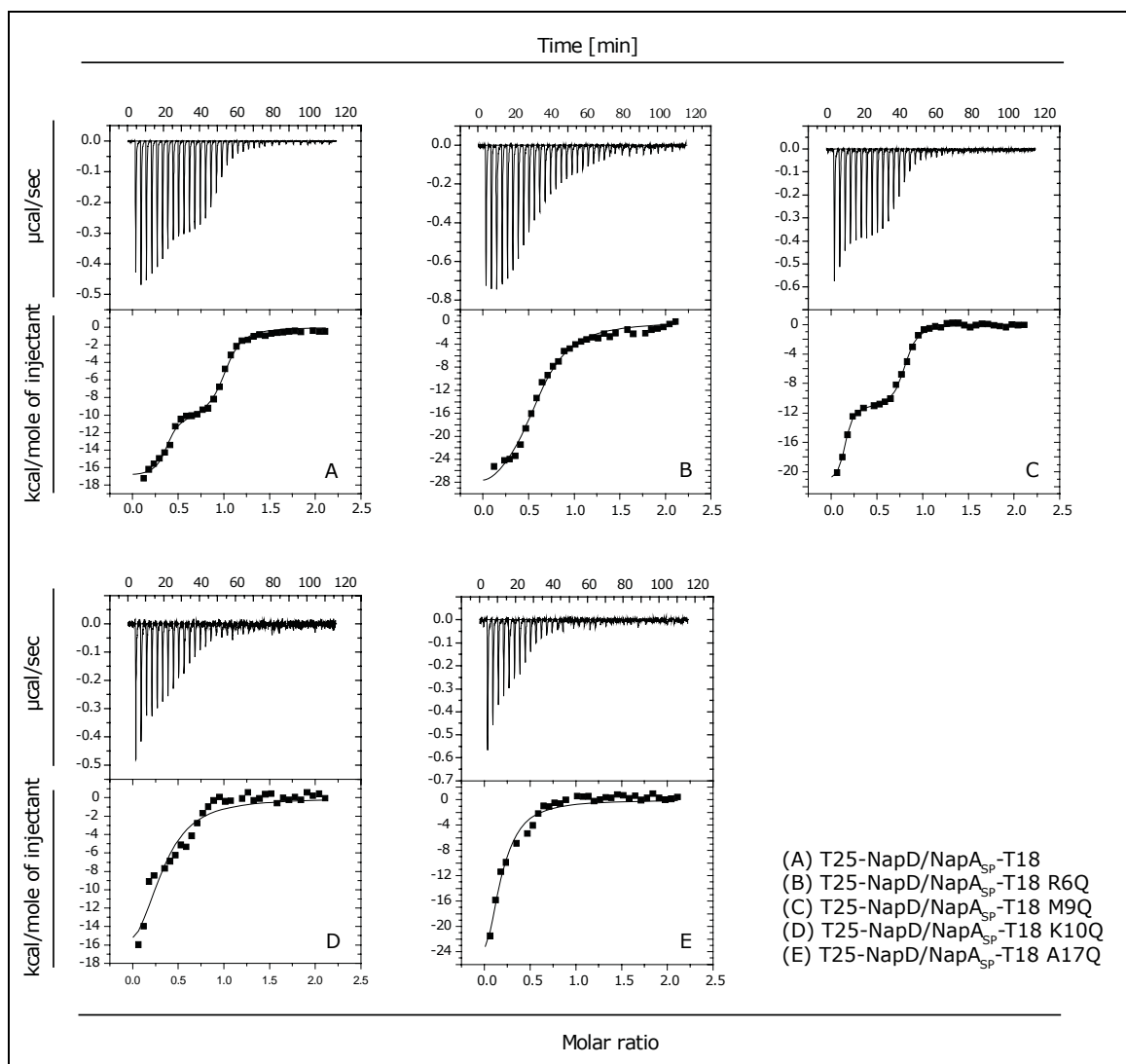
Figure 2.6 Isothermal titration calorimetry analysis of NapD binding to NapA signal peptide variants. All experiments were performed in Tris-HCl buffer under identical conditions and identical protein concentrations. Upper panels show raw data for heat effect during titration. Lower panels are the binding isotherms. Parameters for all runs are summarized in Table 2.1.

Next, four NapA$_{SP}$ variants where glutamine substitutions found to impair NapD binding *in vivo* were chosen for ITC analysis. The plasmid encoding MalE-NapA$_{SP}$ was modified such that it separately encoded R6Q, M9Q and K10Q variants, which form part of the twin-arginine motif, and an A17Q variant, located within the hydrophobic alanine stretch (Figure 2.2). For the R6Q, K10Q and A17Q variants of MalE-NapA$_{SP}$ a single binding event with NapD was observed (Figure 2.6B, D and E and Table 2.1). In all three cases the apparent dissociation constant (K$_D$) increased by one order of magnitude to ~1 µM (Figure 2.6B, D and E and Table 2.1). Also in all three cases the binding stoichiometry *N* remained well below 1 (Table 2.1), suggesting that the second binding site, or second population of binding events as observed for the native proteins (Figure 2.6A), is no longer detectable by this technique. Taken together, these ITC experiments verify that NapA$_{SP}$ residues R6, K10, and A17 are important for recognition and binding by NapD.

35

NapD variant	NapASP variant	analysis	N value				K_D [nM]		
native	native	two sets of	pop. 1	0.35	+/-	0.02	3	+/-	1
		sites	pop. 2	0.64	+/-	0.02	143	+/-	29
	R6Q	one set of sites	pop. 1	0.60	+/-	0.02	725	+/-	90
			pop. 2	0.40			∞		
	M9Q	two sets of	pop. 1	0.13	+/-	0.01	1	+/-	0.3
		sites	pop. 2	0.65	+/-	0.01	75	+/-	1
	K10Q	one set of sites	pop. 1	0.33	+/-	0.05	1,297	+/-	498
			pop. 2	0.67			∞		
	A17Q	one set of sites	pop. 1	0.16	+/-	0.03	1,100	+/-	193
			pop. 2	0.84			∞		

Table 2.2.1 Binding constants between NapD and variants of the NapA signal peptide. Summary of stoichiometry and binding constants determined by isothermal titration calorimetry. In the experiments carried out two populations of NapD were found to bind the NapA signal peptide (pop. 1 and pop. 2). For infinite binding constants second N values were estimated and coloured in grey.

Interestingly, the MalE-NapA$_{SP}$ M9Q variant showed similar NapD binding characteristics to that observed for the un-modified native NapA signal peptide using the *in vitro* ITC approach (Figure 2.6C and Table 2.1). This is in contrast to the *in vivo* data obtained by bacterial two-hybrid assay (Figure 2.3), but most likely indicates that the M9Q substitution destabilises the NapA signal peptide that it leads in-turn to a 'false-negative' result in the BTH (Figure 2.3).

The importance of three specific NapA residues (R6, K10 and A17) for NapD binding has therefore been confirmed by both *in vivo* and *in vitro* analyses. Thus a revised helical wheel projection now narrows the NapD binding epitope down to a distinct binding face on one side of an α-helix. The NapD binding epitope comprises residues that cross the boundary between the twin-arginine motif and the h-region within the N-terminal half of the signal peptide (Figure 2.7).
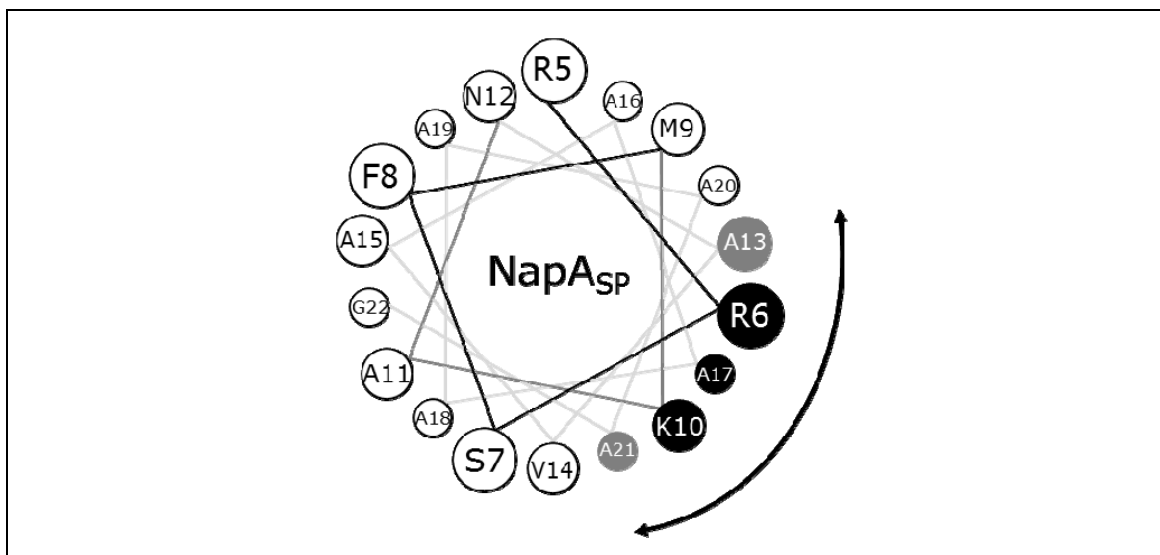
Figure 2.7 The verified NapD binding site on the NapA signal peptide following ITC analysis. α-helical wheel of the NapA signal peptide shows residues predicted by BTH to be involved in NapD binding in grey and residues confirmed by ITC in black. Site of NapD interaction is highlighted by the double arrow. The online applet at http://cti.itc.virginia.edu/~cmg/Demo/wheel/wheelApp.html was used to generate the helical wheel.

2.2.3 The roles of the signal peptide binding epitope residues in nitrate reductase activity

Having identified three key residues within the NapA signal peptide important for NapD binding (R6, K10 and A17), the next step was to assess their roles in assembly and activity of the periplasmic nitrate reductase. To this end three new *E. coli* strains were constructed, each carrying a point mutation at the native *napA* locus on the chromosome. The parental strain chosen was LCB2048 (Table 7.1-1) a seminal strain in the nitrate respiration field that is devoid of the two cytoplasmically-oriented nitrate reductases (NarGHI and NarZYV; Blasco et al, 1992). Thus LCB2048 produces only a single nitrate reductase, the periplasmic isoenzyme, and was further genetically modified here by the introduction of individual glutamine codons at positions normally coding for either R6, K10 or A17 (see Materials & Methods). The resulting strains were designated as SGQ061 (as LCB2048, *napA* R6Q), SGQ101 (as LCB2048, *napA* K10Q), and SGQ171 (as LCB2048, *napA* A17Q).

In order to determine the levels of physiological nitrate reductase activity a colorimetric assay was employed. The product of nitrate (NO_3^-) reduction, nitrite (NO_2^-), can be readily quantified using the Grieß test, where nitrite is further converted by an aminobenzene-based substance to a pink coloured azo compound, which can be spectroscopically quantified by its absorbance at 540 nm (Figure 2.7B).
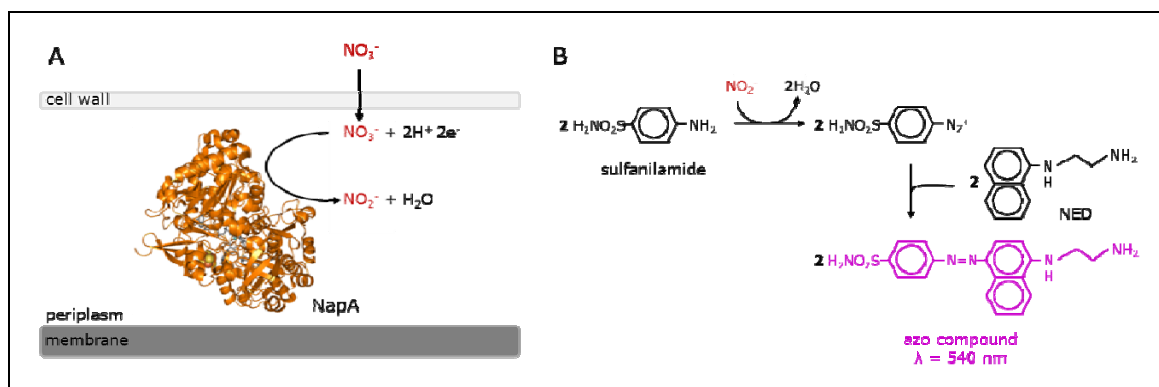
Figure 2.8 *In vivo* **nitrite production assay.** (A) NapA catalyzes the reduction of nitrate to nitrite in the periplasm. Shown is the crystal structure of *E. coli* NapA (PDB ID code 2nya). (B) The Grieß reaction for quantification of produced nitrite. Nitrite reacts with sulfanilamide and NED (*N*-(1-napthyl)ethylenediamine) under acidic conditions to generate a pink coloured azo compound, which has maximum absorption at 540 nm. (Adopted from www.promega.com/tbs/tb229/tb229. pdf)

All four strains (LCB2048, SGQ061, SGQ101 and SGQ171) were tested for their ability to reduce exogenous nitrate added to live cell cultures (Figure 2.8). The parental LCB2048 (*napA*$^+$) strain was capable of nitrate reduction and reached a peak in nitrite production ~2.5 hours following nitrate addition, after which the nitrite is itself metabolised to a basal level (Figure 2.8). This secondary nitrite metabolism is presumably catalysed by the respiratory cytochrome *c* nitrite reductase, which is also located in the periplasm (Simon, 2002). Conversely, strain SGQ061 (*napA* R6Q) did not exhibit any detectible nitrite production over the entire monitoring period of 8 hours (Figure 2.8). It is clear, therefore, that the *napA* R6Q strain is completely devoid of periplasmic nitrate reductase activity. In contrast, SGQ101 (*napA* K10Q) retained an *in vivo* nitrate reductase activity with a similar profile to that observed for the parental strain LCB2048 (Figure 2.8). Finally, strain SGQ171 (*napA* A17Q) exhibited an intermediate phenotype by producing lower levels of nitrite (approx. 50%) as the parental strain (Figure 2.8). In addition, a delay in the onset of nitrite production was observed for SGQ171 (*napA* A17Q) that was not observed in the other strains (Figure 2.8).

It can be concluded that NapA residue R6 within the Tat motif of the signal peptide is essential for *in vivo* nitrate reductase activity. In contrast, substitution of residues K10 and A17 within the NapA signal peptide with glutamine is not sufficient to completely block assembly of the periplasmic nitrate reductase.
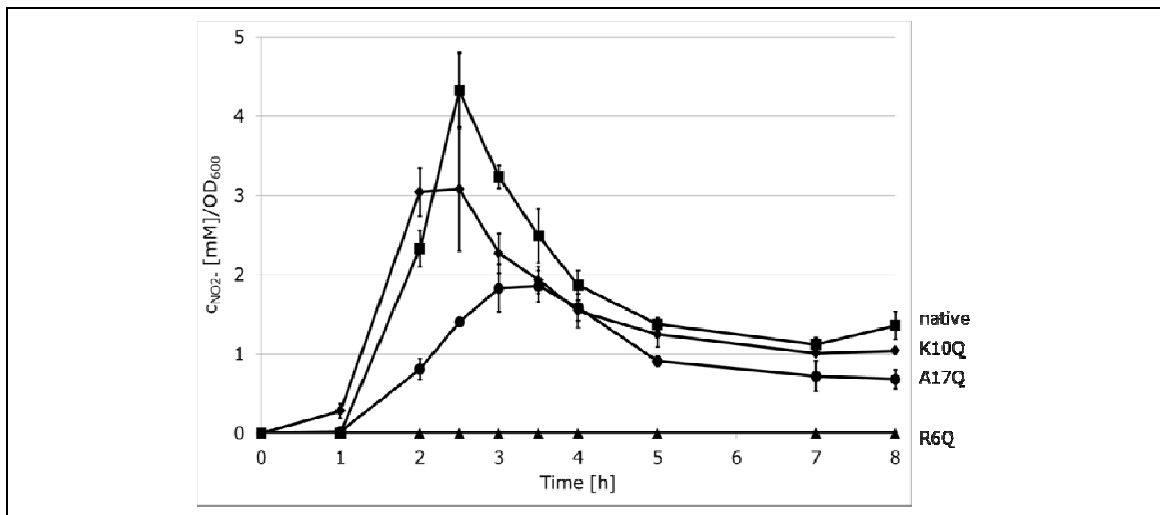
Figure 2.9 Importance of specific NapA signal peptide residues in NapA biosynthesis. *E. coli* strains with individual chromosomal glutamine substitutions were grown anaerobically in LB medium supplemented with 0.5% glycerol, 0.4% fumarate and 0.2% nitrate. Aliquots were taken at indicated time points and OD_{600} noted. The amount of produced nitrite from cell-free supernatant was quantified according to the Grieß test. Strains are labelled as wild type LCB2048 (*nap*[+]) (■), SGQ061/NapA R6Q (▲), SGQ101/NapA K10Q (◆), SGQ171/NapA A17Q (●).

2.2.4 The roles of the signal peptide binding epitope residues in Tat transport

Having studied the roles of NapA residues R6, K10 and A17 in both NapD binding and nitrate reductase activity the third aspect to consider in terms of signal peptide structure/function is their specific roles in Tat transport. In order to study signal peptide activity in isolation (i.e. in the absence of other competing processes such as cofactor insertion) a suitable reporter protein is required. Chloramphenicol acetyl transferase (CAT) has proven to be one of the most useful reporter proteins for Tat transport activity. This enzyme is not compatible for Sec-dependent export but is efficiently translocated to the periplasm by the Tat machinery (Stanley et al, 2002). This is useful as it means there can be no defaulting of export to the Sec machinery, if Tat transport is blocked. In addition, the CAT enzyme is only active in the cell cytoplasm. This is because the reaction to detoxify chloramphenicol is dependent upon acetyl-CoA as cofactor, which is not present in the periplasm. As a result CAT is a robust indicator of impaired Tat transport function, since retention of CAT in the cytoplasm leads to increasing chloramphenicol resistance of the host cell.

A vector encoding a NapA$_{SP}$-CAT fusion has already been prepared (Maillard et al, 2007; Stanley et al, 2002). This fusion directs efficient export of CAT across the cytoplasmic membrane *via* the Tat pathway (Maillard et al. 2007) and the *E. coli* host cells therefore exhibit sensitivity to high concentrations of chloramphenicol (Cml) (Figure 2.9A). Cells blocked for Tat transport, either through lesions in the *tat* genes or through carrying mutations within the signal peptide encoding region, show Cml resistance (Figure 2.9B). Assuming expression levels are similar in any given experiment, the degree of resistance to chloramphenicol is proportional to the amount of CAT retained in the cytoplasm.
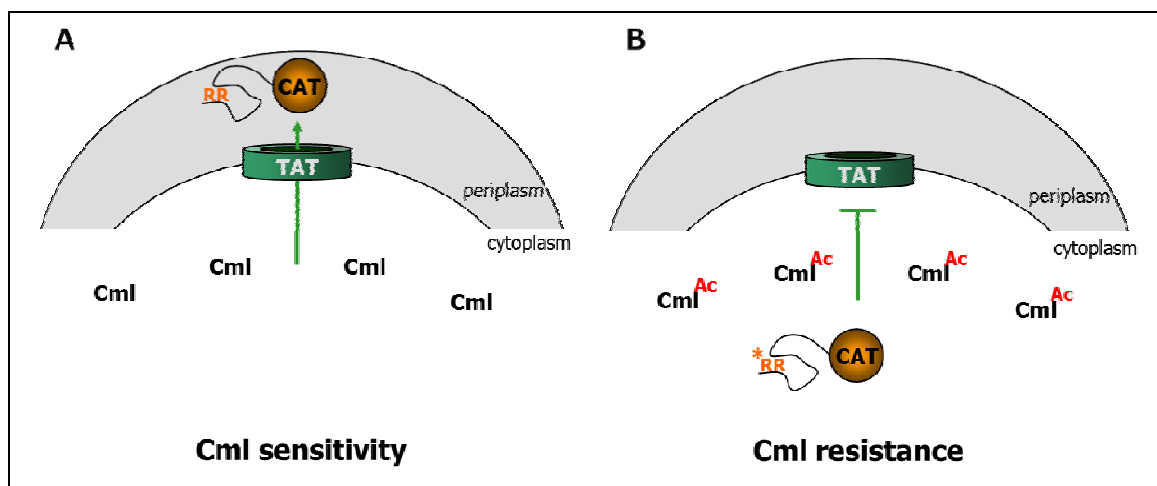
Figure 2.10 *In vivo* **Tat transport assay.** (A) Plasmid encoded chloramphenicol acetyl transferase (CAT) is fused to a Tat signal peptide (labelled 'RR'). Recognition and transport of CAT by the Tat complex results in cells being sensitive to high concentrations of chloramphenicol (Cml). (B) Mutation of e.g. the Tat signal peptide (*RR) causes rejection of CAT for export. Thus CAT remains in the cytoplasm and inactivates chloramphenicol by acetylation (Cml^{Ac}).

In this work, the plasmid encoding NapA$_{SP}$-CAT (Maillard et al, 2007) was modified to encode NapA$_{SP}$ R6Q, K10Q and A17Q derivatives. The four vectors were used to separately transform the *E. coli* wild type strain MG1655 (*tat$^+$*) and growth of the transformants was then monitored in the absence or presence of chloramphenicol (Figure 2.10). All four transformants showed similar growth characteristics when grown aerobically in rich media in the absence of the antibiotic (Figure 2.10). As previously published (Maillard et al., 2007), cells producing the native NapA$_{SP}$-CAT fusion showed no growth in the presence of Cml (Figure 2.10), indicating that CAT had been efficiently targeted to the periplasm. In contrast, cells expressing the R6Q NapA$_{SP}$-CAT variant were able to grow in the presence of 200 µg/ml chloramphenicol, a clear indication that export of CAT from the cytoplasm was severely compromised by this signal peptide modification (Figure 2.10).

Substitution of residues K10 and A17 with glutamine within the NapA$_{SP}$-CAT fusion resulted in intermediate growth phenotypes (Figure 2.10). Cells harbouring the plasmid encoding the NapA$_{SP}$-CAT K10Q glutamine variant began to show detectible signs of growth after a very long lag-phase (~7 hours) and reached only ~10% of the cell density attained by the native system (Figure 2.10). This suggests strongly that the NapA K10Q substitution severely impaired Tat export activity of the signal peptide, but is not sufficient to completely block protein transport.
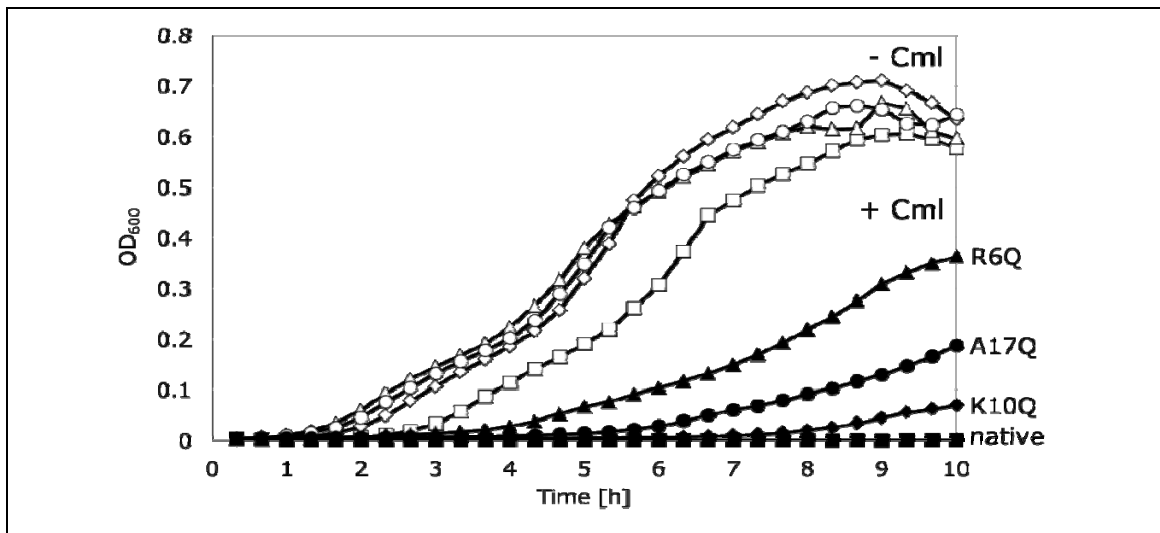
Figure 2.11 Importance of specific NapA signal peptide residues in Tat transport. *E. coli* strain MG1655 was transformed with pUNI-NapA containing a fusion of the NapA signal peptide to CAT (NapA$_{SP}$-CAT). Cells were grown aerobically in LB medium and 0.5% glycerol in presence (+ Cml; closed symbols) or absence (- Cml; open symbols) of chloramphenicol (200 µg/ml final concentration). NapA signal peptide variants are indicated as followed: native (■), R6Q (▲), K10Q (◆), A17Q (●).

2.3 DISCUSSION

2.3.1 NapA residues important for NapD binding

Published work by Maillard et al (2007) showed the very specific and tight binding of the proofreading chaperone NapD to the twin-arginine signal peptide of NapA. Those results provided the basis for the *in vivo* mapping of the binding interface described in the initial part of this Chapter. The NapA residues making up the minimal NapD binding epitope were further verified *in vitro* using isothermal titration calorimetry. This resulted in the identification of NapA R6, K10 and A17 residues as central to the NapD recognition mechanism.

Looking at the h-region of the NapA signal sequence a long alanine stretch stands out (Figure 2.2A), which could in itself indicate that the signal peptide likely adopts an α-helical conformation (Marqusee & Baldwin, 1987; Rohl et al, 1999). Moreover, when the signal peptide was plotted as a canonical helical wheel, residues R6, K10 and A17 (as well as A13 and A21) are predicted to cluster together to form a distinct binding face on the signal peptide.

Comparison of the Tat signal sequence from *E. coli* NapA with the NapA signal peptide of other microorganisms shows that the Tat motif and the hydrophobic region are very well conserved (Figure 2.11). Also all identified NapA residues (R6, K10, A13, A17 and A21) are found to be well conserved in other biological systems, suggesting an important role in NapD binding in general (Figure 2.11).

41

Figure 2.12 Sequence alignment of different NapA twin-arginine signal peptides. Homologs from *Escherichia coli* (*Ec*), *Agrobacterium tumefaciens* (*At*), *Bradyrhizobium japonicum* (*Bj*), *Cupriavidus necator* (*Cn*), *Desulfovibrio desulfuricans* (*Dd*), *Paracoccus pantotrophus* (*Pp*), *Rhodobacter sphaeroides* (*Rs*) and *Shewanella oneidensis* (*So*) are shown. Identified residues for NapD binding by BTH and ITC are highlighted with an arrow. Highly conserved residues are highlighted in orange. Amino acid residues with similar properties are shown in grey.

2.3.2 The bi-phasic binding character of NapD

Interestingly, a two-tier biphasic binding event was observed for NapD binding to the native NapA signal sequence during ITC titrations. This observation was apparently in contrast to previous published work (Maillard et al, 2007). At first glance this biphasic binding curve may appear to suggest two binding sites for the signal peptide on the NapD protein, however it should be noted that the total Molar binding stoichiometry (*N*) consistently adds up to 1, as opposed to 2. In this case, such a biphasic binding curve could be best explained by either NapD or the NapA signal peptide existing as two subpopulations with subtly different properties (Maillard et al, 2007). Why was such biphasic binding not observed by Maillard et al. (2007)? In this work higher protein concentrations were used, so it is likely that Maillard et al. (2007) were focussed on the first, highest affinity, binding site and were not saturating the second site. This would explain why the *N* value obtained by Maillard et al. (2007) was never more than 0.56.

Similarly, Zakian et al (2010) noticed biphasic binding between the chaperone NarJ and the N-terminus of NarG, which is an evolutionary remnant Tat signal peptide (Ize et al, 2009). In addition, it was demonstrated by NMR that the NarG N-terminus has only one binding site on NarJ (Zakian et al, 2010). In this case slight changes in pH were able produce single monophasic binding curves and it was concluded that NarJ consists in two subpopulations with different protonation states, and that this is sufficient to observe subtle differences in binding characteristics (Zakian et al, 2010).

2.3.3 NapA residues R6, K10 and A17 and their importance in NapA assembly

Initial studies of signal peptide binding by Tat proofreading chaperones involved the TorD-TorA system from *E. coli*. Indeed, the TorD binding epitope on the TorA signal peptide was mapped by glutamine-scanning mutagenesis using identical methodology as

described here for NapD-NapA (Buchanan et al, 2008). In this case, the TorD binding epitiope was located at the C-terminus of the TorA signal peptide – relatively far, in molecular terms, from the conserved twin-arginine motif (Buchanan et al, 2008). Work outlined in this Chapter demonstrates that the NapD-NapA system follows its own rules in this regard, since the NapA Tat motif overlaps with the NapD chaperone-binding motif considerably.

First, the NapA R6 residue clearly has overlapping functions in both assembly and export of the nitrate reductase. A strain carrying a chromosomal NapA R6Q allele was completely devoid of nitrate reductase activity, and a reporter assay suggested this substitution was a signal peptide defective in Tat transport. These data point to a role for NapA R6 in Tat transport. In addition, however, both *in vivo* and *in vitro* binding studies identified R6 as being important for the NapD interaction. This could suggest that the role of NapD is focussed entirely on the Tat transport step on nitrate reductase biosynthesis, rather than in cofactor insertion as it is often assumed.

The NapA K10 residue lies within the Tat motif and is very highly conserved in nitrate reductase signal peptide primary sequences (Figure 2.11). In this case, however, a K10Q substitution had little effect on the overall nitrate reductase activity *in vivo*. Similarly, a strain carrying a *napA* A17Q allele at the native chromosomal locus had low, but still detectible, periplasmic nitrate reductase activity. These data suggest cofactor insertion and protein export can continue to a significant extent. This seems at odds with the NapD binding experiments, however, which suggest both K10Q and A17Q NapA substitutions drastically impair NapD binding. Given that NapD is essential for nitrate reductase activity (Maillard et al, 2007), how can these results be reconciled? One possibility is that the detection limit of the BTH system, which these data suggest must lie above an apparent K_D of 750 nM (Table 2.1), bears little relation to the binding constants required for NapD function in the living cell. Indeed, the variant NapA signal peptides reported here to be 'devoid' of chaperone binding still retain some ability to interact with NapD with apparent K_Ds of ~1 μM (Table 2.1), and a binding constant of 1 μM would be considered relatively 'tight' for many biological systems (e.g. Hatzixanthis et al, 2005). It is therefore conceivable that NapD function is continuing to some extent in the mutant strains. The key experiment to test this, of course, would be to further delete the *napD* gene in the SGQ061, SGQ101, and SGQ171 mutant backgrounds. This would demonstrate if nitrate reductase activity was now NapD-independent when the NapA K10Q and A17Q substitutions were made.

It is also possible that the NapA K10Q substitution exhibits compensatory effects across different activities. For example, substitution of the equivalent residue of the Tat motif

with alanine in the cofactor-less Tat substrate SufI resulted in faster, more efficient export (Stanley et al, 2002). It is possible that the impairment of NapD function caused by the NapA K10Q substitution is compensated for by faster export of the enzyme.

A similar observation as seen for NapA K10Q and A17Q was made for TorA variant L31Q, where this glutamine substitution is part of the hydrophobic region of the Tat signal peptide and causes a drastic decrease in binding affinity for TorD as shown by ITC. Surprisingly, reduced interaction with the TorD chaperone does not affect TMAO reductase activity and Tat transport of TorA L31Q when compared to the native enzyme (Buchanan et al, 2008). This indicates that TorA residue L31 is important for chaperone binding, but has no influence on signal peptide recognition by the Tat complex. Hence, NapD interaction is dependent on NapA K10 and A17, whereas Tat transport is independent of residue K10 and to a lesser extent of residue A17. However, it should be noted that TorA biosynthesis is not entirely dependent on TorD, since an *E. coli* Δ*torD* mutant still exhibits significant TorA activity (Pommier et al, 1998), which is in stark contrast to the *nap* system.

It should also be considered that the *in vivo* nitrite production assays give very little information on the amount of nitrate reductase enzyme present in the periplasm of the mutant strains. Conceivably, very little enzyme could support significant nitrate reduction. Attempts were made here to visualise the relative amounts of NapA in the periplasms of the SGQ061, SGQ101 and SGQ171 strains by subcellular fractionation and Western immunoblotting. Unfortunately, the data were of poor quality and the blots were therefore unconvincing.

In summary, this Chapter has combined genetic and biochemical approaches to convincingly define, for the first time, the NapD binding epitope on the NapA twin-arginine signal peptide. These data suggest an intimate link between the Tat translocation activity of the signal peptide and the NapD binding site, possibly pointing to a dedicated role for NapD in protein transport as opposed to cofactor insertion.

3 Structural features of NapD important in NapA binding

3.1 *INTRODUCTION*

As described in Chapter 2, specific NapA residues have been identified within the NapA twin-arginine signal peptide that are important for the interaction with the NapD chaperone both *in vivo* and *in vitro*. These NapA residues are R6, K10 and A17.

In early work designed to identify regions of the NapD molecule involved in the NapA signal peptide interaction Maillard and co-workers (2007) carried out [^{1}H-^{15}N]– heteronuclear single quantum correlation (HSQC) NMR spectroscopy, where MalE-NapA$_{SP}$ was titrated into a ^{15}N-labelled sample of NapD. This binding experiment identified NapD residues 9-11, 35, 37 and 74-76 as being involved in recognition and binding of the twin-arginine signal peptide (Figure 3.1). The NMR solution structure of NapD (PDB ID code 2jsx) shows a single, large β-sheet face and all of the residues identified by Maillard et al (2007) cluster within that specific part of NapD (Figure 3.1) indicating that the β-sheet face is the major region that is physically binding to the NapA signal peptide. Although the initial NMR experiments conducted by Maillard et al (2007) were an excellent first glimpse at the possible signal peptide binding site on NapD, they were also fraught with difficulties.

Classically, NMR-based ligand binding experiments involve complexes that are in 'fast exchange' or 'slow exchange' on the NMR timescale. For 'fast exchange', this normally means studying interactions with K$_D$'s in the low millimolar range (i.e. relatively weak binding) and using 2D HSQC spectroscopy to track the gradual movement of cross-peaks, corresponding to the ligand binding site on the protein of interest, as ligand is titrated (Vaynberg & Qin, 2006). This is the 'best case scenario' for an NMR spectroscopist as it is not necessary to re-assign cross-peaks to specific amino acids in the complex. For 'slow exchange', this means studying very strong interactions by again using 2D HSQC spectroscopy but this time tracking the gradual disappearance of cross-peaks in the 'free' protein spectrum and simultaneously recording the appearance of new cross-peaks for the ligand-bound form, which usually correspond directly to the ligand binding site on the protein of interest (D'Silva et al, 2005). In this case each new cross-peak in the spectrum should be carefully re-assigned to the corresponding amino acid residue.

Now in the experiments of Maillard et al. (2007) the chaperone-peptide complex was in 'intermediate exchange', which meant the free NapD cross-peaks gradually broadened and 'disappeared' as peptide was titrated but no new cross-peaks replaced them. Thus, some information on the initial amino acid side-chains of NapD to be affected upon

peptide binding could be obtained, but it was impossible to extrapolate to the structure of NapD in the peptide-bound state. This demonstrates clearly the limits of NMR when studying interactions with K_D's in the low micromolar and nanomolar ranges.
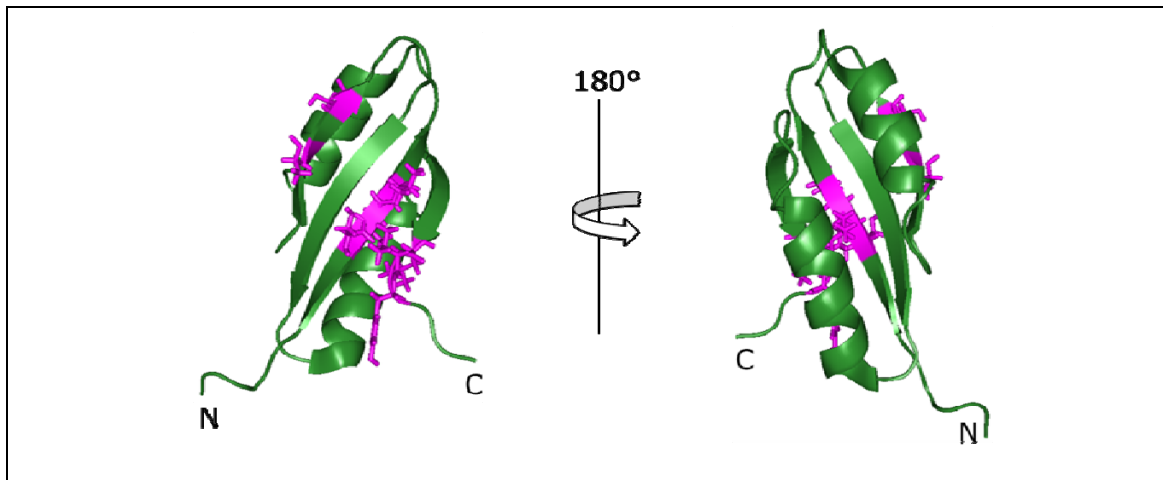
Figure 3.1 NapD residues involved in NapA signal peptide binding. Amino acid residues of NapD identified by HSQC spectroscopy to bind the twin-arginine signal peptide of NapA are highlighted in magenta (Maillard et al, 2007). (PDB ID code 2jsx)

Although good progress has been made in understanding the key requirements for signal peptide recognition by NapD (see Chapter 2), there are still many questions that remain. One question revolves around the twin-arginine motif of the signal peptide: why is it so important for NapD binding, and how does NapD recognise it? A second question concerns the trigger that releases the signal peptide from NapD: how does the chaperone sense that folding of NapA is complete and so releases the signal peptide for export to commence?

What is clear from the original binding studies is that the two α-helices that support the β-sheet from 'beneath'; the loop regions that link the helices and strands; and the long flexible C-terminal tail (residues 78-87), are not implicated in binding the signal peptide directly (Maillard et al, 2007). Moreover, Maillard et al. (2007) studied the role of the flexible C-terminal tail of NapD by attempting to complement a Δ*napD* strain using a vector encoding a truncated NapD protein (Figure 3.2). These experiments suggested the truncated NapD was still able to interact with NapA$_{SP}$ since some periplasmic nitrate reductase activity could be detected. Hence, NapD missing its C-terminus still retained some activity. Note, however, that the nitrite production profile generated by the truncated NapD variant was different to that observed with full-length native NapD (Maillard et al, 2007). Indeed, it resulted in clearly reduced NapA activity perhaps suggesting an important, if not essential, role for the flexible C-terminus of NapD in NapA biosynthesis (Maillard et al, 2007).

Figure 3.2 Amino acid sequence and secondary structure of *E. coli* NapD. The position for the published C-terminal truncation is marked by an arrow (Maillard et al, 2007). Glutamic acid residues subjected to lysine mutations are highlighted in bold orange.

The C-terminal tail of *E. coli* NapD is negatively charged and contains four glutamate side-chains (Figure 3.2). With only a few exceptions, the negative charge in the C-tail is conserved in the vast majority of NapD homologs (Maillard et al, 2007). It is tempting to speculate that this conserved negative charge may be involved in the initial recognition of the conserved positive charge within the Tat motif of the signal peptide.

In general, the question of how NapD somehow 'senses' the folded state of NapA is a difficult one to address. Certainly there are big differences in how NapD behaves when it binds to the native NapA precursor, compared to when it binds the NapA signal peptide fused to a reporter protein. For example, co-expression of plasmid-encoded NapD with a plasmid-encoded NapA$_{SP}$-CAT fusion protein produced a surprising result: export of the CAT reporter protein was completely blocked (Maillard et al, 2007). One interpretation of this data is that the NapD chaperone is unable to release the NapA signal peptide when it is part of such an artificial fusion, possibly because NapD cannot sense the folded state of the alien passenger protein.

In this Chapter structural features of the NapD chaperone important for signal peptide binding were investigated. The role of the flexible C-tail in NapD function was addressed. In addition, highly specific *napD* suppressor mutations were isolated that restored the interaction of the chaperone with the loss-of-binding NapA signal peptide variants identified in Chapter 2.

3.2 RESULTS

3.2.1 Role of the flexible C-terminal tail of NapD in NapA biosynthesis

Solution NMR studies of monomeric, recombinant NapD revealed that the extreme C-terminal region of the protein formed an unstructured, flexible 'C-tail' (Maillard et al,

2007). The C-terminus of NapD has four glutamic acid residue arranged in the sequence 'E-E-x-x-E-E' located at position 80, 81, 84 and 85, respectively (Figure 3.2). While these precise residues are not completely conserved amongst NapD homologs, an overall negative charge in the C-tail is widely retained across many biological systems. For example, the *W. succinogenes* NapD has a very long C-tail of 46 amino acids, of which nine are glutamate, two are aspartate, and only two are lysine or arginine. Similarly, the NapD homolog of the opportunistic pathogen *P. aeruginosa* has a 33-residue C-tail containing four glutamate, six aspartate, and only one arginine. Removal of the last 10 amino acids of *E. coli* NapD (residues 78 to 87), which form the flexible C-terminus, resulted in decreased NapA activity *in vivo* (Maillard et al, 2007). In this work it was decided to take a closer look at the roles of the acidic residues within the C-tail.
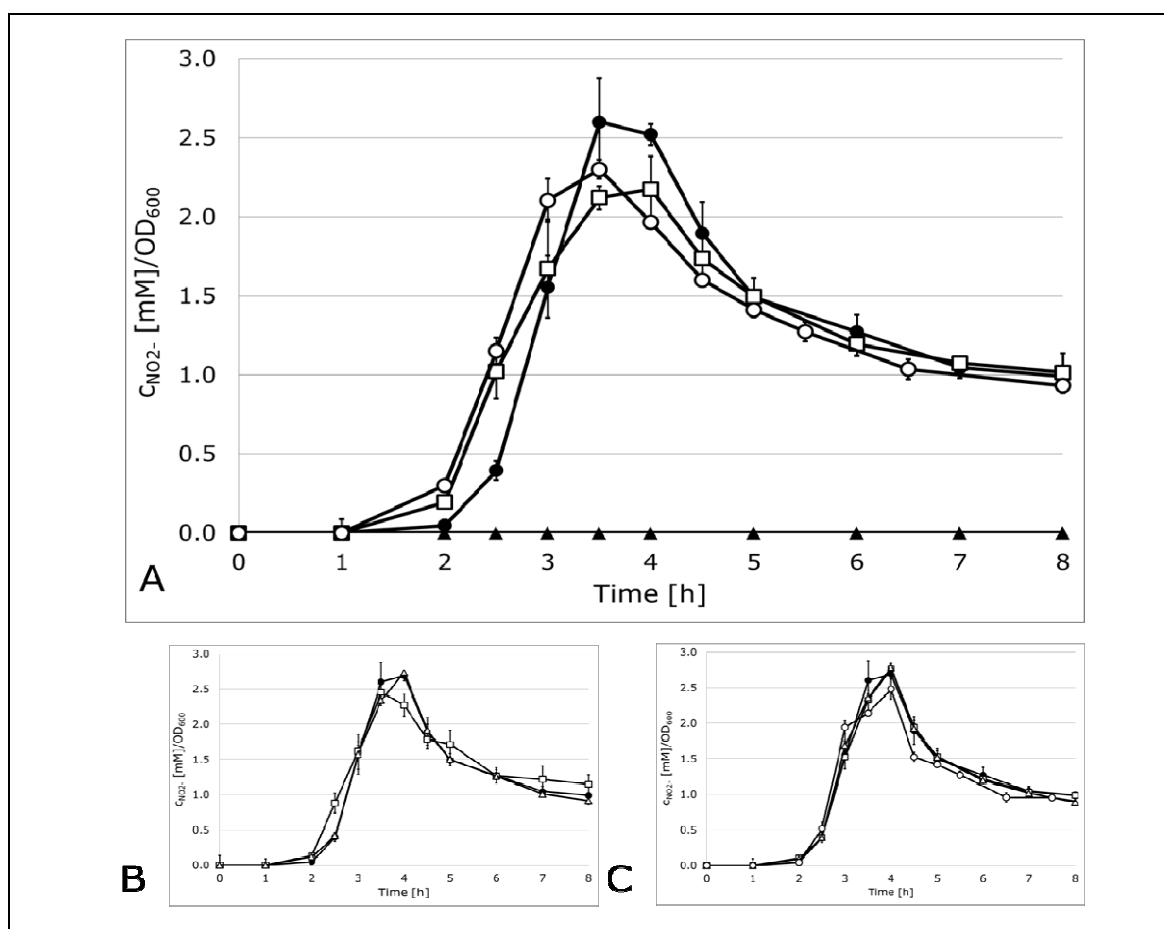
Figure 3.3 Role of C-terminal NapD mutations on NapA activity. Strain LP202$_S$, which has no NapA activity was either transformed with the original vector pUNI-Prom, pUP-NapD or plasmids containing NapD mutations E→K. To measure NapA activity cells were cultured in LB, 0.5% glycerol, 0.4% fumarate and 0.2% nitrate. At indicated time points aliqotes were taken, OD$_{600}$ noted and produced nitrite quantified according to the Grieß test (Chapter 2). For clarity transformants and their enzyme activity are shown in separate graphs. Labels are as followed: (A) LP202$_S$ (Δ*napD*) (▲), LP202$_S$/NapD (●), LP202$_S$/E80K (□), LP202$_S$/E80/81/84/85K (○). (B) LP202$_S$/NapD (●), LP202$_S$/E81K (□), LP202$_S$/E80/81K (Δ). (C) LP202$_S$/NapD (●), LP202$_S$/E84K (□), LP202$_S$/E85K (Δ), LP202$_S$/E84/85K (○).

NapD residues E80, E81, E84 and E85 were substituted with the basic amino acid lysine either individually, in pairs (E80/81K and E84/85K), or all together (E80/81/84/85K).

The influence of each substitution on *in vivo* NapA activity was then determined by a nitrite production assay (Figure 3.3). *E. coli* strain LP202$_S$ (as LCB2048, Δ*napD*), which is devoid of any NapA activity (Maillard et al, 2007; Potter & Cole, 1999), was transformed either with vector only (control) or plasmids encoding native NapD and its C-tail variants. The LP202$_S$ (Δ*napD*) strain is unable to reduce nitrate (Figure 3.3) as the NapA protein is not assembled correctly and so rapidly degraded in the absence of NapD (Maillard et al, 2007). This phenotype can be rescued upon expression of *napD* in *trans* (Figure 3.3). All of the NapD C-tail variants, including one containing no negative charges whatsoever, retained the ability to rescue the nitrate reductase-negative phenotype of the Δ*napD* strain (Figure 3.3). Therefore, it must be concluded that the negative charges in the NapD C-tail do not play a critical role in the assembly of the periplasmic nitrate reductase.

3.2.2 Generation of random mutant libraries of *napD* by error-prone PCR

Genetics can be a powerful tool in unravelling complex biological systems – especially if the genetic screens devised are robust and reliable. In this section it was decided to use a *napD* suppressor mutant library in combination with the bacterial two-hybrid system described in Chapter 2 to further dissect the chaperone-signal peptide relationship. 'Suppression genetics' is an approach that has been used to good effect to decipher complex protein targeting systems in bacteria (e.g. the outer membrane Bam system – Chimalakonda et al, 2011; and the function of TorD on the *E. coli* Tat pathway – Buchanan et al 2008) and involves the selection of secondary mutations that can rescue a particular mutant phenotype.

In Chapter 2 three distinct NapA signal peptide mutations were identified that disrupted the interaction with NapD. These were the NapA$_{SP}$ R6Q, K10Q and A17Q variants. To find NapD variants able to rebind to the corresponding glutamine substituted NapA signal peptides two *napD* mutant libraries were constructed. Error-prone PCR was performed using unequal amounts of dinucleotides and manganese supplemented buffer (Pritchard et al, 2005). The chosen theoretical error rates for the PCR reactions were 1.0% and 1.5%, which should give approximately one mutation per clone. The PCR products were cloned into vector pT25 from the BTH system and provided around 100,000 clones per library.
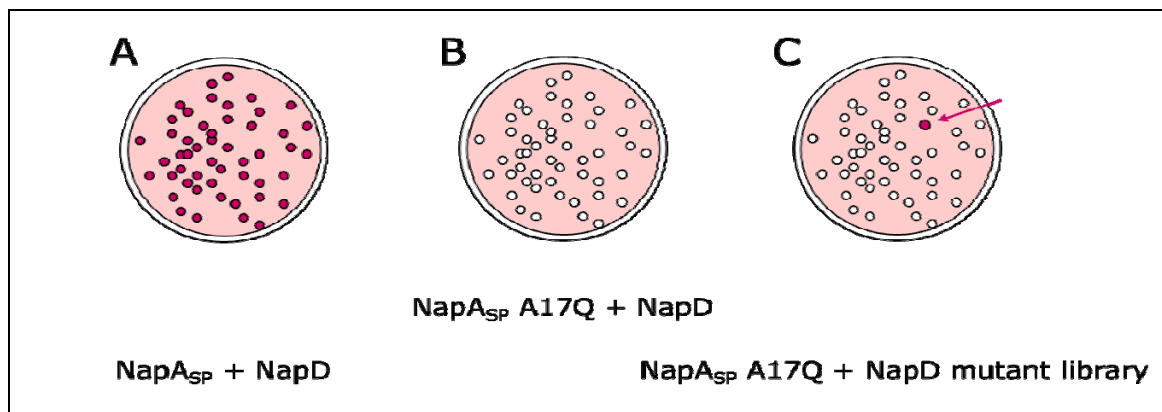
Figure 3.4 Devising a suppressor screen based on the bacterial two-hybrid system. A cartoon outlining the proposed methodology for isolating *napD* suppressor mutants able to interact with variant signal peptides (A) Using the BTH system developed by Karimova et al (1998) NapD can be observed to bind to Tat signal peptide of NapA (NapA$_{SP}$) resulting in red (positive) colony formation on MacConkey-maltose indicator plates. (B) Specific glutamine substitutions within NapA$_{SP}$ (e.g. A17Q) impair NapD binding such that the cells cannot metabolise maltose and so form white (negative) colonies on the indicator plates. (C) By first generating a random library of *napD* mutants and then screening against NapA$_{SP}$ A17Q within the BTH system, any suppressors that are able to re-bind the signal peptide variant can be detected as red (positive) colonies, isolated and further characterised.

3.2.3 Screening the *napD* mutant libraries for suppressors

In Chapter 2 it was clearly shown that a number of NapA$_{SP}$ variants consistently produced 'white' (negative) colonies on MacConkey-maltose indicator plates when co-transformed with the vector encoding native NapD. This plate test can therefore be used as a basis to select for *napD* mutants that are able to re-bind the glutamine substituted NapA signal peptides (see Figure 3.4).

To identify regions of NapD important in Tat signal peptide binding the pT25-NapD libraries were screened against the NapA$_{SP}$ variants (R6Q, K10Q and A17Q) known to be impaired in binding native NapD, as well as the M9Q variant. The *E. coli* reporter strain BTH101 (Δ*cya*) was therefore co-transformed with plasmids encoding either NapA$_{SP}$ R6Q-T18, NapA$_{SP}$ M9Q-T18, NapA$_{SP}$ K10Q-T18, and NapA$_{SP}$ A17Q-T18 together with the pT25-NapD-based mutant libraries. Positive interactions between NapD suppressors and NapA$_{SP}$ variants were visualized as red colonies on MacConkey-maltose indicator plates (Figure 3.4). Overall, 40 suppressors were isolated that, following isolation and re-transformation, consistently formed red colonies on MacConkey-maltose plates (Table 3.1 – 3.3).

The screen against NapA$_{SP}$ R6Q resulted in a total of 25 suppressors that could apparently interact with this normally defective signal peptide (Table 3.1). However, when the 'specificity' of each newly-isolated suppressor was tested by BTH against other glutamine-substituted NapA variants (M9Q, K10Q and A17Q) it became clear that none of the 25 suppressors were specific for the R6Q substitution (Table 3.1). It is possible

that this screen has isolated variant NapD proteins with a generally enhanced affinity for the NapA signal peptide.

Bait: NapA$_{SP}$-T18	Prey: T25-NapD mutant #	Testing T25-NapD mutants for specificity versus NapA$_{SP}$-T18 variants				
		native	R6Q	M9Q	K10Q	A17Q
R6Q	1	orange	gray	green	orange	orange
	2	orange	gray	orange	orange	orange
	3	orange	gray	orange	orange	orange
	4	orange	gray	orange	orange	orange
	5	orange	gray	orange	orange	orange
	6	orange	gray	orange	orange	orange
	7	orange	gray	orange	orange	orange
	8	orange	gray	orange	orange	orange
	9	orange	gray	green	orange	green
	10	orange	gray	green	orange	green
	11	orange	gray	orange	orange	orange
	12	orange	gray	orange	orange	orange
	13	orange	gray	orange	orange	orange
	14	orange	gray	green	orange	orange
	15	orange	gray	orange	orange	orange
	16	orange	gray	green	orange	orange
	17	orange	gray	orange	orange	orange
	18	orange	gray	orange	orange	orange
	19	orange	gray	green	orange	orange
	20	orange	gray	orange	orange	orange
	21	orange	gray	orange	orange	orange
	22	orange	gray	orange	green	green
	23	orange	gray	orange	orange	green
	24	orange	gray	orange	orange	green
	25	orange	gray	orange	green	green

Table 3.1 Screening NapD suppressor mutants for their specificity to NapA$_{SP}$ R6Q by bacterial two-hybrid. *E. coli* BTH101 cells were co-transformed with pT25 producing isolated NapD variants from the *napD* mutant libraries and pT18 with individual NapA$_{SP}$ variants. Colonies were grown on MacConkey indicator plates containing 1% maltose. Positive interactions are indicated in the table by an orange box. Non-interacting combinations are shown in green.

The screen against NapA$_{SP}$ M9Q resulted in no suppressors whatsoever, which is most probably further proof that the NapA$_{SP}$ M9Q-T18 fusion is unstable and actually a 'false negative'.

Bait:	Prey:	Testing T25-NapD mutants for specificity				
NapA$_{SP}$-T18	T25-NapD mutant #	*versus* NapA$_{SP}$-T18 variants				
		native	R6Q	M9Q	K10Q	A17Q
K10Q	1**	🟧	🟩	🟩	▓	🟩
	2	🟧	🟧	🟧	▓	🟧
	3	🟧	🟧	🟧	▓	🟧

Table 3.2 Screening NapD suppressor mutants for their specificity to NapA$_{SP}$ K10Q by bacterial two-hybrid. *E. coli* BTH101 cells were co-transformed with pT25 producing isolated NapD variants from the *napD* mutant libraries and pT18 with individual NapA$_{SP}$ variants. Colonies were grown on MacConkey indicator plates containing 1% maltose. Positive interactions are indicated in the table by an orange box. Non-interacting combinations are shown in green. Specific binding of NapD variants to NapA signal peptide K10Q are tagged with asterisks (**).

The screen against the NapA K10Q signal peptide identified only three suppressors able to re-bind this signal peptide (Table 3.2). In this case, however, one of the suppressors (#1** - Table 3.2) was unable to interact with the R6Q, M9Q or A17Q variants of the NapA signal peptide and so was considered specific for the K10Q substitution. Sequence analysis revealed four NapD mutations: S9G, I22T, V36I and G68S were present in the product of the #1** clone (Figure 3.5). It should be noted that two of these residues (S9 and V36) had been implicated by Maillard and co-workers (2007) in NapA signal peptide binding.
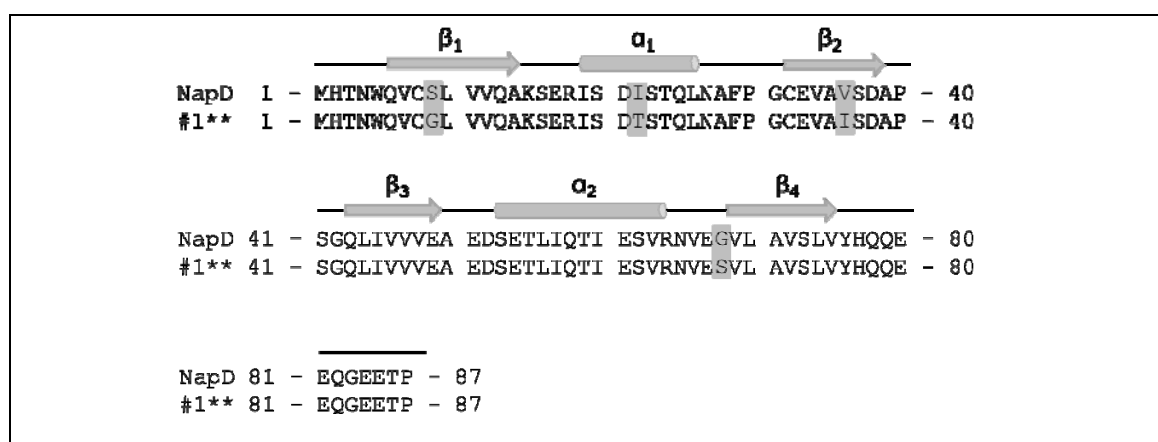
Figure 3.5 Sequence alignment and secondary structure of NapD and mutant suppressor #1 for NapA$_{SP}$ K10Q.** Mutations are highlighted in grey. The alignment programme ClustalW was used.

Finally, the screen against the NapA$_{SP}$ A17Q signal peptide identified 12 suppressors apparently able to re-bind this signal peptide *in vivo* (Table 3.3). Here, three of the suppressors (#2**, #9**, and #11** - Table 3.3) were highly specific for the A17Q substitution (Table 3.3) and sequencing of the mutant *napD* genes gave following amino acid substitutions in the gene products:

- #2**   I19F
- #9**   A14T and A71T

▪ #11**   I19F and T59I

Bait: NapA$_{SP}$-T18	Prey: T25-NapD mutant #	Testing T25-NapD mutants for specificity versus NapA$_{SP}$-T18 variants				
		native	R6Q	M9Q	K10Q	A17Q
A17Q	1	orange	green	green	orange	grey
	2**	orange	green	green	green	grey
	3	orange	orange	green	green	grey
	4	orange	orange	green	green	grey
	5	orange	orange	orange	orange	grey
	6	orange	orange	green	orange	grey
	7	orange	orange	green	green	grey
	8	orange	orange	green	green	grey
	9**	orange	green	green	green	grey
	10	orange	orange	orange	orange	grey
	11**	orange	green	green	green	grey
	12	orange	green	orange	green	grey

Table 3.3 Screening NapD suppressor mutants for their specificity to NapA$_{SP}$ A17Q by bacterial two-hybrid. *E. coli* BTH101 cells were co-transformed with pT25 producing isolated NapD variants from the *napD* mutant libraries and pT18 with individual NapA$_{SP}$ variants. Colonies were grown on MacConkey indicator plates containing 1% maltose. Positive interactions are indicated in the table by an orange box. Non-interacting combinations are shown in green. Specific binding of NapD variants to NapA signal peptide A17Q are tagged with asterisks (**).

From Figure 3.6 it can be seen that the mutations are localized at either the N- or C-terminal regions of NapD. Surprisingly, the NapD I19F substitution was isolated twice by the suppressor screen, suggesting immediately that this was possibly an important residue in signal peptide recognition. These suppressors were chosen for further *in vitro* analysis to establish their role in NapA$_{SP}$ A17Q binding.
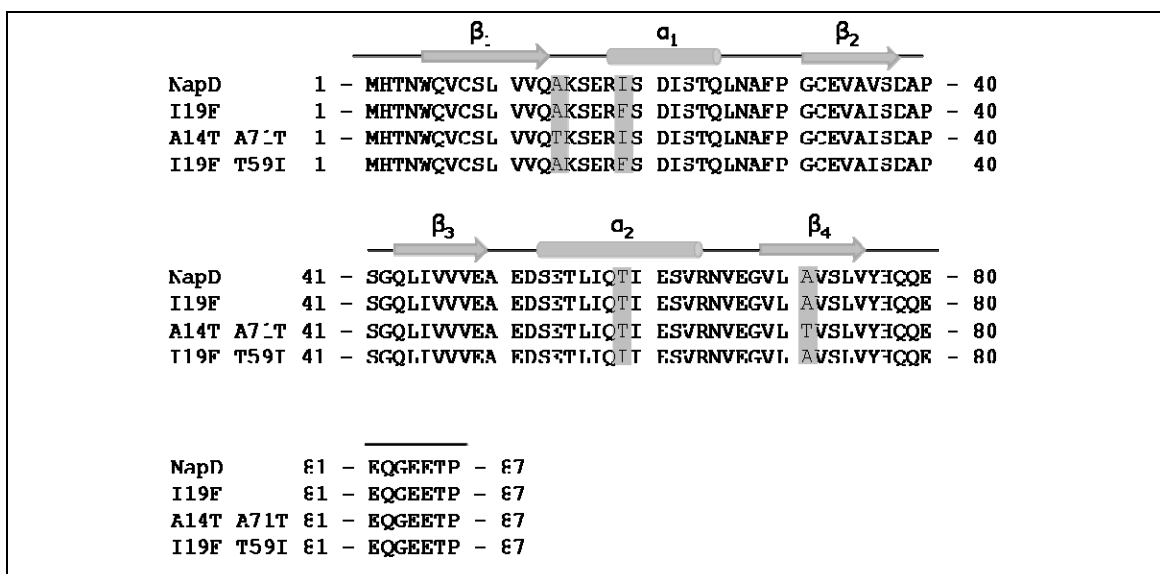
Figure 3.6 Alignment and secondary structure of NapD and NapA$_{SP}$ A17Q suppressors. Amino acid substitutions are framed with grey boxes. The alignment programme ClustalW2 was used.

3.2.4 Verification of *napD* suppressor binding to NapA A17Q by ITC

As outlined in Chapter 2, it is important to verify any BTH experiments with a secondary *in vitro* assay. Here, we turned again to ITC and so constructed *napD* overexpression vectors that would encode six different NapD variants: the I19F (suppressor #2**) single substitution; the A14T A71T (suppressor #9**) and I19F T59I (suppressor #11**) double substitutions; and the A14T, T59I, and A71T single substitutions. Each variant was then purified and tested for signal peptide binding *in vitro* against native MalE-NapA$_{SP}$ and its A17Q variant by ITC (Table 3.4).

(A) MalE::NapA$_{SP}$ A17Q/NapD A14T A71T
(B) MalE::NapA$_{SP}$ A17Q/NapD A14T
(C) MalE::NapA$_{SP}$ A17Q/NapD A71T
(D) MalE::NapA$_{SP}$ A17Q/NapD I19F T59I
(E) MalE::NapA$_{SP}$ A17Q/NapD I19F
(F) MalE::NapA$_{SP}$ A17Q/NapD T59I
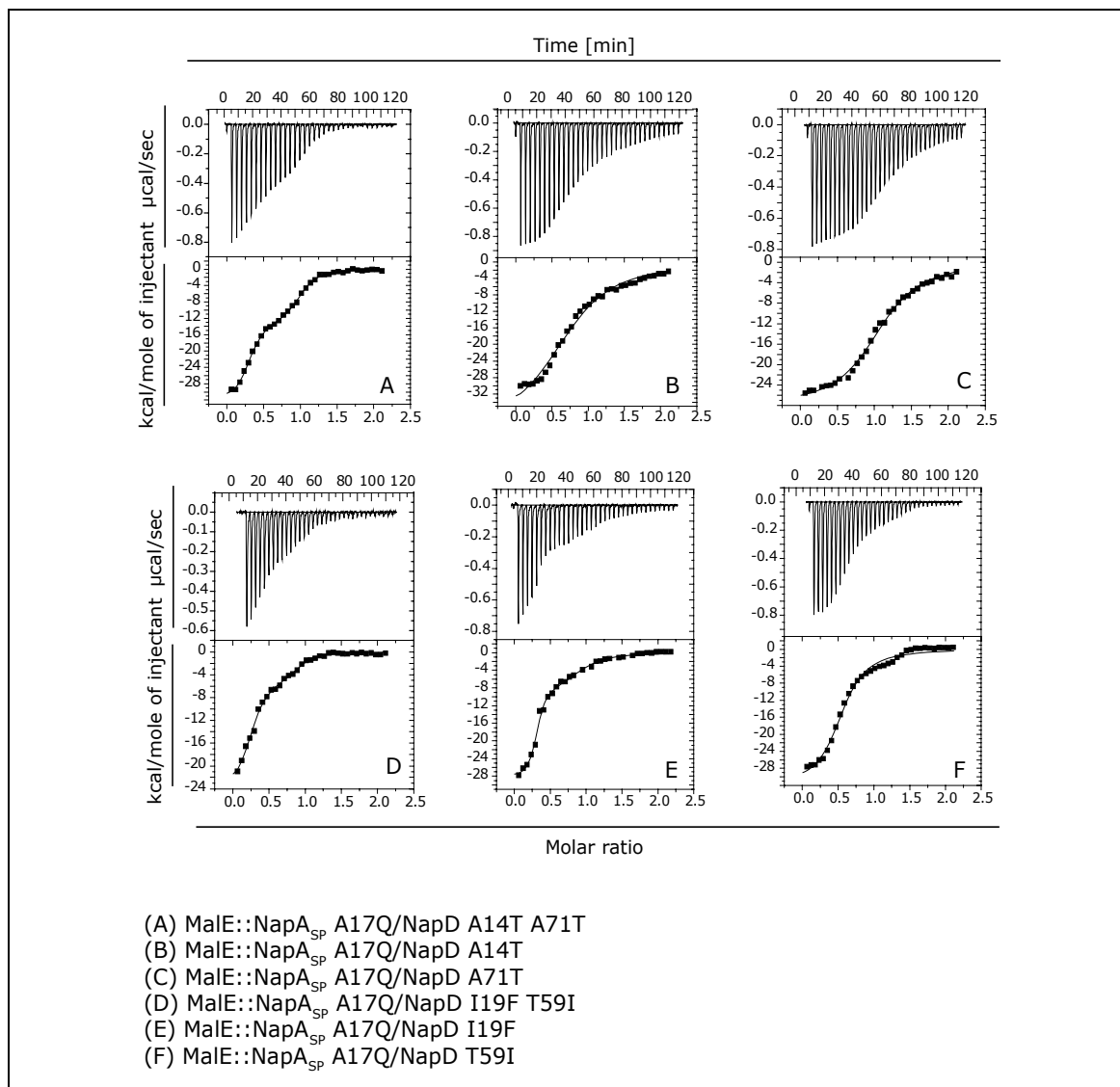
Figure 3.7 *In vitro* binding analysis of NapD suppressor mutants and NapA signal peptide variant A17Q. Shown are ITC graphs of NapD suppressors A14T A71T (A), A14T (B), A71T (C), I19F T59I (D), I19F (E) and T59I (F) with MalE-NapA$_{SP}$ variant A17Q.

As shown in Chapter 2, NapD binds the NapA signal peptide in bi-phasic manner with a relatively low (3 nM) and a higher (143 nM) dissociation constant (K_D). Titration of native NapD against MalE-NapA$_{SP}$ A17Q resulted in a single binding event with an apparent K_D of 1.1 µM. In contrast here, when suppressor #2** (NapD I19F) was titrated against

MalE-NapA$_{SP}$ A17Q this resulted in a bi-phasic binding with a relatively low (14 nM) and a higher (704 nM) dissociation constant (K_D) (Figure 3.7C, Table 3.2). These data suggest strongly that a single I19F substitution in NapD is sufficient to restore binding to the NapA A17Q signal peptide.

The #9** suppressor (NapD A14T A71T) was also isolated and titrated against MalE-NapA$_{SP}$ A17Q (Figure 3.7A, Table 3.4) in the calorimeter. This resulted in a bi-phasic binding curve (Figure 3.7A) with a relatively low (12 nM) and a higher (218 nM) dissociation constant (K_D) (Table 3.4), which is broadly similar to that seen for the native interaction (Chapter 2). As there were multiple amino acid substitutions in suppressor #9**, the corresponding single substitutions were also purified. Interestingly, the NapD A14T variant was essentially incapable of binding to the native NapA signal peptide, or the NapA A17Q variant, with characteristics anything like those previously described: when titrated against MalE-NapA$_{SP}$ A17Q a single binding event was observed with an apparent K_D of ~2 μM (Table 3.4). Similarly, the single A71T NapD variant bound MalE-NapA$_{SP}$ A17Q with single binding event and an apparent K_D of 833 nM (Figure 3.7C, Table 3.4). Thus, it appears that a combination of both A14T and A71T is necessary to restore native-like binding of NapD to the A17Q variant signal peptide.

Finally, the #11** suppressor (NapD I19F T59I) was isolated and titrated against MalE-NapA$_{SP}$ A17Q (Figure 3.7 D, Table 3.4). This too resulted in a bi-phasic binding curve with a relatively low (22 nM) and a higher (261 nM) dissociation constant (K_D) (Table 3.4), again similar to that seen for that observed for both native interaction (Chapter 2) and the interaction of the single substitution, I19F – suppressor #2**. In this case the second amino acid substitution (T59I) does not contribute very much to the binding event: the NapD T59I single variant was isolated and titrated against MalE-NapA$_{SP}$ A17Q. In this case only single binding event was observed (Figure 3.7F) with an apparent K_D of 633 nM (Table 3.4).

Taken together, these experiments have identified an I19F single substitution and an A14T A71T double substitution as being sufficient to restore binding of NapD both *in vivo* and *in vitro* to the A17Q variant NapA signal peptide.

NapD variant	NapA$_{SP}$ variant	analysis		N value			K$_D$ [nM]		
native	native	two sets of sites	pop. 1	0.35	+/-	0.02	3	+/-	1
			pop. 2	0.64	+/-	0.02	143	+/-	29
	A17Q	one set of sites	pop. 1	0.16	+/-	0.03	1,100	+/-	193
			pop. 2	0.84				∞	
A14T A71T (#9)	A17Q	two sets of sites	pop. 1	0.69	+/-	0.01	218	+/-	28
			pop. 2	0.30		0.01	12	+/-	2
	native	one set of sites		0.91	+/-	0.01	571	+/-	26
A14T	A17Q	one set of sites		0.80	+/-	0.02	1,869	+/-	216
	native	one set of sites	pop. 1	0.70	+/-	0.01	763	+/-	92
			pop. 2	0.30				∞	
A71T	A17Q	one set of sites		1.11	+/-	0.01	833	+/-	60
	native	one set of sites		0.83	+/-	0.01	313	+/-	25
I19F (#2)	A17Q	two sets of sites	pop. 1	0.29	+/-	0.10	14	+/-	6
			pop. 2	0.62	+/-	0.06	704	+/-	312
	native	one set of sites		0.97	+/-	0.01	806	+/-	71
I19F T59I (#11)	A17Q	two sets of sites	pop. 1	0.65	+/-	0.04	261	+/-	107
			pop. 2	0.25	+/-	0.01	22	+/-	8
	native	one set of sites	pop. 1	0.39	+/-	0.02	935	+/-	142
			pop. 2	0.61				∞	
T59I	A17Q	one set of sites	pop. 1	0.57	+/-	0.01	633	+/-	84
			pop. 2	0.43				∞	
	native	one set of sites		0.81	+/-	0.01	328	+/-	40

Table 3.4 Isothermal titration calorimetry of NapD suppressor mutants. Two subpopulations of each NapD variant (pop. 1 and pop. 2) bind to the different NapA signal peptide variations. For infinite binding constants second N values are estimated and coloured in grey.

3.2.5 Physiological activity of the *napD* suppressors

Given that the introduction of the *napA* A17Q mutation onto the chromosome at the native *nap* locus resulted in a strain that had clearly reduced periplasmic nitrate reductase activity (Chapter 2, Figure 2.8), it was investigated here whether the newly-discovered suppressors could restore full physiological NapA activity to the mutant strain. *E. coli* strain SGQ171 (as LCB2048, *napA* A17Q) was transformed with pT25-NapD-based plasmids and the *in vivo* nitrite production assay carried out (Figure 3.8). The SGQ171 (*napA* A17Q) strain characteristically produces nitrite after a long lag-phase of around 3 hours (Figure 3.8). None of the three identified suppressors were able to dramatically increase the degree of nitrate reduction exhibited by this strain (Figure 3.8). Perhaps a slight enhancement in nitrite production could be observed induced by the #11 suppressor (I19F, T59I), however following statistical analysis this proved to be not significant. Note, however, that strain SGQ171 still produces endogenous NapD.

Although native NapD should not interact with NapA$_{SP}$ A17Q, it is conceivable that this protein is interfering, or competing, with some aspect of the assembly process.

In order to address this point, as well as issues raised in the Discussion Section of Chapter 2, a new strain was constructed called LP203$_S$ that, beside the chromosomal codon change for *napA* A17Q, also carries an in-frame deletion of *napD*. This strain (LP203$_S$) was found to be completely devoid of any NapA activity (data not shown). Moreover, nitrate reductase activity could not be restored by any of the *napD* suppressor mutants either (data not shown). Clearly, then, the *napD* suppressor mutants can bind the NapA A17Q signal peptide both *in vivo* and *in vitro* but are apparently devoid of any physiological activity.
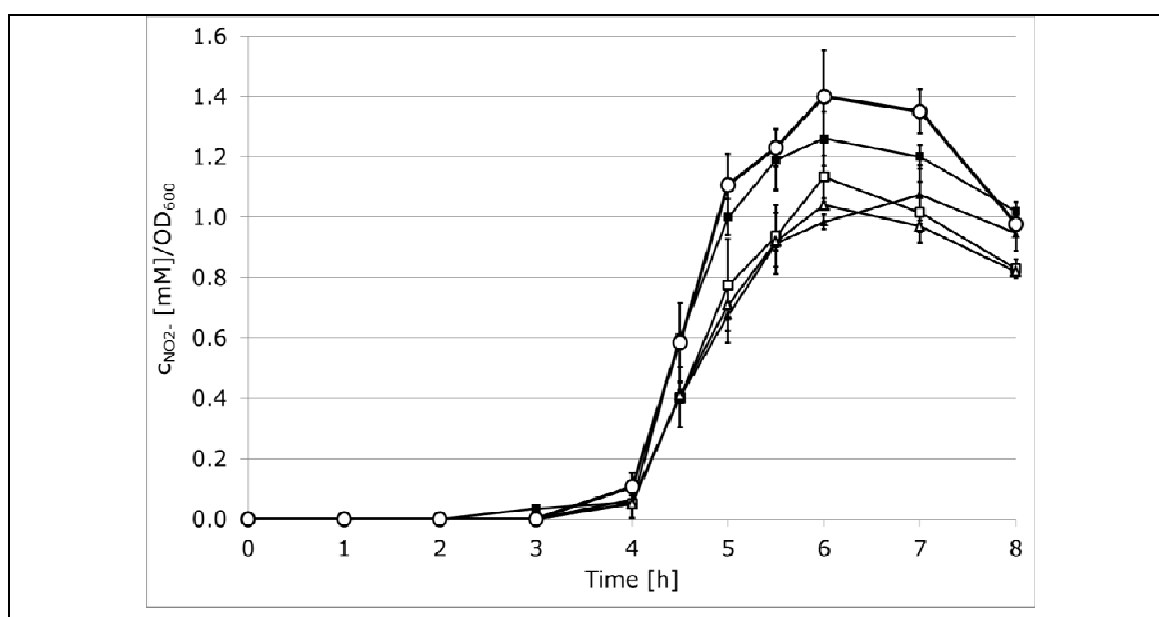
Figure 3.8 Testing for enhanced Tat transport of NapA A17Q by different NapD mutants. *E. coli* strain SGQ171 (NapA A17Q) was transformed with plasmid pT25-NapD or its deduced NapD mutants. Nitrite production was measured in vivo as described in Material & Methods. Strain SGQ171 and transformants are labelled as followed: SGQ171 (■), SGQ171/NapD (▲), SGQ171/NapD #2 (Δ), SGQ171/NapD #9 (□), SGQ171/NapD #11 (○).

3.3 Discussion

3.3.1 Identification of protein-protein interactions using suppression genetics

Genetic suppression is a powerful tool to identify novel functional interactions. There second mutations, which restore function of a protein, are either found on the same gene or on the gene of a binding partner. This either causes new binding sites between both proteins or enables previous sites of interaction to rebind (Sujatha & Chatterji, 2000). Suppression genetics is not only applicable to single-celled organisms such as bacteria or yeast, but is also used for multicellular organisms, e.g. *Caenorhabditis elegans*, *Drosophila melanogaster* and mammalian cells (Dixon et al, 2009).

57

Furthermore, if the structure of a protein complex is known, computational predictions can be made on the roles of mutations that either interrupt binding or restore binding (Sammond et al, 2010).

In bacteria many components and binding partners of protein and membrane assembly pathways have been discovered based on genetic suppressors. For example, to characterise the Sec pathway C-terminal β-galactosidase fusions to either MalE or the maltoporin LamB (λ receptor protein) have been used, where β-galactosidase, because of its folded conformation, jams the Sec translocon after transport is initiated. This causes a lethal maltose-sensitive phenotype. Furthermore, because β-galactosidase is unable to form a homotetramer the enzyme remains inactive and the cells are therefore Lac⁻. These two phenotypes were used to isolate mutations in the Sec signal peptide that prevented export of the fusion proteins and subsequently suppressor mutations were identified in genes encoding the Sec translocon components SecY, SecE and SecA, and the auxiliary components SecB, SecD and SecF (Bieker & Silhavy, 1990).

Recently, the binding between LptE and LptD, proteins believed to participate in the last step of LPS (lipopolysaccharide) insertion into the outer membrane (OM) of Gram-negative bacteria, was also explored by suppression genetics. An LptE mutant was isolated that displayed sensitivity to the antibiotic rifampicin due to increased permeability of the OM. Sequencing revealed a six base pair deletion in *lptE* that resulted in defective binding of LptE to LptD. Suppressor mutants identified through spontaneous resistance to the antibiotic bacitracin were identified in *lptD*, and also in *bamA*, an essential component of the Bam machinery for assembly of β-barrel outer membrane proteins (Chimalakonda et al, 2010).

3.3.2 Suppression mutations in *napD* enable binding to different NapA variants

The purpose of this part of the study was to identify new residues and important structural features of the proofreading chaperone NapD involved in binding to the NapA signal peptide. A genetically engineered random *napD* mutant library was constructed and screened for suppressors able to re-bind variant NapA signal peptides. Notably, none of the isolated suppressors impaired binding of the resultant variant NapD proteins to the native NapA signal peptide. Three mutants that would encode variant chaperones capable of rebinding NapA$_{SP}$ A17Q were chosen for further characterisation and that were the A14T A71T, I19F and I19F T59I NapD proteins. Further *in vitro* interaction studies confirmed that double substitutions of A14T A71T, or a single substitution of I19F, were sufficient to restore binding of NapD to NapA$_{SP}$ A17Q.

I19F was independently identified twice in this work and is therefore strong proof for the importance of NapD I19 in signal peptide binding. Surprisingly, however, I19 is found within the first α-helix of NapD (Figure 3.2 and 3.9), which was previously thought to not take part in signal peptide binding (Maillard et al, 2007). This suggests that at least the first α-helix may exert global control on conformational changes in the β-sheet face during peptide binding.
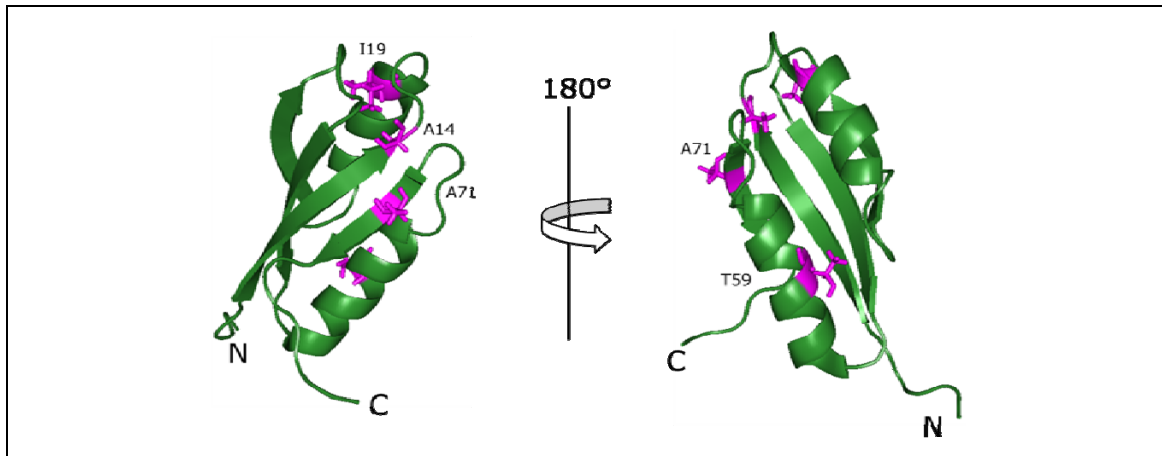
Figure 3.9 Positions of suppressor mutations on NapD for NapA signal peptide variant A17Q. Identified residues from NapD mutant suppressor screen are highlighted in magenta and labelled with their individual positions. For clarity parts of the C-terminus have been removed. (PDB ID code 2jsx)

Importantly, none of the three NapD variants tested were able to rescue full nitrate reductase activity of a *napA* A17Q strain *in vivo*. This would suggest that NapA recognition and transport by the Tat complex is not dependent on signal peptide binding to NapD. Furthermore, it possibly shows that NapA signal peptide residue A17 has a bi-functional role for (i) interaction with NapD during NapA maturation and (ii) binding to the translocase prior export.

Interestingly, a Δ*napD*, *napA* A17Q strain was completely devoid of nitrate reductase activity. This suggests immediately that the residual nitrate reductase present in the *napA* A17Q strain (Chapter 2) is completely dependent upon native NapD and that the suppressor mutants identified here are physiologically inactive, since they cannot complement the Δ*napD*, *napA* A17Q strain. The question therefore remains as to exactly how NapD contributes to the biosynthesis of NapA. It is possible that NapD, even when bound to the signal peptide, has an influence on the mature part of NapA during cofactor insertion, for instance in inducing a 'cofactor-competent state' for the enzyme as hypothesized for the TorD-TorA system (Pommier et al, 1998). To address this, performing a second genetic screen could identify *napD* mutants able to restore NapA activity to the Δ*napD*, *napA* A17Q strain. Here, transformants of strain LP203$_S$ (Δ*napD*, *napA* A17Q) containing the *napD* mutant library would be grown under anaerobic

conditions on minimal media plates supplemented with nitrate. Thus clones that regained the ability to reduce nitrate could be quickly identified.

A broadly similar story as for NapA A17Q was recently told for the cAMP-dependent protein kinase (PKA) from *Saccharomyces cerevisae*. This enzyme consists of two catalytic subunits and two regulatory subunits. A mutant screen revealed an F327A substitution located within the adenosine binding pocket of the catalytic subunit and causes severe growth defects*. In vitro* analysis confirmed a significant decrease in catalytic activity of this variant (Kennedy et al, 2009). Subsequent screening of a suppressor mutant library identified substitution K285P within the catalytic subunit, which was apparently able to restore PKA-dependent growth *in vivo*. Interestingly, however, further biochemical analysis of the new K285P F327A double mutant showed that K285P mutation actually was still not able to restore the activity of the catalytic subunit *in vitro*. Instead it caused reduced binding of the regulatory subunit *in vivo*, thus allowing a very low PKA activity, which was sufficient to restore cell viability (Yang et al, 2009).

Conversely, the identified *napD* mutants were not able to restore NapA activity in variant A17Q *in vivo*, but apparently altered binding affinity to the Tat signal peptide both *in vivo* and *in vitro*.

Further work in this Chapter, not further pursued because of time constrains, involved the identification of *napD* mutant suppressor #1** for NapA$_{SP}$ K10Q. This suppressor encodes a variant NapD protein including two amino acid substitutions at S9G and V36I. Very interestingly, these positions were previously implicated in signal peptide binding during the original NMR study (Maillard et al, 2007).

Finally, the impact of the flexible C-terminus of NapD in NapA activity was investigated further as its deletion was previously shown to reduce nitrite production *in vivo* (Maillard et al, 2007). However, our extensive mutagenesis studies of the NapD C-terminal tail did not lead to any new insights into its role in NapA maturation.

In summary, this Chapter has identified new residues within NapD that are involved in the NapA$_{SP}$ binding event, including a hitherto unexpected role for the first α-helix of the NapD chaperone.

4 Structural studies on NapA and its Tat signal peptide

4.1 INTRODUCTION

Structural studies are the key to fully understanding the mechanism of interplay between proofreading chaperones and their Tat substrates. To this end, several 3D structures of individual Tat chaperones from different organisms have been solved, resulting in the recognition of a surprisingly wide variety of different architectures for these proteins.

TorD and DmsD, two Tat chaperones involved in controlling assembly of TMAO reductase (TorA) and DMSO reductase (DmsAB), respectively, show novel all-helical structures comprising ~10 α-helices that assemble into two domains (Figure 4.1A and 4.1B). The crystal structure of *Sh. massilia* TorD was surprising, however, as it revealed TorD could exist as a domain-swapped homodimer (Tranier et al, 2003). On the other hand, both *E. coli* and *Salmonella* DmsD homologues are monomeric (Ramasamy & Clemons, 2009; Stevens et al, 2009). Both TorD and DmsD have been convincingly shown to bind directly to twin-arginine signal peptides.

Two other proteins, HyaE and HybE, suggested to be Tat proofreading chaperones for *E. coli* hydrogenase-1 and hydrogenase-2, respectively (Dubini & Sargent, 2003) show very distinct structures unrelated to TorD and DmsD. The structures of these proteins were modelled by high-resolution multi-dimensional solution NMR data. HyaE adopts a thioredoxin-like fold (Figure 4.1C), despite not containing any cysteine residues whatsoever (Parish et al, 2008). In contrast, HybE adopts a novel fold described as a 'three layer sandwich fold' with two α-helices flanking a six-stranded β-sheet (Figure 4.1D) (Shao et al, 2009). The evidence for direct signal peptide binding by these chaperones is not strong. However, far-Western analysis of the *Ralstonia eutropha* HyaE homologue HoxO suggests this protein can interact with a hydrogenase Tat signal peptide (Schubert et al, 2007).

The FdhE protein was shown to interact with the catalytic subunits of the respiratory formate dehydrogenases FdnGHI and FdoGHI, and an *E. coli fdhE* mutant was shown to be deficient in formate dehydrogenase activity (Lüke et al, 2008; Mandrand-Berthelot et al, 1988). It was suggested that in the case of FdnG the accessory protein FdhE binds a region that comprises the C-terminal part of the Tat signal peptide and parts of the surrounding mature region (Chan et al, 2010), though it should be noted that there is no experimental evidence for this statement. The crystal structure of *Pseudomonas* FdhE shows a mostly helical protein with two domains containing three non-haem iron ions (Figure 4.1E). Indeed, EPR analysis of *E. coli* FdhE confirmed the protein was a rubredoxin (Lüke et al, 2008). The role of the iron in this accessory protein is unknown,

but mutations that prevented iron binding or redox cycling inactivated the protein (Lüke et al, 2008).
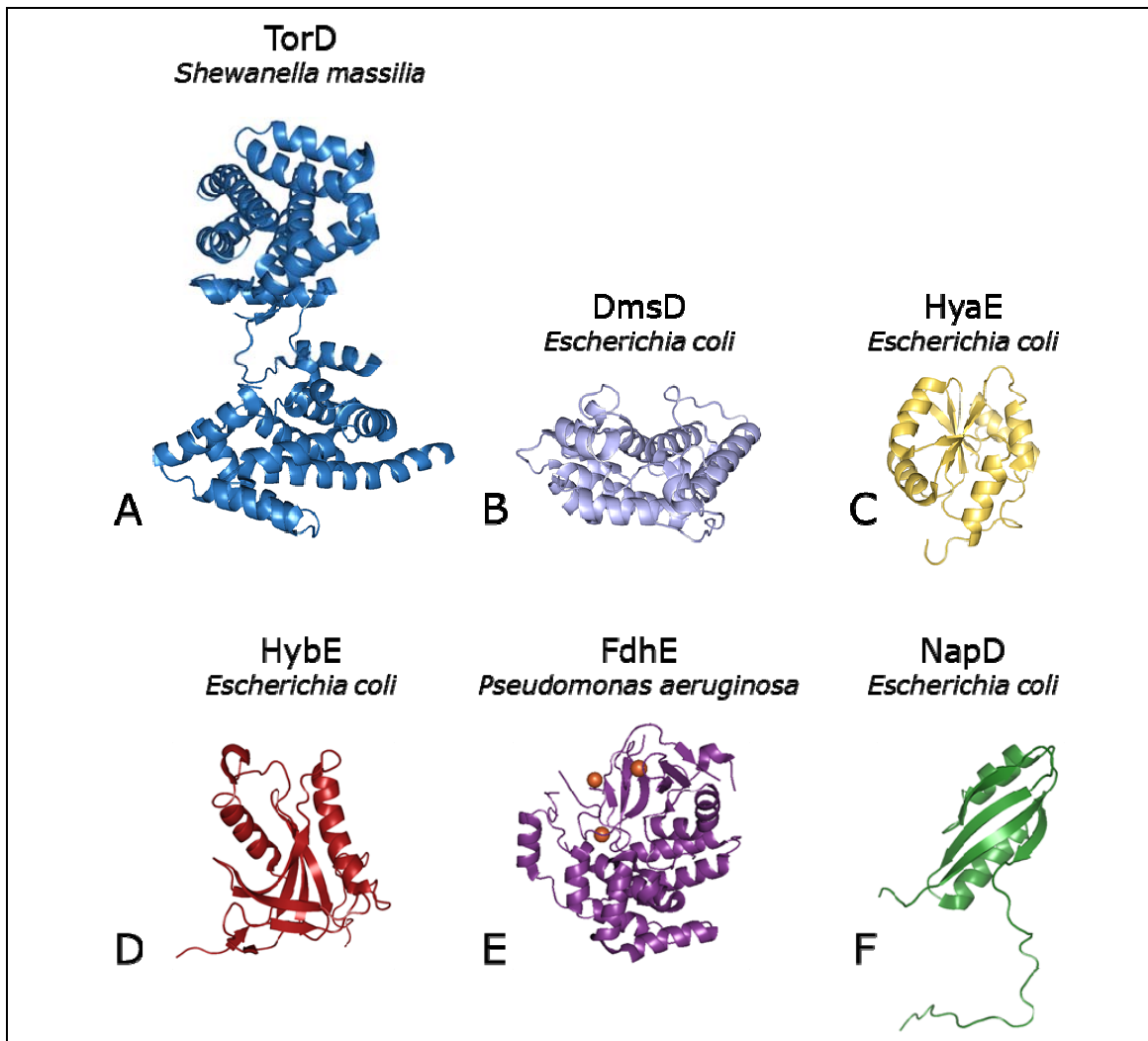
Figure 4.1 Proofreading chaperones show a great structural variety. All structures except for TorD and FdhE are from *E. coli*. (A) *Sh. massilia* TorD adopts an all-helical architecture and exists as a domain swapped dimer (PDB ID code 1n1c). (B) DmsD from the same family as TorD consists of helices, but is monomeric (PDB ID code 3cw0). (C) HyaE shows a thioredoxin-like fold (PDB ID code 2hfd). (D) In HybE two helices imbed a six β-sheet face (PDB ID code 2kc5). (E) FdhE from *P. aeruginosa* contains irons (brown spheres) and belongs to the family of rubredoxins (PDB ID code 2fiy). (F) NapD shows a ferredoxin-like fold (PDB ID code 2jsx).

The proofreading chaperone NapD further contributes to the structural diversity of bacterial Tat chaperones. So far it is the only type that has a ferredoxin-like structure with a β-α-β-β-α-β fold (Figure 4.1F; Maillard et al., 2007). In this case, however, some structural analysis of the signal peptide-chaperone interaction has been studied by 2D NMR spectroscopy. HSQC experiments were performed by titrating unlabelled NapA signal peptide into a sample of ^{15}N-labeled NapD in the NMR spectrometer. The resultant data showed that the cross-peaks of residues corresponding to the β-sheet face of NapD are most obviously shifted upon signal peptide binding. This gave initial strong evidence that the β-sheet face of NapD is directly involved in signal peptide recognition (Maillard

et al, 2007). In addition, work in this thesis has now established that one of the two α-helices of NapD also has an important, possibly indirect, role in NapA signal peptide recognition (Chapter 3).

In 2007, the crystal structure of the periplasmic nitrate reductase (NapA) from *E. coli* was solved (Figure 4.2; Jepson et al, 2007). It shows the mature part of NapA and its two cofactors; a [4Fe-4S] cluster and a Mo-*bis*-MGD cofactor. NapA exists in the periplasm as a heterodimer together with NapB, a dihaem *c*-type cytochrome electron transferring partner subunit. However, *E. coli* NapA was purified without NapB due to the relatively weak binding affinity between the two proteins (Jepson et al, 2007). This is in contrast to available structures of the periplasmic nitrate reductases from *R. sphaeroides* and, very recently, *Cupriavidus necator*, where NapAB purifies as an extremely stable complex (Arnoux et al, 2003; Coelho et al, 2011). Clearly, these structures represent the mature, fully folded, periplasmic and enzymatically-active versions of NapA. The Tat signal peptides are not present and a NapD protein is not stably bound.
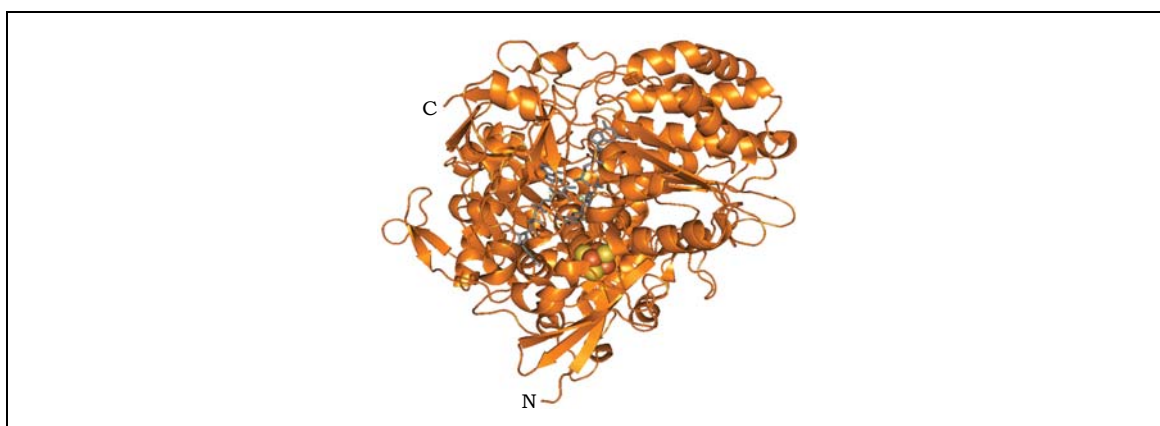
Figure 4.2 Crystal structure of *E. coli* NapA. Shown is the mature part with N- and C-terminus indicated. The [4Fe-4S] cluster is depicted as yellow and brown spheres. The Mo-*bis*-MGD cofactor is shown in ball and stick format and coloured in grey. (PDB ID code 2nya).

Several other structures of mature Tat substrates have been published, however so far no structure exists showing a complete precursor form (comprising twin-arginine signal peptide and mature part) in complex with a specific proofreading chaperone.

Attempts have been made to analyse the conformation of Tat signal peptides. The crystal structure of SufI, a cofactor-free Tat substrate, which apparently does not need a proofreading chaperone, was recently obtained (Tarry et al, 2009a). Here, SufI was found to missing the first 17 residues of its signal peptide, presumably due to non-specific proteolysis during preparation. The remaining 10 amino acids of the signal sequence showed a high degree of disorder (Tarry et al, 2009a). Prior to this it was shown that a synthesized SufI signal peptide was unstructured in an aqueous solution,

but adopted up to 40% helical conformation when placed in a more hydrophobic environment (San Miguel et al, 2003).

Furthermore, NMR studies on the precursor of HiPIP (high potential iron-sulphur protein) from *Allochromatium vinosum* indicated that the signal peptide forms no secondary structure *in vitro* (Kipping et al, 2003). Similar results regarding the Tat signal peptide were obtained for the crystal structure of full-length GFOR (glucose-fructose oxidoreductase) from *Zymomonas mobilis* (Nurizzo et al, 2001). Electron density for the signal peptide could not be assigned and it was therefore concluded that the N-terminus of GFOR was either very flexible or lacked any specific structure (Nurizzo et al, 2001). Taken altogether, it seems that Tat signal peptides commonly adopt no clearly defined secondary structure in their free state.

The objectives of this Chapter were to attempt to isolate and visualize the precursor form of NapA in complex with NapD, and to determine any structural changes of the NapA signal peptide during the chaperone binding event using different structural and biophysical approaches.

4.2 RESULTS

4.2.1 Towards a crystal structure for NapA in complex with NapD

The natural genetic organisation of the *E. coli nap* operon places the *napA* gene immediately downstream of *napD* (Figure 1.11). Thus a construct was made (pQE80-NapDA) in order to co-express *napDA* maintaining the natural translational coupling between the two genes. NapD was also N-terminally tagged with hexa-Histidine. *E. coli* MC4100 cells were transformed with the construct and *napDA* overexpressed under aerobic conditions (see Material & Methods). A crude extract was applied to an IMAC column and bound proteins eluted with an imidazole gradient. All eluted proteins were pooled and subjected to size exclusion chromatography (Figure 4.3). SDS-PAGE analysis of the eluted fractions possibly showed some co-elution of NapDA, but possibly in varying ratios of NapD to NapA (Figure 4.3). In addition large amounts of free NapD were identified (Figure 4.3). Subsequent pooling of the NapA-containing fractions followed by a second gel filtration step, resulted in further separation of the remaining NapD from NapA (data not shown). Taken together, this suggests NapD does interact with NapA in this system (otherwise the initial purification would not have been possible), but that the complex dissociates over time.
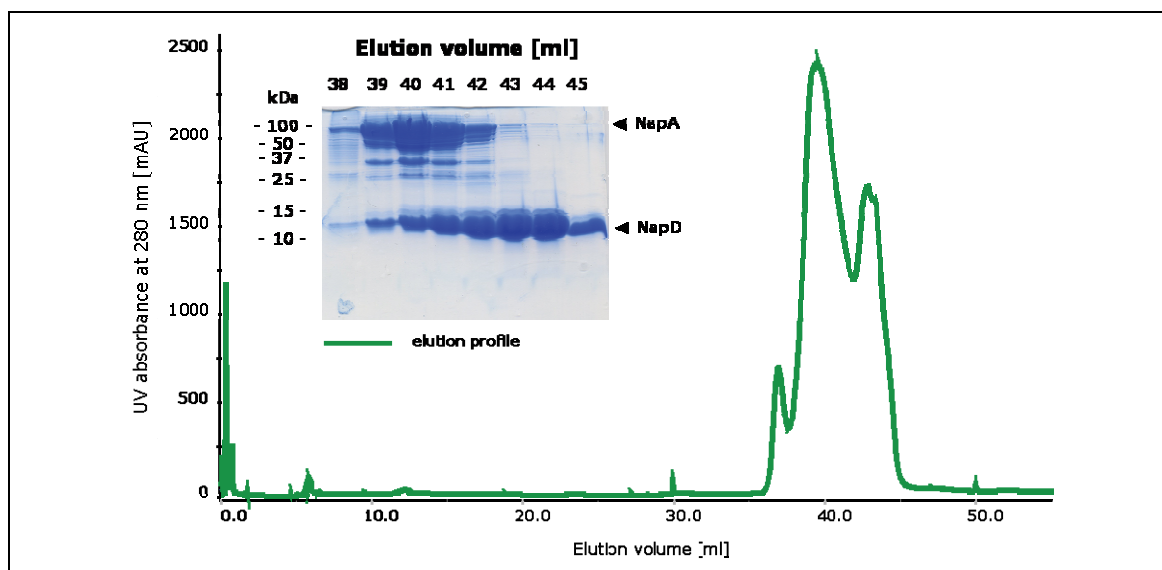
Figure 4.3 Elution profile of the NapDA complex. IMAC purified NapDA was pooled and concentrated to a volume of 500 µl using Vivaspin 20 columns (50,000 MCO PES). A Superdex75 column (GE Healthcare) was pre-equilibrated in 20 mM Tris-HCl, pH 7.6 and 250 mM NaCl. After loading of the NapDA protein sample fractions were collected and aliquots diluted in 1:1 Lämmli buffer followed by protein separation on a 15% SDS-PAGE.

During the purification process a deep brown colour was observed in the NapDA containing samples. Analysis by UV-Vis (ultraviolet-visible) absorption spectroscopy yielded a spectrum with a broad peak of an absorbance at ~420 nm, which is commonly indicative of iron-containing proteins and possibly suggests the presence of an [Fe-S] cluster (Figure 4.4). The spectral features were lost when the sample was reduced by the addition of excess sodium dithionite (Figure 4.4). If the sample was stored as-purified at 4°C a gradual loss of the brown colour could be observed (data not shown).

The crystal structure of mature, active, NapA contains a [4Fe-4S] cluster (Jepson et al, 2007). From the UV-Vis spectrum it is not possible to easily distinguish between an intact [4Fe-4S] or the oxidised breakdown product of this, which is usually a [3Fe-4S] cluster. However, EPR spectroscopy can usually easily distinguish between these two types of cofactor. Under oxidised conditions, a typical $[3Fe-4S]^+$ cluster has a distinctive EPR spectrum while a $[4Fe-4S]^{2+}$ cluster is EPR silent (Lubitz et al, 2007). When reduced by the addition of dithionite the $[4Fe-4S]^+$ cluster becomes detectible with a characteristic spectrum, while the $[3Fe-4S]^0$ cluster is EPR silent (Lubitz et al, 2007). In collaboration with Dr David J. Keeble (University of Dundee), low-temperature X-band EPR spectra were collected of the NapDA sample. The as-purified (presumably oxidised) sample did not show any distinctive features suggesting a [3Fe-4S] cluster is not present, however the reduced sample equally did not show any features of a [4Fe-4S] either (data not shown). A possible explanation could be found in a study carried out by Müllner and co-workers, where the histidine sensor kinase NreB from *Staphylococcus carnosus*, which also contains an EPR silent $[4Fe-4S]^{2+}$ cluster, was analysed (Müllner et

65

al, 2008). In this case the iron-sulphur cluster was reduced by dithionite however the reduced form was not stable and quickly degraded (Müllner et al, 2008). It is possible, therefore, that the [Fe-S] cluster bound by the NapDA complex is in a similar unstable form. In contrast, Jepson et al (2007) performed EPR analysis on purified mature NapA and obtained a strong signal for the reduced $[4Fe-4S]^+$ cluster, calculating one [4Fe-4S] cluster per NapA molecule. In addition, up to 90% total molybdenum in their fully mature and enzymatically-active NapA sample was detected (Jepson et al, 2007).
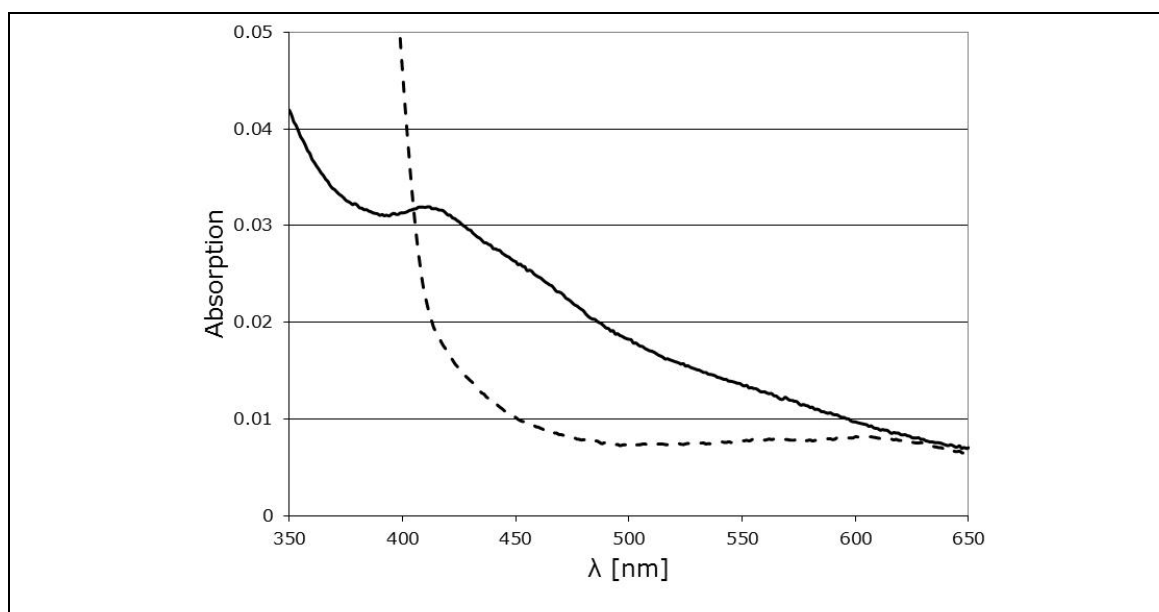
Figure 4.4 Spectrophotometrical analysis of a putative iron sulphur cluster in NapDA. Nickel infinity purified NapDA was diluted 1:100 in 20 mM Tris-HCl, pH 7.6, 250 mM NaCl, 2 mM DTT and 170 mM imidazole. The peak at ~420 nm is indicative for an iron sulphur cluster (solid line). Reduction of the protein sample was achieved by adding dithionate (dashed line). The increase in absorbance in the reduced sample is due to the added dithionate (Gibney et al, 1996).

Despite the evidence presented above that suggested the NapDA complex was heterogeneous (i.e. unstable binding between NapD and full-length NapA, and gradual loss of any possible cofactors) crystallisation trials were set up in co-operation with Prof William Hunter and Dr Alice Dawson, University of Dundee. However, perhaps unsurprisingly, no crystals were obtained.

4.2.2 Stabilizing the NapDA complex

In an attempt to artificially stabilise the binding between NapD and full length NapA for structural studies a covalent linker (L) region was introduced between NapD and NapA. The linker region had the sequence 'RSNLGIEGRPG', which contains a Factor Xa protease site, and was used to fuse the extreme C-terminus of NapD to the extreme N-terminus of the NapA Tat signal peptide.

First, it was important that the influence of the linker on physiological NapA activity was determined. Therefore, *E. coli* strain LCB2048 (*nap*[+]) was genetically modified such that

it carried the *napD-L-napA* fusion at the native *nap* locus on the chromosome (resulting in strain SGDLA10). An *in vivo* nitrite production assay showed that SGDLA10 (*napDLA*) retained some physiological nitrate reductase activity, but that this activity was reduced in comparison to the parent strain (Figure 4.5). A further deletion of the genes encoding the Tat translocase in the *napDLA* background (SGDLA11, *napDLA tat⁻*) was shown to completely block *in vivo* nitrate reduction, i.e. no nitrite was produced (Figure 4.5).
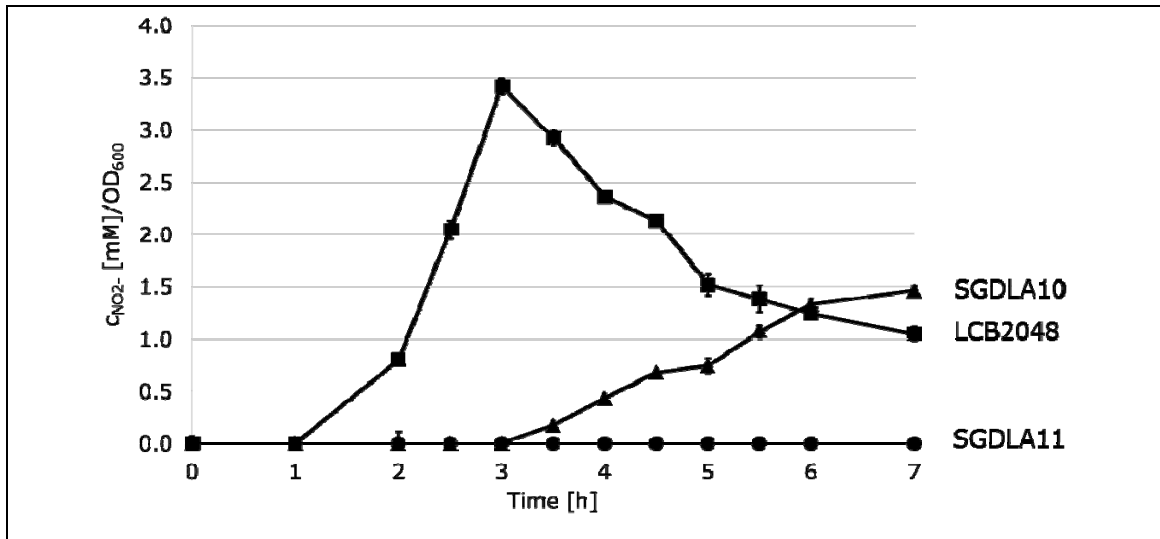
Figure 4.5 Chromosomal fusion of NapD to NapA shows Tat dependent nitrate reducing activity. *In vivo* nitrite production was measured as described in Figure 2.9 Strains are labelled as LCB2048 (*nap⁺*) (■), SGDLA10/NapDLA (▲) and SGDLA11/NapDLA (*tat⁻*) (●).

The artificial fusion between NapD and NapA therefore results in reduced NapA activity *in vivo*, but the activity that is present can be attributed to a properly assembled, periplasmic, Nap system.

Next, MC4100 cells were transformed with plasmid pET15-NapDLA and the NapDLA fusion was overproduced to a high level. A crude extract was then applied to an IMAC column and the NapDLA complex was observed to elute as a broad single peak (Figure 4.6A). SDS-PAGE analysis showed large overloaded bands corresponding to the NapDLA fusion, demonstrating that the fusion protein was stable to purification and water-soluble. However, several impurities and breakdown products were also evident (Figure 4.6B). The IMAC fractions containing NapDLA were pooled and adjusted to a stock concentration of 1 mg/ml. The solution molecular mass of this protein was then estimated using sedimentation velocity ultracentrifugation (performed as a service by Dr Mark Agacan, University of Dundee). The majority of the protein present has an apparent molecular mass of 102 kDa (Figure 4.6C), which correlates well with the predicted molecular mass of the NapDLA fusion (106,278 Da).
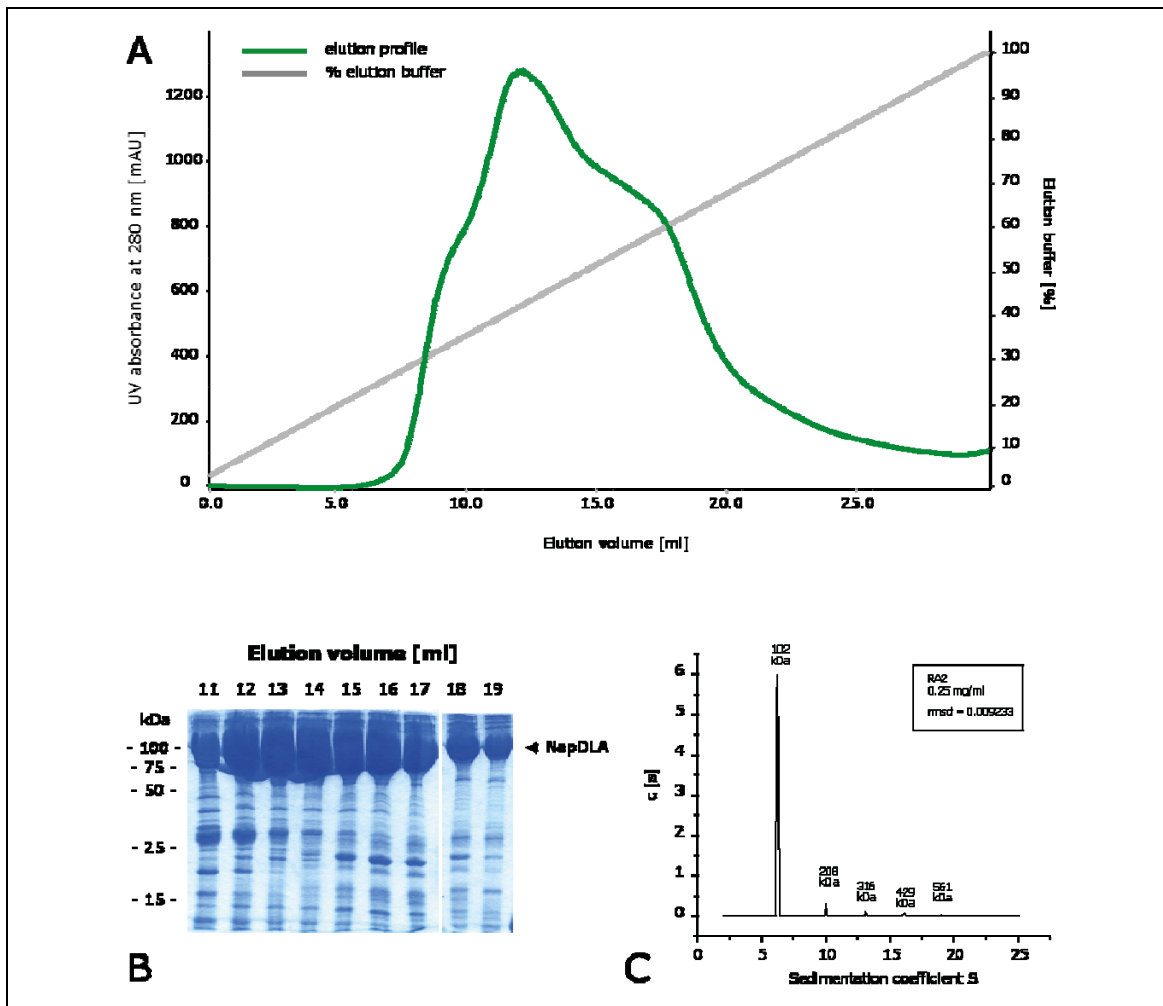
Figure 4.6 Mass determination of NapDLA. (A) Elution profile of NapDLA from a HisTrap™ HP column after applying a linear gradient of imidazole (0-500 mM). (B) To 10 µl of affinity purified NapDLA Lämmli sample buffer was added in a 1:1 ratio and proteins separated on a 10% SDS-PAGE. (C) The oligomeric state of NapDLA was determined by sedimentation velocity ultracentrifugation.

In the case of NapDLA, a deep brown colour was again observed during protein purification. Absorption spectroscopy revealed a spectrum containing a broad peak at ~420 nm, again indicating the presence of an [Fe-S] cluster (Figure 4.7). For the NapDLA protein, however, the brown colour was very stable over several weeks, when stored in solution at 4°C.
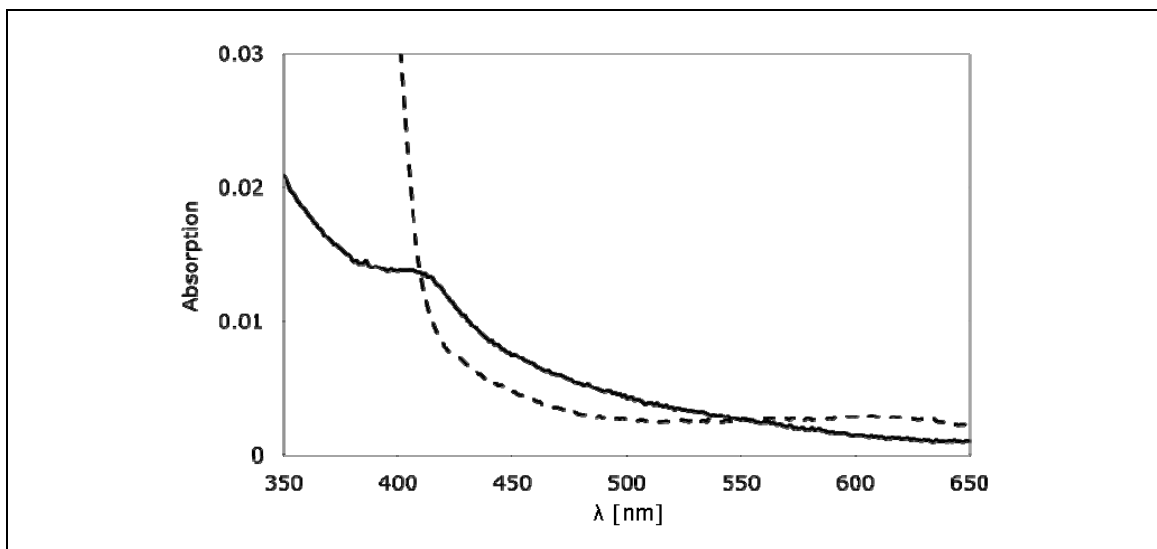
Figure 4.7 Spectroscopical analysis of [Fe-S] in NapDLA. Straight after IMAC purification NapDLA was diluted 1:100 in the same buffer as described in figure 4.4. The iron sulphur cluster shows absorption at ~420 nm (solid line). The sample was reduced by adding dithionite (dashed line).

Next, the metal content of NapDLA was analysed, this time by ICP-MS (inductively coupled plasma mass spectroscopy), instead of EPR, with a focus on iron and molybdenum (performed as a service by Dr Lorna Eades, University of Edinburgh). The results obtained gave 4080 ppb Fe and 17 ppb Mo, on average. From there a Molar ratio of iron to molybdenum can be calculated as 430:1. The NapDLA sample had a protein concentration of 8.3 µmol/l. Therefore, the number of metal atoms per molecule NapDLA can be set as 8 Fe and 0.02 Mo per mol of NapDLA. If accurate, this ratio of Fe to NapDLA would indicate that two [4Fe-4S] are present in the fusion protein, which however is in disagreement with several published observations (e.g. Jepson et al, 2007). Nevertheless, it proves that the sample certainly contains iron, probably to a full complement, but only trace amounts of molybdenum. This suggests the [Fe-S] cluster is present in the NapDLA fusion protein, but that the majority of the sample lacks any molybdenum cofactor.

Finally, the NapDLA fusion was subjected to further purification using size exclusion chromatography where NapDLA was eluted in a single peak (Figure 4.8), followed by crystallisation trials (carried out by Dr Alice Dawson, University of Dundee). Unfortunately, all attempts to obtain crystals for NapDLA under different conditions failed, and could not be further improved even by *in vitro* lysine methylation (Walter et al, 2006).
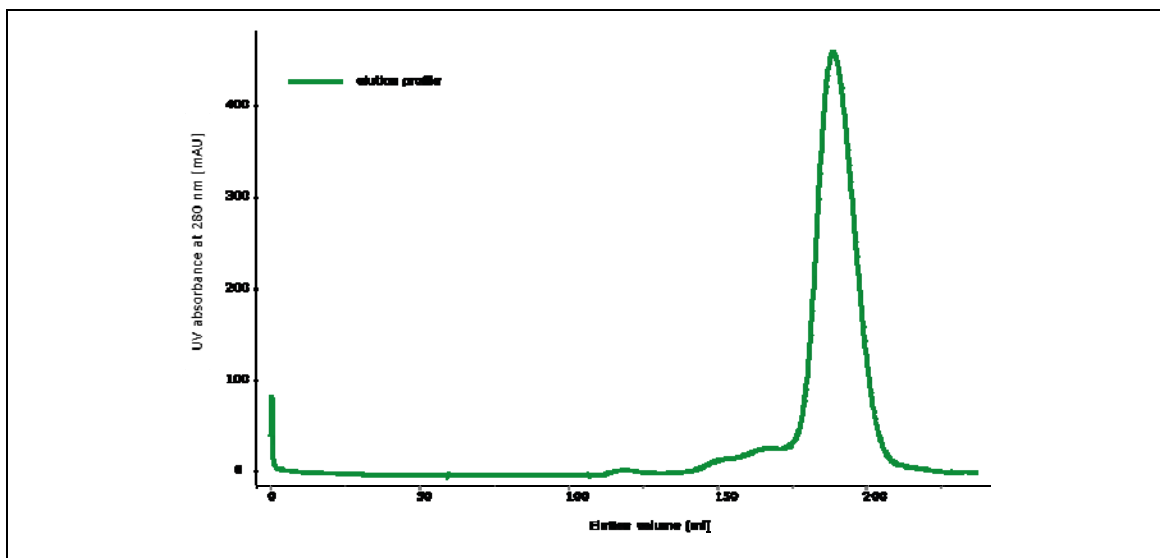
Figure 4.8 Size-exclusion profile of NapDLA. IMAC purified NapDLA was applied to a Superdex200 column (GE Healthcare), which had been equilibrated in 20 mM Tris-HCl, pH 7.6 and 150 mM NaCl. Eluted NapDLA was collected, pooled and subjected to crystallisation trials.

4.2.3 NMR analysis of NapD in complex with the NapA Tat signal peptide

Due to the continued failure to obtain crystals for NapD complexed with full-length NapA precursor, it was decided to focus on structural studies between NapD and the NapA signal peptide only. Maillard et al. (2007) solved a solution NMR structure of NapD, which revealed a new family of Tat proofreading chaperones with a ferredoxin fold. In the same study, unlabelled MalE-NapA$_{SP}$ was titrated into ^{15}N-labelled NapD and analysed by 2D NMR spectroscopy (Maillard et al, 2007), which gave an early indication of the NapD residues mostly affected by binding by the signal peptide (Maillard et al, 2007). These residues all mapped to the single β-sheet face of NapD. Following the difficulties to obtain crystals for NapD in complex with NapA, emphasis was again put on structural analysis of the NapDA interaction using NMR.

The NapA signal peptide contains a long stretch of alanine and valine residues (Figure 2.2). which makes it difficult to synthesize sufficient amounts of the peptide *in vitro*. Therefore, the Tat signal peptide (residues M1 to V33) was fused to the flexible C-terminus of NapD *via* a linker resulting in the protein NapDA$_{SP}$. The linker sequence 'RSNLGIEGRPG' was identical to the one described for the full length NapDLA fusion. It was shown that *E. coli* cells harbouring a chromosomal fusion of *napD-L-napA* were still able to reduce nitrate *in vivo*, so this fusion allows a functional interaction between NapD and the signal peptide (Figure 4.5). The resultant NapDA$_{SP}$ fusion protein was 139 amino acid residues long where residues M1-P87 corresponded to the NapD protein, residues R88-G98 to the linker region, side-chains M99-V131 to the NapA signal peptide, and amino acids R132-H139 to the hexa-Histidine tag.

70

Preliminary experiments using ITC suggested that the NapA signal peptide is stably bound to, or at least occluding, the native binding site in the NapDA$_{SP}$ fusion. Dr Julian Maillard from the Sargent group performed a titration of NapDA$_{SP}$ into a sample of MalE-NapA$_{SP}$. In this case, no binding of the signal peptide by NapD could be detected, suggesting the binding sites on the NapDA$_{SP}$ fusion are already fully occupied (data not shown).

For NMR analysis 100% ^{15}N- and ^{13}C-labelled NapDA$_{SP}$ was prepared, isolated under denaturing conditions, and subsequently refolded on the IMAC column. Subsequent elution of NapDA$_{SP}$ resulted in a protein prep of high yield and purity (Figure 4.9).
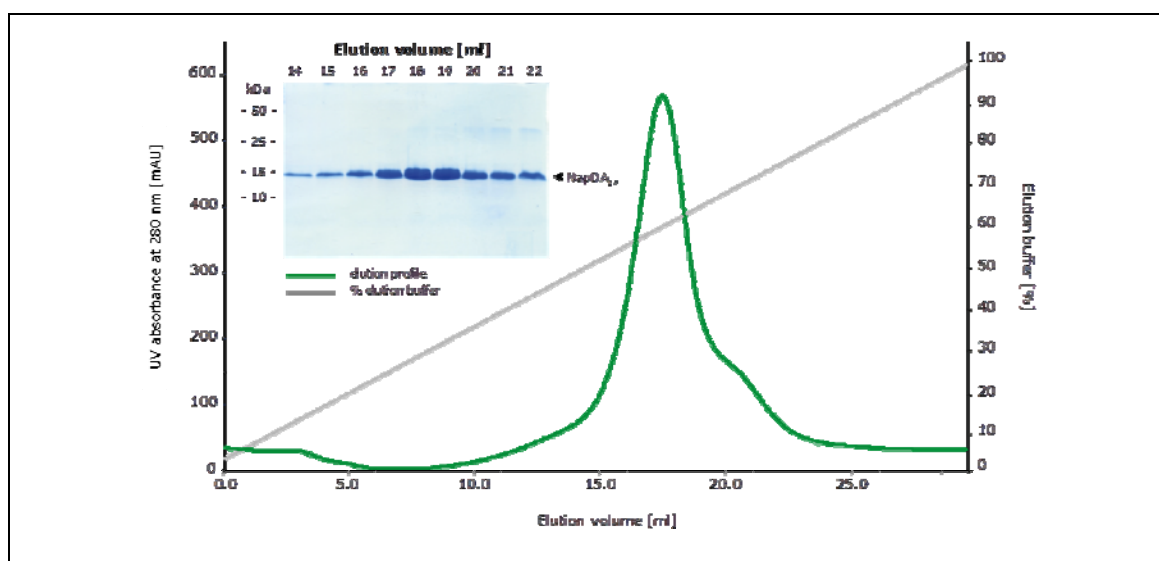
Figure 4.9 Purification of NapDA$_{SP}$. For ^{15}N-^{13}C-labelling of the fusion protein NapDA$_{SP}$ cells were grown in M9 minimal medium supplemented with 0.1 mM CaCl$_2$, 0.2% ^{13}C-glucose and 0.1% ^{15}NH$_4$Cl. Protein purification was carried out under denaturing conditions as described in Figure 2.5.

Collection of NMR data and analysis was done in collaboration with Prof Geerten W. Vuister, Radboud University, The Netherlands and Department of Biochemistry, University of Leicester. Backbone and sidechain assignments of NapDA$_{SP}$ were obtained using triple-resonance experiments HNCACB, CBCACONH, HN(CA)HA and (H)CCH-TOCSY at 600 MHz resonance frequency. Three-dimensional NOESY experiments were recorded at 800 MHz.

An overlay of the [^{15}N]-HSQC spectra of the NapD and NapDA$_{SP}$ proteins showed additional peaks in the latter, presumably originating from the additional residues of NapDA$_{SP}$ (Figure 4.10). In addition, considerable differences in the positions of the cross-peaks previously assigned to native NapD were observed in the NapDA$_{SP}$ spectrum (Figure 4.10). Together, these effects are indicative of the formation of a complex between the NapD core and the final ~40 residues of the NapDA$_{SP}$ construct, which correspond to the NapA Tat signal peptide. Using triple-resonance NMR spectroscopy,

71

the backbone and β-carbon assignments for residues T3-E85 of the NapDA$_{SP}$ protein (corresponding to the NapD part) and residues A109-A127 (corresponding to NapA signal peptide residues A11-A29) were made. Residues 86-108 of the NapDA$_{SP}$ fusion, which include NapA signal peptide residues M1-K10, could not be identified in the spectra, presumably because they adopt a random unstable conformation or are in intermediate exchange leading to line broadening beyond detection.
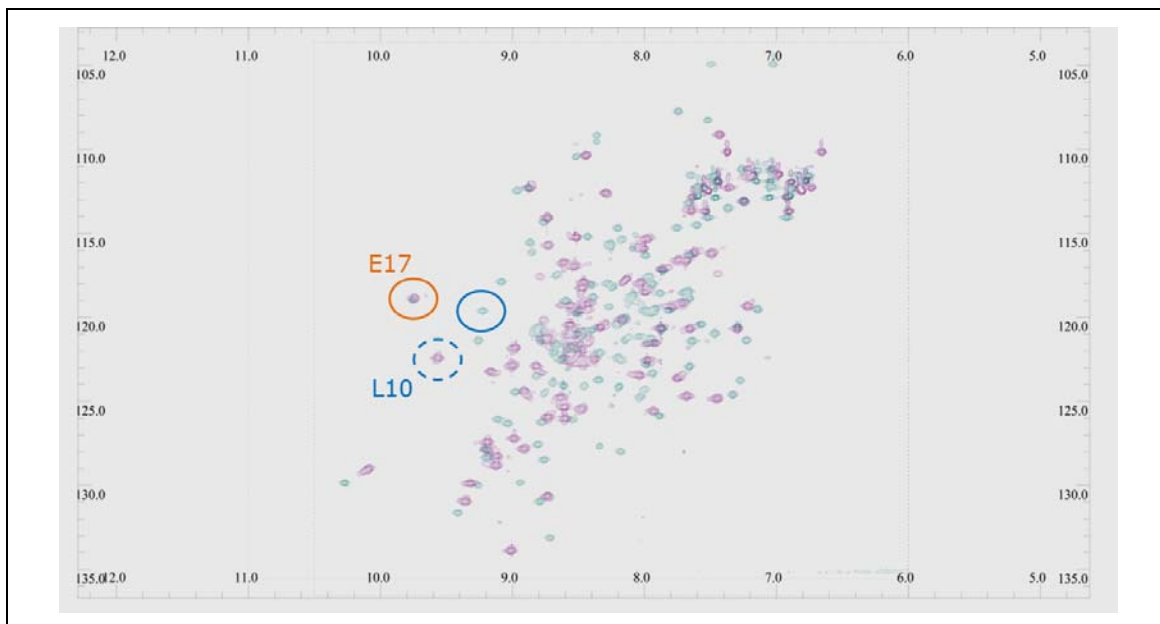
Figure 4.10 Structural changes of NapD during Tat signal peptide binding. 2D [^{1}H-^{15}N]–HSQC spectra of NapD (purple) and NapDA$_{SP}$ (green). For comparison of bound and unbound NapD residues L10 (blue) and E17 (orange) are highlighted. (In cooperation with Dr Martyn James, University of Dundee and Dr Chris Spronk and Prof Geerten Vuister, Radboud University, Nijmegen, Netherlands)

Prof Vuister then analysed the per-residue chemical shift differences between the two samples and used that information to predict secondary structure changes and finally generated a model for the NapDA$_{SP}$ complex (Figure 4.11). It is clear from this model that NapDA$_{SP}$ residues A109-V122, corresponding to the NapA signal peptide residues A11-V25, are well-ordered and adopt α-helical conformation. These helical residues are followed by three residues in a turn-like conformation. The signal peptide is positioned neatly on top of the flat β-sheet face of NapD (Figure 4.11A). The interface between the signal peptide and NapD comprises an extensive surface with hydrophobic interactions, and the close packing appears to explain the need for the poly-alanine stretch of the NapA signal peptide. Changes to the conformation of the NapD protein itself during peptide binding include V75-Q79 pairing-up with residues W5-V7 to extend the first β-strand and together increase the β-sheet sufficiently enough to line one side of the peptide interface (compare with Figure 3.1). Notably, V75 and Y76 together now form a β-bulge, where those two residues extend the β-strand and enable interaction with the signal peptide.

The model also predicts that NapA signal peptide residue K10 engages in a salt-bridge interaction with E49 of NapD (Figure 4.11B). In addition, the aliphatic sidechain atoms of NapA$_{SP}$ K10 are packed against NapD V47. The NapA signal peptide residue R6 wedges in between NapD residues E49 and W5 with its sidechain atoms pack against the NapD W5 sidechain, whereas the guanidinium groups of NapA R6 are oriented towards the highly acidic loop-region, comprising the E51, D52 and E54 side-chains of NapD, between the third β-strand and second α-helix (Figure 4.11B). At the C-terminal end of the NapA signal peptide the backbone oxygen of NapA A21 is hydrogen bonded to the sidechain of NapD Q43, and the NapA L22 sidechain packs into a cavity formed by NapD residues V37 and D38 (Figure 4.11B).
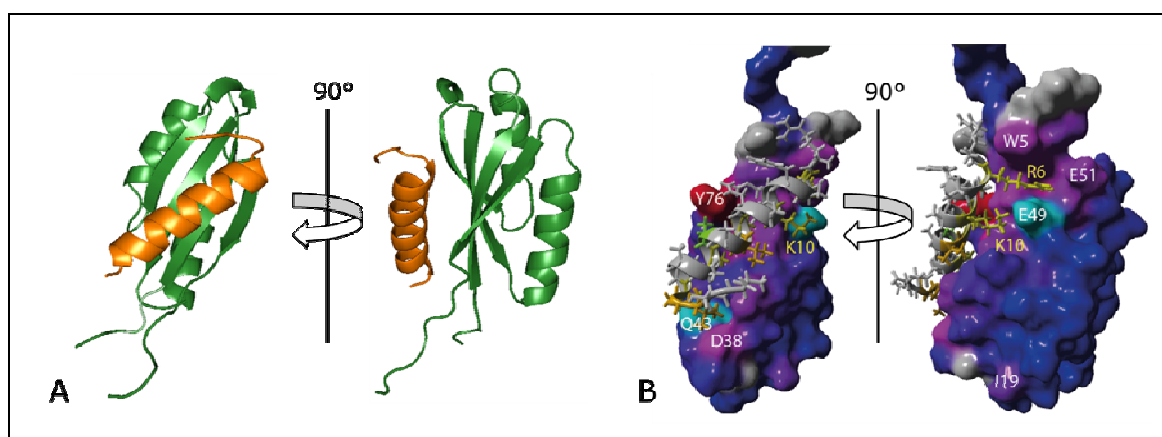
Figure 4.11 NMR structure of NapD in complex with the NapA signal peptide. (A) NapA signal peptide residues R5 to V25 are shown in orange. NapD is depicted in green. (B) Highlighted are interacting residues between NapD (depicted with its surface) and NapA$_{SP}$ (in grey, amino acid residues illustrated in stick form).

4.2.4 Structural analysis of the NapA signal peptide in its free state

Several structural and biophysical studies on different twin-arginine signal peptides hypothesized that they are unstructured in solution (e.g. HiPIP – Kipping et al., 2003, SufI – San Miguel et al., 2003). However, the NMR structure of the chaperone-bound form of the NapA signal peptide presented in this Chapter revealed an α-helical conformation. To investigate the natural unbound state of NapA$_{SP}$ site-directed spin labelling (SDSL) of the signal peptide and pulsed electron-electron double resonance (PELDOR) spectroscopy were carried out (Hubbell et al, 2000). This work was done in collaboration with Dr David Norman and Dr Richard Ward at the University of Dundee.

For this study, the previously described fusion protein MalE-NapA$_{SP}$ was modified by substituting residues S4 and S24 of the NapD signal peptide by cysteines (Figure 12A). Purified MalE-NapA$_{SP}$ S4/24C was then site-specifically labelled with MTSL (*S*-(2,2,5,5-tetramethyl-2,5-dihydro-1H-pyrrol-3-yl)methylmethanesulfonothioate), a chemical com-pound that interacts covalently with the thiol groups of cysteines (Figure 12B). MTSL contains a nitroso radical that allows the compound to be used as a spin label in EPR

experiments. Thus, with a double-spin-labelled sample PELDOR can be used to carry out highly accurate measurements of the distances between the two spins in a range of 2-8 nm, or sometimes longer (Ward et al, 2010). In addition, information about the distribution of distances between the unpaired electrons can be collected. These types of experiments were expected to give an indication of the different conformational states of the NapA signal peptide.
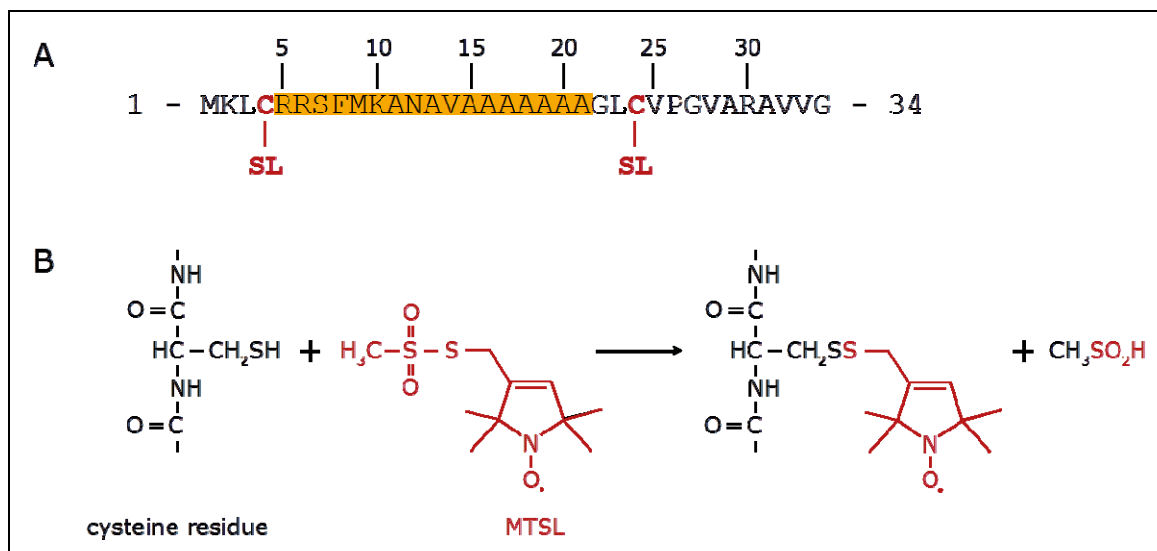
Figure 4.12 Site-directed spin labelling of the NapA signal peptide. (A) Shown is the primary sequence of NapA$_{SP}$, amino acids M1 to G34. Introduced cysteine residues on position 4 and 24 are marked in red with attached spin labels (SL). Secondary helical structure is highlighted on orange background. (B) The spin label MTSL [(*S*-(2,2,5,5-tetramethyl-2,5-dihydro-1H-pyrrol-3-yl)methylmethane-sulfonothioate; highlighted in red] reacts with the thiol group of a cysteine residue.

MalE-NapA$_{SP}$ S4/24C was purified under denaturating conditions as described in Chapter 2 and labelled with MTSL. The efficiency of labelling was monitored by MALDI-TOF (matrix assisted laser desorption ionisation - time of flight) mass spectrometry since each MTSL molecule adds 186.3 Da to the mass of the target protein. After the labelling reaction the apparent molecular mass of MalE-NapA$_{SP}$ S4/24C had increased to ~47,834 Da (Figure 4.13A) as compared to ~47,500 Da for the untreated control (Figure 4.13B). This corresponds to an addition of 334 Da, which indicates successful attachment of the two MTSL molecules to the cysteine residues C4 and C24 of the NapA signal peptide since there are no other cysteine side chains in the remainder of the fusion protein.

74
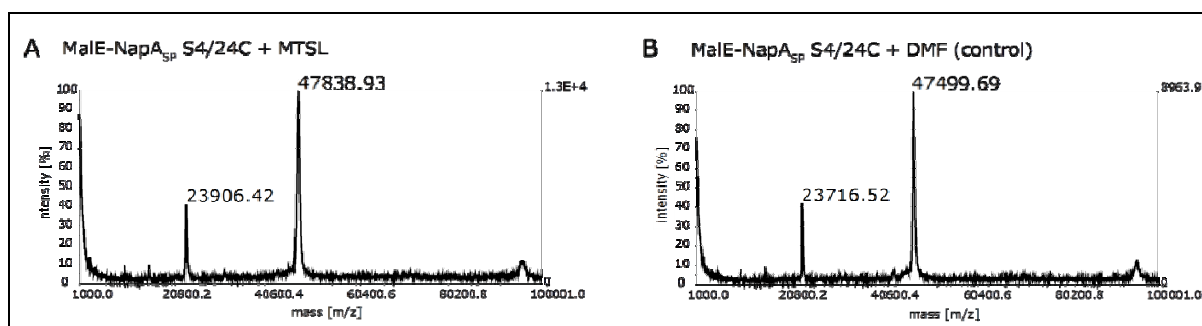
Figure 4.13 Mass spectrometry profile of unlabelled and labelled MalE-NapA$_{SP}$ S4/24C. Purified protein was incubated with either (A) a 10-fold molar excess of MTSL or (B) DMF (dimethylformamide) as a negative control for 4 hours at room temperature followed by 4°C overnight. One molecule of MTSL adds 186.3 Da to the weight of a protein. Labelling was confirmed by MALDI-TOF (FingerPrints Proteomics Facility, University of Dundee).

The double MTSL-labelled MalE-NapA$_{SP}$ S4/24C fusion protein was then analysed by PELDOR (Figure 4.14). To obtain the distance distribution P(r) for the spin labels in the free NapA signal peptide Tikhonov regularisation was applied to the raw data by using the appropriate alpha factor. This type of regularisation is most commonly used where the data is fitted on certain, prior made restrictions, thus reducing the number of possible solutions. The correct regularisation factor (alpha) gives the best fit to the experimental data, whilst suppressing artefactual distributions. A plot of alpha factor versus the goodness of fit (mean squared deviation of the simulated *versus* experimental data) reveals a characteristic 'L' curve (data not shown). The alpha term closest to the point of inflexion is therefore the most appropriate. Observable oscillations and baseline decay usually results in a single, discrete distribution. Care needs to be taken in data interpretation when only small oscillations observed. This produces usually broad distributions that are mostly likely the result of structural heterogeneity within the sample. Here, the resultant PELDOR data for free MalE-NapA$_{SP}$ S4/24C did not show a clear oscillation that would convincingly indicate spin-spin coupling (Figure 4.14A). Correspondingly, the main distance between the two MTSL labels on free NapA$_{SP}$ is not sharply defined and covers a broad range from 2 to 5 nm (Figure 4.14B).

Initial experiments mixing MTSL-labelled MalE-NapA$_{SP}$ S4/24C with native NapD seemed to result in many of the spin labels being lost or disengaging. In order to counter this problem a cysteine-free (Cys⁻; C8S C32A) variant of NapD was prepared, purified under denaturing conditions and refolded. This NapD variant was initially tested using the previously described nitrite production assay by complementing a Δ*napD* strain and restoring NapA activity. Here, no difference could be seen between Cys⁻ and native NapD thus demonstrating that the Cys⁻ NapD variant was physiologically active (data not shown).

The Cys⁻ NapD variant was then mixed with MTSL-labelled MalE-NapA$_{SP}$ S4/24C fusion at an equimolar ratio and the complex subjected to PELDOR analysis (Figure 4.14). In comparison to free NapA signal peptide, the addition of NapD resulted in a clear oscillation indicative of spin-spin interaction (Figure 4.14A), as well as a shortening of the distances between the spins (Figure 4.14B). In the presence of NapD a main distance at 2.4 nm and a minor distance at 2.9 nm could be calculated (Figure 4.14B).

These data clearly indicate structural changes are induced in the NapA signal peptide upon binding by NapD. Also a change in distance distribution can be observed, from

approximately 2 nm for free NapA$_{SP}$ at half height to about 1 nm for NapD-bound signal peptide (Figure 4.14B), which suggests a more defined conformation of NapA$_{SP}$ upon NapD binding.
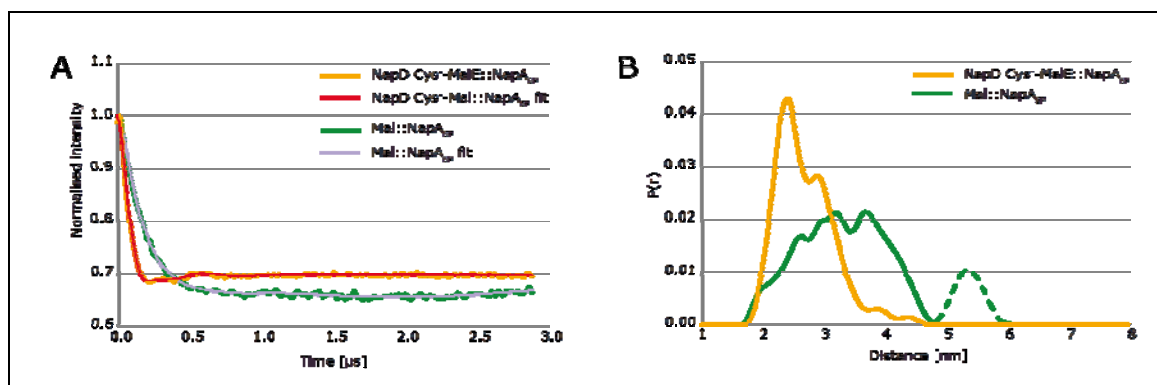
Figure 4.14 Conformational changes of the NapA signal peptide during binding. (A) PELDOR experimental data. (B) Tikhonov derived distance distribution. The dashed line indicates a long distance Tikhonov derived truncation artefact. Data for MalE-NapA$_{SP}$ bound to NapD Cys⁻ is represented in orange, data for unbound MalE-NapA$_{SP}$ is represented in green. (In cooperation with Dr David Norman and Dr Richard Ward, University of Dundee)

The PELDOR data need to be interpreted with caution, however, because the distance distribution for free NapA$_{SP}$ is heterogenous and the oscillation is lacking depth (Figure 4.14). MALDI analysis of purified MalE-NapA$_{SP}$ S4/24C shows a minor protein band of around 23.7 kDa, which is singly labelled upon MTSL addition (Figure 4.13). Therefore, size exclusion chromatography on a calibrated column of MalE-NapA$_{SP}$ S4/24C in complex with NapD was performed to separate individual complexes (Figure 4.15). However, only a single peak was eluted, which corresponds to a molecular weight of 108 kDa (Figure 4.15). Fractions run on a SDS-PAGE show up to three bands showing NapD, the NapA$_{SP}$ fusion and possibly degradation products of MalE-NapA$_{SP}$ S4/24C (Figure 4.15). This suggests that not only NapD and MalE-NapA$_{SP}$ S4/24C form a complex, but that NapD may also interact with truncated MalE-NapA$_{SP}$ fragments. Thus our data for the distance distribution is not only gained from the two nitroxide spin labels on MalE-NapA$_{SP}$ S4/24C, but also takes in account the influence of non-specific, contaminating neighbouring spin labels
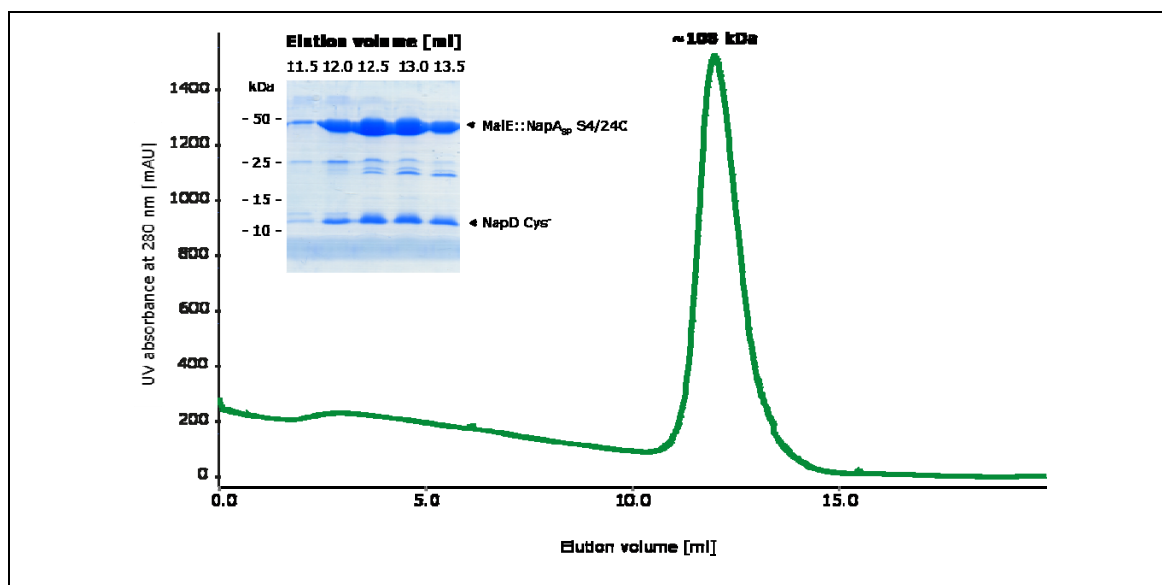
Figure 4.15 Elution profile of NapD in complex with MalE-NapA$_{SP}$ S4/24C. Nickel affinity purified NapD Cys$^-$ (13 kDa) and MalE-NapA$_{SP}$ S4/24C (47 kDa) was mixed with same concentrations and run on a Superdex75 size exclusion column. The NapD/MalE-NapA$_{SP}$ complex eluted as a single peak at ~108 kDa indicating an oligomeric state. The inset shows eluted fractions run on a 15% SDS-PAGE.

4.3 DISCUSSION

4.3.1 NapA in complex with NapD

Several structures of Tat substrates and proofreading chaperones have been solved. However, so far no structure has been published showing either the full length precursor or its signal peptide in complex with its specific chaperone. In this study attempts were made to gain structural information on the interrelationship between the periplasmic nitrate reductase NapA and its chaperone NapD.

Co-overproduction of NapD and NapA resulted in the formation of an initial complex, which could be purified by IMAC. However, the complex was observed to dissociate over time. In addition, the dissociation of NapD and NapA was accompanied by an apparent loss of stable binding of a putative iron-sulphur cluster from the complex. Finding of a loose binding between the two proteins is somewhat surprising since work outlined in Chapter 2 here, as well as that published by Maillard et al. (2007), showed NapD has an apparent dissociation constant in the low nanomolar range for the NapA signal peptide. However, it needs to be noted that those experiments had been carried out with an isolated signal peptide (fused to a carrier protein), which could induce changes in the binding behaviour of NapD. In the light of this it should be considered that NapD dissociation is triggered by maturation or folding of native NapA.

Attempts were made to stabilise the complex by fusing the C-terminus of NapD *via* a linker to the twin-arginine signal peptide of NapA. This approach certainly stabilised the binding of the [Fe-S] cluster, since the brown colour persisted for a considerably longer

77

time. However, so far it is not been proven if additional NapD binding sites, beside the signal peptide itself, are present on NapA. So inserting a linker could have major influences on the NapD/NapA interaction and limit the number of binding sites available. Indeed, while some nitrate reductase activity was still present in a strain carrying the NapDLA fusion, this was clearly reduced by two-fold compared to the parent strain. Therefore, certainly the linker between NapD and NapA changes the binding characteristics.

A possible explanation could be that the linker hinders the release from the NapA signal peptide, which in turn slows down Tat transport resulting in reduced NapA activity in the periplasm. Another possibility is that the C-terminus as a whole structural unit is important for the NapA interaction, indeed both its complete removal (Maillard et al, 2007), or fusion of its C-terminal tail, reduces NapA activity.

Concerning the number of binding sites on NapA for NapD not much is known so far. For proofreading chaperones of the TorD family, for example, it was shown that they not only bind to the Tat signal peptide of their specific substrates, but also interact with the mature part of the precursor, and in doing so play a direct role in cofactor insertion (Genest et al, 2009). However, a recent publication by Chan and co-workers (2010) looking for interactions between NapD and different truncated or modified versions of NapA by bacterial two-hybrid, suggests that NapD is only interacting with the Tat signal peptide.

4.3.2 Co-factor insertion into NapA and the role of NapD

Analysis of a possible NapDA complex revealed the presence of a putative iron-sulphur cluster. The crystal structure of NapA showed (beside the presence of a Mo-*bis*-MGD) a [4Fe-4S] cluster and this was confirmed by EPR analysis (Jepson et al, 2007). To determine the nature of the [Fe-S] cluster in the NapDA complex low-temperature X-band EPR spectroscopy was performed. However, no spectra for the [4Fe-4S] cluster or its reduced form could be detected, possibly due to unstable iron-sulphur intermediates upon reduction (Müllner et al, 2008). Over time the iron-sulphur cluster was gradually lost, possibly indicating its accessibility to surrounding oxygen or other environmental factors.

Fusing the chaperone NapD to the Tat signal peptide of NapA stabilized the [Fe-S] cluster. ICP-MS analysis showed the presence of Fe and traces of Mo, where however eight molecules of Fe were found per molecule NapDLA, which possibly indicates an excess accumulation of iron in the sample, but most likely reflects errors in estimating protein concentrations. Concerning the order of cofactor assembly, it was shown for the catalytic subunits of the DMSO reductase, DmsA, and the nitrate reductase, NarG, that

the molybdenum cofactor (MoCo) is only inserted after [4Fe-4S] assembly, and that oxidative damage of this cluster to a [3Fe-4S] blocks insertion of MoCo (Lanciano et al, 2007; Tang et al, 2011). Clearly, the data presented here concur with those observations and suggest that the [Fe-S] cluster can be inserted first and in the absence of MoCo. In conclusion, the NapDA and NapDLA complexes contain a [4Fe-4S] cluster, but only insignificant amounts of molybdenum, thus indicating that NapA maturation is not yet completed or the molybdenum cofactor is extremely unstable under those purifying conditions used.

Interestingly, cofactor insertion into NapA and NapD binding seem to be connected: the dissociation of NapD from the complex was followed by loss of [Fe-S] in the sample, whereas fusing NapD to NapA stabilized the [Fe-S] cluster considerably. Interaction studies on the proofreading chaperones TorD and DmsD suggested possible participation at least in the molybdenum cofactor biosynthesis pathway (Genest et al, 2008; Li et al, 2010). It was also proven that TorD binds to the precursor and mature forms of Mo-*bis*-MGD (Genest et al, 2008). One possible hypothesis is that TorD and DmsD keep their substrate in a 'cofactor competent state' by binding to the mature part (Genest et al, 2009). Regarding NapD, so far it is not known if this chaperone interacts with the biosynthesis pathway for molybdenum or iron-sulphur cofactors. However, one could propose that NapD, even so assuming its 'only' binding site is at the NapA signal peptide, has an structural influence on the mature part, which helps to facilitate co-factor insertion.

Another factor that needs to be considered in the complete maturation pathway of NapA is the role of a second accessory protein encoded by the *nap* operon - the iron-sulphur protein NapF. It has not been fully elucidated what role NapF has in the nitrate reduction pathway of Nap. It is possible that NapF has a function in cofactor assembly and NapA maturation, but possibly also in electron transfer to NapA (Kern & Simon, 2009; Nilavongse et al, 2006). Furthermore, it should be considered that Jepson et al. (2007) were able to purify mature NapA containing a [4Fe-4S] and Mo-*bis*-MGD by expressing the whole *E. coli napFDAGHBC* operon on a plasmid under anaerobic conditions. This suggests a stabilizing effect of one or more additional factors on the maturation of NapA. In the experiments carried out in this Chapter cells used for overproducing NapDA and NapDLA contained endogenous *napF*. However, protein production was performed under aerobic conditions, thus the *nap* operon would not be expected to be expressed. The work carried out in this Chapter therefore shows that NapF is not essential for [4Fe-4S] assembly into NapA. Therefore, future work could include the overproduction of NapFDA, which could possibly result in the extraction of a stable NapFA complex.

4.3.3 NMR analysis on NapDA$_{SP}$

High-resolution NMR spectroscopy is a powerful tool to study the structure, dynamics and interactions of biomolecules. The NMR data presented here shows the formation of a specific complex between the Tat signal peptide of NapA and its chaperone NapD. This interaction induces an extension of the fourth β-strand of NapD, however leaves the overall conformation of the NapD molecule unaffected.

The model shows that the signal peptide traverses the β-sheet face of NapD almost completely. Glutamine scanning mutagenesis and bacterial two-hybrid studies described in Chapter 2, revealed NapA residues R6, K10, A13, A17 and A21 to be important for NapD binding. The NapDA$_{SP}$ structure presented here strongly supports the mutagenesis study.

NapA residues R6 and K10 are predicted to form salt bridges to negatively charged E51 and E49 of NapD, respectively (Figure 4.16A). Hydrogen bonding occurs for NapA A13 and A21 with NapD S9 and Q43, respectively (Figure 4.16B). Maillard et al (2007) showed already that those three NapD residues (S9, Q43 and E49) are part of the Tat signal peptide binding event, being highly conserved within the large family of NapD-like proteins. The effect of alanine mutations within the hydrophobic region of the signal peptide can be explained by the spatial constraints exerted by the interface, where substitutions of alanine residues with glutamines would disrupt the tight packing of the helix onto NapD due to steric clashes.

Screening of a NapD mutant suppressor library revealed the single mutant I19F and the double mutant A14T A71T as being able to restore binding to the NapA signal peptide variant A17Q (Chapter 3). Residue I19 is positioned at the N-terminal end of the first α-helix, and is therefore not located in direct vicinity of the NapD/NapA interface (Figure 4.11B). However, a possible explanation for the effect of I19F on NapA$_{SP}$ A17Q binding comes from inspection of our NapDA$_{SP}$ structure. The I19 side-chain forms hydrophobic interactions with L44 on the third β-strand, and one of the neighbouring residues to L44, I45, has direct contact to NapA$_{SP}$ residue A17. Thus, it is conceivable that a NapD I19F substitution could have a long-range influence on the conformation of I45, which could in-turn allow binding of the NapA$_{SP}$ variant A17Q (Figure 4.17C). Moreover, further NMR spectroscopic analysis supports this hypothesis since I19 and S20 are the only residues on this face of the NapD molecule that display significant chemical shift perturbations upon signal peptide binding (data not shown).

The effect of NapD mutant A14T A71T is more difficult to estimate, because the NMR structure of NapDA$_{SP}$ shows no direct binding of those two residues to the signal peptide (Figure 4.16D). However, local, but strong conformational changes of NapD upon

threonine substitution cannot be excluded and could contribute to a variant structure that could interact with NapA A17Q. Clearly, only a detailed structural analysis of the NapD A14T A71T/NapA A17Q complex will reveal the true molecular basis for this interaction.
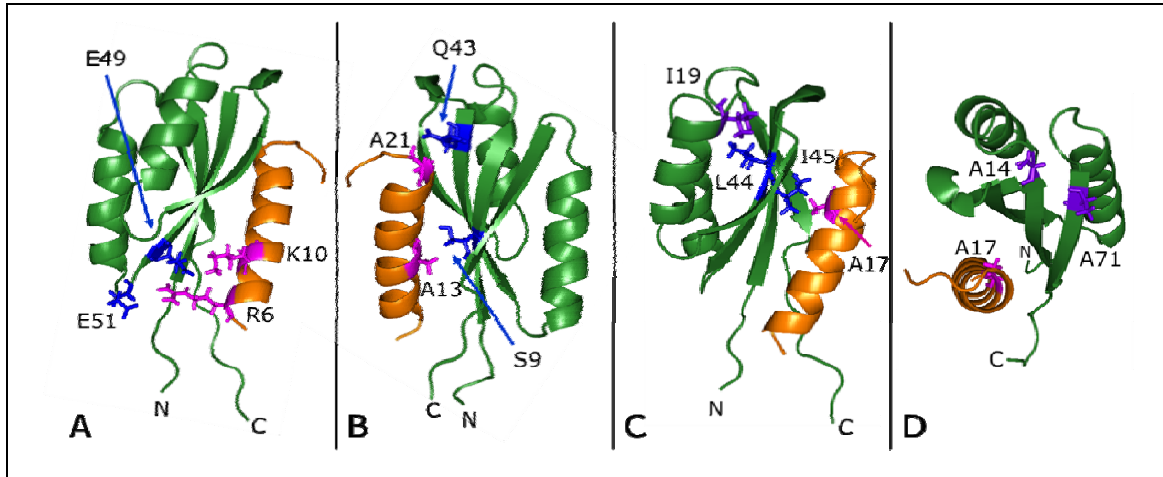
Figure 4.16 Highlighting the interaction between residues of the NapA signal peptide and NapD. The NMR structure of NapDA$_{SP}$ with NapD shown in green and the signal peptide in orange. NapA residues identified by glutamine scanning mutagenesis and BTH are highlighted in magenta. NapD residues involved in NapA$_{SP}$ binding are highlighted in blue and residues identified by a NapD mutant suppressor screen for NapA signal peptide variant A17Q are shown in purple. (A) NapA residues R6 and K10 interact with NapD E51 and E49, respectively. (B) NapD S9 and Q43 interact with NapA A13 and A21, respectively. (C) NapA A17 can interact with NapD I45. However, a I19F mutations possibly influences I45 to be able to bind a NapA A17Q mutation. (D) NapD residues A14T and A71T are supposed to interact with NapA$_{SP}$ variant A17Q.

During this study the NMR structure of another NapD-NapA complex was deposited (PDB ID code 2pq4; Minailiuc, O.M., Ekiel, I., Cheng, J., Milad, M.; Bacterial Structural Genomics Initiative, Canada), which is referred here from now on as NapD-NapA$_{SP}$. This structure also shows the NapA signal peptide binding to the β-sheet face of NapD (Figure 4.17A). However, when it is compared to our NapDA$_{SP}$ structure it can be seen that the models are not entirely in agreement. In particular the experimentally-derived important roles of NapA residues R6 and K10 in NapD binding is not apparent from the alternative NapD-NapA$_{SP}$ complex structure. Also, NapD residues that take part in signal peptide binding as predicted by Maillard et al (2007) do not stand out in the alternative NapD-NapA$_{SP}$ complex structure. In addition, the conformation of the hydrophobic alanine-rich region of the signal peptide in NapD-NapA$_{SP}$ is in disagreement with our predicted secondary structure when analysed using the programme Talos+, which is used to predict protein backbone torsion angles (Shen et al, 2009). The prominent bend of the NapA$_{SP}$ helix in the alternative NapD-NapA$_{SP}$ complex structure, and its angle of contact with respect to NapD, are major differences compared to our NapDA$_{SP}$ model (Figure 4.11 and 4.17A). Finally, analysis of the available (incomplete) data for the alternative NapD-NapA$_{SP}$ complex for overall structural quality shows very poor scores (data not shown). However, the NapD-NapA$_{SP}$ structure does agree with some of our findings:

certainly the position of NapA$_{SP}$ residues A21 to L24 on the third β-strand, and the extension of the fourth β-strand (residues V75 and Y76) upon peptide binding, are in agreement with the work presented here. Differences between the two structures of NapD-NapA$_{SP}$ and NapDA$_{SP}$ are indicated by an alignment in Figure 4.17B.
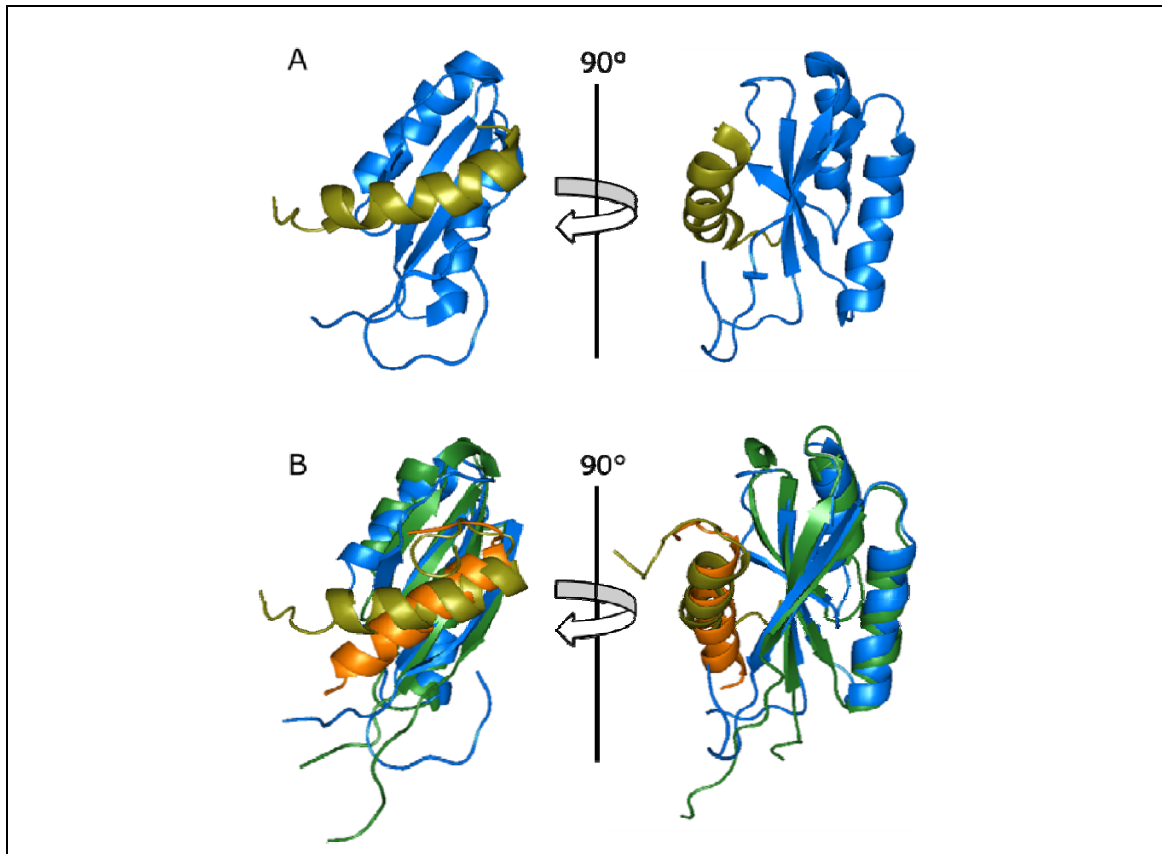
Figure 4.17 Comparison of two different structures of the NapA signal peptide bound to NapD. (A) Pre-deposited NMR structure NapD-NapA$_{SP}$ (PDB ID code 2pq4; Minailiuc, O.M., Ekiel, I., Cheng, J., Milad, M.; Bacterial Structural Genomics Initiative). NapD is shown in blue and the NapA signal peptide in olive. (B) Overlay of NapD-NapA$_{SP}$ with NapDA$_{SP}$ from Figure 4.11.

Overall, the NMR analysis of NapDA$_{SP}$ shows for the first time that the twin-arginine signal peptide of NapA adopts an α-helical structure during NapD binding (Figure 4.11). In contrast, docking simulations of the *E. coli* DmsD chaperone with the Tat signal peptide of DmsA proposed that the peptide could adopt an extended conformation devoid of secondary structure when bound to DmsD (Stevens et al, 2009). However, this conclusion is based on an extrapolation of genetic and biochemical work onto a ligand-free chaperone structure, and the work presented here demonstrates amino acids involved in long-range indirect effects, distant from the actually signal peptide binding site, are commonly identified by these methods. It is possible that a genuine chaperone-peptide complex will be required to reveal the true nature of the peptide binding site on TorD/DmsD family chaperones.

4.3.4 Structure of the NapA signal peptide in solution

The NMR structure of NapDA$_{SP}$ in this Chapter assigns the secondary structure of the NapA signal peptide to be helical when bound to the proofreading chaperone NapD (Figure 4.11). However, what conformational changes does the signal peptide undergo during the transition from an unbound to a bound state?

Previously, it was shown that free Tat signal peptides are highly flexible and unstructured (e.g. GFOR – Nurizzo et al, 2001; HiPIP – Kipping et al, 2003). The same was observed *in vitro* for a synthetic Tat signal peptide of SufI, which however became helical in a more hydrophobic environment (San Miguel et al, 2003).

Here, site-directed spin labelling and PELDOR analysis carried out on the NapA signal peptide revealed that there are structural changes upon NapD binding. Comparison of the distance distributions obtained for bound and unbound signal peptide suggest a more relaxed structure for free NapA$_{SP}$. However, the alanine repeat in the hydrophobic region of the signal peptide suggests an overall maintenance of at least some helical structure even in solution (Rohl et al, 1999). Similarly, the free N-terminus of NarG, which is proposed to be a remnant signal peptide and binding site for the NarJ chaperone, shows a helical conformation when analysed in solution (Zakian et al, 2010).

Overall, however, the EPR data shown here for NapA$_{SP}$ need to be taken with caution because of the lack of depth in oscillation. The quality of the spectra could be improved by deuteration of the protein sample (Ward et al, 2010). Further EPR-based structural analysis of the NapA signal peptide will also focus on conformational changes during interaction with the Tat complex. Fincher and colleagues published work on the signal sequence of a precursor of the Delta pH pathway in the thylakoid membrane of chloroplasts that showed Tat signal peptides may form a loop after binding to the translocase and prior to export (Fincher et al, 1998). By using purified TatBC complex (Tarry et al. 2009) and MTSL-labelled NapA$_{SP}$ it should be possible to study such conformational changes in the signal peptide using PELDOR. Taken together with our studies of signal binding by NapD, such work will give a complete picture of the role of the signal peptide at different steps on the bacterial Tat pathway.

5 Interaction studies between the proofreading chaperone NapD and the Tat translocase

5.1 Introduction

Tat proofreading chaperones are involved in processes such as Tat substrate folding, cofactor insertion and maturation (Sargent, 2007b). A common feature of those chaperones is the direct binding to Tat signal peptides and one of the first proofreading chaperones to be identified was the *E. coli* DmsD protein (Chan et al, 2009). Pull-down experiments using the immobilized twin-arginine signal peptide from DmsA (catalytic subunit of the DMSO reductase) incubated with *E. coli* cell extract identified DmsD as a specific binding partner. The authors also proposed DmsD to behave as a 'signal recognition particle' specifically targeting DmsA to the Tat machinery for export (Oresnik et al, 2001). The same study showed that a *ΔdmsD* strain was devoid of any DMSO reductase activity, suggesting that DmsD is involved in fundamental aspects of DmsA assembly. Indeed, a later *in vivo* study showed DmsD-independent Tat transport of a DmsA signal peptide/GFP fusion (Ray et al, 2003), which suggested the DmsA signal peptide did not have an obligation to be escorted to the Tat translocase by DmsD. Further work by the same group involving cell fractionations and immunoblotting revealed an association of DmsD with the inner membrane, and that this localisation was dependent on the interaction with both subunits of the Tat signal recognition complex, TatB and TatC (Papish et al, 2003). Those findings had been recently supported by the same authors in a study using bimolecular fluorescence complementation (BiFC) microscopy. In this method, a fluorescent protein is split into two non-fluorescent fragments, which are then fused to two putative binding partners. Interaction of those two proteins brings the fragments back into close proximity, which reconstitutes fluorescence. Use of this method suggested again that DmsD could interact with the TatBC complex (Kostecki et al, 2010).

The question of whether a Tat substrate would need a soluble target factor for the initial stages of transport is one that has dominated the field from the outset. In the ubiquitous and very heavily studied Sec pathway, there are several soluble proteins involved in signal peptide recognition and guiding substrates to the Sec translocon. For integral membrane proteins, and some soluble substrates, a ribonucleoprotein termed the signal recognition particle (SRP) recognises the first transmembrane helix or signal peptide of the substrate, binds to it, and then guides the whole complex, *via* a membrane-bound receptor, to the Sec translocon. In the eukaryotic endoplasmic reticulum (ER) this process allows co-translational translocation across the ER membrane. It remains unknown whether translation of membrane proteins is stalled by SRP binding in the

bacterial system. For most soluble Sec substrates transport is post-translational but again soluble factors are involved in guiding the Sec signal peptide to the translocon. In most cases SecA, a large ATPase, binds directly to the Sec signal peptide and also the SecY protein of the translocon, thus bringing the Sec signal close to the export apparatus. A final soluble factor on the Sec pathway is SecB, which does not bind directly to Sec signal peptides, but instead helps some Sec substrates maintain an unfolded conformation until transport is completed (Driessen & Nouwen, 2008). Given this huge body of evidence for soluble targeting factors in general protein export it was perhaps understandable that many believe Tat signal peptides should also benefit from a targeting factor that would guide them to the Tat translocon.

The evidence for the existence of a general Tat signal recognition protein is not strong. In the homologous plant thylakoid Tat pathway, export was seen to proceed *in vitro* in the absence of any soluble factors (Cline & Henry, 1996; Mori & Cline, 1998). However, in *E. coli* the heavily-studied TorA signal peptide remains active in the absence of its chaperone TorD, but export of passenger proteins seems to be enhanced *in vivo* upon over-expression of *torD*. Very similar observations were made for DmsD improving Tat transport of GFP fused to the DmsA signal peptide (Lee et al, 2010; Li et al, 2006).

The aim of this final Chapter was to begin to explore whether NapD acts in shuttling NapA to the Tat complex. In order to tackle this question biochemical and genetic approaches were taken. First, a collaboration with the Matthias Müller group, University of Freiburg, Germany, was established with the aim of utilising *in vitro* site-specific cross-linking technology to study the Nap/Tat interrelationship. In addition, a bank of new *E. coli* strains were designed and constructed with a view to using fluorescence correlation spectroscopy (FCS) to study the Nap/Tat interactions in living cells.

5.2 Results

5.2.1 NapD mediated NapA export – an attempt to study *in vitro* interactions between NapD and the Tat translocase

Matthias Müller (University of Freiburg, Germany) is a pioneer of the study of protein targeting and secretion systems *in vitro*. In recent years the focus has been on establishing a reliable and reproducible *in vitro* transport assay for the Tat pathway (Panahandeh & Müller, 2010). The starting point is the *in vitro* transcription of a plasmid based gene encoding the protein of interest, for example a cofactor-less Tat substrate. The gene in question is first placed under the control of the T7 promoter (Figure 5.1). This is followed by a transcription-translation process under semi-defined conditions where radioactive methionine and cysteine is incorporated into the newly synthesised

protein thus enabling sensitive visualization of the protein by autoradiography after separation by SDS-PAGE (Figure 5.2C)
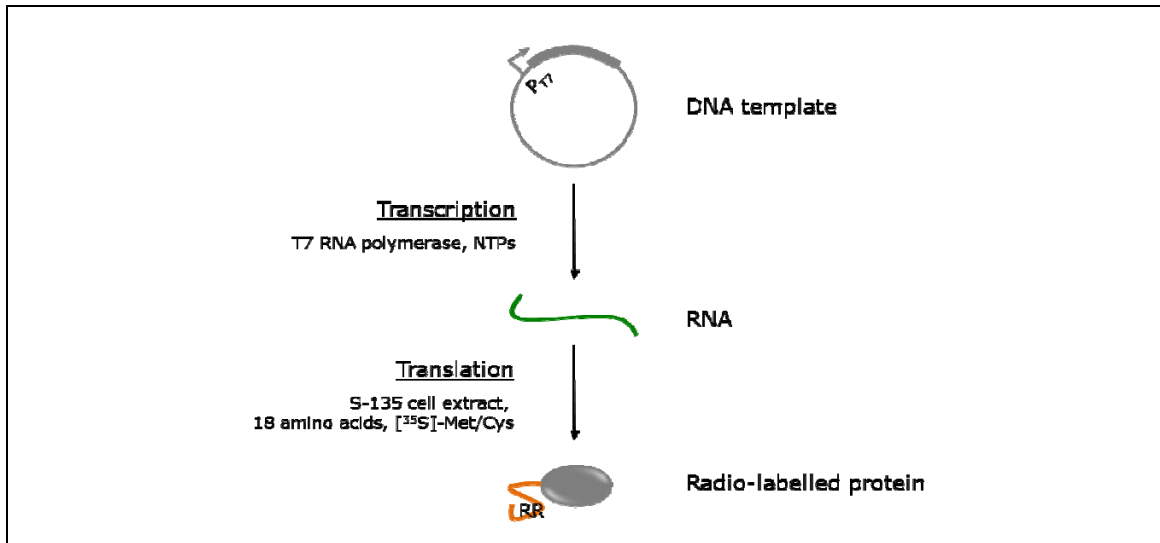
Figure 5.1 *In vitro* transcription and translation. Expression of the gene of interest is under the control of a T7 promoter (P_{T7}). All components for transcription (i.e. plasmid DNA, purified T7 RNA polymerase, NTPs) and translation (membrane-free but ribosome-containing S-135 extract, amino acids) are mixed and buffer conditions are adjusted. The resulting protein, depicted here to harbour a Tat signal peptide ('RR') will be immediately subjected to *in vitro* transport (Figure 5.2).

The next critical step is the preparation of inside-out inner membrane vesicles (INVs) obtained from an *E. coli* strain overexpressing *tatABC* (Figure 5.2A). If these are sealed and transport active the radio-labelled *in vitro* synthesised Tat precursor can be mixed with the INVs. If the protein is successfully transported into a vesicle then its N-terminal signal peptide is normally processed, which is evident in a size difference after SDS-PAGE (Figure 5.2C), and in addition proteins inside the vesicles are protected from externally-added proteases (e.g. Proteinase K; Figure 5.2B). The following work described here was done in cooperation with Matthias Müller and involved a four-month visit to his laboratory in Freiburg.
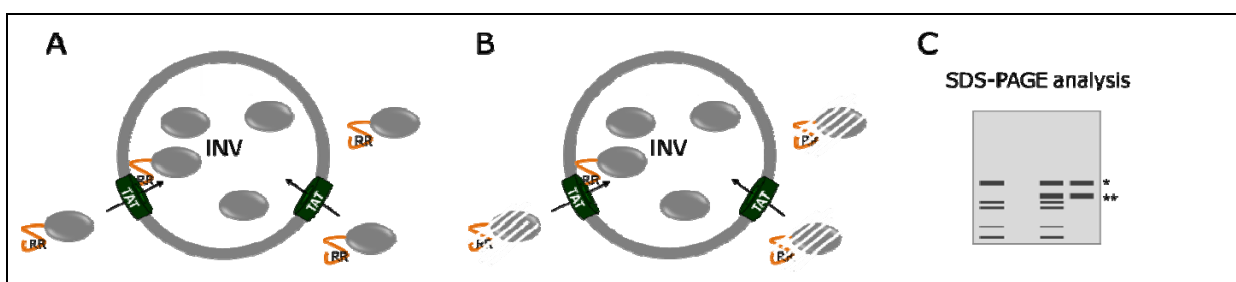
Figure 5.2 Schematic description of *in vitro* transport into inside-out inner membrane vesicles. (A) The protein of interest is recognized *via* its Tat signal peptide ('RR') by the Tat complex and transported into the vesicle (INV). To generate a proton motif force excess amounts of ATP are used. (B) Non-exported proteins are degraded upon addition of proteinase (i.e. Proteinase K). (C) Precursor (*) and processed form (**) of the Tat substrate can be visualized after SDS-PAGE separation by autoradiography.

5.2.2 *In vitro* analysis of Tat transport using CAT signal peptide fusions

Initially, two constructs were available for *in vitro* transcription/translation experiments and both of these employed chloramphenicol acetyl transferase as a Tat passenger protein replacing the nitrate reductase catalytic domain. The decision to use signal peptide fusions to CAT was made because native NapA requires cofactor insertion before folding and transport and this is a process that cannot be reliably provided in this *in vitro* assay. In addition, it had been already established that NapA$_{SP}$-CAT was an ideal artificial Tat substrate to study the Tat export process *in vivo* (Maillard et al, 2007; Stanley et al, 2002). The first construct therefore encoded a NapA$_{SP}$-CAT fusion only, while the second coded for NapD fused *via* a linker (L) to NapA$_{SP}$-CAT (NapDLA$_{SP}$-CAT). The linker sequence used is identical to the one described in Chapter 4 and this is known to not block protein transport *in vivo* or signal peptide binding by NapD *in vitro* (Chapter 4, Figure 4.5).

Figure 5.3A shows radiolabelled NapDLA$_{SP}$-CAT and NapA$_{SP}$-CAT after *in vitro* translation and clearly demonstrates that both proteins have been produced in high amounts. Next, *in vitro* Tat transport of each individual protein was initiated by adding TatABC-containing INVs followed by a Proteinase K digest. Treatment of the vesicles with this protease degrades all proteins that are not protected inside the INVs. However, this experiment showed that neither NapDLA$_{SP}$-CAT nor NapA$_{SP}$-CAT had been transported. In both cases addition of Proteinase K after a 20 minute import regimen led to the degradation of all protein (Figure 5.3A).

To show the efficiency of the *in vitro* Tat transport assay a fusion comprising the TorA signal peptide to the fluorescent protein mCherry was chosen (TorA$_{SP}$-mCherry). This protein is now used as a standard Tat substrate by the Müller group (Fröbel et al, submitted). Here, a portion of TorA$_{SP}$-mCherry was successfully transported and processed (Figure 5.3B), which indicates the functional set up of the assay. Note that two forms of TorA$_{SP}$-mCherry are protease-resistant and therefore inside the INVs. The first corresponds to the fully-processed imported mCherry protein (** band, Figure 5.3B), while the other corresponds to TorA$_{SP}$-mCherry in an unprocessed, but transported, form (* band, Figure 5.3B). It is believed that not all vesicles contain sufficient quantities of the LepB leader peptidase to process all imported substrates. Note also that the imported TorA$_{SP}$-mCherry protein appears to be slightly smaller compared to the initial *in vitro*-produced precursor. It is hypothesised that the N-terminus of the long TorA signal peptide (46 amino acids) remains exposed outside the INVs even after transport and is hence not completely protected from the Proteinase K digest (Figure 5.3B).
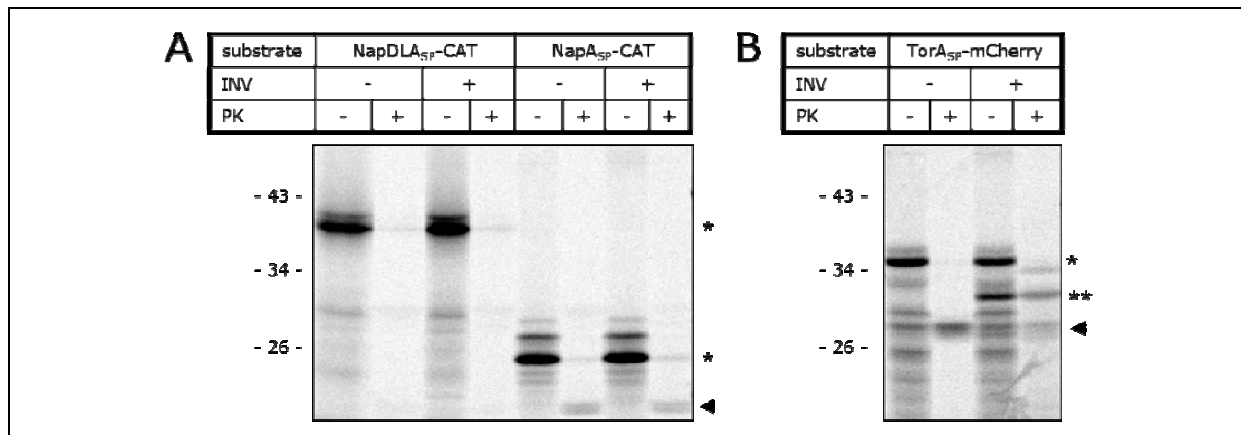
Figure 5.3 *In vitro* transport assay of CAT fusions. (A) Proteins were synthesised *in vitro* and transported into inside-out inner membrane vesicles (INV) from a *tatABC* overexpressing strain. Control is buffer only (-). Transport efficiency was tested by Proteinase K (PK) digest. Proteins and their correlating bands are indicated by an asterisk. (B) For TorA$_{SP}$-mCherry transported and processed form are indicated by one or two asterisks, respectively. Molecular weights are given in kDa. PK resistant bands are highlighted by an arrow.

5.2.3 *In vivo* assays for Tat transport using CAT

The *in vitro* data obtained for NapA$_{SP}$-CAT is in contrast to the *in vivo* data presented in Chapter 2 and by Maillard et al (2007) where this fusion protein is readily transported through the Tat translocase into the periplasm. Thus to investigate the effect of fusing NapD to NapA$_{SP}$-CAT on *in vivo* transport efficiency the previously described chloramphenicol-resistance assay was used (e.g. Chapter 2). In short, CAT is an enzyme that detoxifies chloramphenicol in the cytoplasm by acetylation. Fusions of Tat signal peptides to CAT result in periplasmic localisation of the enzyme where it is ineffective, thus cells grown in the presence of chloramphenicol are inhibited for growth (Figure 5.4B; Stanley et al, 2000). However, modifications inactivating the Tat signal peptide or Tat translocase result in retention of CAT in the cytoplasm thus enabling the cells to gain resistance to chloramphenicol.

Here, *E. coli* strain MG1655 (*tat*[+]) producing NapA$_{SP}$-CAT alone are not resistant to chloramphenicol and so no cell growth is observed (Figure 5.4A and B), which is in exact agreement to previous experiments (Chapter 2; Maillard et al., 2007). Co-expression of plasmids individually encoding NapA$_{SP}$-CAT and also NapD results in clear chloramphenicol resistance (Figure 5.4A and D), indicating that the presence of excess NapD hinders signal peptide function in this assay. Interestingly, production of the NapDLA$_{SP}$-CAT fusion alone enabled growth after addition of chloramphenicol, which indicates CAT is functional in the cytoplasm (Figure 5.4A and C).

Taken together, it can be concluded that neither NapDLA$_{SP}$-CAT nor NapA$_{SP}$-CAT is efficiently transported *in vitro*, whereas NapA$_{SP}$-CAT is readily exported to the periplasm *in vivo*, but the NapDLA$_{SP}$-CAT fusion is not.
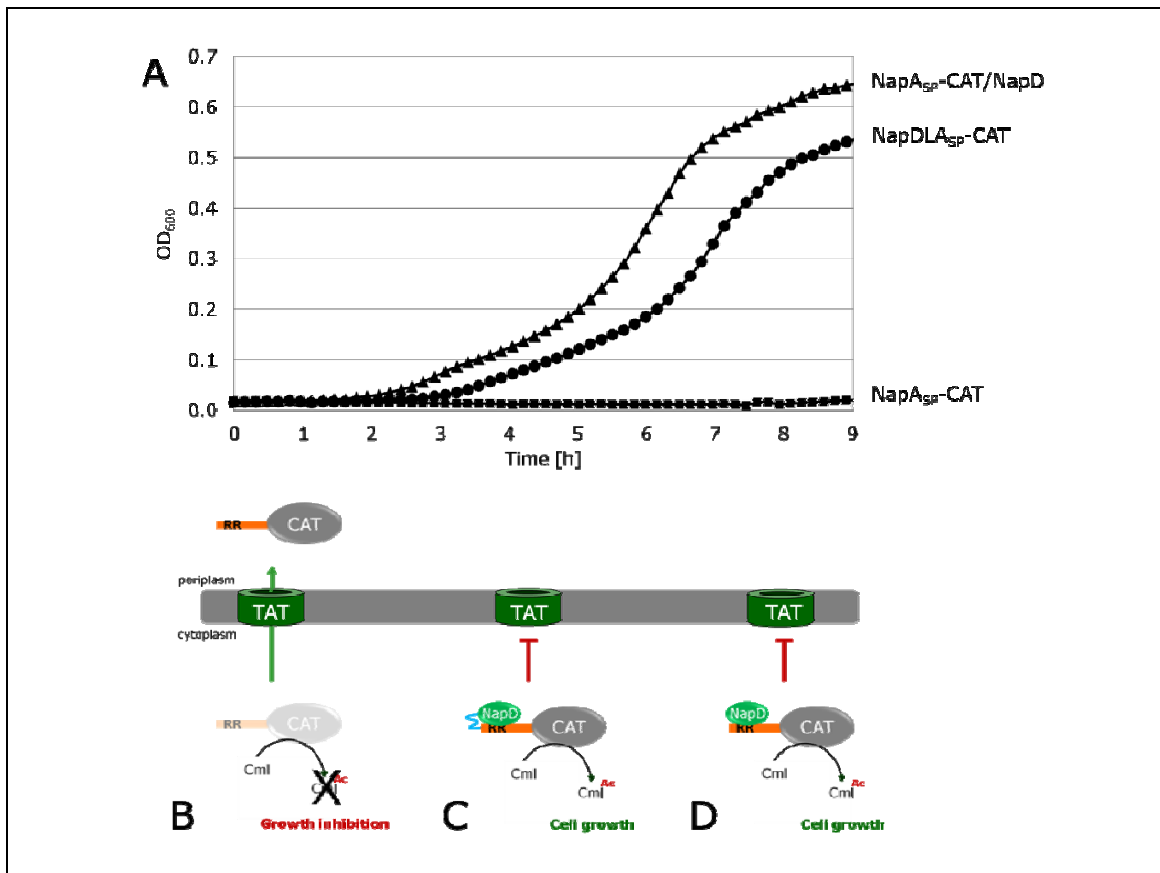
Figure 5.4 *In vivo* transport of CAT fusions. (A) *E.coli* strain MG1655 (*tat*[+]) producing plasmid based fusions of NapA$_{SP}$-CAT (■), NapDLA$_{SP}$-CAT (●) or co-producing NapA$_{SP}$-CAT and NapD (▲). Cells were grown in presence of 200 µg/ml chloramphenicol (Cml) and growth was monitored by measuring OD$_{600}$. (B) NapA$_{SP}$-CAT is transported *via* the Tat pathway into the periplasm, thus CAT cannot inactivate Cml by acetylation (Ac), which inhibits cell growth. (C) Fusion of NapD to NapA$_{SP}$ (indicated in blue) shields the Tat motif (RR) from Tat recognition, therefore no transport across the cytoplasmic membrane. CAT is acetylating Cml. Hence, the antibiotic has only little effect on cell growth. (D) Similar effects as for (C) can be observed when NapD and NapA$_{SP}$-CAT are co-produced. The NapA signal peptide is depicted in orange with 'RR'.

5.2.4 Utilising mCherry as a substrate for *in vitro* Tat transport assays

Given the inconsistent behaviour of the NapA$_{SP}$-CAT fusion protein, the possibility of CAT being an unsuitable *in vitro* substrate for the assay developed by Panahandeh et al (2010) was considered. Therefore, to proceed in the attempts to investigate to role of NapD in targeting NapA to the Tat complex the CAT reporter was substituted for mCherry.

Plasmids encoding NapDLA$_{SP}$-mCherry and NapA$_{SP}$-mCherry were constructed and *in vitro* translation and transport assay performed. Figure 5.5A shows after *in vitro* synthesis both NapDLA$_{SP}$-mCherry and NapA$_{SP}$-mCherry were generated in high amounts. However, upon addition of INVs NapDLA$_{SP}$-mCherry and NapA$_{SP}$-mCherry were not protected from degradation after Proteinase K treatment, suggesting efficient Tat transport did not take place (Figure 5.5A).

Note that the *in vitro* transport assay for all CAT fusion as well as mCherry fusion proteins was performed at the same time under identical conditions. Therefore, Figure 5.5B shows the same TorA$_{SP}$-mCherry control as in Figure 5.3B, where TorA$_{SP}$-mCherry is transported into INVs and processed by the leader peptidase.
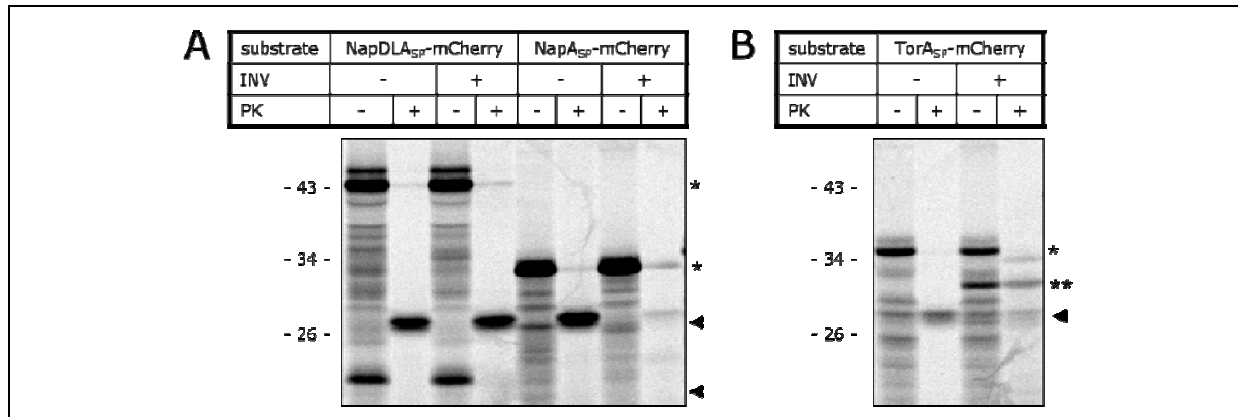
Figure 5.5 *In vitro* **transport assay of mCherry fusions.** Experimental set up for (A) NapDLA$_{SP}$-mCherry, NapA$_{SP}$-mCherry and (B) TorA$_{SP}$-mCherry is identical to figure 5.3. Precursor (*) and mature form (**) are indicated. A Proteinase K resistant band is highlighted by an arrow. The molecular weight of proteins is given in kDa.

5.2.5 An *in vitro* cross-linking study between Tat signal peptide and Tat components

One powerful aspect of the *in vitro* transport assay is that it can be further modified in order to study substrate-translocase interactions by including, site-specifically, photosensitive non-natural amino acids, e.g. *p*Bpa (*p*-benzoyl-L-phenylalanine; Figure 5.6A) (Chin et al, 2002; Maurer et al, 2010). The phenylalanine analogue *p*Bpa can be activated to form a free radical by UV light, which in turn will cross-link covalently by C-H bonding to any other organic molecule in the "molecular neighbourhood". Although, no in vitro transport was detected for NapDLA$_{SP}$-mCherry and NapA$_{SP}$-mCherry an attempt was made to further analyse the interrelationship between those fusion proteins and the Tat complex using site-specific cross-linking. The following experiment was carried out in collaboration with Julia Fröbel, University of Freiburg.

Initially, the gene encoding the protein of interest is mutated in such changing a specific codon for the amber stop codon 'TAG'. Here a plasmid was used that expressed tatABC where tatA carried such TAG mutations either at codons 11 (normally isoleucine) or 32 (normally leucine codon), which are localized in the transmembrane domain or aliphatic helix, respectively. Cells producing the individual TatA variants also contained a plasmid (pSUP), which encodes an amber-suppressor-tRNA and a *p*Bpa-specific-tRNA-synthetase. The synthetase loads externally added *p*Bpa on to the suppressor-tRNA during cell growth, which suppresses the amber stop codon and specifically incorporates pBpa into

the protein nascent chain of TatA (resulting in TatA variant I11pBpa and L32pBpa; schematic description in Figure 5.6B).
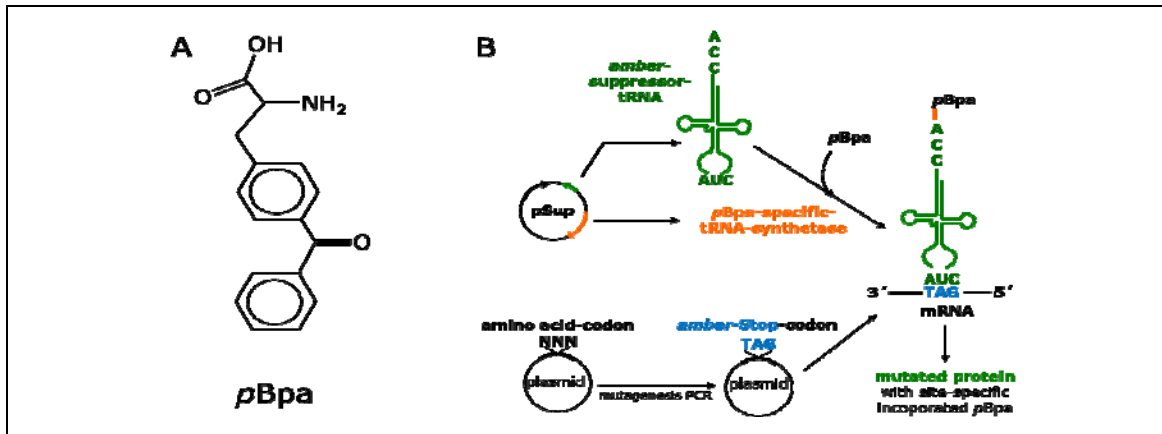
Figure 5.6 pBpa insertion into proteins. (A) Chemical structure of unnatural amino acid pBpa (p-benzoyl-L-phenylalanine). (B) First, the plasmid based gene of interest is subjected to mutagenizing PCR, substituting site-specifically one codon ('NNN') for an amber stop codon ('TAG'). Next, cells expressing an amber-suppressor-tRNA and a pBpa-specific-tRNA-synthetase (plasmid pSUP) are grown pBpa externally added to the medium. The cells specifically integrate pBpa into the newly synthesised protein. Courtesy Prof Peter G. Schultz, Scripps Research Institute, California.

Next, cells overproducing pBpa-containing TatABC were harvested and INVs prepared as described in Material and Methods. After *in vitro* transcription/translation of NapDLA$_{SP}$-mCherry and NapA$_{SP}$-mCherry, the INVs were added and the reaction subjected to UV light treatment for 20 minutes on ice (Figure 5.7 A and B). Possible cross-links between TatA variants I11pBpa and L32pBpa were analysed by SDS-PAGE and phosphor-imaging (Figure 5.7C).
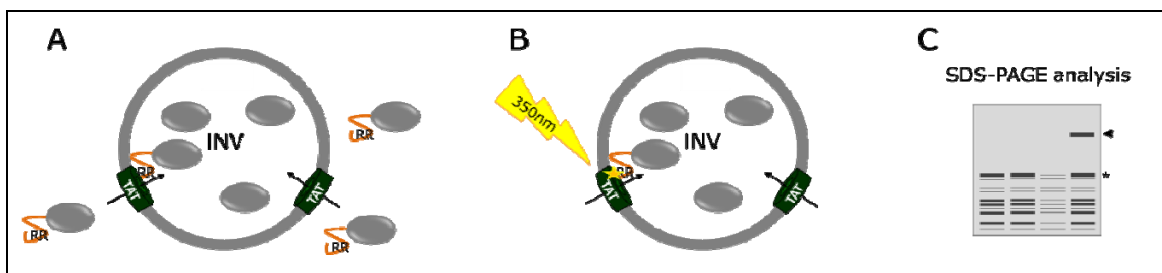
Figure 5.7 pBpa-based cross-linking between two binding partners. (A) Transport of the Tat substrate ('RR') is initiated by adding INVs containing TatABC. (B) The interaction between translocase and substrate is captured by applying UV light (350-360 nm wavelength), which activates pBpa (shown by a yellow star) and cross-links to any amino acid in close proximity. (C) The binding between two proteins is visualized as a band shift (arrow) by SDS-PAGE.

Figure 5.8A shows very efficient protein synthesis of NapDLA$_{SP}$-mCherry and NapA$_{SP}$-mCherry. However, no cross-links are visible between TatA variant I11pBpa or L32pBpa and the mCherry fusions. In contrast, control TorA$_{SP}$-mCherry interacts specifically with TatA L32pBpa, but not with TatA I11pBpa (Figure 5.8B). Binding of TorA$_{SP}$-mCherry to TatA at position L32 is in agreement with previous observations indicating the

importance of the aliphatic helix of TatA in signal peptide recognition (Fröbel et al, submitted).

In conclusion, NapA$_{SP}$ fusions to the reporter proteins CAT or mCherry are not transported *in vitro* by the Tat translocase.
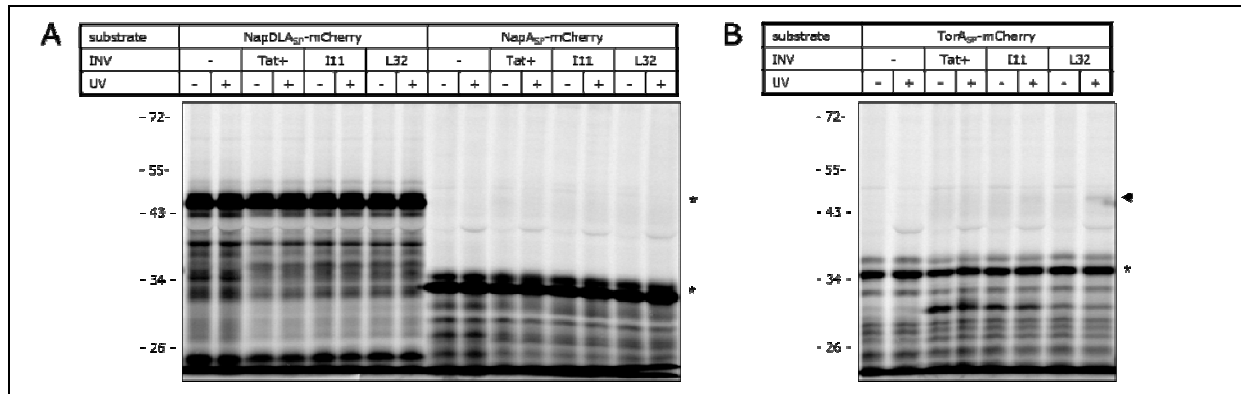
Figure 5.8 Cross-linking trials between mCherry fusions and the Tat complex. INVs were prepared from strains overexpressing TatABC (Tat+) or in addition have incorporated *p*Bpa in TatA on position I11 or L32. After *in vitro* translation of (A) NapDLA$_{SP}$-mCherry, NapA$_{SP}$-mCherry and (B) TorA$_{SP}$-mCherry proteins INVs were added and subjected to UV for 20 min. Mature forms are indicated by an asterisk, crosslink between TorA$_{SP}$-mCherry and TatA variant L32 highlighted by an arrow.

5.2.6 Utilising mCherry as a substrate for *in vivo* Tat transport assays

NapDLA$_{SP}$-mCherry and NapA$_{SP}$-mCherry were subjected to fluorescence microscopy to test for Tat export *in vivo* (Figure 5.9). The construct encoding NapDLA$_{SP}$-mCherry was slightly modified in that an additional C-terminal SsrA-tag (sequence 'AANDENYALAA') was included at the C-terminus of mCherry. Proteins with this specific tag are subjected to the cytoplasmic SsrA-SmpB system and quickly degraded by proteases (Karzai et al, 2000). Thus high levels of fluorescence inside the cell by non-exported proteins are dramatically reduced and make it possible to identify periplasmically-localised proteins, which are shielded from proteolysis.

E. coli strain BL21, which is able to express genes under the control of the T7 promoter, was individually transformed with plasmids encoding NapDLA$_{SP}$-mCherry-SsrA and NapA$_{SP}$-mCherry (Figure 5.9A and 5.9C). Fluorescence observed for cells producing NapDLA$_{SP}$-mCherry-SsrA is equally distributed over each cell. No increased fluorescence is detected around the membrane region (Figure 5.9C). The level of fluorescence is most possibly the lowest background level (Figure 5.9D). Cells producing NapA$_{SP}$-mCherry, however, show a distinct brighter rim around the cytoplasmic membrane (Figure 5.9A), which is indicative of Tat transport, or at least membrane association, of this protein (Figure 5.9B).
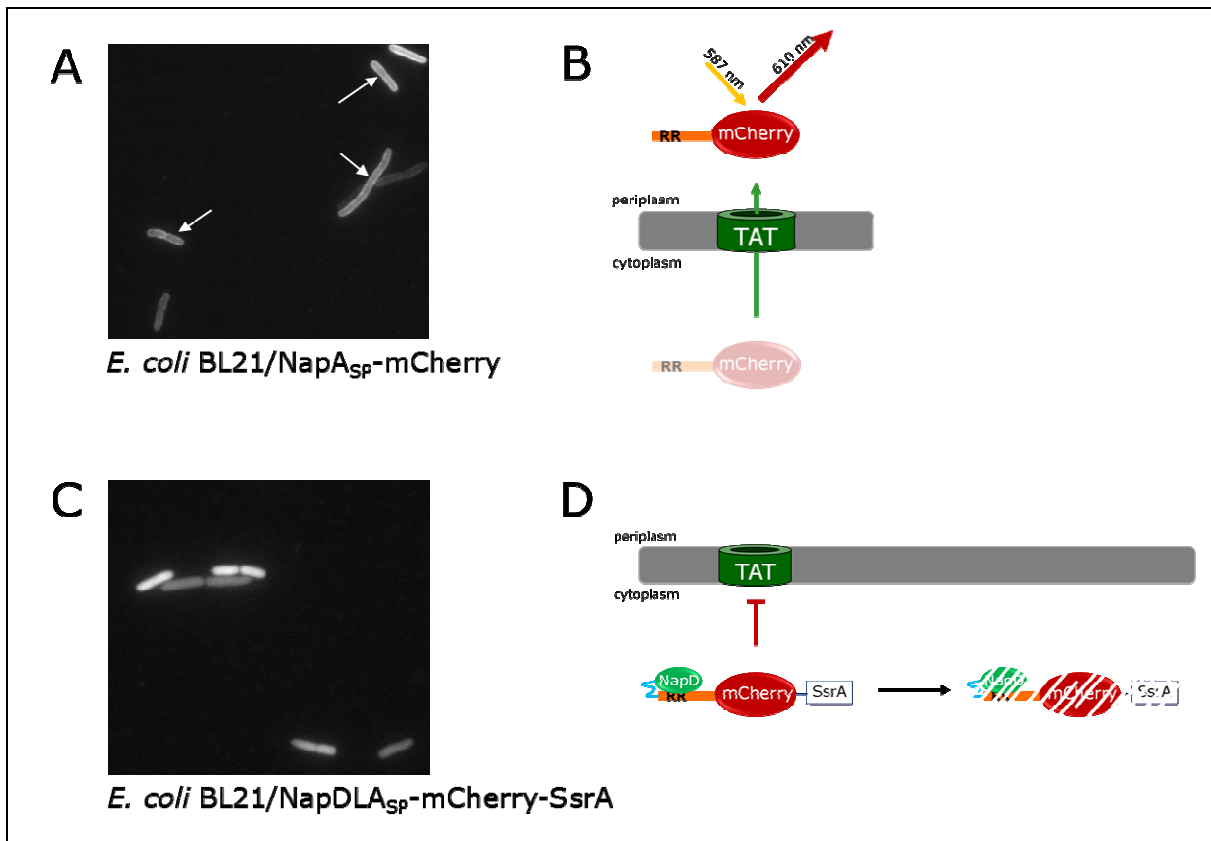
Figure 5.9 Visualizing the _in vivo_ transport efficiancy of mCherry fusion proteins by fluorescence microscopy. (A) _E. coli_ BL21 cells producing NapA$_{SP}$-mCherry exhibit a typical rim stain around the membrane region, which is indicated by white arrows. (B) In explanation of (A), fusion of mCherry to the NapA signal peptide ('RR') is recognized by the Tat complex and transported across the cytoplasmic membrane. Excitation of mCherry at ~587 nm wavelength results in fluorescence at 610 nm. (C) NapDLA$_{SP}$-mCherry-SsrA causes diffused fluorescence in BL21 cells. This point to (D) non transported protein resulting in degradation of NapDLA$_{SP}$-mCherry-SsrA by recruited proteases.

5.2.7 Towards visualizing the relationship between NapD and Tat

To understand and dissect possible interactions between NapD and the Tat complex under physiological conditions, fluorescence correlation spectroscopy (FCS) was chosen. This method measures the fluctuation of fluorescent labelled molecules diffusing in and out of a small detection volume (usually $\leq 10^{-15}$ l) and because of the restricted measurement volume it is important to keep the number of biomolecules to be analysed as low as possible (i.e. single-molecule-level). Therefore, the _nap_ operon and its resulting proteins are ideal candidates for FCS due to their naturally low expression levels. Also FCS is non-invasive thus perfectly situated for detecting interactions in living cells (Van den Wildenberg et al, 2011).
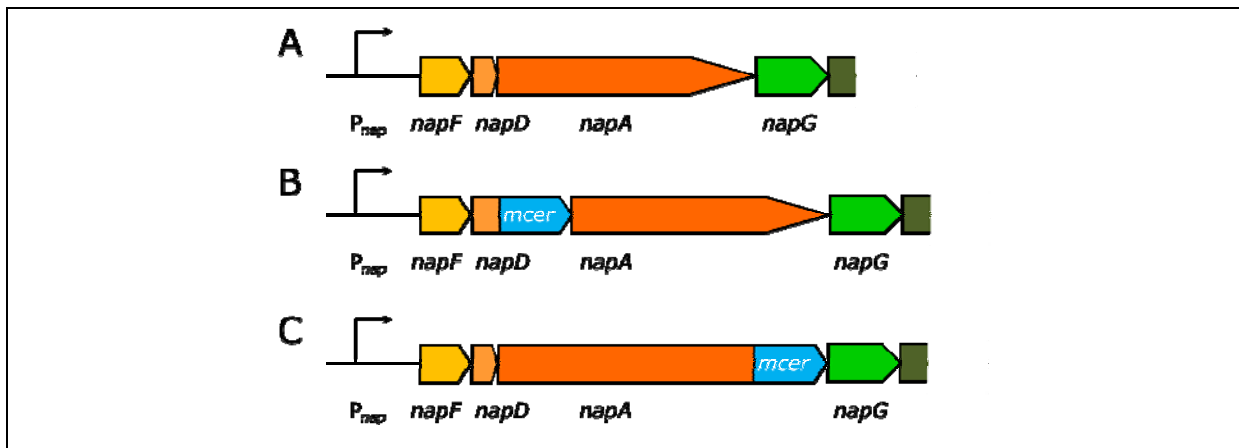
Figure 5.10 Chromosomal mCer fusions to *napD* and *napA*. (A) The *E. coli nap* operon showing the first four genes *napF, napD, napA and napG*. The gene encoding for mCer was either fused to (B) *napD* or (C) *napA*.

E. coli strains were constructed with chromosomal mCerulean (mCer) fusions to the 3' end of either *napD* or *napA* in the native *nap* operon (Figure 5.10). All mCer fusions are based on parental strain LCB2048, which expresses *nap* as the only nitrate reductase. To check if attachment of mCer has any influence on NapA activity or Tat transport, nitrite production assays were carried out (Figure 5.11). Strain LCBAmCer (NapA-mCer) retains similar levels of NapA activity as LCB2048 (Figure 5.11). Also, LCBDmCer (NapD-mCer) is able to reduce nitrate. However, the amount of produced nitrite in this strain is almost half compared to the parent strain, with a longer lag-phase (~3 hours compared to 2 hours) (Figure 5.9).
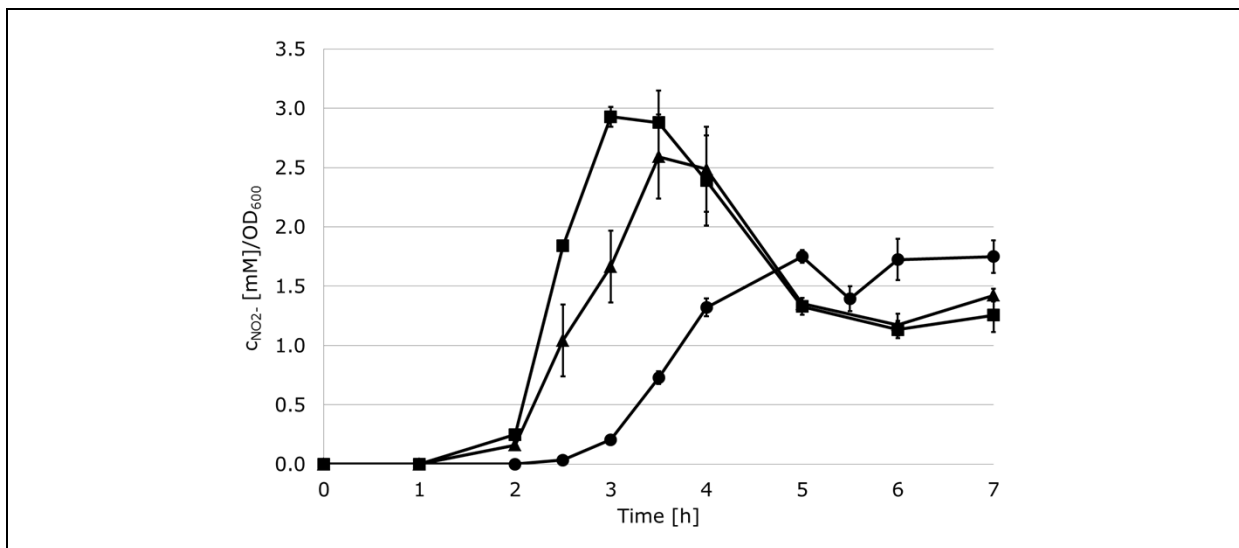
Figure 5.11 Chromosomal mCerulean fusions and their influence on NapA activity. Strains harbouring mCer fusions were tested for NapA activity. Strains are labelled as follows: wild type LCB2048 (*nap*[+]) (■), LCBAmCer/NapA-mCer (▲), LCBDmCer/NapD-mCer (●).

In summary, cells expressing either *napA-mCer* or *napD-mCer* show NapA activity. This forms a good basis for future work, which would involve the introduction of a second

fluorophore (e.g. YFP) to different possible interaction partners (e.g. individual Tat components).

5.3 DISCUSSION

5.3.1 *In vitro* and *in vivo* transport of Tat signal peptides containing reporter proteins

The aim of this Chapter was to establish if NapD, besides its role as a proofreading chaperone, could specifically target its substrate, NapA, to the Tat translocase for export. Previously it has been shown that another Tat chaperone, DmsD, is associated with the membrane and possibly interacts with the TatBC complex (Kostecki et al, 2010; Papish et al, 2003). Thus the authors hypothesized DmsD is escorting DmsA to initiate the interaction between TatBC and the signal peptide.

To determine if NapD could fulfil a similar function, fusions were prepared between NapD itself and the NapA signal peptide (NapDLA$_{SP}$), substituting the mature part of NapA for proteins CAT or mCherry. Previously it was shown that a NapD-NapA fusion using a linker retains NapA activity *in vivo* (Chapter 4) and that CAT and mCherry are excellent reporters for Tat transport when fused to a Tat signal peptide *in vivo* and *in vitro*, respectively (Chapter 2; Fröbel et al., submitted; Maillard et al., 2007; Stanely et al., 2002).

In vitro transport was carried out according to Panahandeh et al (2010) using TatABC containing INVs. However, none of the NapDLA$_{SP}$ fusion proteins was exported in this assay; neither had been NapA$_{SP}$-CAT and NapA$_{SP}$-mCherry. In contrast a substitution for the Tat signal peptide of TorA (TorA$_{SP}$-mCherry) was transported into INVs followed by signal peptide cleavage. It needs to be noted that transport efficiency of TorA$_{SP}$-mCherry in this *in vitro* assay is very low in relation to available synthesised protein. Usually, only a maximum of up to 20% translocation is achieved for *in vitro* synthesised proteins (Alami et al, 2002). If the amount of NapA$_{SP}$ fusion proteins being transported is 50% less then shown for TorA$_{SP}$-mCherry, it would not be detected in this assay, showing its strong limitation on sensitivity.

In vivo analysis monitoring growth of CAT fusion producing cells in the presence of chloramphenicol and protein localisation by fluorescence for mCherry fusions revealed that proteins containing only the NapA signal peptide were transported by Tat, whereas N-terminal fusion to NapD blocked transport.

Here, it has been already proposed that in order to trigger NapD release from the signal peptide cofactor insertion into the mature part of NapA has to be completed first (Chapter 4). This suggests that NapD might not act as targeting protein for NapA. In

addition NapD is localized in the cytoplasm (Maillard et al, 2007), but DmsD (Kostecki et al, 2010; Papish et al, 2003) and overproduced TorD (K. McGowan & F. Sargent, unpublished) have been found to be partly membrane associated. Therefore, if a targeting mechanism for Tat substrates exists, it might be a sole function of the TorD/DmsD family.

Still, the question remains why NapA signal peptide containing proteins are not transported efficiently *in vitro* but are transported very efficiently *in vivo*? Holzapfel et al (2009) using the same *in vitro* translation/transport approach, reported that the signal peptide of SufI was interacting non-specifically with the periplasmic chaperone FkpA. The binding between those two proteins was due to the application of extract for the translation process prepared from whole cells (Holzapfel et al, 2009).

In order to test the possibility of a periplasmic contamination blocking the transport of NapA signal peptide containing proteins, an *in vitro* transport assay was carried out (Yufan Zhou, University of Freiburg) using the PURE (protein synthesis using recombinant elements) system. The PURE system consists of all necessary components for in vitro transcription and translation, which were highly purified and combined in a defined buffer system (Holzapfel et al, 2009). Even so good synthesize rate of NapDLA$_{SP}$-mCherry, NapA$_{SP}$-mCherry and TorA$_{SP}$-mCherry were achieved, none of those three proteins was transported into TatABC containing INVs (data not shown). Thus a careful optimisation of the PURE system would be needed for further investigation on the *in vitro* transport of NapA$_{SP}$ containing proteins.

5.3.2 Initial *in vivo* analysis of the interrelationship between NapD and Tat on native level

To establish, if NapD targets NapA specifically to the Tat complex and to understand the interaction between NapD and NapA in more detail an *in vivo* approach was chosen with the ultimate aim of using fluorescence correlation spectroscopy. *E. coli* strains harbouring chromosomal mCer fusions to the C-terminus of either NapD or NapA were constructed and retained Tat dependent NapA activity. Those are the first steps towards the spectroscopic analysis of the two Nap proteins and their interaction with the Tat subunits. To see a correlation between binding and release of NapD/NapA and the Tat components a second fluorophore (e.g. YFP) could be inserted into each strain in order to test different protein interactions:

1. A NapD-mCer/NapA-YFP combination in *tat*[+] and *tat*[-] background could be analysed as it has been suggested that interactions between NapD and NapA is dependent on the presence of the Tat complex (Chan et al, 2010).

2. FCS studies on NapD-mCer and TatA-, TatB- or TatC-YFP could shed more light on interaction between NapD and any of the Tat subunits, drawing conclusions about the possibility of Tat substrate targeting for export. Strains producing such YFP fusions at single copy are already available (e.g. Tarry et al. 2009).

3. In addition, the combination of NapA-mCer and YFP-fusions to the Tat components could give more insight into the substrate/translocase relationship.

It needs to be noted that besides the several advantages of FCS (non-invasive, native protein levels avoiding artefacts from overexpression) also disadvantages have been reported, such as small size of bacteria, photo-bleaching and, for detection of membrane proteins, membrane curvature and different refraction index of lipids compared to aqueous environment of the cytoplasm (Medina & Schwille, 2002). However, a study exists that shows successful tracking of TatA in bacteria by FCS giving promising opportunities for further studies (Van den Wildenberg et al, 2011). Overall, FCS analysis will need careful set up and optimisation as well as committed collaboration from experts in this area.

6 Conclusions and future perspectives

6.1 *THE NITROGEN CYCLE AND NAPA*

The nitrogen cycle is one of the most important nutrition cycles on Earth. However, with industrial development humans had a big influence in the global nitrogen balance through processes such as new agricultural practises and combustion of fossil fuels (Canfield et al, 2010). In the last 50 years an increase of over 800% in the use of nitrogen-based fertilizers was observed (Fixen & West, 2002). Furthermore, the efficiency of certain kind of crops for nitrogen uptake is below 40%, thus a large amount of nitrogen compounds in the soil are either washed out from the root zone or converted back into N_2 by denitrification. Also during denitrification NO and N_2O are produced, which partially escape into the atmosphere. N_2O, together with CO_2 and CH_4, is one of the most important greenhouse gases where the global warming potential of N_2O is even 300 times greater than that of CO_2 (Richardson et al, 2009). In addition, NO and N_2O have large effects on the depletion of the ozone layer (Lassey et al, 2007).

A key step in the denitrification process is the conversion of nitrate to nitrite, which is performed by nitrate reductases. Considering the huge influence of denitrification by bacteria in agriculture it is important to study those nitrate reductase regarding their assembly and function. In *E. coli*, as well as in other bacteria, two types of nitrate reductases are found: the membrane-bound nitrate reductases NarGHI and NarZYV in the cytoplasm, and the periplasmic nitrate reductase NapA. Both enzymes contain Mo-bis-MGD in their active centre and [Fe-S] clusters for electron transfer (Bertero et al, 2003; Jepson et al, 2007). But how is it possible that NarGHI/NarZYV and NapA possess the same cofactors and perform the same reaction even though they are localized in different compartments of the cell?

NapA contains an N-terminal signal peptide with an 'S-R-R-s-F-M-K' motif, which targets NapA to the Tat pathway for transport into the periplasm. Importantly, NapA folding and cofactor insertion needs to be completed in the cytoplasm prior to export. A key question is how maturation of NapA is controlled and assessed. Therefore, molecular and structural studies were performed here to understand the complex process of cofactor assembly and NapA maturation in relation to Tat transport.

6.2 *PROOFREADING OF NAPA BY THE CHAPERONE NAPD*

6.2.1 NapD binding to the Tat signal peptide of NapA

Many cofactor-containing Tat substrates interact with very specific chaperones in the cytoplasm, which ensures protein folding, cofactor insertion and assembly in a process

named collectively as 'Tat proofreading' (Sargent, 2007b). It was shown that NapD is the proofreading chaperone for NapA binding very specifically and tightly to its Tat signal peptide (Maillard et al, 2007). Here, *in vivo* and *in vitro* interaction studies identified residues R6, K10 and A17 within the NapA signal peptide to be important for NapD binding, with NapA R6 and A17 also participating in Tat transport.

In addition, to highlight structural regions within NapD that participate in NapA signal peptide binding a screen of a *napD* mutant suppressor library was performed. Suppression genetics is a powerful tool to identify novel protein interactions or functions. It is often used when difficulties occur in obtaining the crystal structure of proteins or complexes, e.g. for a multimeric membrane protein complexes. The group of Thomas Silhavy has made many great contributions in understanding the assembly of outer membrane proteins or the insertion of lipopolysaccharides in Gram-negative bacteria by the Bam complex using this technique (e.g. Chimalakonda et al, 2010; Ruiz et al, 2006). In this study, *napD* mutants were identified that showed increased affinity for the NapA A17Q signal peptide variant. However rather than isolate direct compensatory mutations as would be the best-case scenario, here mutation such as NapD I19F, located on the first α-helix, were identified that must be having long-range effects on the signal peptide binding site.

Surprisingly, none of the *napD* mutants was able to restore full nitrate reductase activity to NapA variant A17Q, even in a Δ*napD* strain (LP203$_S$). It can only be concluded that even though those NapD variants are able to interact with the Tat signal peptide, somehow biosynthesis of NapA remains impaired. Therefore, to further investigate the mechanism of Tat proofreading, future work could include the extension of the screen using *E. coli* strain LP203$_S$. Growth tests on nitrate could identify new NapD variants that would enabling not just signal peptide binding, but also full maturation and thus nitrate reduction activity of the NapA A17Q variant. Overall, however, residues as part of the interaction interface between NapD and NapA identified here, but also by Maillard et al (2007), were well supported by an NMR structure of NapD in complex with the NapA signal peptide.

However, how does NapD recognize the NapA signal peptide? Does NapD receive the signal peptide immediately at the ribosomal exit tunnel, and is binding initiated by nucleotide binding as shown for TorD (Hatzixanthis et al, 2005)? As for TorD, no specific nucleotide binding motif is found within NapD either (Turner et al, 2004). Considering the high affinity of NapD for the NapA signal peptide, it could be possible that NapD out-competes general chaperones such as TF and SRP at this early stage. Future experiments could include nucleotide binding analysis by NapD as well as cross-linking

experiments between NapD and the NapA signal peptide-producing ribosome. Given the high number of alanine and valine residues within the NapA signal peptide h-region, it may be hard for SRP to resist binding to this protein as it emerges from the ribosome. Perhaps fusion of NapA$_{SP}$ to a Sec-dependent membrane protein (e.g. LepB) followed by expression in +/- *napD* strains would give insight into possible competition between SRP and NapD for this signal peptide.

6.2.2 Does NapD participate in cofactor insertion?

Purification studies of NapD in complex with NapA suggest dissociation of NapD occurs after cofactor insertion. A covalent fusion of NapD to NapA, on the other hand, had a stabilizing effect on the NapA iron-sulphur cluster under aerobic conditions. Indeed the fusion experiment probably also supports the hypothesis that NapD binds only to the Tat signal peptide, and nowhere else on NapA (Maillard et al, 2007; Chan et al, 2010).

Still, it is not known if NapD is actively participating in cofactor insertion into NapA, as been shown for two other Tat proofreading chaperones, TorD and DmsD. There, some data has been presented that suggests both chaperones interact *in vitro* with components of the molybdenum cofactor biosynthesis pathway, and were even able to bind the precursor and mature forms of the Mo-*bis*-MGD cofactor itself (Genest et al, 2008; Li et al, 2010). If this is true for NapD may need to be established in the future. Also the possibility should be considered that NapD acts as a scaffold protein for assembly of the [4Fe-4S] cluster, especially considering its ferredoxin-like structure. It has already been shown that the chaperones HscA/HscB, homologues of Hsp70, bind to IscU, which is an iron-sulphur template protein in one of the iron-sulphur cluster pathways (Bonomi et al, 2008). To test if any NapD residues could have an influence on iron-sulphur cluster insertion into NapA single substitutions at positions H2, C8 and C32 were constructed. However, none of the resulting variants (H2A, C8S or C32A) had any effect on the enzymatic activity of NapA (data not shown). Nevertheless, cluster coordination can also be dependent on amino acid side-chains such as Asp or Ser, and even backbone amides can be involved (Moulis et al, 1996). Thus it is probable that only multiple mutations in *napD* would be required to negatively affect the cofactor assembly activity of the protein.

Overall, only structural studies will give further understanding on the interaction between NapD and NapA. In this project crystal trials were performed on the *E. coli* NapDA complex, however to date no crystals were obtained. This is one area that definitely needs further investigation and investment of time and effort. Perhaps more, automated, crystallisation screens, or changing to NapDA from another organism, e.g. *R.*

sphaeroides or *C. necator*, where the structure of mature NapA has already been successfully solved.

6.3 TAT TRANSPORT OF NAPA

One of the main general questions remaining to be answered in Tat transport field is what triggers chaperone release so the Tat signal peptide can bind to the TatBC complex? Based on interaction and purification studies it was proposed for TorD and DmsD that they would indeed specifically target their respective passenger proteins to the Tat machinery (Kostecki et al, 2010; Papish et al, 2003).

In this work *in vitro* cross-linking experiments were planned to detect possible interactions between NapD, the NapA signal peptide, and the Tat complex. However were not successful. The biggest problem was that the Tat transport assays suggest that the activities of NapD and the NapA signal peptide *in vivo* is very different to what is observed *in vitro*. In particular, the transport activity of NapA$_{SP}$ *in vitro* was so low as to be undetectable.

For further investigation on NapD interaction with the Tat translocase fluorescence correlation spectroscopy could be the method of choice. This technique allows measuring binding kinetics between two partners on a native protein level in the living cell (Sahoo and Schwille, 2011). Here, strains were prepared that produce active NapD-mCer and NapA-mCer fusions from the chromosome. This forms a good base for future studies and might demonstrate targeting of NapA by NapD for transport.

Already one can speculate if NapD acts as a shuttle protein like a signal recognition particle. Some evidence would suggest 'no': for example, DmsD was proposed to target DmsA$_{SP}$ to the TatBC complex and is already associated with the membrane (Papish et al, 2003). In contrast, NapD was shown to be localized in the cytoplasm, at least in resting cells (Maillard et al, 2007). Furthermore, purification of the NapDA complex resulted in dissociation of NapD from NapA, possibly triggered by completed NapA folding and/or maturation. For NapD to act as signal recognition particle / shuttle protein it would need to remain tightly associated with the signal peptide after the passenger enzyme has been folded.

In relation to Tat transport another question concerns the structural transitions that the signal peptide undergoes during binding to the translocase. *In vitro* studies on a Tat signal peptide showed that it was unstructured in solution, however became helical in a more hydrophobic environment (San Miguel et al, 2003). Here, the NMR structure of the NapA signal peptide is α-helical when bound to NapD and PELDOR analysis suggests that overall this conformation is broadly retained, even when the signal peptide is in its free

state. Fincher and co-workers did transport studies on a Tat substrate of the Delta pH pathway in chloroplasts and concluded that the signal sequence forms a loop when it is bound to the translocase (Fincher et al, 1998). A similar observation can be made for NarG. This nitrate reductase contains an N-terminal extension with a remnant Tat motif indicating its evolutionary relation to Tat substrates (Ize et al, 2009). In the crystal structure of the water-soluble NarGH complex this N-terminus is unstructured (Jormakka et al, 2004), which is in agreement with the CD study of SufI$_{SP}$. In contrast, in the NarGHI holoenzyme the very N-terminus forms an α-helix followed by a twisted β-hairpin, which results from binding to the NarI subunit (Bertero et al, 2003). Thus it was hypothesized that this interaction of NarG to the membrane protein NarI reflects binding of a Tat signal peptide to the TatBC complex (Sargent, 2007a).

Regarding Tat signal peptide binding by the TatBC complex one obstacle that needs to be overcome is the determination of the number of signal peptide binding sites. Single-particle electron microscopy revealed up to two SufI molecules bound per TatBC (Tarry et al, 2009) and even up to four substrates on the Hcf106:cpTatC in chloroplasts (Ma & Cline, 2010). Assuming that TatBC consists of six or seven subunits of TatB and TatC each should provide six or seven possible binding sites (Oates et al, 2005; Tarry et al, 2009). ITC analysis suggests that one binding site is available with high binding affinity, whereas the others possess a relatively much lower affinity (M. Krehenbrick & B. Berks, unpublished).

6.4 ROLE OF NAPF IN NAPA MATURATION

6.4.1 Predicting the structure of NapF

A component that needs to be considered for the NapA maturation process is the iron-sulphur protein NapF. Protein data banks label NapF as a ferredoxin-like protein and sequence analysis shows four tetra-cysteine motifs. Mutational analysis of *W. succinogenes napF* revealed that the third cysteine motif is important for NapA maturation and activity (Kern & Simon, 2009). Bacterial two-hybrid analysis showed that *E. coli* NapF interacts with the precursor form of NapA, and the *R. sphaeroides* NapF was able to restore the [4Fe-4S] cluster into NapA (Nilavongse et al, 2006; Olmo-Mira et al, 2004). Therefore, two roles have been proposed for NapF: (i) facilitating cofactor insertion into NapA; and (ii) participating in electron transfer to the membrane complex NapGH.

Using the modelling programme Phyre (Kelley et al, 2009) *E. coli* NapF aligns with the β-subunit FdnH, which is part of the molybdenum-dependent formate dehydrogenase (Figure 6.1A). FdnH is membrane associated and transfers electrons from the catalytic α-subunit FdnG to the γ-subunit FdnI (Jormakka et al, 2002). However, the model of NapF

shows that the cysteine residues do not align with the iron-sulphur clusters of FdnH and the overall structure has many flexible unstructured parts (Figure 6.1B). Therefore, the actual NapF protein might be more compact. Nevertheless, because of structural relation between NapF and FdnH it might point to a role in electron transport for NapF.
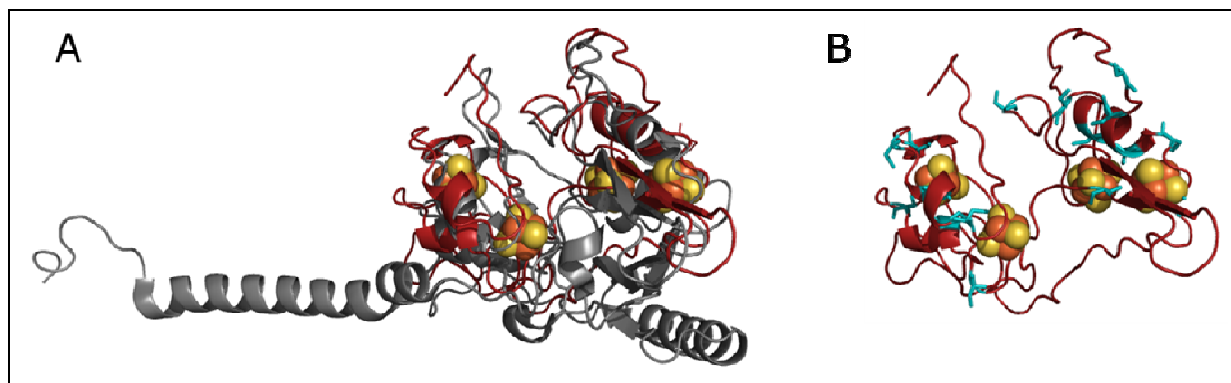
Figure 6.1 Predicted structure of *E. coli* NapF. (A) Alignment of NapF (red) with the β-subunit FdnH of the formate dehydrogenase-N (grey). The four [4Fe-4S] clusters are cofactors of FdnH and depicted as brown/yellow spheres. For modelling the programme Phyre was used (http://www.sbg.bio.ic.ac.uk/~phyre/). (B) NapF with its cysteine residues highlighted in cyan. The [4Fe-4S] clusters are kept from FdnH.

As part of this study two NapF constructs were made for protein overproduction. The first plasmid contained *napF* only with an N-terminal hexa-Histidine tag. Initial protein production tests did not give any protein, thus conditions for growth of the *E. coli* cells and for protein induction would need to be optimized. This would be followed by subjection of NapF to crystallisation trials, which should provide definitive information on NapF folding and the state of its cofactors.

The second construct encodes *napFDA*, exactly following the native *nap* operon, again with a hexa-Histidine tag at the N-terminus of NapF. Protein production from this plasmid was not tested. However, if successful, this could help conclude whether: (i) NapF stabilizes binding of NapD to NapA; or (ii) that NapF forms even a tighter complex with NapA. Again, the main goal would be structural analysis of the NapF complex.

6.4.2 NapF contains a remnant Tat motif

The N-terminal part of some NapF-like proteins bears a motif with two arginine residues, which is very similar to that of *bona fide* Tat signal peptides. In *E. coli* this N-terminal NapF sequence is 6-SRRGILT-13. However, the remainder of the N-terminus does not have the characteristic hydrophobic properties of a Tat signal peptide. Furthermore, cell fractionation established a cytoplasmic localisation of NapF in both *R. sphaeroides* and *E. coli* (Olmo-Mira et al, 2004; Nilavongse et al, 2006). Furthermore, also some NapD proteins, especially those from organisms that have no obvious NapF homolog, have an N-terminal extension containing a Tat-like motif (Martinez-Espinosa et al, 2007).

This phenomenon has been found for other proteins, where the N-terminus has sequence similarities with Tat signal peptides. However, as for NapF and NapD, none of those proteins are either predicted or proven to be transported by the Tat pathway (Turner et al, 2004). Interestingly, for NarG and BisC (biotin sulfoxide reductase) it was shown that six and five amino acid substitutions, respectively within those 'remnant signal peptides' located at the N-termini are enough to initiate export by the Tat complex in *E. coli* (Ize et al, 2009). It was proposed that those N-terminal extensions are important in biosynthesis of the proteins (Sargent, 2007a). Indeed, the chaperone NarJ binds to the N-terminus of NarG during cofactor insertion (Lanciano et al, 2007) and the BisC variant was inactive upon mutation (Ize et al, 2009), suggesting functional importance for remnant signal peptides.

Furthermore, TtrB and STM0612 from *Salmonella* contain remnant Tat signal peptides, but form tight complexes with other Tat dependent partner proteins in the cytoplasm before transport. It was speculated that TtrB and STM0612 had been originally individually exported by the Tat pathway, but this activity had been possibly lost during the course of evolution (Ize et al, 2009). Hence it is one possibility that forms of NapF and NapD once existed that were transported by the Tat complex into the periplasm. Considering the structure of both proteins (NapF contains [Fe-S] cluster, NapD has a ferredoxin-like fold) the participation in electron transfer to NapA, perhaps in reductive activation, would have been likely.

6.5 *Tat proofreading and quality control*

It is not possible to describe a general model for the Tat proofreading process, but what all Tat proofreading chaperones seem to have in common is their ability to bind to specific Tat signal peptides. The specificity between each chaperone and their individual Tat substrates might be initially defined by length and amino acid sequence of the Tat signal peptide, but also surrounding residues of the mature passenger domain (e.g. Ray et al, 2002; Maurer et al, 2010). Furthermore, at least five different families of proofreading chaperones are known so far based on their structural variability, which contributes further to the complexity of the system.

Interestingly, a few Tat substrates do not interact with proofreading chaperones. They are either cofactor-free or bind cofactors after transport into the periplasm. It was hypothesized that those Tat substrates fold too quickly, which prevents transport by the Sec pathway (Berks et al, 2003; Sturm et al, 2006). But how is it ensured that they are properly folded and thus active? An intrinsic quality control of the Tat complex was proposed, where unfolded Tat substrates were rejected from transport (DeLisa et al, 2003). This is probably caused by exposed hydrophobic patches, which preclude

interaction with the Tat complex. However, the translocase also shows relaxed specificity for folded proteins. For example small hydrophilic peptides fused *via* long unstructured linker were transported (Lindenstrauß & Brüser, 2009; Richter et al, 2007). However it should be noted that this does not necessarily reflect a physiological situation in the cell and therefore investigation on the possibility of a Tat quality control should include true Tat substrates.

6.6 *FUTURE WORK*

Research regarding the Tat proofreading process and the export of proteins *via* the Tat pathway still leaves many unanswered questions.

With regards to NapD, it is known that it recognises and binds to the Tat signal peptide of NapA (Maillard et al, 2007). However, it is not known, if there are additional binding sites on the mature region of NapA, as exists for TorA and its proofreading chaperone TorD (Jack et al, 2004; Tranier et al, 2002). Further structural knowledge could help in answering such questions, such as the co-crystallisation of the full-length NapDA complex.

NapD also stabilizes NapA during folding (Maillard et al, 2007). However, how far NapD participates in the folding process itself is unknown. Possibly, NapD, as hypothesised for DmsD, is guiding NapA through a cascade of general chaperones, including DnaK-DnaJ-GrpE and GroEL-GroES (Li et al, 2010). Yet evidence for such a 'chaperone cascade' is lacking, leading to a possible role of NapD during cofactor insertion into NapA. It was shown for TorD and DmsD that both proteins interact with components of the molybdenum cofactor biosynthesis (Genest et al, 2008; Li et al, 2010). Regarding NapD, with its ferredoxin-like fold, it is DmsD may also participate in [Fe-S] cluster insertion into NapA, however, specific motifs in the amino acid sequence have yet to be discovered (Turner et al, 2004). It may also be possible that NapD is involved in a transient transfer of the [Fe-S] from one of the scaffold proteins to apo-NapA. Chapter 4 of this study showed already that NapD is able to stabilize the [Fe-S] cluster into NapA.

If NapD is important for co-factor insertion, we would hypothesize that completed cofactor insertion (either after [Fe-S] cluster or after the MoCo insertion) into NapA acts as a trigger for NapD release. Following on, this hypothesis therefore suggests that NapA is not targeted to the TatBC complex, as suggested for DmsA through DmsD (Papish et al, 2003; Kostecki et al, 2010), but rather finds its way through simple diffusion. It also means that NapD, assuming it only binds to the Tat signal peptide, 'senses' completed NapA maturation through strong conformation changes, which influence the structure of the signal peptide itself. This also points to the major role of NapD: shielding the Tat signal peptide from pre-mature interactions with the Tat translocase.

Another question arising is how NapA binds to the TatBC complex. It was shown that TatC first recognises the Tat motif (Alami et al, 2003) and, subsequent to this event, TatB interacts with residues of the hydrophobic region and of the mature part of the substrate (Gérard & Cline, 2006; Maurer et al, 2010). It has been suggested that the Tat signal peptide forms a loop-like structure during binding to TatBC (Fincher et al, 1998). However, these suggestions pose additional questions, such as the valency of such interactions with the multiply heteromeric TatBC complex (Bolhuis et al, 2001). Also, how is TatA arranged in the membrane and later recruited to the TatBC complex? Which role does TatE play? Does TatE extend the TatA conducting channel? Regarding even the topology of the TatA complex contradicting results exist (e.g. Gouffi et al, 2004; Chan et al, 2011). And how are membrane bound Tat substrates inserted into the membrane *via* the Tat pathway?

Further, detailed biochemical investigations, aided by broader structural coverage, shall be required to answer the questions posed here. It is hoped that worked carried out in this current study will have provided a beneficial platform on which to build future investigations into this interesting field of microbiology.

7 Material and methods

7.1 E. COLI *STRAINS AND PLASMIDS*

Strain	Genotype	Resistance	Application	Reference
BL21 (DE3)	F⁻ *ompT gal dcm lon hsdS$_B$(r$_B$⁻ m$_B$⁻) λ(DE3)*	None	Preparation of inner membrane vesicles (INV)	New England Biolabs
BL21 (DE3) pLysS	F⁻ *ompT gal dcm lon hsdS$_B$(r$_B$⁻ m$_B$⁻) λ(DE3) (pLysS Cml^R)*	Chloramphenicol	Protein overproduction	New England Biolabs
BTH101	F⁻ *cya-99 araD139 galE15 galK16 rpsL1* (Str^r) *hsdR2 mcrA1 mcrB1*	None	Bacterial two-hybrid system	(Karimova et al, 1998)
BW25113 *ΔtatABCD::Apra*	Δ(araD-araB)567, ΔlacZ4787(::rrnB-3), lambda⁻, rph-1, Δ(rhaD-rhaB)568, hsdR514 ΔtatABCD::Apra	Apramycin	Lysate for P1 transduction	Kindly provided by Dr Berengere Ize
LCB2048	*nar25(narGH), thi-1, leu-6, thr-1, rpsL175, lacY,*Km^R, *narZ*::Ω, Spec^R	Kanamycin, Spectinomycin	*In vivo* nitrite production assay	(Blasco et al, 1992)
LCBAmCer	As LCB2048, but chromosomal fusion of *napA::mCerulean*	Kanamycin, Spectinomycin	*In vivo* nitrite production assay	This study
LCBDmCer	As LCB2048, but chromosomal fusion of *napD::mCerulean*	Kanamycin, Spectinomycin	*In vivo* nitrite production assay	This study

Table 7.1-1 Strains used in this study.

Strain	Genotype	Resistance	Application	Reference
LP202$_s$	As LCB2048, but Δ*napD*	Kanamycin, Spectinomycin	*In vivo* nitrite production assay	This study
LP203$_s$	AS LP202$_s$, but *napA* A17Q	Kanamycin, Spectinomycin	*In vivo* nitrite production	This study
MC4100	F⁻ *araD139 Δ(argF-lac)U169 rpsL150 relA1 deoC1 rbsR fthD5301 fruA25* λ⁻	None	Protein overproduction in combination with pREP4 and pQE70 overexpression plasmids	Lab stock
MG1655	F- λ- *rph-1*	None	*In vivo* Tat transport assay	Lab stock
SG3000	As MG1655, but Δ*tatABCD*	None	*In vivo* Tat transport assay	This study
SGDLA10	As LCB2048, but chromosomal fusion of *napDA via* linker (L) sequence	Kanamycin, Spectinomycin	*In vivo* nitrite production assay	This study
SGDLA11	As SGDLA10, but Δ*tatABC::Apra*	Kanamycin, Spectinomycin	*In vivo* nitrite production assay	This study

Table 7.1-2 Strains used in this study.

Strain	Genotype	Resistance	Application	Reference
SGQ061	As LCB2048, but *napAR6Q*	Kanamycin, Spectinomycin	*In vivo* nitrite production assay	This study
SGQ101	As LCB2048, but *napAK10Q*	Kanamycin, Spectinomycin	*In vivo* nitrite production assay	This study
SGQ171	As LCB2048, but *napAA17Q*	Kanamycin, Spectinomycin	*In vivo* nitrite production assay	This study
TOP10	F⁻ *mcrA D(mrr-hsd RMS-mcrBC) F 80lacZDM15 DlacX74 deoR recA1 araD139 D(araA-leu)697 galU galK*	None	Plasmid amplification	Invitrogen
XL10-Blue	*endA1 gyrA96(nal^R) thi-1 recA1 relA1 lac glnV44 F'[::Tn10 proAB⁺ lacI^q (lacZ)M15] hsdR17 (r$_K$⁻, m$_K$⁺)*	Tetracycline	Plasmid amplificatiom for NapD mutant supressor library	Invitrogen
DH5α	F- Φ80*lacZ*ΔM15 Δ(*lacZYA-argF*) U169 *recA1 endA1 hsdR17* (r$_K$-, m$_K$+) *gal⁻ phoA supE44* λ⁻ *thi⁻1 gyrA96 relA1*	None	Plasmid amplificatiom	Invitrogen

Table 7.1-3 Strains used in this study

109

Plasmid	Vector	Relevant characteristics	Resistance	Reference
pUT18	pUT18	Encoding the adenylate cyclase dpmain T18 from *Bordutella pertussis*	Ampicillin	Karimova et al, 1998
pUT18-NapA	pUT18	N-terminal fusion of NapA signal sequence to T18 fragment	Ampicillin	Maillard et al, 2007
pUT18-NapA K2Q	pUT18-NapA	K2Q substitution in NapA signal sequence by Quickchange	Ampicillin	This study
pUT18-NapA L3Q	pUT18-NapA	L3Q substitution in NapA signal sequence by Quickchange	Ampicillin0	This study
pUT18-NapA S4Q	pUT18-NapA	S4Q substitution in NapA signal sequence by Quickchange	Ampicillin	This study
pUT18-NapA R5Q	pUT18-NapA	R5Q substitution in NapA signal sequence by Quickchange	Ampicillin	This study
pUT18-NapA R6Q	pUT18-NapA	R6Q substitution in NapA signal sequence by Quickchange	Ampicillin	This study
pUT18-NapA S7Q	pUT18-NapA	S7Q substitution in NapA signal sequence by Quickchange	Ampicillin	This study
pUT18-NapA F8Q	pUT18-NapA	F8Q substitution in NapA signal sequence by Quickchange	Ampicillin	This study
pUT18-NapA M9Q	pUT18-NapA	M9Q substitution in NapA signal sequence by Quickchange	Ampicillin	This study
pUT18-NapA K10Q	pUT18-NapA	K10Q substitution in NapA signal sequence by Quickchange	Ampicillin	This study
pUT18-NapA A11Q	pUT18-NapA	A11Q substitution in NapA signal sequence by Quickchange	Ampicillin	This study

Table 7.2-1 Plasmids used in this study.

Plasmid	Vector	Relevant characteristics	Resistance	Reference
pUT18-NapA N12Q	pUT18-NapA	N12Q substitution in NapA signal sequence by Quickchange	Ampicillin	This study
pUT18-NapA A13Q	pUT18-NapA	A13Q substitution in NapA signal sequence by Quickchange	Ampicillin	This study
pUT18-NapA V14Q	pUT18-NapA	V14Q substitution in NapA signal sequence by Quickchange	Ampicillin	This study
pUT18-NapA A15Q	pUT18-NapA	A15Q substitution in NapA signal sequence by Quickchange	Ampicillin0	This study
pUT18-NapA A16Q	pUT18-NapA	A16Q substitution in NapA signal sequence by Quickchange	Ampicillin	This study
pUT18-NapA A17Q	pUT18-NapA	A17Q substitution in NapA signal sequence by Quickchange	Ampicillin	This study
pUT18-NapA A17L	pUT18-NapA	A17L substitution in NapA signal sequence by Quickchange	Ampicillin	This study
pUT18-NapA A18Q	pUT18-NapA	A18Q substitution in NapA signal sequence by Quickchange	Ampicillin	This study
pUT18-NapA A19Q	pUT18-NapA	A19Q substitution in NapA signal sequence by Quickchange	Ampicillin	This study
pUT18-NapA A20Q	pUT18-NapA	A20Q substitution in NapA signal sequence by Quickchange	Ampicillin	This study
pUT18-NapA A21Q	pUT18-NapA	A21Q substitution in NapA signal sequence by Quickchange	Ampicillin	This study
pUT18-NapA G22Q	pUT18-NapA	G22Q substitution in NapA signal sequence by Quickchange	Ampicillin	This study

Table 7.2-2 Plasmids used in this study.

111

Plasmid	Vector	Relevant characteristics	Resistance	Reference
pUT18-NapA G22Q	pUT18-NapA	G22Q substitution in NapA signal sequence by Quickchange	Ampicillin	This study
pUT18-NapA L23Q	pUT18-NapA	L23Q substitution in NapA signal sequence by Quickchange	Ampicillin	This study
pUT18-NapA S24Q	pUT18-NapA	S24Q substitution in NapA signal sequence by Quickchange	Ampicillin	This study
pUT18-NapA V25Q	pUT18-NapA	V25Q substitution in NapA signal sequence by Quickchange	Ampicillin0	This study
pUT18-NapA P26Q	pUT18-NapA	P26Q substitution in NapA signal sequence by Quickchange	Ampicillin	This study
pUT18-NapA G27Q	pUT18-NapA	G27Q substitution in NapA signal sequence by Quickchange	Ampicillin	This study
pUT18-NapA V28Q	pUT18-NapA	V28Q substitution in NapA signal sequence by Quickchange	Ampicillin	This study
pUT18-NapA A29Q	pUT18-NapA	A29Q substitution in NapA signal sequence by Quickchange	Ampicillin	This study
pUT18-NapA R30Q	pUT18-NapA	R30Q substitution in NapA signal sequence by Quickchange	Ampicillin	This study
pUT18-NapA A31Q	pUT18-NapA	A31Q substitution in NapA signal sequence by Quickchange	Ampicillin	This study
pUT18-NapA V32Q	pUT18-NapA	V32Q substitution in NapA signal sequence by Quickchange	Ampicillin	This study
pUT18-NapA V33Q	pUT18-NapA	V33Q substitution in NapA signal sequence by Quickchange	Ampicillin	This study

Table 7.2-3 Plasmids used in this study.

Plasmid	Vector	Relevant characteristics	Resistance	Reference
pUT18-NapA G34Q	pUT18-NapA	G34Q substitution in NapA signal sequence by Quickchange	Ampicillin	This study
pT25		Encoding the adenylate cyclase dpmain T25 from *Bordutella pertussis*	Chloramphenicol	Karimova et al, 1998
pT25-NapD	pT25	C-terminal fusion of NapD to T25 fragment	Chloramphenicol	Maillard et al, 2007
pT25-NapD I19F T59I	pT25-NapD	Mutations introduced by error prone PCR	Chloramphenicol	This study
pT25-NapD I19F	pT25-NapD	Mutations introduced by error prone PCR	Chloramphenicol	This study
pT25-NapD T59I	pT25-NapD	T59I substitution in Nap D by Quickchange	Chloramphenicol	This study
pT25-NapD A14T A71T	pT25-NapD	Mutations introduced by error prone PCR	Chloramphenicol	This study
pQE70		IPTG inducible overexpression vector for C-terminal His-tagged proteins	Ampicillin	Invitrogen
pQE70-NapD	pQE70	C-terminal His-tagged NapD	Ampicillin	Maillard et al, 2007
pQE70-NapD I19F T59I	pQE70-NapD	I19F and T59I substitutions in NapD by Quickchange	Ampicillin	This study
pQE70-NapD I19F	pQE70-NapD	I19F substitution in NapD by Quickchange	Ampicillin	This study
pQE70-NapD T59I	pQE70-NapD	T59I substitution in NapD by Quickchange	Ampicillin	This study

Table 7.2-4 Plasmids used in this study.

113

Plasmid	Vector	Relevant characteristics	Resistance	Reference
pQE70-NapD A14T A71T	pQE70-NapD	A14T and A71T substitutions in NapD by Quickchange	Ampicillin	This study
pQE70-NapD A14T	pQE70-NapD	A14T substitution in NapD by Quickchange	Ampicillin	This study
pQE70-NapD A71T	pQE70-NapD	A71T substitution in NapD by Quickchange	Ampicillin	This study
pQE70-NapD Cys⁻	pQE70-NapD	C8S and C32A substitutions in NapD by Quickchange	Ampicillin	This study
pQE70-NapDA$_{SP}$	pQE70	Fusion of NapD *vis* linker sequence to NapA signal peptide	Ampicillin	Kindly provided by Dr. Julian Maillard
pQM-NapA	pQE70	C-terminal fusion of NapA signal sequence to MalE	Ampicillin	Maillard et al, 2007
pQM-NapA R6Q	pQM-NapA	R6Q substitution in NapA signal sequence by Quickchange	Ampicillin	This study
pQM-NapA M9Q	pQM-NapA	M9Q substitution in NapA signal sequence by Quickchange	Ampicillin	This study
pQM-NapA K10Q	pQM-NapA	K10Q substitution in NapA signal sequence by Quickchange	Ampicillin	This study
pQM-NapA A17Q	pQM-NapA	A17Q substitution in NapA signal sequence by Quickchange	Ampicillin	This study
pQM-NapA S4C S24C	pQM-NapA	S4C and S24C substitutions in NapA signal sequence by Quickchange	Ampicillin	This study

Table 7.2-5 Plasmids used in this study.

Plasmid	Vector	Relevant characteristics	Resistance	Reference
pREP4		Encoding *lacI* gene. Therefore thight regulation of gene expression.	Kanamycin	Invitrogen
pET15bTEV		IPTG inducible overexpression vector for C-terminal His-tagged proteins. Cleavable His-tag *via* TEV site	Ampicillin	Kindly provided by Prof William Hunter
pET15-NapDLA	pET15bTEV	Fusion of NapD to NapA *via* linker sequence (L)	Ampicillin	This study
pET-TEV	pET derivativ	His-tagged TEV protease	Ampicillin	Kindly provided by Prof William Hunter
pET22b(+)		Constitutively expressing vector with N-terminal *pelB* sequence and C-terminal His-tag	Ampicillin	Novagen
pET22-NapA$_{SP}$-mCherry	pET22b(+)	Fusion of NapA signal sequence to mCherry. PelB signal sequence is removed.	Ampicillin	This study
pET22-NapDLA$_{SP}$-mCherry	pET22b(+)	Fusion of NapD *via* linker and NapA signal sequence to mCherry. PelB signal sequence is removed.	Ampicillin	This study
pET22-NapDLA$_{SP}$-mCherry-SsrA	pET22-NapDLA-mCherry	C-terminal SsrA-tag for cytoplasmic degradation	Ampicillin	This study
pET22-TorA$_{SP}$-mCherry	pET22b(+)	Fusion of TorA signal sequence to mCherry. PelB signal sequence is removed.	Ampicillin	Kindly provided by Prof Matthias Müller
pMAK705		Suicide vector for gene deletion or insertion by homologues recombination	Chloramphenicol	Hamiltonet al, 1989

Table 7.2-6 Plasmids used in this study.

Plasmid	Vector	Relevant characteristics	Resistance	Reference
pMAK705 Δ*napD*	pMAK705	Suicide plasmid to delete *napD*	Chloramphenicol	Kindly provided by Dr Julian Maillard
pMAK705 Δ*napD napA* A17Q	pMAK705	Suicide plasmid to delete *napD* and insert an A17Q substitution on the NapA signal peptide	Chloramphenicol	This study
pMAK705 *napA* R6Q	pMAK705	Suicide plasmid to insert a R6Q substitution on the NapA signal peptide	Chloramphenicol	This study
pMAK705 *napA* K10Q	pMAK705	Suicide plasmid to insert a K10Q substitution on the NapA signal peptide	Chloramphenicol	This study
pMAK705 *napA* A17Q	pMAK705	Suicide plasmid to insert an A17Q substitution on the NapA signal peptide	Chloramphenicol	This study
pMAK705 *napD-L-A*	pMAK705	Suicide plasmid to fuse *napD* to *napA via* a linker sequence	Chloramphenicol	This study
pMAK705 *napD*-mCerulean	pMAK705	Suicide plasmid to fuse *napD* tomCerulean	Chloramphenicol	This study
pMAK705 *napA*-mCerulean	pMAK705	Suicide plasmid to fuse *napA* tomCerulean	Chloramphenicol	This study
pMAK705 Δ*narJ*	pMAK705	Suicide plasmid to delete *narJ*	Chloramphenicol	Kindly provided by Dr Julian Maillard
pMAK705 Δ*narW*	pMAK705	Suicide plasmid to delete *narW*	Chloramphenicol	Kindly provided by Dr Julian Maillard

Table 7.2-7 Plasmids used in this study.

Plasmid	Vector	Relevant characteristics	Resistance	Reference
pUNIProm	pT7.5	Constitutively expression from *tat* promotor	Ampicillin	(Jack et al, 2004)
pUNI-NapD	pUNIProm	Encoding for NapD	Ampicillin	Maillard et al, 2007
pUNI-NapD H2A	pUNI-NapD	H2A substitution in NapD by Quickchange	Ampicillin	This study
pUNI-NapD W5A	pUNI-NapD	W5A substitution in NapD by Quickchange	Ampicillin	This study
pUNI-NapD C8S	pUNI-NapD	C8S substitution in NapD by Quickchange	Ampicillin	This study
pUNI-NapD C32A	pUNI-NapD	C32A substitution in NapD by Quickchange	Ampicillin	This study
pUNI-NapDE80K	pUNI-NapD	E80K substitution in NapD by Quickchange	Ampicillin	This study
pUNI-NapD E81K	pUNI-NapD	E81K substitution in NapD by Quickchange	Ampicillin	This study
pUNI-NapD E84K	pUNI-NapD	E84K substitution in NapD by Quickchange	Ampicillin	This study
pUNI-NapD E85K	pUNI-NapD	E85K substitution in NapD by Quickchange	Ampicillin	This study
pUNI-NapD E80/81K	pUNI-NapD	E80K and E81K substitutions in NapD by Quickchange	Ampicillin	This study
pUNI-NapD E84/85K	pUNI-NapD	E84 and E85K substitutions in NapD by Quickchange	Ampicillin	This study

Table 7.2-8 Plasmids used in this study.

Plasmid	Vector	Relevant characteristics	Resistance	Reference
pUNI-NapD E80/81/84/85K	pUNI-NapD	E80K, E81K, E84 and E85K substitutions in NapD by Quickchange	Ampicillin	This study
pUNI-Rep	pUNIProm	Encoding CAT	Ampicillin	Maillard et al, 2007
pUNI-NapA	pUNI-Rep	N-terminal fusion of the NapA signal sequence to CAT	Ampicillin	Maillard et al, 2007
pUNI-NapA R6Q	pUNI-NapA	R6Q substitution in NapA signal sequence by Quickchange	Ampicillin	This study
pUNI-NapA K10Q	pUNI-NapA	K10Q substitution in NapA signal sequence by Quickchange	Ampicillin	This study
pUNI-NapA A17Q	pUNI-NapA	A17Q substitution in NapA signal sequence by Quickchange	Ampicillin	This study
pUNI-NapDLA$_{SP}$	pUNI-NapA	Fusion of NapD via a linker and the NapA signal sequence to CAT	Ampicillin	This study
pSUProm		Constitutively expressing vector under the control of the E. coli tat promoter	Kanamycin	Jack et al, 2004
pSU-NapD	pSUProm	Encoding NapD	Kanamycin	Maillard et al, 2007
P8737	pET22b(+)	Overexpression of tatABC	Ampicillin	(Alami et al, 2002)

Table 7.2-9 Plasmids used in this study.

118

7.2 ANTIBIOTIC CONCENTRATIONS

Antibiotic	Final concentration
Ampicillin	50 µg/ml
Apramycin	50 µg/ml
Chloramphenicol (in 100% ethanol)	20 µg/ml
Kanamycin	30 µg/ml
Tetracycline (in 100% methanol)	15 µg/ml

Table 7.3 Antibiotics used in this study.

7.3 MOLECULAR BIOLOGICAL METHODS

7.3.1 Site-directed mutagenesis by PCR (polymerase chain reaction)

Site-directed mutagenesis was performed according to the Quickchange manual from Stratagene. To introduce specific mutations on a given plasmid complementary primers were designed of 33 base pairs length each (Sigma). The mutated codon of interest was thereby positioned in the middle of each primer. For each PCR concentrations as described in table 6.4 were used. PCR was performed in Eppendorf Mastercycle Personal machine with running conditions summarized in table 7.9. To digest non-mutated, methylated DNA 1 µl of restriction enzyme *Dpn*I (Roche) was added and incubated overnight at 37°C. Subsequently plasmids were transformed into competent *E. coli* DH5α.

Component	Concentration
DNA template (plasmid)	10-20 ng
Primer 1 (forward)	100 ng
Primer 2 (reverse)	100 ng
Pfu Turbo DNA polymerase (2.5U/µl)[a]	1 µl
10x *Pfu* DNA polymerase reaction buffer	5 µl
dNTP mix[b]	1 µl
H_2O	ad 50 µl

Table 7.4 Composition for one PCR reaction. [a] *Pfu* Turbo DNA polymerase was purchased from Stratagene. [b] dNTP mix consists of 10 mM each of dATP, dCTP, dGTP, dTTP (Roche).

Segment	Cycle	Temperature	Time
1	1	95°C	30 sec
2	18	95°C	30 sec
		53°C	1 min
		68°C	1 min/kb of plasmid length
3	1	68°C	10 min

Table 7.5 Cycling parameters for site-directed mutagenesis.

7.3.2 Preparation of competent *E. coli* cells and plasmid transformation

An overnight culture of *E. coli* cells was diluted 1:100 into 5 ml LB (Luria-Bertani) medium (10 g/l tryptone, 5 g/l yeast extract, 10 g/l NaCl) and aerobically incubated for 90 min at 37°C. Cells were harvested at 4,000 rpm, 10 min, 4°C and resuspended in 500 μl filter sterilized transformation buffer (LB medium, 50 mM $MgSO_4$, 5% (v/v) DMSO, 10% (w/v) PEG6000). Cells were prepared for plasmid transformation by chilling on ice for 30 min together with 1-100 ng DNA. This was followed by a heat shock at 42°C for 90 sec. After cooling on ice 1 ml of LB was added and cells recovered at 37°C for one hour. Cells were plated on LB agar plates (LB medium, 1.5% agar) and colonies grown at 37°C overnight.

7.3.3 In-frame chromosomal gene deletion and insertion

7.3.3.1 pMAK705 vector-based recombination

Gene deletion or replacement on the chromosome of *E.coli* was achieved by a homologues recombination according to Hamilton et al using the suicide vector pMAK705 (Hamilton et al, 1989). Plasmids were transformed into a competent $recA^+$ target strain performing the heat shock state at 37°C for 5 min and cell recovery at 30°C for one hour. All following steps were performed using selective LB, if not differently stated. Colonies were grown at 30°C for 48 hours on LB agar plates from which an overnight culture was inoculated. Serial dilutions up to 10^{-7} were prepared and 200 μl plated on several LB plates. Except dilution 10^{-7}, which was incubated at 30°C as control, all plates were kept at 44°C to induce recombination of the plasmid's encoded gene or gene segment into the chromosome. Per mutation five 10 ml cultures with several colonies were set up and incubated aerobically for 24 hours at 30°C followed by two repeated 1:1000 dilutions under same growth conditions. Single colonies were isolated on a LB agar plate. To cure the pMAK705 plasmids from those colonies 16 liquid cultures in 10 ml LB medium free of antibiotics were set up with individual colonies and grown overnight at 44°C. Single colonies were purified by striking onto LB plates and subsequent incubation at 44°C. Around 10 colonies per curing were tested for chloramphenicol sensitivity at 30°C and verified by sequencing (DNA Sequencing and Services, University of Dundee).

7.3.3.2 Preparation of P1 lysate

E. coli strain BW25113 Δ*tatABCD::Apra* was grown aerobically overnight in 5 ml LB medium at 30°C. After adding 5 ml MC buffer (100 mM $MgSO_4$, 10 mM $CaCl_2$) cells were grown for additional 30 min at 37°C. Serial dilutions of phage P1 (lab stock) ranging from 10^0 to 10^{-3} were prepared in LB medium and subsequently 100 µl of each added to individual 150 µl of cells. After incubation for 15 min at 37°C, 3 ml LBMC soft agar (LB medium, 10 mM $CaCl_2$, 10 mM $MgSO_4$, 0.65% agar) was added and cells were poured on freshly prepared thick R-plates (LB medium, 0.1% glucose, 2 mM $CaCl_2$, 1.2% agar) containing 50 µg/ml apramycin. Colonies were allowed to grow for 5-7 hours at 37°C, after which soft agar from partial lysed plates was taken off into 2 ml LB medium. This was followed by adding 50 µl/volume chloroform and centrifugation for 15 min at 12,000 rpm. Supernatant was stored at 4°C in additional 50 µl/volume chloroform.

7.3.3.3 P1-transduction

A 5 ml overnight culture of the recipient strain was mixed with 5 ml MC buffer and incubated for 30 min at 37°C. The culture was divided into 2 x 2 ml (P1 transduction and negative control) and centrifuged at 4,000 rpm for 10 min. Control cells were resuspended in 200 µl TGYES (LB medium plus 0.2% (w/v) glucose) and recipient cells resuspended in 100 µl TGYES, 100 µl P1 phage solution and 10 µl 100 mM $CaCl_2$. Attachment of P1 phage was allowed to proceed for 30 min at 37°C without shaking and terminated by adding 5 ml 1M sodium citrate. Cells were harvested at 4,000 rpm, 10 min, washed in LB medium and resuspended in 5 ml TGYES supplemented with 20 mM sodium citrate. Cell recovery was achieved for 3 hours incubation at 37°C followed by a washing step with LB medium and cell uptake in 1.5 ml TGYES (plus 20 mM sodium citrate). An aliquot of 100 µl cells was plated on selective LB agar plates containing 3 mM pyrophosphate and colonies grown at 37°C overnight. To ensure complete removal of P1 phage single colonies were streaked out up to three times on selective LB plates in presence of pyrophosphate. Strains were stored at -80°C in LB medium and 25% (w/v) glycerol.

7.4 BIOCHEMICAL METHODS

7.4.1 Protein overproduction of NapDA$_{SP}$ for NMR analysis

E. coli strain MC4100 pREP4 overproducing NapDA$_{SP}$ was grown in a 50 ml pre-culture of M9 medium (2 mM $MgSO_4$, 0.1 mM $CaCl_2$, 12.8 g/l $Na_2HPO_4 \cdot 7H_2O$, 3 g/l KH_2PO_4, 0.5 g/l NaCl) supplemented with 0.2% D-glucose-$^{13}C_6$ and 0.1% $^{15}NH_4Cl$. Incubation was carried out aerobically at 37°C overnight and used to inoculate 1l of M9 medium. Cells were grown until an OD_{600} of ~0.4 and protein production induced with 1 mM IPTG (isopropyl β-D-1-thiogalactopyranoside, Sigma) for 4 hours at 37°C. Cells were harvested at 4,000

rpm, 4°C for 10 min and washed in 20 mM Tris-HCl, pH 7.6. Finally, cells were flash frozen in liquid nitrogen and kept at -20°C until further purification.

7.4.2 Protein overproduction of other hexa-Histidine-tagged proteins

Overnight cultures of *E. coli* harbouring overexpression plasmids were diluted 1:100 into LB medium (except for BL21(DE3) pLysS producing TEV (tobacco etch virus) protease: LB was supplemented with 1 mM $MgCl_2$, 0.5 mM $CaCl_2$, 0.2% (w/v) glucose) and grown at 37°C under aerobic conditions. At OD_{600} of ~0.5 induction conditions with IPTG were carried out as summarized in table 7.6. Cell harvesting, wash and storage was performed as for protein $NapDA_{SP}$ (Section 7.4.1).

Protein	TEV protease	NapD variants	MalE-NapA$_{SP}$ variants	NapDLA
IPTG (final concentration)	1 mM	1 mM	1 mM	0.25 mM
Induction time	overnight	4 hours	4 hours	overnight
Incubation temperature	25°C	37°C	37°C	30°C

Table 7.6 Conditions for His-tagged proteins regarding induction and overproduction.

7.4.3 Purification of NapDA$_{SP}$ and different variants of NapD and MalE-NapA$_{SP}$ using nickel affinity chromatography

Cells overproducing either variants of NapD or MalE-NapA$_{SP}$ were lysed by denaturing in Buffer A (20 mM Tris-HCl, pH 7.6, 250 mM NaCl, 25 mM imidazole, 2 mM DTT) and 5 M urea and subjected to sonication. Crude extracts were centrifuged at 12,000 rpm, 4°C for 20 min and loaded onto 5-ml HisTrap affinity columns (GE Healthcare) equilibrated in Buffer A and urea. Proteins were gradual refolded over 18 column volumes in Buffer A and subsequently eluted with 6 column volumes of a linear gradient in Buffer B (20 mM Tris-HCl, pH 7.6, 250 mM NaCl, 500 mM imidazole, 2 mM DTT). Fractions containing His-tagged protein were pooled and proceeded as described in the following sections.

7.4.4 Purification of TEV (tobacco etch virus) protease using nickel affinity chromatography

Per one gram of cells producing TEV protease 10 ml of purification buffer (50 mM $Na_2H_2PO_4$, pH 8.0, 300 mM NaCl, 1 mM DTT, 25 mM imidazole, 10% (w/v) glycerol) was added and cell suspension passed two times through a French Press Cell Disrupter (Thermo Scientific). The homogenate was centrifuged at 15,000 rpm for 20 min at 4°C. A pre-equilibrated 5-ml HisTrap HP column was loaded with the resulting supernatant and TEV protease eluted by applying a linear imidazole gradient from 25 mM to 250 mM over 12 column volumes. Pooled fractions were subjected to buffer exchange (purification buffer supplemented with 2 mM DTT and 20% (w/v) glycerol) *via* a Vivaspin

20 column (10,000 MWCO PES; Sartorius). Protein concentration was adjusted to 10 mg/ml and the protein kept at -80°C after flash freezing in liquid nitrogen.

7.4.5 Purification of NapDLA using nickel affinity chromatography

Cells were resuspended in 10 ml/g Buffer A and twice broken by French pressing. Crude extract was spun down at 12,000 rpm, 4°C for 20 min and supernatant loaded onto a pre-equilibrated 5 ml HisTrap HP column. NapDLA^{his} was eluted with a linear gradient of Buffer over 6 column volumes. To remove the cleavable His-tag fractions were pooled and concentrated to ~1 ml using a Vivaspin 20 column (50,000 MCO PES). Protein concentration was calculated with its specific extinction coefficient using Nanotrop ND-1000 (Thermo Scientific). NapDLA^{his} was diluted in 50 ml TEV buffer (50 mM Tris-HCl, pH7.8, 0.5 mM EDTA, 10% (w/v) glycerol, 2 mM DTT) and purified TEV^{his} protease added in a 1:20 molar ratio followed by an overnight incubation at 4°C, rocking. To separate cleaved NapDLA from non-cleaved NapDLA^{his} and TEV^{his} protease reverse nickel affinity chromatography was carried out on the same HisTrap HP column in Buffer A. The flow through containing NapDLA was collected, concentrated (final concentration 10-20 mg/ml) and passed on to Dr Alice Dawson (University of Dundee) for further purification and crystal trial set up.

7.4.6 Protein characterisation using size-exclusion chromatography

Nickel affinity purified NapD Cys$^-$ and MalE-NapA$_{SP}$ S4/24C were concentrated using Vivaspin 20 columns with 5,000 Da MWCO and 10,000 Da MWCO cut off, respectively followed by a buffer exchange to 20 mM Tris-HCl, pH 7.6 and 50 mM NaCl. Both proteins were mixed with 100 μM each and incubated at room temperature for 10 min. Protein sample was loaded on a pre-equilibrated Superdex75 column (GE Healthcare). Fractions were collected and from each 10 μl mixed with Lämmli sample buffer and run on a 15% SDS-PAGE. Size of the protein complex was calculated from a standard curve using a Gel Filtration Molecular Weight Markers Kit (29,000-200,000 Da; Sigma).

7.4.7 Site-directed spin labelling (SDSL) of MalE-NapA$_{SP}$ S4/24C variant

MalE-NapA$_{SP}$ S4/24C was reduced with 20 mM DTT followed by immediate buffer exchange of seven volumes of 20 mM Tris-HCl, pH 7.6, 50 mM NaCl using Vivaspin 20 columns (10,000 MWCO PES). The protein was labelled with a 10-fold molar excess of MTSL (S-(2,2,5,5-tetramethyl-2,5-dihydro-1H-pyrrol-3-yl)methylmethanesulfonothioate; Toronto Research Chemicals). Labelling was allowed to proceed for 4 hour at room temperature followed by an overnight incubation at 4°C. Unbound MTSL was removed by a final buffer exchange to deuterated 20 mM Tris-HCl, pH 7.6, 50 mM NaCl. Labelling was confirmed my mass spectrometry (FingerPrints Proteomics Facility, University of Dundee). One hundred micromolar MalE-NapA$_{SP}$ S4/24C were mixed in a 1:1 ratio with

NapD in presence of 50% D8-glycerol (Cambridge Isotope Laboratories) and stored at -80°C until EPR measurements were carried out. PELDOR (pulsed electron-electron double resonance) spectroscopy and data analysis was done by Dr Richard Ward and Dr David Norman, University of Dundee.

7.4.8 Isothermal titration calorimetry (ITC)

Nickel affinity purified variants of NapD and MalE-NapA$_{SP}$ were dialyzed in 20 mM Tris-HCl, pH 7.6. For ITC a VP-ITC microcalorimeter (MicroCal Inc., Northampton,MA) was used. Protein concentration of NapD was adjusted to 100 µM and 500 µl were loaded into the syringe. The sample cell contained 1.4 ml of 10 µM MalE-NapA$_{SP}$. Each experiment consisted of 35 x 8 µl injections at 28°C. Data analysis was performed with Origin 7.0 software (MicroCal; OriginLab Corp., Northhampton, MA).

7.5 TAT TRANSPORT IN A CELL-FREE SYSTEM

7.5.1 Preparation of S-135 cell extract

E. coli TOP10 cells were grown aerobically at 37°C in 1l batches of S-30 medium (9 g/l tryptone, 0.8 g/l yeast extract, 5.6 g/l NaCl, 1 mM NaOH, 0.08% (w/v) glucose) until late log-phase (OD$_{600}$ = 1.0-1.2). All subsequent steps were performed at 4°C. Cells were harvested at 5,000 rpm for 10 min and washed with S-30 buffer (10 mM TEAOAc, 14 mM Mg(OAc)$_2$, 60 mM KOAc, 1 mM DTT). After resuspension in 1 ml/g S-30 buffer (+ 0.5 mM PMSF) cells were passed twice through a French Press and crude extract centrifuged for 30 min at 15,000 rpm. To degrade endogenous mRNA from the obtained supernatant (S-30) readout of polysomal mRNA at 37°C for one hour was performed with the set up shown in table 5:

Stock solution		Volume [µl]/ml S-30	
1 M	TEAOAc	60.0	
1 M	DTT	0.6	
1 M	Mg(AOc)$_2$	1.6	
1 mM	18 amino acids	6.0	
1 mM	Methionine	6.0	
1 mM	Cysteine	6.0	
0.25 M	ATP (neutralized)	2.0	
0.2 M	Phosphoenol pyruvate	27.0	
2 mg/ml	Pyruvate kinase	2.4	

Table 7.7 Set up for readout of polysomal mRNA from S-30 extract. The reaction was performed at 37°C for 30 min.

To remove all readout components S-30 was three times dialyzed in 1l cold S-30 buffer for one hour followed by centrifugation at 88,000 rpm for 13 min. Resulting S-135 extract was flash frozen in liquid nitrogen and stored at -80°C.

7.5.2 Preparation of inside-out inner membrane vesicles (INV)

E. coli BL21(DE3) overexpressing *tatABC* genes were grown in INV medium (10 g/l yeast extract, 10 g/l tryptone, 28.9 g/l K_2HPO_4, 5.6 g/l KH_2PO_4, 10 g/l glucose) at 37°C. Protein production was induced at an OD_{600} of ~0.5 with 1 mM IPTG and incubated for 3 hours at 37°C. Cells were harvested at 5,000 rpm for 10 min, washed in Buffer A-INV (50 mM TEAOAc, pH 7.5, 250 mM sucrose, 1 mM EDTA, pH7.0, 1 mM DTT) and resuspended in 1 ml/g Buffer A-INV (+ 0.5 mM PMSF). After breakage of the cells two times by French pressing cell suspension was centrifuged for 2 hours at 40,000 rpm, 4°C. The crude membrane extract was resuspended in 2 ml Buffer A-INV per 1l starting batch and set on top of a sucrose gradient (0.77 M, 1.44 M, 2.02 M in a 1:1:1 ration of sucrose in Buffer A). After ultracentrifugation at 25,000 rpm for 16 hours the inner membrane fraction was visible as a yellow layer at the interface between sucrose step 0.77 M and 1.44 M. Inner membranes were collected and diluted in 25 ml 50 mM TEAOAc, pH 7.5. After centrifugation at 40,000 rpm for 2 hours membranes were resuspended in ~100 µl INV buffer (50 mM TEAOAc, pH 7.5, 250 mM sucrose, 1 mM DTT). This will result in absorption of 50 units/ml at 280 nm. INVs were aliquoted and kept at -80°C after flash freezing.

7.5.3 DNA preparation for *in vitro* transcription/translation

Template DNA for *in vitro* translation was prepared using a Maxiprep Kit according to supplier's instructions (Qiagen). To obtain high and pure DNA concentrations the standard protocol was changed in that way that after isopropanol wash and pelleting the DNA was solved in 700 µl EB buffer (10 mM Tris-HCl, pH 8.5, Qiagen), 70 µl P3 buffer (3 M potassium acetate, pH 5.5, Qiagen) and filled up to 2 ml with 100% ethanol. After 20 min incubation at -80°C and spinning for 15 min at 14,000 rpm DNA was washed with 70% ethanol, centrifuged again and resolved in EB buffer to a concentration of 1 µg/µl.

7.5.4 *In vitro* translation and transport

In vitro translation and transport was performed as described in Panahandeh et al and given again in detail below (Panahandeh & Müller, 2010).

To perform optimal transcription and translation *in vitro* buffer composition is crucial. The compensating buffer (CB) consists of 40 mM TEAOAc, pH 7.5, 140 mM KOAc, 6 mM $Mg(OAc)_2$. However, ion concentrations from DNA preparation, S-135 and INV need to be taken into account. Therefore CB is calculated as shown in table 6. Each reaction consists of 24 µl total volume reaction mix (RM) is prepared as shown in table 7.

	TEA/Tris [nmol]	K$^+$ [nmol]	Mg^{2+} [nmol]	Spermidine [nmol]	H$_2$O
3 µl S-135 *10 mM TEA, 60 mM K$^+$, 14 mM Mg^{2+a}*	30	180	42		
1 µl DNA *10 mM Tris^a*	10				
1 µl INV *50 mM TEA^a*	50				
Total (1)	90	180	42		
Desired final concentration: *40 mM TEA, 140 mM K$^+$,* *6 mM Mg^{2+}, 0.8 mM spermidine* *→ in 25 µl reaction* (2)	1000	3500	150	20	
Difference (2)–(1) *→ required for 25 µl reaction to be added via CB* (3)	960	3320	108	20	
Required nmol (3) are added in 5 µl CB **→ required nmol/µl CB** (4) *(= mM concentration of CB)*	192	664	21.6	4	
To prepare 1 ml of such CB *from 1 M TEA, 4 M K$^+$, 1 M Mg^{2+}, 0.1 M spermidine stocks* **add [µl]**	**192**	**166**	**21.6**	**40**	**580.4**

Table 7.8 Calculating the compensating buffer (CB). [a] Components that contribute relevantly to the ionic composition of the reaction mixture. Modified from Panahandeh et al, 2010.

Component	Concentration of stock solution	Final concentration	Volume [µl]/25 µl
CB[a]	5x	1x	5
H$_2$O			7.9
PEG6000	40% (w/v)	3.2% (w/v)	2
18 amino acids	1 mM each	0.04 mM each	1
DTT	200 mM	2 mM	0.25
dNTP mixture *dATP* *dGTP, dCTP, dUTP*	50 mM 10 mM each	2.5 mM 0.5 mM each	1.25
Phosphoenol pyruvate	200 mM	12 mM	1.5
Creatine phosphate	500 mM	8 mM	0.4
Creatine phosphokinase	10 mg/ml	40 µg/ml	0.1
DNA	1 mg/ml	40 µg/ml	1
S-135			3
T7 RNA polymerase			0.1[b]
[^{35}S]-Met/Cys			0.5
Total			**24**

Table 7.9 Calculating the reaction mixture (RM). [a] See table 4. [b] Depends on activity; use 5-10U of a commercial enzyme. Modified from Panahandeh et al, 2010.

To perform *in vitro* translation followed by transport into inside-out inner membrane vesicle the experiments were set up according to the following scheme:

Sample	1		2 (control)	
$V_{Reaction\ mixture\ (RM)}$ [µl]	48		48	

10 min, 37°C synthesis reaction

$V_{INV/Buffer}$ [µl]; add	2 (INV)		2 (INV buffer)	

20 min, 37°C transport

Divide samples [µl]	15	30	15	30
$V_{PK}{}^{a}$ [µl]; add		30		30
PK digest		25 min, 25°C		25 min, 25°C
$V_{TCA}{}^{b}$ [µl]; add	15	60	15	60
PK inactivation		10 min, 56°C		10 min, 56°C

30 min, ice
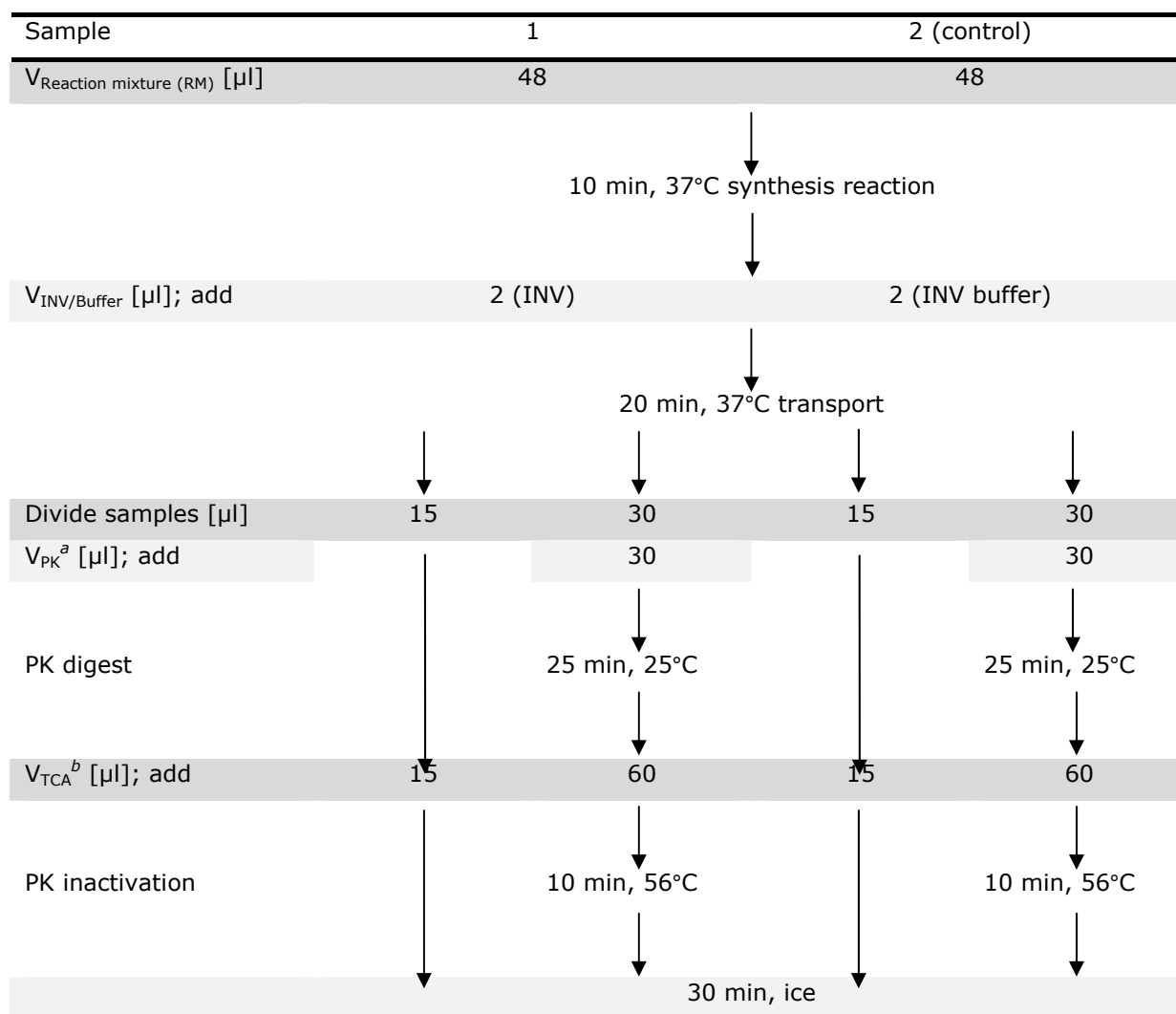
Table 7.10 Pipetting scheme for *in vitro* translation and transport. [a] Proteinase K (PK) concentration 1 mg/ml. [b] 10% trichloracetic acid (TCA).

Precipitated protein is pelleted by centrifugation at 13,000 rpm, 10 min. Supernatant is removed and protein dissolved by shaking in 30 µl SDS sample buffer (table 9) at 37°C. Proteins are separated on SDS-PAGE and analysed by radiography.

Solution	Component	Concentration
Solution I	Tris Base	0.2 M
	EDTA, pH 7.5	20 mM
Solution II	SDS	8.3% (v/v)
	Tris Base	83.3 mM
	Glycerol	29.2% (w/v)
	Bromphenol Blue	0.03% (w/v)
SDS sample buffer	Solution I	500 µl
	Solution II	400 µl
	1 M DTT	100 µl

Table 7.11 Composition of SDS sample buffer.

7.6 PROTEIN ASSAYS

7.6.1 Bacterial two-hybrid (BTH) system and β-galactosidase assay

The bacterial two-hybrid system is based on the reconstitution of the adenylate cyclase domain of CyaA toxin from *B. pertussis* (Karimova et al, 1998). Thereby the two domains T18 and T25 of CyaA produce cAMP (cyclic adenosine monophosphate) from ATP, if in close proximity. Plasmids encoding fusion proteins of T25 and T18 to different variants of NapD and the NapA signal peptide, respectively were transformed into the *cya* deficient *E. coli* strain BTH101. Transformants were plated on McConkey agar containing 1% maltose and incubated for 48 hours at 30°C. Red colony formation was indicative for positive protein interaction. To quantify the strength of the interaction β-galactosidase activity was measured. Cultures were grown in LB medium at 30°C until an OD_{600} of ~0.5 was reached. Cell density was measured and 1 ml vortexed together with 50 μl toluene followed by a 15 min incubation on ice. Crude cell extract was diluted 1:10 in Buffer Z (16.1 g/l of $Na_2HPO_4 \cdot 7H_2O$, 5.5 g/l of $NaH_2PO_4 \cdot H_2O$, 0.75 g/l of KCl, 0.246 g/l $MgSO_4 \cdot 7H_2O$) and 0.07% β-mercaptoethanol and equilibrated at 28°C. After adding 4 mg/ml ONPG (*o*-Nitrophenyl-β-galactoside) development of a yellow product was monitored and reaction stopped by adding 0.5 M Na_2CO_3. Time of reaction was noted and absorption measured at 420 nm.

The specific β-galactosidase activity is calculated as followed (Equation 7.1):

$$\beta - \text{galactosidase activity [Miller units]} = \frac{A_{420} \times 10^3}{t \times V \times OD_{600}}$$

Equation 7.1

t = time of reaction [min]

V = volume of cells [ml]

7.6.2 *In vivo* Tat transport assay

E. coli strain MG1655 producing NapA signal peptide fusions to CAT (chloramphenicol acetyl transferase; $NapA_{SP}$-CAT) from plasmid pUNI-REP (Maillard et al, 2007) was incubated aerobically at 37°C in LB medium. Growth rate was monitored at an OD_{600} in a Synergy 2 plate reader/incubator (BioTek, Winooski, VT) in absence and presence of high concentration of chloramphenicol (200 μg/ml).

7.6.3 *In vivo* nitrite production assay (Grieß method)

Strains were grown anaerobically at 37°C in 100 ml LB medium supplemented with 0.5% (v/v) glycerol, 0.4% (w/v) fumarate and 0.2% (w/v) nitrate. Aliquots were taken every 30 or 60 min for OD_{600} measurement and nitrite quantification. To calculate the concentration of nitrite 200 μl of cell-free supernatant were diluted in 600 μl 100 mM

Tris-HCl, pH 7.6 and 400 µl of 2:1 mix of 4% sulphanilamide (in 25% (v/v) conc. HCl) and 0.08% (w/v) *N*-(1-naphthyl)ethylendiamine. Samples were incubated for 15 min at room temperature and absorption measured at 540 nm. Nitrite concentration was calculated from a standard curve and normalized to cell density.

References

Alami M, Lüke I, Deitermann S, Eisner G, Koch HG, Brunner J, Müller M (2003) Differential interactions between a twin-arginine signal peptide and its translocase in Escherichia coli. Molecular Cell 12(4): 937-946

Alami M, Trescher D, Wu LF, Müller M (2002) Separate analysis of twin-arginine translocation (Tat)-specific membrane binding and translocation in Escherichia coli. Journal of Biological Chemistry 277(23): 20499-20503

Arnoux P, Sabaty M, Alric J, Frangioni B, Guigliarelli B, Adriano JM, Pignol D (2003) Structural and redox plasticity in the heterodimeric periplasmic nitrate reductase. Nature Structural Biology 10(11): 928-934

Arp DJ, Sayavedra-Soto LA, Hommes NG (2002) Molecular biology and biochemistry of ammonia oxidation by Nitrosomonas europaea. Archives of Microbiology 178(4): 250-255

Bageshwar UK, Musser SM (2007) Two electrical potential-dependent steps are required for transport by the Escherichia coli Tat machinery. Journal of Cell Biology 179(1): 87-99

Bageshwar UK, Whitaker N, Liang FC, Musser SM (2009) Interconvertibility of lipid- and translocon-bound forms of the bacterial Tat precursor pre-SufI. Molecular Microbiology 74(1): 209-226

Behrendt J, Standar K, Lindenstrauß U, Brüser T (2004) Topological studies on the twin-arginine translocase component TatC. FEMS Microbiology Letters 234(2): 303-308

Bendtsen JD, Nielsen H, Widdick D, Palmer T, Brunak S (2005) Prediction of twin-arginine signal peptides. BMC Bioinformatics 6

Bennett B, Berks BC, Ferguson SJ, Thomson AJ, Richardson DJ (1994) Mo(V) electron paramagnetic resonance signals from the periplasmic nitrate reductase of Thiosphaera pantotropha. European Journal of Biochemistry 226(3): 789-798

Bennett B, Charnock JM, Sears HJ, Berks BC, Thomson AJ, Ferguson SJ, Garner CD, Richardson DJ (1996) Structural investigation of the molybdenum site of the periplasmic nitrate reductase from Thiosphaera pantotropha by X-ray absorption spectroscopy. Biochemical Journal 317(2): 557-563

Berks BC (1996) A common export pathway for proteins binding complex redox cofactors? Molecular Microbiology 22(3): 393-404

Berks BC, Ferguson SJ, Moir JWB, Richardson DJ (1995) Enzymes and associated electron transport systems that catalyse the respiratory reduction of nitrogen oxides and oxyanions. Biochimica et Biophysica Acta - Bioenergetics 1232(3): 97-173

Berks BC, Palmer T, Sargent F (2003) The Tat protein translocation pathway and its role in microbial physiology. Advances in Microbial Physiology 47: 187-254

Bertero MG, Rothery RA, Boroumand N, Palak M, Blasco F, Ginet N, Weiner JH, Strynadka NCJ (2005) Structural and biochemical characterization of a quinol binding site of Escherichia coli nitrate reductase A. Journal of Biological Chemistry 280(15): 14836-14843

Bertero MG, Rothery RA, Palak M, Hou C, Lim D, Blasco F, Weiner JH, Strynadka NCJ (2003) Insights into the respiratory electron transfer pathway from the structure of nitrate reductase A. Nature Structural Biology 10(9): 681-687

Berthelmann F, Mehner D, Richter S, Lindenstrauß U, Lünsdorf H, Hause G, Brüser T (2008) Recombinant expression of tatABC and tatAC results in the formation of interacting cytoplasmic TatA tubes in Escherichia coli. Journal of Biological Chemistry 283(37): 25281-25289

Bieker KL, Silhavy TJ (1990) The genetics of protein secretion in E. coli. Trends in Genetics 6(10): 329-334

Biswas L, Biswas R, Nerz C, Ohlsen K, Schlag M, Schäfer T, Lamkemeyer T, Ziebandt AK, Hantke K, Rosenstein R, Götz F (2009) Role of the twin-arginine translocation pathway in Staphylococcus. Journal of Bacteriology 191(19): 5921-5929

Blasco F, Iobbi C, Ratouchniak J, Bonnefoy V, Chippaux M (1990) Nitrate reductases of Escherichia coli: Sequence of the second nitrate reductase and comparison with that encoded by the narGHJI operon. Molecular and General Genetics 222(1): 104-111

Blasco F, Pommier J, Augier V, Chippaux M, Giordano G (1992) Involvement of the narJ or narW gene product in the formation of active nitrate reductase in Escherichia coli. Molecular Microbiology 6(2): 221-230

Blattner FR, Plunkett Iii G, Bloch CA, Perna NT, Burland V, Riley M, Collado-Vides J, Glasner JD, Rode CK, Mayhew GF, Gregor J, Davis NW, Kirkpatrick HA, Goeden MA, Rose DJ, Mau B, Shao Y (1997) The complete genome sequence of Escherichia coli K-12. Science 277(5331): 1453-1462

Blaudeck N, Kreutzenbeck P, Freudl R, Sprenger GA (2003) Genetic analysis of pathway specificity during posttranslational protein translocation across the Escherichia coli plasma membrane. Journal of Bacteriology 185(9): 2811-2819

Bogsch E, Brink S, Robinson C (1997) Pathway specificity for a ΔpH-dependent precursor thylakoid lumen protein is governed by a 'Sec-avoidance' motif in the transfer peptide and a 'Sec-incompatible' mature protein. EMBO Journal 16(13): 3851-3859

Bogsch EG, Sargent F, Stanley NR, Berks BC, Robinson C, Palmer T (1998) An essential component of a novel bacterial protein export system with homologues in plastids and mitochondria. Journal of Biological Chemistry 273(29): 18003-18006

Bolhuis A, Mathers JE, Thomas JD, Claire M, Barrett L, Robinson C (2001) TatB and TatC Form a Functional and Structural Unit of the Twin-arginine Translocase from Escherichia coli. Journal of Biological Chemistry 276(23): 20213-20219

Bonomi F, Iametti S, Morleo A, Ta D, Vickery LE (2008) Studies on the mechanism of catalysis of iron-sulfur cluster transfer from IscU [2Fe-2S] by HscA/HscB chaperones. Biochemistry 47(48): 12795-12801

Braun NA, Davis AW, Theg SM (2007) The chloroplast tat pathway utilizes the transmembrane electric potential as an energy source. Biophysical Journal 93(6): 1993-1998

Breton J, Berks BC, Reilly A, Thomson AJ, Ferguson SJ, Richardson DJ (1994) Characterization of the paramagnetic iron-containing redox centres of Thiosphaera pantotropha periplasmic nitrate reductase. FEBS Letters 345(1): 76-80

Brondijk THC, Fiegen D, Richardson DJ, Cole JA (2002) Roles of NapF, NapG and NapH, subunits of the Escherichia coli periplasmic nitrate reductase, in ubiquinol oxidation. Molecular Microbiology 44(1): 245-255

Brondijk THC, Nilavongse A, Filenko N, Richardson DJ, Cole JA (2004) NapGH components of the periplasmic nitrate reductase of Escherichia coli K-12: Location, topology and physiological roles in quinol oxidation and redox balancing. Biochemical Journal 379(1): 47-55

Brown CT, Callan Jr CG (2004) Evolutionary comparisons suggest many novel cAMP response protein binding sites in Escherichia coli. Proceedings of the National Academy of Sciences of the United States of America 101(8): 2404-2409

Brüser T (2007) The twin-arginine translocation system and its capability for protein secretion in biotechnological protein production. Applied Microbiology and Biotechnology 76(1): 35-45

Brüser T, Sanders C (2003) An alternative model of the twin arginine translocation system. Microbiological Research 158(1): 7-17

Buchanan G, Maillard J, Nabuurs SB, Richardson DJ, Palmer T, Sargent F (2008) Features of a twin-arginine signal peptide required for recognition by a Tat proofreading chaperone. FEBS Letters 582(29): 3979-3984

Buchanan G, Sargent F, Berks BC, Palmer T (2002) A genetic screen for suppressors of Escherichia coli Tat signal peptide mutations establishes a critical role for the second arginine within the twin-arginine motif. Archives of Microbiology 177(1): 107-112

Canfield DE, Glazer AN, Falkowski PG (2010) The evolution and future of earth's nitrogen cycle. Science 330(6001): 192-196

Chan CS, Chang L, Rommens KL, Turner RJ (2009) Differential interactions between tat-specific redox enzyme peptides and their chaperones. Journal of Bacteriology 191(7): 2091-2101

Chan CS, Chang L, Winstone TML, Turner RJ (2010) Comparing system-specific chaperone interactions with their Tat dependent redox enzyme substrates. FEBS Letters 584(22): 4553-4558

Chan CS, Haney EF, Vogel HJ, Turner RJ (2011) Towards understanding the Tat translocation mechanism through structural and biophysical studies of the amphipathic region of TatA from Escherichia coli. Biochimica et Biophysica Acta - Biomembranes 1808(9): 2289-2296

Chan CS, Zlomislic MR, Tieleman DP, Turner RJ (2007) The TatA subunit of Escherichia coli twin-arginine translocase has an N-in topology. Biochemistry 46(25): 7396-7404

Chimalakonda G, Ruiz N, Chng SS, Garner RA, Kahne D, Silhavy TJ (2011) Lipoprotein LptE is required for the assembly of LptD by the β-barrel assembly machine in the outer membrane of Escherichia coli. Proceedings of the National Academy of Sciences of the United States of America 108(6): 2492-2497

Chin JW, Martin AB, King DS, Wang L, Schultz PG (2002) Addition of a photocrosslinking amino acid to the genetic code of Escherichia coli. Proceedings of the National Academy of Sciences of the United States of America 99(17): 11020-11024

Choe M, Reznikoff WS (1993) Identification of the regulatory sequence of anaerobically expressed locus aeg-46.5. Journal of Bacteriology 175(4): 1165-1172

Cline K, Henry R (1996) Import and routing of nucleus-encoded chloroplast proteins. Annual Review of Cell and Developmental Biology
 12: 1-26

Cline K, McCaffery M (2007) Evidence for a dynamic and transient pathway through the TAT protein transport machinery. EMBO Journal 26(13): 3039-3049

Coelho C, González PJ, Moura JG, Moura I, Trincão J, João Romão M (2011) The crystal structure of Cupriavidus necator nitrate reductase in oxidized and partially reduced states. Journal of Molecular Biology 408(5): 932-948

Cristóbal S, De Gier JW, Nielsen H, Von Heijne G (1999) Competition between Sec- and TAT-dependent protein translocation in Escherichia coli. EMBO Journal 18(11): 2982-2990

Cunha CA, Macieira S, Dias JM, Almeida G, Gonçalves LL, Costa C, Lampreia J, Huber R, Moura JJG, Moura I, Romão MJ (2003) Cytochrome c nitrite reductase from Desulfovibrio desulfuricans ATCC 27774. The relevance of the two calcium sites in the structure of the catalytic subunit (NrfA). Journal of Biological Chemistry 278(19): 17455-17465

D'Silva L, Ozdowy P, Krajewski M, Rothweiler U, Singh M, Holak TA (2005) Monitoring the effects of antagonists on protein-protein interactions with NMR spectroscopy. Journal of the American Chemical Society 127(38): 13220-13226

Dance I (2007) Elucidating the coordination chemistry and mechanism of biological nitrogen fixation. Chemistry - An Asian Journal 2(8): 936-946

Darwin AJ, Stewart V (1995) Nitrate and nitrite regulation of the Fnr-dependent aeg-46.5 promoter of Escherichia coli K-12 is mediated by competition between homologous response regulators (NarL and NarP) for a common DNA-binding site. Journal of Molecular Biology 251(1): 15-29

Darwin AJ, Ziegelhoffer EC, Kiley PJ, Stewart V (1998) Fnr, NarP, and NarL regulation of Escherichia coli K-12 napF (periplasmic nitrate reductase) operon transcription in vitro. Journal of Bacteriology 180(16): 4192-4198

De Buck E, Lammertyn E, Anné J (2008) The importance of the twin-arginine translocation pathway for bacterial virulence. Trends in Microbiology 16(9): 442-453

DeLisa MP, Tullman D, Georgiou G (2003) Folding quality control in the export of proteins by the bacterial twin-arginine translocation pathway. Proceedings of the National Academy of Sciences of the United States of America 100(10): 6115-6120

Dixon SJ, Costanzo M, Baryshnikova A, Andrews B, Boone C (2009) Systematic mapping of genetic interaction networks. Annual Review of Genetics 43: 601-625

Dreusch A, Bürgisser DM, Heizmann CW, Zumft WG (1997) Lack of copper insertion into unprocessed cytoplasmic nitrous oxide reductase generated by an R20D substitution in the arginine consensus motif of the signal peptide. Biochimica et Biophysica Acta - Bioenergetics 1319(2-3): 311-318

Drew D, Sjöstrand D, Nilsson J, Urbig T, Chin CN, De Gier JW, Von Heijne G (2002) Rapid topology mapping of Escherichia coli inner-membrane proteins by prediction and

PhoA/GFP fusion analysis. Proceedings of the National Academy of Sciences of the United States of America 99(5): 2690-2695

Driessen AJM, Nouwen N (2008) Protein translocation across the bacterial cytoplasmic membrane. Annual Review of Biochemistry 77: 643-667

Du Plessis DJF, Nouwen N, Driessen AJM (2011) The Sec translocase. Biochimica et Biophysica Acta - Biomembranes 1808(3): 851-865

Dubini A, Sargent F (2003) Assembly of Tat-dependent [NiFe] hydrogenases: Identification of precursor-binding accessory proteins. FEBS Letters 549(1-3): 141-146

Einsle O (2011) Structure and function of formate-dependent cytochrome c nitrite reductase, NrfA. Methods in Enzymology 496: 399-422

Einsle O, Stach P, Messerschmidt A, Klimmek O, Simon J, Kröger A, Kroneck PMH (2002) Crystallization and preliminary X-ray analysis of the membrane-bound cytochrome c nitrite reductase complex (NrfHA) from Wolinella succinogenes. Acta Crystallographica Section D: Biological Crystallography 58(2): 341-342

Fan E, Jakob M, Klösgen RB (2010) One signal is enough: Stepwise transport of two distinct passenger proteins by the Tat pathway across the thylakoid membrane. Biochemical and Biophysical Research Communications 398(3): 438-443

Fay D, Johnson W (2006) Genetic mapping and manipulation: chapter 10--Suppressor mutations. WormBook : the online review of C elegans biology: 1-4

Feltcher ME, Sullivan JT, Braunstein M (2010) Protein export systems of Mycobacterium tuberculosis: Novel targets for drug development? Future Microbiology 5(10): 1581-1597

Filenko N, Spiro S, Browning DF, Squire D, Overton TW, Cole J, Constantinidou C (2007) The NsrR regulon of Escherichia coli K-12 includes genes encoding the hybrid cluster protein and the periplasmic, respiratory nitrite reductase. Journal of Bacteriology 189(12): 4410-4417

Fincher V, McCaffery M, Cline K (1998) Evidence for a loop mechanism of protein transport by the thylakoid Delta pH pathway. FEBS Letters 423(1): 66-70

Fisher AC, Delisa MP (2004) A little help from my friends: Quality control of presecretory proteins in bacteria. Journal of Bacteriology 186(22): 7467-7473

Fisher AC, DeLisa MP (2009) Efficient Isolation of Soluble Intracellular Single-chain Antibodies using the Twin-arginine Translocation Machinery. Journal of Molecular Biology 385(1): 299-311

Fisher AC, Kim W, Delisa MP (2006) Genetic selection for protein solubility enabled by the folding quality control feature of the twin-arginine translocation pathway. Protein Science 15(3): 449-458

Fixen PE, West FB (2002) Nitrogen Fertilizers: Meeting contemporary challenges. Ambio 31(2): 169-176

Fontecilla-Camps JC, Volbeda A, Cavazza C, Nicolet Y (2007) Structure/function relationships of [NiFe]- and [FeFe]-hydrogenases. Chemical Reviews 107(10): 4273-4303

Genest O, Ilbert M, Méjean V, Iobbi-Nivol C (2005) TorD, an essential chaperone for TorA molybdoenzyme maturation at high temperature. Journal of Biological Chemistry 280(16): 15644-15648

Genest O, Méjean V, Iobbi-Nivol C (2009) Multiple roles of TorD-like chaperones in the biogenesis of molybdoenzymes. FEMS Microbiology Letters 297(1): 1-9

Genest O, Neumann M, Seduk F, Stöcklein W, Méjean V, Leimkühler S, Iobbi-Nivol C (2008) Dedicated metallochaperone connects apoenzyme and molybdenum cofactor biosynthesis components. Journal of Biological Chemistry 283(31): 21433-21440

Genest O, Seduk F, Ilbert M, Méjean V, Iobbi-Nivol C (2006a) Signal peptide protection by specific chaperone. Biochemical and Biophysical Research Communications 339(3): 991-995

Genest O, Seduk F, Théraulaz L, Méjean V, Iobbi-Nivol C (2006b) Chaperone protection of immature molybdoenzyme during molybdenum cofactor limitation. FEMS Microbiology Letters 265(1): 51-55

Gérard F, Cline K (2006) Efficient twin arginine translocation (Tat) pathway transport of a precursor protein covalently anchored to its initial cpTatC binding site. Journal of Biological Chemistry 281(10): 6130-6135

Gibney BR, Mulholland SE, Rabanal F, Dutton PL (1996) Ferredoxin and ferredoxin-heme maquettes. Proceedings of the National Academy of Sciences of the United States of America 93(26): 15041-15046

Giel JL, Rodionov D, Liu M, Blattner FR, Kiley PJ (2006) IscR-dependent gene expression links iron-sulphur cluster assembly to the control of O2-regulated genes in Escherichia coli. Molecular Microbiology 60(4): 1058-1075

Gohlke U, Pullan L, McDevitt CA, Porcelli I, De Leeuw E, Palmer T, Saibil HR, Berks BC (2005) The TatA component of the twin-arginine protein transport system forms channel complexes of variable diameter. Proceedings of the National Academy of Sciences of the United States of America 102(30): 10482-10486

González ET, Brown DG, Swanson JK, Allen C (2007) Using the Ralstonia solanacearum Tat secretome to identify bacterial wilt virulence factors. Applied and Environmental Microbiology 73(12): 3779-3786

Gouffi K, Gérard F, Santini CL, Wu LF (2004) Dual Topology of the Escherichia coli TatA Protein. Journal of Biological Chemistry 279(12): 11608-11615

Graubner W, Schierhorn A, Brüser T (2007) DnaK plays a pivotal role in Tat targeting of CueO and functions beside SlyD as a general Tat signal binding chaperone. Journal of Biological Chemistry 282(10): 7116-7124

Grove J, Tanapongpipat S, Thomas G, Griffiths L, Crooke H, Cole J (1996) Escherichia coli K-12 genes essential for the synthesis of c-type cytochromes and a third nitrate reductase located in the periplasm. Molecular Microbiology 19(3): 467-481

Guymer D, Maillard J, Agacan MF, Brearley CA, Sargent F (2010) Intrinsic GTPase activity of a bacterial twin-arginine translocation proofreading chaperone induced by domain swapping. FEBS Journal 277(2): 511-525

Hamilton CM, Aldea M, Washburn BK, Babitzke P, Kushner SR (1989) New method for generating deletions and gene replacements in Escherichia coli. Journal of Bacteriology 171(9): 4617-4622

Hatzixanthis K, Clarke TA, Oubrie A, Richardson DJ, Turner RJ, Sargent F (2005) Signal peptide-chaperone interactions on the twin-arginine protein transport pathway. Proceedings of the National Academy of Sciences of the United States of America 102(24): 8460-8465

Hatzixanthis K, Palmer T, Sargent F (2003) A subset of bacterial inner membrane proteins integrated by the twin-arginine translocase. Molecular Microbiology 49(5): 1377-1390

Hino T, Nagano S, Sugimoto H, Tosha T, Shiro Y (2011) Molecular structure and function of bacterial nitric oxide reductase. Biochimica et Biophysica Acta - Bioenergetics: doi:10.1016/j.bbabio.2011.1009.1021

Hinsley AP, Stanley NR, Palmer T, Berks BC (2001) A naturally occurring bacterial Tat signal peptide lacking one of the 'invariant' arginine residues of the consensus targeting motif. FEBS Letters 497(1): 45-49

Hoeren FU, Berks BC, Ferguson SJ, McCarthy JEG (1993) Sequence and expression of the gene encoding the respiratory nitrous-oxide reductase from Paracoccus denitrificans. New and conserved structural and regulatory motifs. European Journal of Biochemistry 218(1): 49-57

Hofmann K, Stoffel W (1993) TMbase - A database of membrane spanning protein segments. Biological Chemistry Hoppe-Seyler 374(166): 166

Holzapfel E, Eisner G, Alami M, Barrett CML, Buchanan G, Lüke I, Betton JM, Robinson C, Palmer T, Moser M, Müller M (2007) The entire N-terminal half of TatC is involved in twin-arginine precursor binding. Biochemistry 46(10): 2892-2898

Holzapfel E, Moser M, Schiltz E, Ueda T, Betton JM, Müller M (2009) Twin-arginine-dependent translocation of SufI in the absence of cytosolic helper proteins. Biochemistry 48(23): 5096-5105

Hoppe A, Pandelia ME, Gärtner W, Lubitz W (2011) [Fe4S4]- and [Fe3S4]-cluster formation in synthetic peptides. Biochimica et Biophysica Acta - Bioenergetics 1807(11): 1414-1422

Hu Y, Fay AW, Chi CL, Yoshizawa J, Ribbe MW (2008) Assembly of nitrogenase MoFe protein. Biochemistry 47(13): 3973-3981

Hu Y, Zhao E, Li H, Xia B, Jin C (2010) Solution NMR structure of the TatA component of the twin-arginine protein transport system from gram-positive bacterium Bacillus subtilis. Journal of the American Chemical Society 132(45): 15942-15944

Hubbell WL, Cafiso DS, Altenbach C (2000) Identifying conformational changes with site-directed spin labeling. Nature Structural Biology 7(9): 735-739

Ignatova Z, Hörnle C, Nurk A, Kasche V (2002) Unusual Signal Peptide Directs Penicillin Amidase from Escherichia coli to the Tat Translocation Machinery. Biochemical and Biophysical Research Communications 291(1): 146-149

Ilbert M, Méjean V, Giudici-Orticoni MT, Samama JP, Iobbi-Nivol C (2003) Involvement of a mate chaperone (TorD) in the maturation pathway of molybdoenzyme TorA. Journal of Biological Chemistry 278(31): 28787-28792

Ilbert M, Méjean V, Iobbi-Nivol C (2004) Functional and structural analysis of members of the TorD family, a large chaperone family dedicated to molybdoproteins. Microbiology 150(4): 935-943

Iobbi-Nivol C, Santini CL, Blasco F, Giordano G (1990) Purification and further characterization of the second nitrate reductase of Escherichia coli K12. European Journal of Biochemistry 188(3): 679-687

Ize B, Coulthurst SJ, Harzixanthis K, Caldelari I, Buchanan G, Barclay EC, Richardson DJ, Palmer T, Sargent F (2009) Remnant signal peptides on non-exported enzymes: Implications for the evolution of prokaryotic respiratory chains. Microbiology 155(12): 3992-4004

Ize B, Stanley NR, Buchanan G, Palmer T (2003) Role of the Escherichia coli Tat pathway in outer membrane integrity. Molecular Microbiology 48(5): 1183-1193

Jack RL, Buchanan G, Dubini A, Hatzixanthis K, Palmer T, Sargent F (2004) Coordinating assembly and export of complex bacterial proteins. EMBO Journal 23(20): 3962-3972

Jack RL, Sargent F, Berks BC, Sawers G, Palmer T (2001) Constitutive expression of Escherichia coli tat genes indicates an important role for the twin-arginine translocase during aerobic and anaerobic growth. Journal of Bacteriology 183(5): 1801-1804

Jepson BJN, Mohan S, Clarke TA, Gates AJ, Cole JA, Butler CS, Butt JN, Hemmings AM, Richardson DJ (2007) Spectropotentiometric and structural analysis of the periplasmic nitrate reductase from Escherichia coli. Journal of Biological Chemistry 282(9): 6425-6437

Jones CM, Stres B, Rosenquist M, Hallin S (2008) Phylogenetic analysis of nitrite, nitric oxide, and nitrous oxide respiratory enzymes reveal a complex evolutionary history for denitrification. Molecular Biology and Evolution 25(9): 1955-1966

Jong WSP, Ten Hagen-Jongman CM, Genevaux P, Brunner J, Oudega B, Luirink J (2004) Trigger factor interacts with the signal peptide of nascent Tat substrates but does not play a critical role in Tat-mediated export. European Journal of Biochemistry 271(23-24): 4779-4787

Jormakka M, Richardson D, Byrne B, Iwata S (2004) Architecture of NarGH Reveals a Structural Classification of Mo-bisMGD Enzymes. Structure 12(1): 95-104

Jormakka M, Törnroth S, Byrne B, Iwata S (2002) Molecular basis of proton motive force generation: Structure of formate dehydrogenase-N. Science 295(5561): 1863-1868

Karimova G, Pidoux J, Ullmann A, Ladant D (1998) A bacterial two-hybrid system based on a reconstituted signal transduction pathway. Proceedings of the National Academy of Sciences of the United States of America 95(10): 5752-5756

Kartal B, Maalcke WJ, de Almeida NM, Cirpus I, Gloerich J, Geerts W, Op den Camp HJM, Harhangi HR, Janssen-Megens EM, Francoijs KJ, Stunnenberg HG, Keltjens JT, Jetten MSM, Strous M (2011) Molecular mechanism of anaerobic ammonium oxidation. Nature 479(7371): 127-130

Karzai AW, Roche ED, Sauer RT (2000) The SsrA-SmpB system for protein tagging, directed degradation and ribosome rescue. Nature Structural Biology 7(6): 449-455

Kelley LA, Sternberg MJ (2009) Protein structure prediction on the Web: a case study using the Phyre server. Nature protocols 4(3): 363-371

Kennedy EJ, Yang J, Pillus L, Taylor SS, Ghosh G (2009) Identifying critical non-catalytic residues that modulate Protein Kinase A activity. PLoS ONE 4(3)

Kern M, Mager AM, Simon J (2007) Role of individual nap gene cluster products in NapC-independent nitrate respiration of Wolinella succinogenes. Microbiology 153(11): 3739-3747

Kern M, Simon J (2009) Periplasmic nitrate reduction in Wolinella succinogenes: Cytoplasmic NapF facilitates NapA maturation and requires the menaquinol dehydrogenase NapH for membrane attachment. Microbiology 155(8): 2784-2794

Kiley PJ, Beinert H (1998) Oxygen sensing by the global regulator, FNR: The role of the iron-sulfur cluster. FEMS Microbiology Reviews 22(5): 341-352

Kiley PJ, Reznikoff WS (1991) Fnr mutants that activate gene expression in the presence of oxygen. Journal of Bacteriology 173(1): 16-22

Kipping M, Lilie H, Lindenstrauß U, Andreesen JR, Griesinger C, Carlomagno T, Brüser T (2003) Structural studies on a twin-arginine signal sequence. FEBS Letters 550(1-3): 18-22

Klotz MG, Schmid MC, Strous M, Op Den Camp HJM, Jetten MSM, Hooper AB (2008) Evolution of an octahaem cytochrome c protein family that is key to aerobic and anaerobic ammonia oxidation by bacteria. Environmental Microbiology 10(11): 3150-3163

Kostecki JS, Li H, Turner RJ, DeLisa MP (2010) Visualizing interactions along the Escherichia coli twin-arginine translocation pathway using protein fragment complementation. PLoS ONE 5(2)

Kreutzenbeck P, Kröger C, Lausberg F, Blaudeck N, Sprenger GA, Freudl R (2007) Escherichia coli twin arginine (Tat) mutant translocases possessing relaxed signal peptide recognition specificities. Journal of Biological Chemistry 282(11): 7903-7911

Lanciano P, Vergnes A, Grimaldi S, Guigliarelli B, Magalon A (2007) Biogenesis of a respiratory complex is orchestrated by a single accessory protein. Journal of Biological Chemistry 282(24): 17468-17474

Lassey K, Harvey M (2007) Nitrous oxide: the serious side of laughing gas. Water & Atmosphere 15: 10-11

Leake MC, Greene NP, Godun RM, Granjon T, Buchanan G, Chen S, Berry RM, Palmer T, Berks BC (2008) Variable stoichiometry of the TatA component of the twin-arginine protein transport system observed by in vivo single-molecule imaging. Proceedings of the National Academy of Sciences of the United States of America 105(40): 15376-15381

Lee PA, Buchanan G, Stanley NR, Berks BC, Palmer T (2002) Truncation analysis of TatA and TatB defines the minimal functional units required for protein translocation. Journal of Bacteriology 184(21): 5871-5879

Lee PA, Orriss GL, Buchanan G, Greene NP, Bond PJ, Punginelli C, Jack RL, Sansom MSP, Berks BC, Palmer T (2006) Cysteine-scanning mutagenesis and disulfide mapping studies of the conserved domain of the twin-arginine translocase TatB component. Journal of Biological Chemistry 281(45): 34072-34085

Lee Y-F, Hsieh H-Y, Tullman-Ercek D, Chiang T-K, Turner RJ, Lin S-C (2010) Enhanced translocation of recombinant proteins via the Tat pathway with chaperones in Escherichia coli. Journal of the Taiwan Institute of Chemical Engineers 41(5): 540-546

Li H, Chang L, Howell JM, Turner RJ (2010) DmsD, a Tat system specific chaperone, interacts with other general chaperones and proteins involved in the molybdenum cofactor biosynthesis. Biochimica et Biophysica Acta - Proteins and Proteomics 1804(6): 1301-1309

Li S-Y, Chang B-Y, Lin S-C (2006) Coexpression of TorD enhances the transport of GFP via the TAT pathway. Journal of Biotechnology 122(4): 412-421

Lindenstrauß U, Brüser T (2009) Tat transport of linker-containing proteins in Escherichia coli. FEMS Microbiology Letters 295(1): 135-140

Lindenstrauß U, Matos CFRO, Graubner W, Robinson C, Brüser T (2010) Malfolded recombinant Tat substrates are Tat-independently degraded in Escherichia coli. FEBS Letters 584(16): 3644-3648

Lubitz W, Reijerse E, van Gastel M (2007) [NiFe] and [FeFe] hydrogenases studied by advanced magnetic resonance techniques. Chemical Reviews 107(10): 4331-4365

Lüke I, Butland G, Moore K, Buchanan G, Lyall V, Fairhurst SA, Greenblatt JF, Emili A, Palmer T, Sargent F (2008) Biosynthesis of the respiratory formate dehydrogenases from Escherichia coli: Characterization of the FdhE protein. Archives of Microbiology 190(6): 685-696

Lüke I, Handford JI, Palmer T, Sargent F (2009) Proteolytic processing of Escherichia coli twin-arginine signal peptides by LepB. Archives of Microbiology 191(12): 919-925

Ma X, Cline K (2010) Multiple precursor proteins bind individual Tat receptor complexes and are collectively transported. EMBO Journal 29(9): 1477-1488

Magalon A, Asso M, Guigliarelli B, Rothery RA, Bertrand P, Giordano G, Blasco F (1998) Molybdenum cofactor properties and [Fe-S] cluster coordination in Escherichia coli nitrate reductase A: Investigation by site-directed mutagenesis of the conserved His-50 residue in the NarG subunit. Biochemistry 37(20): 7363-7370

Maillard J, Spronk CAEM, Buchanan G, Lyall V, Richardson DJ, Palmer T, Vuister GW, Sargent F (2007) Structural diversity in twin-arginine signal peptide-binding proteins. Proceedings of the National Academy of Sciences of the United States of America 104(40): 15641-15646

Maldonado B, Buchanan G, Müller M, Berks BC, Palmer T (2011a) Genetic Evidence for a TatC Dimer at the Core of the Escherichia coli Twin Arginine (Tat) Protein Translocase. Journal of Molecular Microbiology and Biotechnology 20(3): 168-175

Maldonado B, Kneuper H, Buchanan G, Hatzixanthis K, Sargent F, Berks BC, Palmer T (2011b) Characterisation of the membrane-extrinsic domain of the TatB component of the twin arginine protein translocase. FEBS Letters 585(3): 478-484

Mandrand-Berthelot MA, Couchoux-Luthaud G, Santini CL, Giordano G (1988) Mutants of Escherichia coli specifically deficient in respiratory formate dehydrogenase activity. Journal of General Microbiology 134: 3129-3139

Marqusee S, Baldwin RL (1987) Helix stabilization by Glu-...Lys+ salt bridges in short peptides of de novo design. Proceedings of the National Academy of Sciences of the United States of America 84(24): 8898-8902

Martens-Habbena W, Stahl DA (2011) Nitrogen metabolism and kinetics of ammonia-oxidizing archaea. Methods in Enzymology 496: 465-487

Martínez-Espinosa RM, Cole JA, Richardson DJ, Watmough NJ (2011) Enzymology and ecology of the nitrogen cycle. Biochemical Society Transactions 39(1): 175-178

Martinez-Espinosa RM, Dridge EJ, Bonete MJ, Butt JN, Butler CS, Sargent F, Richardson DJ (2007) Look on the positive side! The orientation, identification and bioenergetics of 'Archaeal' membrane-bound nitrate reductases. FEMS Microbiology Letters 276(2): 129-139

Maurer C, Panahandeh S, Jungkamp AC, Moser M, Müller M (2010) TatB functions as an oligomeric binding site for folded tat precursor proteins. Molecular Biology of the Cell 21(23): 4151-4161

Maurer C, Panahandeh S, Moser M, Müller M (2009) Impairment of twin-arginine-dependent export by seemingly small alterations of substrate conformation. FEBS Letters 583(17): 2849-2853

Mayhew M, Hartl FU (1996) Molecular Chaperone Proteins in Escherichia coli and Salmonella and Molecular Biology. ASM Press, Washington DC 2nd edition

McNicholas PM, Gunsalus RP (2002) The molybdate-responsive Escherichia coli ModE transcriptional regulator coordinates periplasmic nitrate reductase (napFDAGHBC) operon expression with nitrate and molybdate availability. Journal of Bacteriology 184(12): 3253-3259

Medina MA, Schwille P (2002) Fluorescence correlation spectroscopy for the detection and study of single molecules in biology. BioEssays 24(8): 758-764

Moir JWB (2011) Nitrogen Cycle in Bacteria. Caister Academic Press

Mori H, Cline K (1998) A signal peptide that directs non-Sec transport in bacteria also directs efficient and exclusive transport on the thylakoid Delta pH pathway. Journal of Biological Chemistry 273(19): 11405-11408

Mori H, Cline K (2001) Post-translational protein translocation into thylakoids by the Sec and ΔpH-dependent pathways. Biochimica et Biophysica Acta - Molecular Cell Research 1541(1-2): 80-90

Moulis JM, Davasse V, Golinelli MP, Meyer J, Quinkal I (1996) The coordination sphere of iron-sulfur clusters: Lessons from site-directed mutagenesis experiments. Journal of Biological Inorganic Chemistry 1(1): 2-14

Müller M, Klösgen RB (2005) The Tat pathway in bacteria and chloroplasts. Molecular Membrane Biology 22(1-2): 113-121

Müllner M, Hammel O, Mienert B, Schlag S, Bill E, Unden G (2008) A PAS domain with an oxygen labile [4Fe-4S]2+ cluster in the oxygen sensor kinase NreB of Staphylococcus carnosus. Biochemistry 47(52): 13921-13932

Nilavongse A, Brondijk THC, Overton TW, Richardson DJ, Leach ER, Cole JA (2006) The NapF protein of the Escherichia coli periplasmic nitrate reductase system: Demonstration of a cytoplasmic location and interaction with the catalytic subunit, NapA. Microbiology 152(11): 3227-3237

Nolandt OV, Walther TH, Roth S, Bürck J, Ulrich AS (2009) Structure analysis of the membrane protein TatCd from the Tat system of B. subtilis by circular dichroism. Biochimica et Biophysica Acta - Biomembranes 1788(10): 2238-2244

Nurizzo D, Halbig D, Sprenger GA, Baker EN (2001) Crystal structures of the precursor form of glucose-fructose oxidoreductase from Zymomonas mobilis and its complexes with bound ligands. Biochemistry 40(46): 13857-13867

Oates J, Barrett CML, Barnett JP, Byrne KG, Bolhuis A, Robinson C (2005) The Escherichia coli twin-arginine translocation apparatus incorporates a distinct form of TatABC complex, spectrum of modular TatA complexes and minor TatAB complex. Journal of Molecular Biology 346(1): 295-305

Olmo-Mira MF, Gavira M, Richardson DJ, Castillo F, Moreno-Vivián C, Roldán MD (2004) NapF is a cytoplasmic iron-sulfur protein required for Fe-S cluster assembly in the periplasmic nitrate reductase. Journal of Biological Chemistry 279(48): 49727-49735

Oresnik IJ, Ladner CL, Turner RJ (2001) Identification of a twin-arginine leader-binding protein. Molecular Microbiology 40(2): 323-331

Palmer T, Sargent F, Berks BC (2005) Export of complex cofactor-containing proteins by the bacterial Tat pathway. Trends in Microbiology 13(4): 175-180

Panahandeh S, Maurer C, Moser M, DeLisa MP, Müller M (2008) Following the path of a twin-arginine precursor along the TatABC translocase of Escherichia coli. Journal of Biological Chemistry 283(48): 33267-33275

Panahandeh S, Müller M (2010) Site-specific cross-linking of in vitro synthesized E. coli preproteins for investigating transmembrane translocation pathways. Methods in Molecular Biology 619: 217-240

Papish AL, Ladner CL, Turner RJ (2003) The twin-arginine leader-binding protein, DmsD, interacts with the TatB and TatC subunits of the Escherichia coli twin-arginine translocase. Journal of Biological Chemistry 278(35): 32501-32506

Parish D, Benach J, Liu G, Singarapu KK, Xiao R, Acton T, Su M, Bansal S, Prestegard JH, Hunt J, Montelione GT, Szyperski T (2008) Protein chaperones Q8ZP25_SALTY from Salmonella typhimurium and HYAE_ECOLI from Escherichia coli exhibit thioredoxin-like structures despite lack of canonical thioredoxin active site sequence motif. Journal of Structural and Functional Genomics 9(1-4): 41-49

Penton CR, Devol AH, Tiedje JM (2006) Molecular evidence for the broad distribution of anaerobic ammonium-oxidizing bacteria in freshwater and marine sediments. Applied and Environmental Microbiology 72(10): 6829-6832

Pérez-Rodríguez R, Fisher AC, Perlmutter JD, Hicks MG, Chanal A, Santini CL, Wu LF, Palmer T, DeLisa MP (2007) An Essential Role for the DnaK Molecular Chaperone in

Stabilizing Over-expressed Substrate Proteins of the Bacterial Twin-arginine Translocation Pathway. Journal of Molecular Biology 367(3): 715-730

Peters JW, Boyd ES, Hamilton T, Rubio LM (2011) Biochemistry of Mo-nitrogenases. In J W B Moir, Nitrogen Cycling in Bacteria Caister Academic Press, York, UK: 59-99

Poly F, Wertz S, Brothier E, Degrange V (2008) First exploration of Nitrobacter diversity in soils by a PCR cloning-sequencing approach targeting functional gene nxrA. FEMS Microbiology Ecology 63(1): 132-140

Pommier J, Mejean V, Giordano G, Iobbi-Nivol C (1998) TorD, a cytoplasmic chaperone that interats with the unfolded trimethylamine N-oxide reductase enzyme (TorA) in Escherichia coli. Journal of Biological Chemistry 273(26): 16615-16620

Pomowski A, Zumft WG, Kroneck PMH, Einsle O (2011) N2O binding at a [4Cu:2S] copper-sulphur cluster in nitrous oxide reductase. Nature 477(7363): 234-237

Pop O, Martin U, Abel C, Müller JP (2002) The twin-arginine signal peptide of PhoD and the TatAd/Cd proteins of Bacillus subtilis form an autonomous tat translocation system. Journal of Biological Chemistry 277(5): 3268-3273

Porcelli I, De Leeuw E, Wallis R, Van den Brink-van der Laan E, De Kruijff B, Wallace BA, Palmer T, Berks BC (2002) Characterization and membrane assembly of the TatA component of the Escherichia coli twin-arginine protein transport system. Biochemistry 41(46): 13690-13697

Potter LC, Cole JA (1999) Essential roles for the products of the napABCD genes, but not napFGH, in periplasmic nitrate reduction by Escherichia coli K-12. Biochemical Journal 344(1): 69-76

Pritchard L, Corne D, Kell D, Rowland J, Winson M (2005) A general model of error-prone PCR. Journal of Theoretical Biology 234(4): 497-509

Punginelli C, Maldonado B, Grahl S, Jack R, Alami M, Schröder J, Berks BC, Palmer T (2007) Cysteine scanning mutagenesis and topological mapping of the Escherichia coli twin-arginine translocase TatC component. Journal of Bacteriology 189(15): 5482-5494

Qiu Y, Zhang R, Binkowski TA, Tereshko V, Joachimiak A, Kossiakoff A (2008) The 1.38 Å crystal structure of DmsD protein from Salmonella typhimurium, a proofreading chaperone on the Tat pathway. Proteins: Structure, Function and Genetics 71(2): 525-533

Rabin RS, Stewart V (1993) Dual response regulators (NarL and NarP) interact with dual sensors (NarX and NarQ) to control nitrate- and nitrite-regulated gene expression in Escherichia coli K-12. Journal of Bacteriology 175(11): 3259-3268

Ramasamy SK, Clemons WM (2009) Structure of the twin-arginine signal-binding protein DmsD from Escherichia coli. Acta Crystallographica Section F: Structural Biology and Crystallization Communications 65(8): 746-750

Ray N, Oates J, Turner RJ, Robinson C (2003) DmsD is required for the biogenesis of DMSO reductase in Escherichia coli but not for the interaction of the DmsA signal peptide with the Tat apparatus. FEBS Letters 534(1-3): 156-160

Ribbe MW, Burgess BK (2001) The chaperone GroEL is required for the final assembly of the molybdenum-iron protein of nitrogenase. Proceedings of the National Academy of Sciences of the United States of America 98(10): 5521-5525

Richardson D, Felgate H, Watmough N, Thomson A, Baggs E (2009) Mitigating release of the potent greenhouse gas N2O from the nitrogen cycle - could enzymic regulation hold the key? Trends in Biotechnology 27(7): 388-397

Richardson DJ (2000) Bacterial respiration: a flexible process for a changing environment. Microbiology 146: 551-571

Richardson DJ, Berks BC, Russell DA, Spiro S, Taylor CJ (2001) Functional, biochemical and genetic diversity of prokaryotic nitrate reductases. Cellular and Molecular Life Sciences 58(2): 165-178

Richter S, Brüser T (2005) Targeting of unfolded PhoA to the TAT translocon of Escherichia coli. Journal of Biological Chemistry 280(52): 42723-42730

Richter S, Lindenstrauß U, Lücke C, Bayliss R, Brüser T (2007) Functional tat transport of unstructured, small, hydrophilic proteins. Journal of Biological Chemistry 282(46): 33257-33264

Robinson C, Matos CFRO, Beck D, Ren C, Lawrence J, Vasisht N, Mendel S (2011) Transport and proofreading of proteins by the twin-arginine translocation (Tat) system in bacteria. Biochimica et Biophysica Acta - Biomembranes 1808(3): 876-884

Rodrigue A, Chanal A, Beck K, Müller M, Wu LF (1999) Co-translocation of a periplasmic enzyme complex by a hitchhiker mechanism through the bacterial Tat pathway. Journal of Biological Chemistry 274(19): 13223-13228

Rohl CA, Fiori W, Baldwin RL (1999) Alanine is helix-stabilizing in both template-nucleated and standard peptide helices. Proceedings of the National Academy of Sciences of the United States of America 96(7): 3682-3687

Rose RW, Brüser T, Kissinger JC, Pohlschröder M (2002) Adaptation of protein secretion to extremely high-salt conditions by extensive use of the twin-arginine translocation pathway. Molecular Microbiology 45(4): 943-950

Rothery RA, Bertero MG, Cammack R, Palak M, Blasco F, Strynadka NCJ, Weiner JH (2004) The Catalytic Subunit of Escherichia coli Nitrate Reductase A Contains a Novel [4Fe-4S] Cluster with a High-Spin Ground State. Biochemistry 43(18): 5324-5333

Rothery RA, Blasco F, Weiner JH (2001) Electron transfer from heme bL to the [3Fe-4S] cluster of Escherichia coli nitrate reductase A (NarGHI). Biochemistry 40(17): 5260-5268

Ruiz N, Wu T, Kahne D, Silhavy TJ (2006) Probing the barrier function of the outer membrane with chemical conditionality. ACS chemical biology 1(6): 385-395

Sahoo H, Schwille P (2011) FRET and FCS - Friends or foes? ChemPhysChem 12(3): 532-541

Sammond DW, Eletr ZM, Purbeck C, Kuhlman B (2010) Computational design of second-site suppressor mutations at protein-protein interfaces. Proteins: Structure, Function and Bioformatics 78(4): 1055-1065

San Miguel M, Marrington R, Rodger PM, Rodger A, Robinson C (2003) An Escherichia coli twin-arginine signal peptide switches between helical and unstructured conformations depending on the hydrophobicity of the environment. European Journal of Biochemistry 270(16): 3345-3352

Santini CL, Ize B, Chanal A, Müller M, Giordano G, Wu LF (1998) A novel Sec-independent periplasmic protein translocation pathway in Escherichia coli. EMBO Journal 17(1): 101-112

Sarfo KJ, Winstone TL, Papish AL, Howell JM, Kadir H, Vogel HJ, Turner RJ (2004) Folding forms of Escherichia coli DmsD, a twin-arginine leader binding protein. Biochemical and Biophysical Research Communications 315(2): 397-403

Sargent F (2007a) Constructing the wonders of the bacterial world: Biosynthesis of complex enzymes. Microbiology 153(3): 633-651

Sargent F (2007b) The twin-arginine transport system: Moving folded proteins across membranes. Biochemical Society Transactions 35(5): 835-847

Sargent F, Berks BC, Palmer T (2006) Pathfinders and trailblazers: A prokaryotic targeting system for transport of folded proteins. FEMS Microbiology Letters 254(2): 198-207

Sargent F, Bogsch EG, Stanley NR, Wexler M, Robinson C, Berks BC, Palmer T (1998) Overlapping functions of components of a bacterial Sec-independent protein export pathway. EMBO Journal 17(13): 3640-3650

Sargent F, Stanley NR, Berks BC, Palmer T (1999) Sec-independent protein translocation in Escherichia coli. A distinct and pivotal role for the TatB protein. Journal of Biological Chemistry 274(51): 36073-36082

Schindelin H, Kisker C, Schlessman JL, Howard JB, Rees DC (1997) Structure of ADP·AlF4/--stabilized nitrogenase complex and its implications for signal transduction. Nature 387(6631): 370-376

Schubert T, Lenz O, Krause E, Volkmer R, Friedrich B (2007) Chaperones specific for the membrane-bound [NiFe]-hydrogenase interact with the Tat signal peptide of the small subunit precursor in Ralstonia eutropha H16. Molecular Microbiology 66(2): 453-467

Schwarz G, Mendel RR, Ribbe MW (2009) Molybdenum cofactors, enzymes and pathways. Nature 460(7257): 839-847

Seefeldt LC, Hoffman BM, Dean DR (2009) Mechanism of Mo-dependent nitrogenase. Annual Review of Biochemistry 78: 701-722

Shao X, Lu J, Hu Y, Xia B, Jin C (2009) Solution structure of the Escherichia coli HybE reveals a novel fold. Proteins: Structure, Function and Bioformatics 75(4): 1051-1056

Shen Y, Delaglio F, Cornilescu G, Bax A (2009) TALOS+: A hybrid method for predicting protein backbone torsion angles from NMR chemical shifts. Journal of Biomolecular NMR 44(4): 213-223

Shulman ST, Friedmann HC, Sims RH (2007) Theodor Escherich: the first pediatric infectious diseases physician? Clinical infectious diseases : an official publication of the Infectious Diseases Society of America 45(8): 1025-1029

Simon J (2002) Enzymology and bioenergetics of respiratory nitrite ammonification. FEMS Microbiology Reviews 26(3): 285-309

Sodergren EJ, DeMoss JA (1988) narI region of the Escherichia coli nitrate reductase (nar) operon contains two genes. Journal of Bacteriology 170(4): 1721-1729

Speck J, Arndt KM, Mller KM (2011) Efficient phage display of intracellularly folded proteins mediated by the TAT pathway. Protein Engineering, Design and Selection 24(6): 473-484

Stanley NR, Palmer T, Berks BC (2000) The twin arginine consensus motif of Tat signal peptides is involved in Sec-independent protein targeting in Escherichia coli. Journal of Biological Chemistry 275(16): 11591-11596

Stanley NR, Sargent F, Buchanan G, Shi J, Stewart V, Palmer T, Berks BC (2002) Behaviour of topological marker proteins targeted to the Tat protein transport pathway. Molecular Microbiology 43(4): 1005-1021

Starkenburg SR, Larimer FW, Stein LY, Klotz MG, Chain PSG, Sayavedra-Soto LA, Poret-Peterson AT, Gentry ME, Arp DJ, Ward B, Bottomley PJ (2008) Complete genome sequence of Nitrobacter hamburgensis X14 and comparative genomic analysis of species within the genus Nitrobacter. Applied and Environmental Microbiology 74(9): 2852-2863

Stevens CM, Winstone TML, Turner RJ, Paetzel M (2009) Structural Analysis of a Monomeric Form of the Twin-Arginine Leader Peptide Binding Chaperone Escherichia coli DmsD. Journal of Molecular Biology 389(1): 124-133

Stewart V, Bledsoe PJ (2005) Fnr-, NarP- And NarL-dependent regulation of transcription initiation from the Haemophilus influenzae Rd napF (Periplasmic nitrate reductase) promoter in Escherichia coli K-12. Journal of Bacteriology 187(20): 6928-6935

Stewart V, Bledsoe PJ, Chen LL, Cai A (2009) Catabolite repression control of napF (periplasmic nitrate reductase) operon expression in Escherichia coli K-12. Journal of Bacteriology 191(3): 996-1005

Stewart V, Bledsoe PJ, Williams SB (2003) Dual overlapping promoters control napF (periplasmic nitrate reductase) operon expression in Escherichia coli K-12. Journal of Bacteriology 185(19): 5862-5870

Stewart V, Rabin RS (1995) Dual sensors and dual response regulators interact to control nitrate- and nitrite-responsive gene expression inEscherichia coli. In J A Hoch and T J Silhavy (ed), Two-component signal transduction ASM Press, Washington DC: 233-252

Strauch EM, Georgiou G (2007) Escherichia coli tatC Mutations that Suppress Defective Twin-Arginine Transporter Signal Peptides. Journal of Molecular Biology 374(2): 283-291

Strous M, Pelletier E, Mangenot S, Rattei T, Lehner A, Taylor MW, Horn M, Daims H, Bartol-Mavel D, Wincker P, Barbe V, Fonknechten N, Vallenet D, Segurens B, Schenowitz-Truong C, Médigue C, Collingro A, Snel B, Dutilh BE, Op Den Camp HJM, Van Der Drift C, Cirpus I, Van De Pas-Schoonen KT, Harhangi HR, Van Niftrik L, Schmid M, Keltjens J, Van De Vossenberg J, Kartal B, Meier H, Frishman D, Huynen MA, Mewes HW, Weissenbach J, Jetten MSM, Wagner M, Le Paslier D (2006) Deciphering the evolution and metabolism of an anammox bacterium from a community genome. Nature 440(7085): 790-794

Sturm A, Schierhorn A, Lindenstrauss U, Lilie H, Brüser T (2006) YcdB from Escherichia coli reveals a novel class of Tat-dependently translocated hemoproteins. Journal of Biological Chemistry 281(20): 13972-13978

Sujatha S, Chatterji D (2000) Understanding protein-protein interactions by genetic suppression. Journal of Genetics 79(3): 125-129

Tang H, Rothery RA, Voss JE, Weiner JH (2011) Correct assembly of iron-sulfur cluster FS0 into Escherichia coli dimethyl sulfoxide reductase (DmsABC) is a prerequisite for molybdenum cofactor insertion. Journal of Biological Chemistry 286(17): 15147-15154

Tarry M, Arends SJR, Roversi P, Piette E, Sargent F, Berks BC, Weiss DS, Lea SM (2009a) The Escherichia coli Cell Division Protein and Model Tat Substrate SufI (FtsP) Localizes to the Septal Ring and Has a Multicopper Oxidase-Like Structure. Journal of Molecular Biology 386(2): 504-519

Tarry MJ, Schäfer E, Chen S, Buchanan G, Greene NP, Lea SM, Palmer T, Saibil HR, Berks BC (2009b) Structural analysis of substrate binding by the TatBC component of the twin-arginine protein transport system. Proceedings of the National Academy of Sciences of the United States of America 106(32): 13284-13289

Thammawong P, Kasinrerk W, Turner RJ, Tayapiwatana C (2006) Twin-arginine signal peptide attributes effective display of CD147 to filamentous phage. Applied Microbiology and Biotechnology 69(6): 697-703

Theg SM, Cline K, Finazzi G, Wollman FA (2005) The energetics of the chloroplast Tat protein transport pathway revisited. Trends in Plant Science 10(4): 153-154

Thomas G, Potter L, Cole JA (1999) The periplasmic nitrate reductase from Escherichia coli: A heterodimeric molybdoprotein with a double-arginine signal sequence and an unusual leader peptide cleavage site. FEMS Microbiology Letters 174(1): 167-171

Tranier S, Iobbi-Nivol C, Birck C, Ilbert M, Mortier-Barrière I, Méjean V, Samama JP (2003) A novel protein fold and extreme domain swapping in the dimeric TorD chaperone from Shewanella massilia. Structure 11(2): 165-174

Tranier S, Mortier-Barrière I, Ilbert M, Birck C, Iobbi-Nivol C, Méjean V, Samama JP (2002) Characterization and multiple molecular forms of TorD from Shewanella massilia, the putative chaperone of the molybdoenzyme TorA. Protein Science 11(9): 2148-2157

Tullman-Ercek D, DeLisa MP, Kawarasaki Y, Iranpour P, Ribnicky B, Palmer T, Georgiou G (2007) Export pathway selectivity of Escherichia coli twin arginine translocation signal peptides. Journal of Biological Chemistry 282(11): 8309-8316

Turner RJ, Papish AL, Sargent F (2004) Sequence analysis of bacterial redox enzyme maturation proteins (REMPs). Canadian Journal of Microbiology 50(4): 225-238

Van den Wildenberg SMJL, Bollen YJM, Peterman EJG (2011) How to quantify protein diffusion in the bacterial membrane. Biopolymers 95(5): 312-321

van Niftrik L, Geerts WJC, van Donselaar EG, Humbel BM, Yakushevska A, Verkleij AJ, Jetten MSM, Strous M (2008) Combined structural and chemical analysis of the anammoxosome: A membrane-bounded intracytoplasmic compartment in anammox bacteria. Journal of Structural Biology 161(3): 401-410

van Spanning RJM (2011) Structure, Function, Regulation and Evolution of the Nitrite and Nitrous Oxide Reductases: Denitrification Enzymes with a Beta-propeller Fold. In J W B Moir, Nitrogen Cycling in Bacteria Caister Academic Press, York, UK: 135-162

Vaynberg J, Qin J (2006) Weak protein-protein interactions as probed by NMR spectroscopy. Trends in Biotechnology 24(1): 22-27

Von Heijne G (1992) Membrane protein structure prediction. Hydrophobicity analysis and the positive-inside rule. Journal of Molecular Biology 225(2): 487-494

Walmsley J, Toukdarian A, Kennedy C (1994) The role of regulatory genes nifA, vnfA, anfA, nfrX, ntrC, and rpoN in expression of genes encoding the three nitrogenases of Azotobacter vinelandii. Archives of Microbiology 162(6): 422-429

Walter TS, Meier C, Assenberg R, Au KF, Ren J, Verma A, Nettleship J, Owens RJ, Stuart D, Grimes JM (2006) Lysine Methylation as a Routine Rescue Strategy for Protein Crystallization. Structure 14(11): 1617-1622

Walther TH, Grage SL, Roth N, Ulrich AS (2010) Membrane alignment of the pore-forming component TatAd of the twin-arginine translocase from Bacillus subtilis resolved by solid-state NMR spectroscopy. Journal of the American Chemical Society 132(45): 15945-15956

Wang X, Lavrov DV (2007) Mitochondrial genome of the homoscleromorph Oscarella carmela (Porifera, Demospongiae) reveals unexpected complexity in the common ancestor of sponges and other animals. Molecular Biology and Evolution 24(2): 363-373

Waraho D, DeLisa MP (2009) Versatile selection technology for intracellular protein-protein interactions mediated by a unique bacterial hitchhiker transport mechanism. Proceedings of the National Academy of Sciences of the United States of America 106(10): 3692-3697

Ward R, Bowman A, El-Mkami H, Owen-Hughes T, Norman DG (2009) Long distance PELDOR measurements on the histone core particle. Journal of the American Chemical Society 131(4): 1348-1349

Ward R, Bowman A, Sozudogru E, El-Mkami H, Owen-Hughes T, Norman DG (2010) EPR distance measurements in deuterated proteins. Journal of Magnetic Resonance 207(1): 164-167

White GF, Schermann SM, Bradley J, Roberts A, Greene NP, Berks BC, Thomson AJ (2010) Subunit organization in the TatA complex of the twin arginine protein translocase: A site-directed EPR spin labeling study. Journal of Biological Chemistry 285(4): 2294-2301

Widdick DA, Dilks K, Chandra G, Bottrill A, Naldrett M, Pohlschröder M, Palmer T (2006) The twin-arginine translocation pathway is a major route of protein export in Streptomyces coelicolor. Proceedings of the National Academy of Sciences of the United States of America 103(47): 17927-17932

Widdick DA, Eijlander RT, van Dijl JM, Kuipers OP, Palmer T (2008) A Facile Reporter System for the Experimental Identification of Twin-Arginine Translocation (Tat) Signal Peptides from All Kingdoms of Life. Journal of Molecular Biology 375(3): 595-603

Wu LF, Ize B, Chanal A, Quentin Y, Fichant G (2000) Bacterial twin-arginine signal peptide-dependent protein translocation pathway: Evolution and mechanism. Journal of Molecular Microbiology and Biotechnology 2(2): 179-189

Yahr TL, Wickner WT (2001) Functional reconstitution of bacterial Tat translocation in vitro. EMBO Journal 20(10): 2472-2479

Yang J, Kennedy EJ, Wu J, Deal MS, Pennypacker J, Ghosh G, Taylor SS (2009) Contribution of non-catalytic core residues to activity and regulation in protein kinase A. Journal of Biological Chemistry 284(10): 6241-6248

Zakian S, Lafitte D, Vergnes A, Pimentel C, Sebban-Kreuzer C, Toci R, Claude JB, Guerlesquin F, Magalon A (2010) Basis of recognition between the NarJ chaperone and the N-terminus of the NarG subunit from Escherichia coli nitrate reductase. FEBS Journal 277(8): 1886-1895

Zhang JW, Butland G, Greenblatt JF, Emili A, Zamble DB (2005) A role for SlyD in the Escherichia coli hydrogenase biosynthetic pathway. Journal of Biological Chemistry 280(6): 4360-4366

Zumft WG (2005) Nitric oxide reductases of prokaryotes with emphasis on the respiratory, heme-copper oxidase type. Journal of Inorganic Biochemistry 99(1): 194-215